Overcoming Barriers in the Treatment of Textile Wastewaters using Advanced Oxidation Processes

Thesis submitted in partial fulfilment of the requirements for the degree of Doctor of Philosophy in Environmental Engineering, at the Faculty of Engineering, University of Porto

Petrick Anderson Soares

Supervisor: Vítor Jorge Pais Vilar, Ph.D.

Co-Supervisors: Selene M. A. Guelli U. Souza, Ph.D. [UFSC]

Rui Alfredo da Rocha Boaventura, Ph.D.

LSRE-Laboratory of Separation and Reaction Engineering - Associate Laboratory LSRE-LCM

Department of Chemical Engineering

Faculty of Engineering

University of Porto

December, 2015

Acknowledgments

I would like to acknowledge to my supervisor, Dr. Vítor Vilar, the opportunity given to perform this thesis under his guidance, as well as his enriching presence in the discussion and resolution of the difficulties encountered. I am sure that without his help and valuable knowledge would not have been possible to develop this work.

I am also thankful to my co-supervisors, Dra. Selene M. A. Guelli U. Souza and Dr. Rui Boaventura, for the contribution given for this thesis as well as their constructive criticisms that have become precious.

I am very grateful to Dra. Tânia F. C. V. Silva for her support, ideas and partnership. A great researcher who became my "co-supervisor" over the last years, contributing actively for the accomplishment of my work.

A mention must be made to the following institutions that supported this work: the foundation *Coordenação de Aperfeiçoamento de Pessoal de Nível Superior* (CAPES) for the doctoral grant (BEX 5512-10-7); the Associated Laboratory of Separation and Reaction Engineering (LSRE) and Catalysis Materials (LCM), Faculty of Engineering of the University of Porto (FEUP).

A greeting goes to my esteemed colleagues from LSRE-FEUP (so many that I cannot nominate all of them), for all the good, bad, and overall funny moments spent together, for the coffee break sessions and for all the lunch time conversations. My thanks and appreciations also go to people who have willingly helped me out with their abilities: Dr. Diego Manenti, Dra. Lucila Doumic, Dra. Renata Souza, Eng. Mauro Batalha, Ms. Adriana Arcy and Dr. Juan Escoda.

I would like to express my frank acknowledgment to my family, especially to my parents, Ana and Luis, for all the help and strength that always instilled in me throughout my personal and academic life. In addition, I would like to take and say, I am sorry for the long four years far away from you, I promise that all this will be worth it.

Finally, to my wife, Evelyn, I would like to express my sincere gratitude for her love, friendship and support in all times, for have given me strength in the most difficult moments and for the encouragement along this journey.

With love to Evelyn

No matter how educated, talented,
rich, or cool you believe you are, how
you treat people ultimately tells all.
Integrity is everything.

Unknown Author

Abstract

Currently, the textile industry is one of the most important economic sectors in many countries. Besides, it is known as a major consumer of water and consequently one of the largest groups of industries causing intense water pollution. Chemicals, including surfactants, dyes, resins, dispersants agents, inorganic salts, etc., play a variety of functions during the textile processing and are present as a by-product in large volumes of toxic wastewater. As a consequence, textile industry has been challenged for colour removal, salt content reduction and elimination of the non-biodegradable organic fraction from the generated wastewaters. Biological processes are the preferred choice for textile wastewater treatment because they are less costly, and the by-products resulting from complete degradation are not toxic. However, conventional biological processes do not always provide satisfactory results, since many of the organic substances used in the textile industry are toxic or recalcitrant. Advanced oxidation processes (AOPs) have been considered a promising wastewater treatment technology for the elimination of recalcitrant/toxic organic pollutants, as those present in textile wastewaters. The main aim of this thesis was the study of alternative processes for the treatment of textile wastewaters, combining AOPs and biological oxidation. The treatment strategy was applied to four different textile wastewater, two real textile wastewaters and two synthetic ones.

Firstly, for two textile wastewaters, both with high percentage of recalcitrant organic matter, a treatment strategy including AOPs and biological oxidation was proposed. The efficiency of different AOPs (UVA-Vis; UVA-Vis/TiO_2; UVA-Vis/H_2O_2; UVA-Vis/TiO_2/H_2O_2 and UVA-Vis/Fe^{2+}/H_2O_2) was compared in the treatment of a real cotton-textile dyeing wastewater using a pilot plant under natural sunlight. The obtained results demonstrated that solar-photo-Fenton treatment was the most efficient of all solar AOPs studied, enhancing the biodegradability of the wastewater and making possible its combination with a downstream biological oxidation process. The photo-Fenton reaction rate was also assessed at different iron concentrations, pH, temperature and light intensity, in a lab-scale prototype under controlled conditions using artificial solar radiation. Thus, considering the combination of a photo-Fenton reaction with a biological oxidation process, the energy dose required for the phototreatment was 0.5 kJ_{UV} L^{-1} (T= 30ºC; pH = 2.8), while consuming 7.5 mM of hydrogen peroxide and leading to 58.4% mineralisation (DOC_f = 62.9 mg C L^{-1}).

Afterwards, the enhancement of a solar photo-Fenton reaction by using different ferric-organic ligands (oxalic acid, citrate acid and EDDS-Ethylenediamine-N,N'-disuccinic acid), applied to the treatment of a simulated acrylic-textile dyeing wastewater to increase its biodegradability, was evaluated. The catalytic activity of the organic ligands toward the ferrous-catalysed systems followed this order: Fe(III)-Oxalate > Fe(III)-Citrate > Fe(III)-EDDS, and all were better than the traditional photo-Fenton reaction.

The influence of the main ferrioxalate-solar-photo-Fenton reaction variables, such as iron concentration, pH, temperature, UV irradiance and H_2O_2 concentration and dosage strategy was also investigated. Thus, the ferrioxalate induced photo-Fenton process presented the best results, achieving 87% mineralisation after 9.3 kJ_{UV} L^{-1} and allowing working until pH 5.0. As expected, the biodegradability of the textile wastewater was significantly enhanced during the photo-Fenton treatment, achieving a value of 73%, while consuming 32.4 mM of H_2O_2 and 5.7 kJ_{UV} L^{-1}.

For the other two textile wastewaters, both with high percentage of biodegradable organic matter, a biological oxidation treatment followed by AOPs was proposed. A synthetic polyester-cotton dyeing wastewater was firstly subjected to biological oxidation, achieving a DOC removal of 76%, resulting in a bio-treated wastewater with 84 mg L^{-1} of DOC. The colour reduction was less than 5% (Pt-Co scale), 9% (DFZ_{436nm}), 3% (DFZ_{525nm}) and 0% (DFZ_{620nm}). Thus, UVC/H_2O_2 and photo-Fenton oxidation processes were used as a polishing step for the decolourisation of bio-treated textile wastewater. The photo-Fenton reaction did not promote the decolourisation. Moreover, the addition of oxalic acid did not result in an enhancement of the photo-Fenton reaction. On the other hand, the photolysis of hydrogen peroxide using UVC radiation led to decolourisation efficiencies of 71% (Pt-Co scale), 86% ($DFZ_{436\ nm}$) and 97% ($DFZ_{525\ nm}$) and more than 40% of mineralisation, consuming 14.1 mM H_2O_2 and 2.5 kJ_{UV} L^{-1} of energy (time = 95 min; 6W UVC lamp; natural pH = 8.4; T = 30ºC). The influence of hydrogen peroxide dosage, lamp power, solution pH and temperature on the UVC/H_2O_2 system was evaluated. It was shown that the UVC/H_2O_2 reaction efficiency is mostly affected by the relation between H_2O_2 dosage and lamp power. The integrated treatment strategy was able to achieve a wastewater quality in agreement with the discharge limits imposed by legislation.

Finally, UVC/H_2O_2 and photo-Fenton oxidation processes were used as a polishing step in the decolourisation of a bio-treated real textile wastewater. The photolysis of hydrogen peroxide using UVC radiation achieved decolourisation efficiencies of 86% (Pt-Co scale) and 96% (DFZ_{436nm}), consuming 1.6 mM H_2O_2 after 0.9 kJ_{UV} L^{-1} (time = 35 min; UVC lamp power = 6 W; natural pH = 7.8; T = 30ºC). The photo-Fenton reaction was promoted by different radiation sources (UVC, UVA or UVA-Visible), showing best results under UVC light. The efficiency of the UVC/Fe^{2+}/H_2O_2 system was also studied for different iron concentrations, H_2O_2 availability and pH values. Decolourisation efficiencies of 78% (Pt-Co scale) and 93% (DFZ_{436nm}) were achieved applying the UVC/Fe^{2+}/H_2O_2 system at pH = 2.8 and T = 30ºC, consuming 3.6 mM H_2O_2 after 0.6 kJ_{UV} L^{-1} (time = 25 min; UV lamp power = 6 W). To further investigate the use of solar energy, additional photo-Fenton assays mediated by ferric-organic ligands under UVA-Visible radiation were also performed, considering the effect of the type of ferric-organic ligand as well as the iron/ferric-organic ligand molar ratio, iron concentration and pH. Maximum

values for the decolourisation with UVA-Vis/Fe^{3+}/H_2O_2/oxalic acid were 84% (Pt-Co scale) and 94% (DFZ_{436nm}), consuming 1.9 mM H_2O_2 after 2.9 kJ_{UV} L^{-1} (pH = 2.8). In addition, the costs associated with the processes studied were estimated. For the optimal conditions, aiming at achieving the legal wastewater discharge requirements, the total unit costs were: a) 0.25 € m^{-3} (UVC/H_2O_2 at pH 2.8); b) 0.16 € m^{-3} (UVC/H_2O_2 at natural pH); c) 0.24 € m^{-3} (UVC/Fe^{2+}/H_2O_2 at pH 2.8); d) 0.61 € m^{-3} (UVA-Vis/Fe^{2+}/H_2O_2 at pH 2.8); e) 0.79 € m^{-3} (UVA-Vis/Fe^{3+}/H_2O_2/Oxalic acid at pH 2.8) and; f) 0.83 € m^{-3} (UVA-Vis/Fe^{3+}/H_2O_2/oxalic acid at pH 5.0).

Resumo

Atualmente, a indústria têxtil representa um dos setores mais importantes para a economia de muitos países. Por outro lado, o processamento e tingimento de fibras têxteis são conhecidos pelo elevado consumo de água e, consequentemente, a indústria têxtil é um dos setores industriais que causam intensa poluição da água. Além disso, muitos produtos auxiliares são adicionados para realizar uma variedade de funções durante o processamento das fibras, por exemplo, agentes tensioativos, corantes, resinas, agentes dispersantes, sais inorgânicos, etc., os quais aparecem como subproduto num grande volume de águas residuais tóxicas. Como consequência, a indústria têxtil tem sido desafiada para promover a remoção de cor, redução do teor de sais e eliminação da fração orgânica não-biodegradável das águas residuais geradas. Os processos biológicos são a escolha preferida para o tratamento de águas residuais das indústrias têxteis, principalmente porque são menos dispendiosos, e os subprodutos da degradação biológica não são tóxicos. No entanto, os processos biológicos convencionais nem sempre fornecem resultados satisfatórios, uma vez que muitas das substâncias orgânicas utilizadas na indústria têxtil são potencialmente resistentes à oxidação biológica. Processos oxidativos avançados (POAs) são atualmente considerados uma promissora tecnologia de tratamento de águas residuais, principalmente na eliminação de poluentes orgânicos tóxicos/recalcitrantes, como aqueles presentes em águas residuais têxteis. O principal objetivo desta tese foi estudar processos alternativos para o tratamento de águas residuais têxteis, combinando POAs e oxidação biológica. A estratégia de tratamento foi aplicada a quatro tipos de águas residuais, sendo dois efluentes têxteis reais e dois efluentes têxteis sintéticos.

Inicialmente, para dois dos efluentes têxteis, ambos com elevada percentagem de matéria orgânica recalcitrante, foi proposta uma estratégia de tratamento incluindo POAs seguidos de processos oxidativos biológicos. A eficiência de diferentes POAs (UVA-Vis; UVA-Vis/TiO_2; UVA-Vis/H_2O_2; UVA-Vis/TiO_2/H_2O_2 e UVA-Vis/Fe^{2+}/H_2O_2) foi comparada no tratamento de um efluente real de tingimento de fibras de algodão, usando uma instalação piloto irradiada com luz solar natural. Os resultados obtidos demonstraram que a reação foto-Fenton foi o processo mais eficiente, resultando num efluente de elevada biodegradabilidade, tornando possível a sua combinação com um processo de oxidação biológica a jusante. A velocidade da reação foto-Fenton foi avaliada para diferentes concentrações de ferro, pH, temperatura e intensidade da radiação, num protótipo à escala laboratorial sob condições controladas utilizando radiação solar artificial. Considerando a estratégia de tratamento combinando o POA (reação foto-Fenton) com um sistema de oxidação biológica a jusante, a dose de energia necessária para a fotoreação foi de 0,5 kJ_{UV} L^{-1} (T = 30°C; pH = 2,8) consumindo 7,5 mM de peróxido de hidrogénio, resultando numa mineralização de 58,4% (COD_f = 62,9 mg L^{-1}).

Posteriormente, a reação foto-Fenton foi melhorada através da utilização de diferentes ligantes orgânicos férricos (ácido oxálico, ácido cítrico e EDDS-etilenodiamina-N, N'-disuccínico), sendo aplicada como uma etapa de pré-oxidação para aumentar a biodegradabilidade de um efluente sintético de tingimento de fibras acrílicas. A atividade catalítica dos ligantes orgânicos decresceu pela seguinte ordem: Fe(III)-Oxalato>Fe(III)-Citrato>Fe(III)-EDDS, e todos foram melhores do que a reação tradicional de foto-Fenton. A influência das principais variáveis reacionais, tais como a concentração de ferro, pH, temperatura, intensidade da radiação, e concentração e estratégia de dosagem de H_2O_2, foi investigada. Os resultados obtidos demonstraram que a reação de foto-Fenton com ácido oxálico atingiu 87% de mineralização após 9,3 kJ_{UV} L^{-1}, demonstrando, além disso, possibilidades de funcionar em valores de pH até 5,0. Como já esperado, a biodegradabilidade do efluente têxtil aumentou significativamente durante o tratamento foto-Fenton, atingindo um valor de 73% (teste de Zahn-Wellens), após o consumo de 32,4 mM de H_2O_2 e de 5,7 kJ_{UV} L^{-1} de energia.

Para os outros dois efluentes têxteis, ambos com elevada fração de material orgânico biodegradável, foi proposta uma oxidação biológica seguida de POA. Uma mistura de efluentes sintéticos de tingimento de fibras de poliéster e de algodão foi oxidada num reactor biológico, obtendo-se uma remoção de COD de 76% e resultando um efluente bio-tratado com 84 mg L^{-1} de COD. Por outro lado, a descoloração observada no tratamento biológico foi inferior a 5% (Pt-Co), 9% (DFZ_{436nm}), 3% (DFZ_{525nm}) e 0% (DFZ_{620nm}). Por conseguinte, foram utilizados processos oxidativos avançados (UVC/H_2O_2 e foto-Fenton) como uma etapa de polimento, de forma a promover a redução de cor do efluente já biologicamente tratado. Os resultados obtidos demonstraram a incapacidade da reação foto-Fenton de descolorir as águas residuais. Além disso, foi observado que a adição de ácido oxálico na reação foto-Fenton também não resultou numa remoção significativa da cor. Por outro lado, a fotólise do peróxido de hidrogénio usando radiação UVC mostrou elevada eficiência na remoção de cor do efluente, atingindo 71% (Pt-Co), 86% (DFZ_{436nm}) e 97% (DFZ_{525nm}) bem como, mais de 40% de mineralização, consumindo 14,1 mM H_2O_2 e 2,5 kJ_{UV} L^{-1} de energia (tempo = 95 min; 6W UVC; pH natural = 8,4; T = 30ºC). Foi avaliada a influência da dose de peróxido de hidrogénio, da potência da lâmpada, do pH e da temperatura do efluente sobre o sistema UVC/H_2O_2. Foi observado que a eficiência da reação UVC/H_2O_2 é principalmente afetada pela relação entre a dosagem de H_2O_2 e a potência da lâmpada. A estratégia de tratamento integrado foi capaz de proporcionar uma qualidade nas águas residuais de acordo com os limites de descarga impostos pela legislação.

Por fim, processos de oxidação avançados (UVC/H_2O_2 e foto-Fenton) foram utilizados como uma etapa de polimento na remoção da cor de um efluente real já biologicamente tratado. A fotólise do peróxido de hidrogénio utilizando radiação UVC mostrou eficiência de descoloração de 86% (Pt-Co) e

96% (DFZ_{436nm}), consumindo 1,6 mM de H_2O_2 após 0,9 kJ_{UV} L^{-1} (tempo = 35 min; 6W UVC; pH natural = 7,8; T = 30ºC). A eficiência da reação foto-Fenton foi avaliada usando diferentes fontes de radiação (UVC, UVA ou UVA visível), mostrando melhores resultados sob luz UVC. A eficiência do sistema UVC/ Fe^{2+}/H_2O_2 foi estudada para diferentes concentrações de ferro, disponibilidade de H_2O_2 e valores de pH. Eficiências de remoção de cor de 78% (Pt-Co) e 93% (DFZ_{436nm}) foram observadas para o sistema UVC/Fe^{2+}/H_2O_2 (pH = 2,8 e T = 30ºC), consumindo 3,6 mM de H_2O_2 após 0,6 kJ_{UV} L^{-1} (tempo = 25 min; 6 W UVC). De forma a possibilitar o uso de energia solar, foram realizados ensaios adicionais de foto-Fenton mediado por ligantes orgânicos sob radiação UVA-Visível. Foram avaliados os efeitos na reação foto-Fenton de diferentes ligantes orgânicos, diferentes rácios molares entre o ferro e o ligante orgânico, diferentes concentrações de ferro e diferentes valores de pH da reação. As maiores percentagens de remoção de cor obtidas com o sistema UVA-Vis/Fe^{3+}/H_2O_2/Ácido oxálico foram de 84% (Pt-Co) e 94% (DFZ_{436nm}), consumindo 1,9 mM de H_2O_2 após 2,9 kJ_{UV} L^{-1} (pH = 2,8). Finalmente, foram estimados os custos associados com os processos estudados. Para as condições ideais, visando atingir os requisitos legais de descarga de águas residuais, os custos unitários observados foram: a) 0,25 € m^{-3} (UVC/H_2O_2; pH 2,8); b) 0,16 € m^{-3} (UVC/H_2O_2; pH natural); c) 0,24 € m^{-3} (UVC/ Fe^{2+}/H_2O_2; pH 2,8); d) 0,61 € m^{-3} (UVA-Vis/Fe^{2+}/H_2O_2; pH 2,8); e) 0,79 € m^{-3} (UVA-Vis/Fe^{3+}/H_2O_2/Ácido oxálico; pH 2,8); f) 0,83 € m^{-3} (UVA-Vis/Fe^{3+}/H_2O_2/Ácido oxálico; pH 5,0).

Table of Contents

List of Figures

List of Tables

Notation

Latin letters

A_{CPC}	Total collectors area needed for the treatment of 30,240 m^3 of bio-treated textile wastewater per day (m^2)
ADMI	American Dye Manufacturer Institute
AOP	Advanced Oxidation Process
A_r	Illuminated collector surface area (m^2)
BOD_5	Biochemical oxygen demand (mg O_2 L^{-1})
C_A	DOC of the sample measured 3-h after starting the Zahn-Wellens test (mg L^{-1})
C_B	DOC of the blank measured at the sampling time *t* during the Zahn-Wellens test (mg L^{-1})
C_{BA}	DOC of the blank measured 3-h after starting the Zahn-Wellens test (mg L^{-1})
DFZ	Visual colour number (m^{-1})
COD	Chemical oxygen demand (mg O_2 L^{-1})
COS	Carbon Oxidation State
CPC	Compound parabolic collector
C_t	DOC of the sample measured at the sampling time *t* during the Zahn-Wellens test(mg L^{-1})
DOC	Dissolved organic carbon (mg L^{-1})
DOC_f	Final dissolved organic carbon concentration (mg C L^{-1})
DOC_0	Initial dissolved organic carbon concentration (mg C L^{-1})
D_t	Percentage of biodegradation (%)
E	Energy (J)
E_y	Yearly accumulated UV energy (kJ_{UV} m^{-2})
fc	Global UV irradiance (%)
F_0	Photonic flux (Einstein s^{-1})
I	Irradiation intensity (W m^{-2})
I_m	Yearly average global UV radiation power (W m^{-2})
LMWCA	Low molecular-weight carboxylate anions (mg L^{-1})
N_A	Avogadro´s number (6.022 x 10^{23} mol^{-1})
P	Lamp power (W)
pf	Photonic flux (J s^{-1})
$\overline{pH}$	Average pH
Pt-Co	Platinum-Cobalt method (mg L^{-1})
Q	Flow (L min^{-1})

Q_d	Daily flow (m^3 day^{-1})
$Q_{UV,n}$	Accumulated UV energy received on any surface in the same position with regard to the sun (kJ L^{-1})
Re	Reynolds number
t	Sampling time (h)
T	Temperature (ºC)
$\overline{T}$	Average temperature (ºC)
TCR	Total capital required (€)
t_{dark}	Time in the dark (min)
TDC	Total direct cost (€)
TDI	Total dissolved iron (mg L^{-1})
t_i	Illumination time (min)
t_{ins}	Total yearly hours of insolation (h)
TN	Total nitrogen (mg L^{-1})
t_n	Time corresponding to n-water sample (s)
TOC	Total organic carbon (mg L^{-1})
TSS	Total suspended solids (mg L^{-1})
TYC	Total yearly cost (€)
UC	Unit cost (€ m^{-3})
$\overline{UV}_{G,n}$	Average solar ultraviolet radiation measured during Δt (W m^{-2})
V	Volume (L)
V_i	Illuminated volume (L)
VSS	Volatile suspended solids (mg L^{-1})
V_t	Total reactor volume (L)
V_y	Yearly volume (m^3)
WWTP	Wastewater treatment plant
ΔH	Enthalpy (kcal mol^{-1})
Δt	Time interval between the collection of two samples, during reaction ($t_n - t_{n-1}$) (s)

Greek letters

λ	Wavelength (nm)
ϕ	Quantum yield

1 Introduction

This first chapter presents the background and motivation of this thesis. An overview of the problematics of aquatic pollution by textile wastewaters is provided, as well as of current and potential treatment methods. The operational parameters and concepts of the main advanced oxidation processes herein proposed are presented, complemented with a survey of current literature.

1.1 Motivation and thesis outline

Water is used for very diverse purposes, which include domestic supply, irrigation, transport, industrial processes, recreation and other human activities. These activities often generate heavily contaminated wastewaters, which if discharged without any treatment can cause strong negative impacts on the receiving water bodies. The environmental pressure on water resources resulting from the discharge of wastewaters contaminated with non-biodegradable pollutants all over the world is regarded as a major challenge to be tackled. Textile dyeing industry is a major consumer of water and consequently one of the largest groups of industries causing intense water pollution. According to the European Integrated Pollution Prevention and Control Bureau [1] estimation, the textile industry releases more than 0.2 million of tons of salts in the environment every year and more than 7000 different compounds and additives are used for the preparation of textile goods, and up to 1 kg of these substances are used for each kilogram of fabric. The extensive use of chemicals and water results in the generation of large quantities of highly polluted wastewater with high recalcitrant matter percentage. As a result, textile industry has been confronted with the challenge of colour removal, wastewater salt content reduction and removal of non-biodegradable matter. The current practice in textile industries is the discharge of the wastewater directly into the local environment or into the municipal sewerage systems after appropriated treatment in agreement with the current local legislation, which is becoming more and more stringent. A varied range of methods has been developed for textile wastewater treatment, which were tested at lab, pilot and/or full scale. In many cases, the combination of various basic treatments is needed to improve the overall efficiency of the wastewater treatment systems. The most widely used are adsorption, membrane filtration (ultrafiltration, nanofiltration or reverse osmosis), coagulation-flocculation, biological treatments (aerobic activated sludge, UASB – Upflow Anaerobic Sludge Blanket), and chemical/electrochemical oxidation processes (AOPs - Advanced Oxidation Processes or EAOPs-Electrochemical Advanced Oxidation Processes).

Nowadays, biological processes are the preferred ones for textile wastewater treatment because they are less costly, and the products from complete degradation are not toxic. The biological oxidation shows good results in the mineralisation of the non-recalcitrant fraction of textile wastewater, especially when mixed with other biodegradable wastewaters, e.g., domestic sewage. However, it is known that the biological process cannot fully decolourize textile dyeing wastewater, i.e. very little biodegradation of dyes occurs and adsorption onto biomass seems to be the main colour removal mechanism. Besides, other synthetic organic chemicals, some categorized as ‘‘xenobiotics’’, are used as additives in different stages of textile dyeing, with a wide range of functions (e.g.: sequestering agents, stabilizers, colour

fixers, dispersants, etc.), and confer significant recalcitrant character to textile wastewaters. In this context, conventional biological processes do not always provide satisfactory results, since many of the organic substances produced by the textile industry are toxic or resistant to biological treatment [2].

Advanced oxidation processes (AOPs) have been considered a promising wastewater treatment technology for the elimination of recalcitrant/toxic organic pollutants, as those present in textile wastewaters [3, 4]. In addition, many studies have already demonstrated the great potential of AOPs for wastewater decolourisation [5-7]. The endpoint of these processes would be complete pollutant transformation, through generation and subsequent reaction with hydroxyl radicals ($^{\bullet}OH$), into CO_2, water and inorganic ions (mineralisation), or otherwise conversion of pollutants into non-toxic and more biodegradable intermediaries.

However, the application of AOPs is limited, as the costs involved with the energy requirements and chemicals, especially when the goal is the complete mineralisation, are high and eventually make these technologies non-competitive. Moreover, specifically the photo-Fenton reaction presents some drawbacks when used in textile wastewaters treatment, e.g.: (i) the presence of coloured compounds might reduce light penetration; (ii) textile wastewaters are usually alkaline in nature and, photo-Fenton treatment works efficiently at acid pH, implying additional costs associated with acidification and subsequent neutralization reagents; at this pH value iron precipitation is avoided and the most photoactive ferric ion-water complex ($FeOH^{2+}$) is the predominant iron species in solution; (iii) ferric-dissolved organic matter complexes can be promoted, limiting the photo reduction of Fe^{3+} and decreasing the decomposition of H_2O_2 in the Fenton reaction; (iv) the high content of inorganic ions (Cl^-, SO_4^{2-}, CO_3^-) promotes the hydroxyl radicals scavenger reactions and also the formation of inorganic ion-ferric complexes, which decreases the rate of generation of hydroxyl radicals [8-10].

Research studies in this field have shown that a single, universally applicable end-of-pipe solution is unrealistic, and the combination of different techniques is required to devise a technically and economically feasible option [2, 11]. For these reasons, the AOPs application for the treatment of textile wastewater, combined with biological oxidation, has potential to become a feasible alternative. Experimental examples of sequential chemical and biological oxidation treatments have been previously reviewed by Sarria et al., [12], Mantzavinos and Psillakis [13], Gaya and Abdullah [14] and Oller et al., [2]. Research studies in this field have usually focused on the specific development of the combination of AOPs and biological treatments for industrial wastewater decontamination. They highlight not only efforts in applying AOPs as a pre-treatment, but also in a combination strategy in the opposite direction,

first eliminating the highly biodegradable part of the wastewater and then degrading the recalcitrant contaminants by a AOP post-treatment [2, 15].

The present thesis focuses on the study of the treatment of four different textile wastewaters (two real textile wastewaters and two synthetic textile ones), by means of a solar-driven photo-Fenton reaction, which is compared with other AOPs, namely, Fenton´s reaction, UV/TiO_2, UV/H_2O_2, UV/TiO_2/H_2O_2 and UVC/H_2O_2. The effect of radiation sources, as UVC, UVA and UVA-Visible radiation was assessed. It has also been studied the effect of the main variables on AOPs performance, such as pH, temperature, radiation source and intensity, iron concentration, hydrogen peroxide concentration and dosage strategy, hydrodynamic conditions in the photoreactor and ferric-organic ligands for process enhancement. It is worth noting that two strategies of combined treatment were considered. For two wastewaters, both with high percentage of recalcitrant organic matter, AOPs prior to a biological oxidation treatment have been proposed. For the other two wastewaters, both with high percentage of biodegradable organic matter, a biological oxidation treatment followed by AOPs has been proposed.

This thesis is organized in seven chapters. **Chapter 1** includes this introductory section, wherein the problematics of textile wastewaters, as well as current and potential treatment technologies, are discussed. **Chapter 2** describes the experimental methodology, comprising: i) chemicals and reagents, ii) analytical methods iii) textile wastewaters under study; iv) experimental units and v) experimental procedure.

The subsequent four chapters report on the experimental results obtained. In Chapters 3 and 4, using real and synthetic textile wastewaters, AOP systems were studied as a pre-oxidation step to enhance textile wastewater biodegradability. In Chapters 5 and 6, also using both types of textile wastewaters, AOP systems were assessed as a polishing step, with the main objective of decolourizing bio-treated textile wastewaters.

Chapter 3 reports on a study where the efficiency of different AOPs has been compared in the treatment of a real cotton-textile dyeing wastewater using a pilot plant under natural sunlight. The influence of the main photo-Fenton reaction variables, such as iron concentration, pH, temperature and light intensity, was evaluated in a lab-scale prototype under controlled conditions using artificial solar radiation.

Chapter 4 reports on the evaluation of the treatment of a synthetic acrylic-textile dyeing wastewater by a photo-Fenton process enhanced by ferric-organic ligands (oxalic acid, citrate acid and EDDS-Ethylenediamine-N,N'-disuccinic acid), in a lab-scale prototype under controlled conditions, using artificial solar radiation, and in a pilot plant under natural sunlight. Besides the study of the influence of

the main ferrioxalate-solar-photo-Fenton reaction variables, the effect of hydrodynamics conditions on the reactors performance was also assessed both in dark and light conditions.

In **Chapter 5** is assessed an integrated treatment strategy for synthetic polyester-cotton dyeing wastewater, combining biological and photochemical oxidation processes. The characterization of chemicals used as additives in different stages of cotton and polyester textile manufacturing was carried out. The synthetic wastewater was firstly subject to a biological oxidation with objective to remove the biodegradable matter. Thus, UVC/H_2O_2 and photo-Fenton oxidation processes were used as a polishing step for the decolourisation of bio-treated textile wastewater. The effect of hydrogen peroxide dosage, lamp power, solution pH and temperature on the UVC/H_2O_2 system was evaluated.

Chapter 6 reports on the decolourisation of a bio-treated real textile wastewater by UVC/H_2O_2 and photo-Fenton oxidation, as a polishing step. The effect of hydrogen peroxide photolysis under UVC radiation on the wastewater decolourisation was evaluated at different pHs values, H_2O_2 concentrations and temperature. The effect of radiation sources (UVC, UVA or UVA-Visible), iron concentration, pH value and H_2O_2 concentration on the photo-Fenton reaction was also assessed. The photo-Fenton reaction enhancement by ferric-organic ligands using artificial solar radiation was also evaluated at different iron concentrations, pH values and iron/organic ligand molar ratios. In addition, the costs associated with the studied processes were evaluated and compared.

Chapter 7 is dedicated to final remarks where the main conclusions and subsequent suggestions for future work are presented.

1.2 The textile industry

The textile industry is one of the most important, traditional and representative sectors of the world economy. Presently, the textile industry is featured in the economy of the richest countries and plays a fundamental role in the economic development in emerging countries. Nowadays, it is an important part of the European manufacturing industry with a crucial role on the economy and social well-being in numerous regions of the European Union (EU). According to the latest structural data available, in 2009 there were 190.000 companies employing 1.8 million people which generated a turnover of 153 billion € [16]. Figure 1.1 shows the largest five textile suppliers in the world between 2010 and 2014 [17-21].

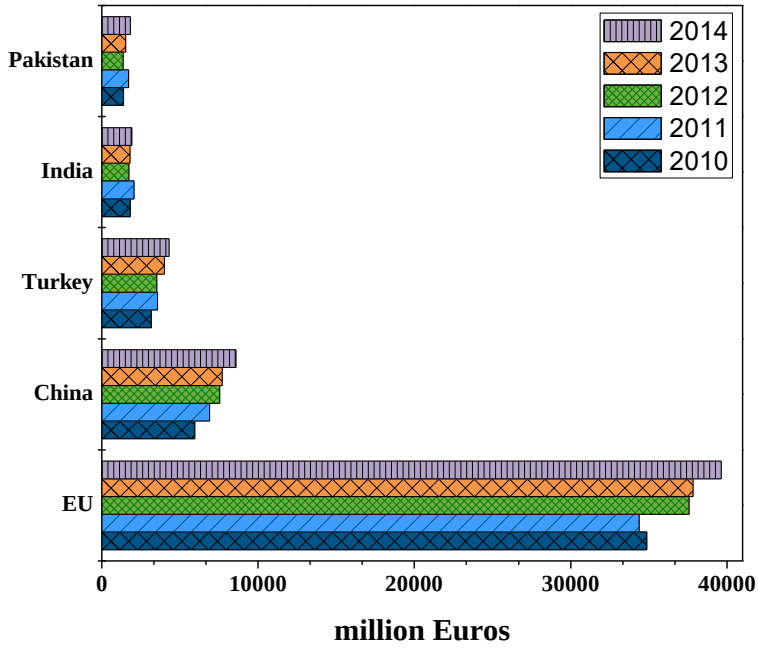

Figure 1.1. Top 5 suppliers in textiles (million Euros) per year (codes NC50 to NC60 and NC63).

Besides its significant economic importance, the textile manufacturing industry presents other characteristics of interest, for example, its complexity, due to the wide variety of used substrates, processes, chemicals, machinery and components, as well as of undertaken finishing steps. Different types of fibres/yarns, methods of fabric production, dyes and chemical auxiliaries, and finishing processes, all interrelate in producing a finished fabric [22]. The inherent complexity in the textile industry, its production chain, the big consumption of materials and energy, and as a consequence, the waste produced, make the textile industry an activity with high potential environmental impact [23-25]. Textile industries are one of the biggest users of water and complex chemicals during textile processing at various processing stages (e.g., sizing, desizing, scouring, bleaching and others) [26]. Water use in textile processing occurs at all the steps of production although the volume may range according textile

fibre and/or finish process; however in most cases, it is an expressive consumption that results in a significant volume of wastewater. Representative magnitudes for water consumption are 100–200 L of water per kilogram of textile product. Considering an annual production of 40 million tons of textile fibres, the release of wasted water can be estimated to exceed 4–8 billion cubic meters per year [27]. Figure 1.2 shows different steps of textile production and their contribution to the wastewater generation [26, 28, 29]. The production of a textile requires several stages of mechanical processing such as spinning, weaving, knitting, and garment production, which seem to be insulated from the wet treatment processes like pre-treatment, dyeing, printing, and finishing operations, but there is a strong interrelation between treatment processes in the dry state and consecutive wet treatments.

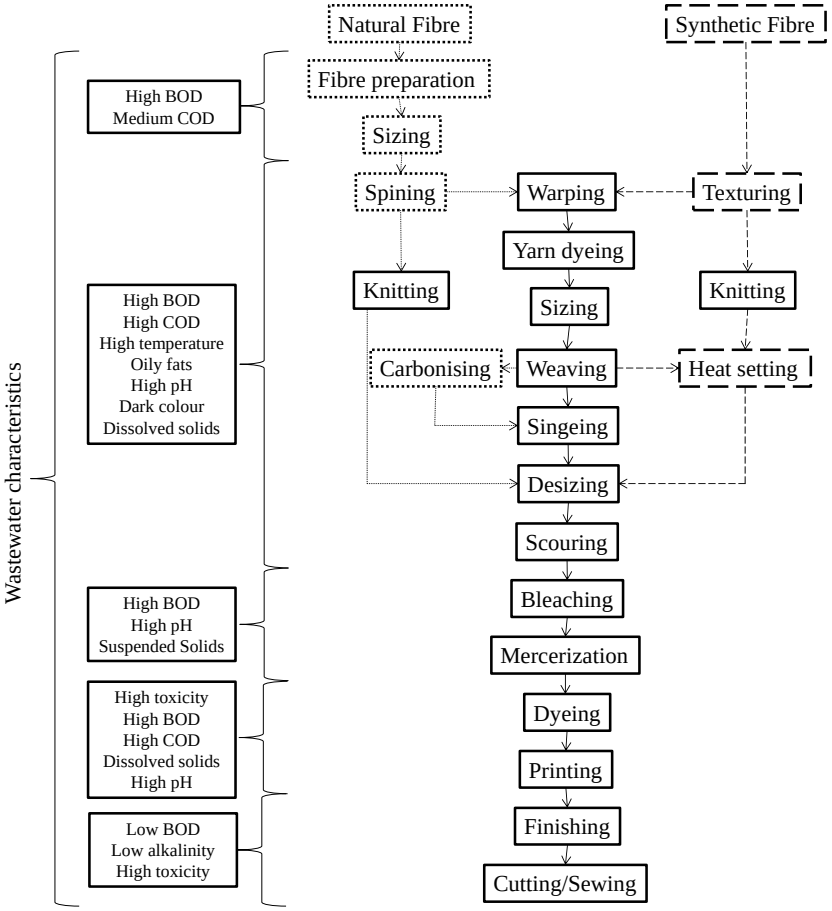

Figure 1.2. General flowchart for textile manufacturing and general characteristics of the wastewater generated on each step of production. The line style indicates which fibre the process refers to: (⋯) natural fibre, (---) synthetic fibre and (-) both. Adapted from Bisschops and Spanjers [29].

The textile industry process is complex and its dynamics can be different depending on the fibres used in the process. Basically, for each fibre type, a specific manufacturing process and, as a consequence, dye and chemical auxiliaries, are employed. Dyeing processes are developed according to the desired results in the fibres and are composed by dye mixtures, salts, acids, bases and chemicals such as wetting,

sequestering and lubricant agents. Currently, many different dyes are commercially available and about 10^6 tons are produced annually worldwide [30, 31]. Nowadays, there are very few natural dyes in use. Almost all are of synthetic origin and are produced using hydrocarbons like benzene, toluene, naphthalene, and others and not always with a known chemical structure. According to their application in dyeing different fibres, dyes can be classified into: Sulphur, Azoic, Reactive, Ingrain, Direct, Basic, Vat, Acid, Mordant, Metal complex, Solvent and Disperse [32, 33]. Table 1.1 shows the suitability for each type of fibre.

Table 1.1. Suitability of substrates for different types of dyes [32, 33].

Dye	Natural fibres		Synthetic fibres		
	Protein	**Cellulosic**	**Polyamide**	**Polyester**	**Acrylic**
Basic					V.S.
Direct	S.	V.S.	S.		
Acid	V.S.		V.S.		
Reactive	V.S.	V.S.	S.		
Azoic		V.S.	S.	S.	S.
Vat	S.	V.S.			
Sulphur		V.S.			
Disperse			V.S.	V.S.	V.S.
Metal complex	V.S.		V.S.		
Mordant	V.S.				

V.S. – Very Suitable
S. – Suitable

The textile manufacturing process, in addition to dyes and fibres, uses a large quantity of chemical auxiliaries at the different process steps with many functions. In the growing or storage of the fibre, it is ordinary the use of chemicals based on chlorinated aromatics, in the finishing products (e.g., synthetic resins), surfactants (e.g., alkyl phenol ethoxylates), solvents, fats, heavy metals, salts, nutrients (e.g., urea), oxidizing agents (e.g., peroxide), reducing agents (e.g., sodium sulphide), and many other chemical auxiliaries are employed in different stages of the manufacturing [34]. Table 1.2 presents the main auxiliary chemicals used in textile industry, their composition and function.

Table 1.2. Main textile auxiliary chemicals, their composition and function [29, 35].

Auxiliary Products	Substances	Function
Acids	Acetic acid, boric acid, formic acid, hydrochloric acid, oxalic acid, sulphuric acid	pH adjustment
Bases	Ammonia, sodium hydroxide	pH adjustment
Bleaching agents	Hypochlorite, hydrogen peroxide	Remove the natural colour of the fibres
Carriers	Perchloroethylene, methyl salicylate, chlorinated aromatics	Increase the absorption of the dye in the fibre
Detergents (surfactants)	Anionic, non-ionic, cationic (e. g., alkyl phenol ethoxylates)	Decrease the surface tension of the fibres when in contact with water
Finishing agents	Formaldehyde-based resins, Flame-proof finishes	Give body and stiffness or/and soften the fibre
Sequestering agents	polyphosphates	Form complexes with metallic ions to prevent their interference in the process

The manufacturing process, due to the wide range of dyes and chemicals involved, together with the different seasons and also fashion contributes to the variability found in textile wastewaters. Wastewater characteristics vary largely between processes and materials; however, some general characteristics (e.g., high temperature, low biodegradability and others) make textile wastewater an exigent waste which needs an appropriate treatment before discharge into water bodies.

1.2.1 Textile wastewater – main characteristics and environmental hazard

Dyes and other chemicals are added to perform a variety of functions during wet processing; even so, it is consensual that these chemicals produce large volumes of toxic wastewater as a by-product. Textile process wastewater must be treated before it can be released safely into receiving water bodies [36]. The dyeing process generates wastewaters with an intense colour, associated with the mixture of different types of dyes and different auxiliary products, such as organic acids, fixing agents, reducing agents, and others. However, textile wastewaters are generically characterized by a moderate organic content, low biodegradability, variable pH values, usually in the alkaline range, and colour [28].

Nearly 40,000 dyes and pigments have been listed, which consist of more than 7,000 different chemical structures [37]. Exact data on the quantity of dyes discharged in the environment are not available. However, some authors estimate that a loss of 1–2% in production and 1–10% loss in use is a fair estimate [38]. Others reported that 10–15 % of the used dyes enter the environment through wastes [11, 39]. In order to meet economic demands, it has become more frequent to use synthetic dyes, less amenable to degradation by aerobic biological processes; these dyes are recalcitrant organic molecules, have complex structure and xenobiotic properties [40, 41]. Most of them are toxic, mutagenic, and carcinogenic and lethal levels may be reached, affecting aquatic systems and associated flora and fauna [42].

Although dyes are recognized as one of the most problematic pollutants of textile wastewater, other pollutant types that exist in this wastewater show undesirable characteristics, e.g., biological persistence, biocide, recalcitrance, toxicity and others, causing them to be characterized as "xenobiotic compounds" [43]. These pollutants are derived from the use of synthetic organic chemicals as additives in different stages of textile manufacturing, with a wide range of functions (e.g.: sequestering agents, stabilizers, colour fixers, dispersants, etc.). Although there is speculation about the types and quantities of chemical auxiliaries released to the environment during textile process, there are only few published studies related to the biodegradability and toxic impact of these chemicals [44, 45].

Some research demonstrated that potential sources of recalcitrance and toxicity in textile wastewater may be attributed to the different types of chemicals applied in the sizing and finishing steps, besides surfactants, most of which are still of poorly biodegradable nature [46]. Whereas textile wastewater characteristics fluctuate and depend on many factors, their potential impact on the environment may also vary. Literature reports that textile wastewaters present toxic compounds [47, 48] with recalcitrant characteristics [49, 50], or with high organic matter content that partly, can be easily removed by biological oxidation [51, 52]. Generically, the main negative effects in environment due to the discharge of textile wastewater without the correct treatment can be seen in Table 1.3.

Table 1.3. Main effects of textile wastewater in the environment. Adapted from Verma, Dash [26].

Indirect Effects	Direct Effects
Killing of aquatic life such as fishes, plants, mammals etc.	Aesthetic problems
Eutrophication	Poor sunlight penetration in the receiving water, damaged flora, fauna of the ecosystem
Coloured allergen accelerates genotoxicity and microtoxicity	Ground water pollution due to leaching of contaminant through soil
Suppression of immune system of human beings	Dissolved oxygen depletion in the receiving water. Suppression of the streams re-oxygenation capacity

Oller et al., [2] showed that typical textile industry wastewater characteristics include a COD range from 150 to 12000 mg L^{-1}, total suspended solids between 2900 and 3100 mg L^{-1}, total Kjeldahl nitrogen from 70 to 80 mg L^{-1}, and BOD_5 range from 80 to 6000 mg L^{-1} leading to a BOD_5/COD ratio of around 0.25, which means that it contains large amounts of non-biodegradable organic matter. As commented, textile wastewater contains the unfixed dyes on the fibres, auxiliary dyeing chemicals, salts, acids, bases, chlorinated compounds and in some cases, heavy metals [30, 53-55]. The composition and, consequently, the characteristics of these wastewaters depend on many factors, including the processed fabric, the type of process, and used chemicals (Table 1.4).

Table 1.4. Characteristics of different dyeing textile wastewaters.

Fibre		Parameter				References
		COD (mg O_2 L^{-1})	BOD_5 (mg O_2 L^{-1})	TOC (mg C L^{-1})	pH	
Natural	Wool	800-7920	380-2200	250	5-8	[28, 29]
	Cotton	684-4585	11-1800	460-1290	5-13	[29, 56-58]
Synthetic	Polyester	518-3365	130-2700	143	4-8	[28, 59]
	Polyamide	1318	1125	640	5	[60]
	Rayon	2400	400	150	7	[61]
	Acetate	2500	2000	930	9	[28]
	Acrylic	828	50-200	334	1-7	[28, 49]

1.2.2 Guidelines and legislation for textile wastewaters

Increasing attention has been paid over the years to the environmental problems related to industrial activities. Environmental standards and control organisms have been established with a view to applying restrictive legislation. Special attention has been given to the textile industry, due to the expressive discharge in the environment of large volumes of strongly coloured wastewaters that are heavily loaded with pollutants and highly concentrated in salts [62]. A great deal of guidelines, legislation, recommendations, and propositions have been developed to try to ensure the protection of receiving water bodies. Over the past decades, new and stricter regulations coupled with increased enforcement concerning wastewater discharges were established in many countries, especially in the developed nations.

Nevertheless, when it comes to specifically coloured wastewater, we can find lots of divergent opinions and different measurement methods [62]. Many countries, as the United States of America (USA), France, Germany, Portugal and Brazil, have national environmental legislation, which establishes the limit values to comply with. In some countries as India, Pakistan and Malaysia, the emission limits are recommended, not mandatory [63].

The USA discharge legislation for textile manufactures, applied by EPA-Environmental Protection Agency, is composed by national standards for wastewater discharges to surface waters and publicly owned treatment works (sometimes called municipal sewage treatment plants). EPA issues wastewater guidelines for categories of existing sources and new sources under Title III of the Clean Water Act [64]. The standards are technology-based (i.e. they are based on the performance of treatment and control technologies); they are not based on risk or impacts upon receiving waters [64, 65]. It is important to note that USA standards set load discharges over the amount of textile articles produced and have different requirements for each type of textile processing industry.

Table 1.5 presents an example of discharge limits for textile industry of fibres and yarn processing [66]. For colour limit values, the USA legislation uses a specific method proposed by the American Dye Manufacturer Institute – ADMI, which uses three special tristimulus light filters, combined with a specific light source and photoelectric cell in a filter photometer, to obtain suitable colour data. The percentage of tristimulus light transmitted by the solution is determined for each of the three filters. The transmittance values are then converted to trichromatic coefficients and colour characteristic values [67]. However, the limit value for colour may vary from state to state, i.e. each state legislates independently and it has a specific ADMI limit value.

Table 1.5. USA discharge limits for textile industry of the fibres and yarn processing [66].

Wastewaters characteristics	Maximum for any one day (kg ton^{-1})	Maximum for monthly average (kg ton^{-1})
BOD_5	3.6	1.9
COD	33.9	21.9
TSS	9.8	4.4
pH	6.0 – 9.0	6.0 – 9.0

Similarly, Brazil has national laws for wastewater discharges to surface waters. The Brazilian National Environmental Council (CONAMA, abbreviation in Portuguese) regularizes the classification of receiving bodies and establishes the limit values for wastewater discharges. The CONAMA Resolution nº357 of 17 March 2005, altered by CONAMA Resolution nº410 of 4 May 2009 and by CONAMA Resolution nº430 of 13 May 2011, applies to discharges of all types of wastewater in national territory [68-70]. Table 1.6 lists the main applicable limits for wastewater discharge.

Table 1.6. Brazilian main discharge limits for wastewater [68-70].

Wastewaters characteristics	Maximum values
BOD_5	Minimum reduction of 60%
Temperature	40ºC
Mineral Oil	20 mg L^{-1}
Vegetal Oil	50 mg L^{-1}
Dissolved Iron	15 mg L^{-1}
Total ammonia nitrogen	20 mg L^{-1}

Brazilian norms do not have limits of colour values for wastewater discharges, but it is described on the CONAMA nº357 [68] that the wastewater cannot bestow characteristics on the receiving bodies in disagreement with the established quality characteristics by resolutions, namely, 75 mg Pt-Co L^{-1} (real colour).

It is an obligation for the European Union member states to comply with European legislation. It is often left to the states to set their own limit values and to decide on how to enforce them. There are different kinds of legislative documents. Directives oblige the European Union member states to achieve certain results [63]. At a European level only domestic wastewater was regulated through Directive 91/271/EEC of 21 May 1991, altered by Directive 98/15/EEC of 27 February 1998 and by Regulation (EC) nº1882 of 29 September 2003 [71-73]. These directives were transposed by each member country to the national legislation. In the case of industrial wastewaters, the limits as well as quality standards and methods are established by each member state for its own territory.

Germany wastewater discharge standards for textile wastewaters, based on the Law on the Regulation of water balance [74], stands out for the use of a simple and efficient technique for the colour measurement through absorbance at 436, 525 and 620 nm wavelengths and is based on a specific method

proposed by DIN ISO:7887 [75]. Table 1.7 shows the main requirements for textile wastewater at the point of discharge.

Table 1.7. German main limits for wastewater whose contaminant load originates primarily from commercial and industrial processing and processing of textile fibres and yarns and textile finishing [74].

Wastewaters characteristics	Qualified random sample or 2 hour composite sample
BOD_5	25 mg L^{-1}
COD	160 mg L^{-1}
Total phosphorous	2 mg L^{-1}
Total ammonia nitrogen	10 mg L^{-1}
Total nitrogen	20 mg L^{-1}
Sulphite	1 mg L^{-1}
Colour (DFZ_{436nm})*	7 m^{-1}
Colour (DFZ_{525nm})*	5 m^{-1}
Colour (DFZ_{620nm})*	3 m^{-1}

(*) DFZ – Visual Colour Number (*DurchsichtFarbZahl*, abbreviation in German).

Another member state of the European Union that has specific legislation to regulate discharges of textile wastewaters is Portugal. Through the Decree Law 236 of 1 August 1998, which limits the emission values of the discharge of all types of wastewater and through the Ordinance 423 of 25 June 1997, which limits specific values of the discharges of textile wastewater, Portugal has established the limits together with quality standards and used methods for its own territory [76, 77]. Table 1.8 lists the main applicable limits for industrial wastewater in general and textile wastewater.

Table 1.8. Portuguese main limits for general type of wastewater (Decree Law 236/98) [77] and specific for textile wastewater (Ordinance 423/97) [76].

Wastewaters characteristics	Decree Law 236/98	Ordinance 423/97
BOD_5	40 mg L^{-1}	100 mg L^{-1}
COD	150 mg L^{-1}	250 mg L^{-1}
pH	6.0 – 9.0	5.5 – 9.0
Total iron	2 mg L^{-1}	-
Total phosphorous	10 mg L^{-1}	-
Total ammonia nitrogen	10 mg L^{-1}	-
Total nitrogen	15 mg L^{-1}	-
Sulphite	mg L^{-1}	-
Colour	No visible colour after dilution 1:20	No visible colour after dilution 1:40

Briefly, it is difficult to draw a simple and global conclusion about the legislation currently applied to textile wastewaters. Parameters and norms vary from one country to the other, as does their enforcement. In certain countries the textile wastewater has special legislation, as EUA, Germany, Portugal etc., while many other countries do not have specific legislation or guidelines to control textile wastewater discharges, as Brazil and others. It should be noted that countries have used different units for their limit values for textile wastewater colour, which makes comparison almost impossible. However, basically,

four methods for colour monitoring have been used, Hazen method (mg Pt-Co L^{-1}) employed by France, Brazil etc., ADMI (ADMI colour unit) employed by the EUA etc., DIN ISO:7887 (DFZ at m^{-1}) employed by Germany, and monitoring of visible colour after dilution, employed by Portugal, France etc. [63, 64, 66, 68-70, 75-78].

1.2.3 Present practices for textile wastewater treatment

The application of a certain technology for wastewater treatment is dependent on the type of wastewater, thus different technologies have been proposed and are applied at present. Normally a combination of procedures and equipment is applied and a big variety of concepts have been realized. To facilitate an overview of the different techniques, the most important processes are discussed in this section. During the last 10 years, publications regarding textile wastewaters treatment rose continuously, achieving more than 230 papers in 2014 (Figure 1.3). Scientific community research interests have been focused in biological, membrane and advanced oxidation processes (AOPs) technologies for the treatment of textile wastewaters. Although biological processes present competitive costs, they are often ineffective in degradation of complex organic dye molecules.

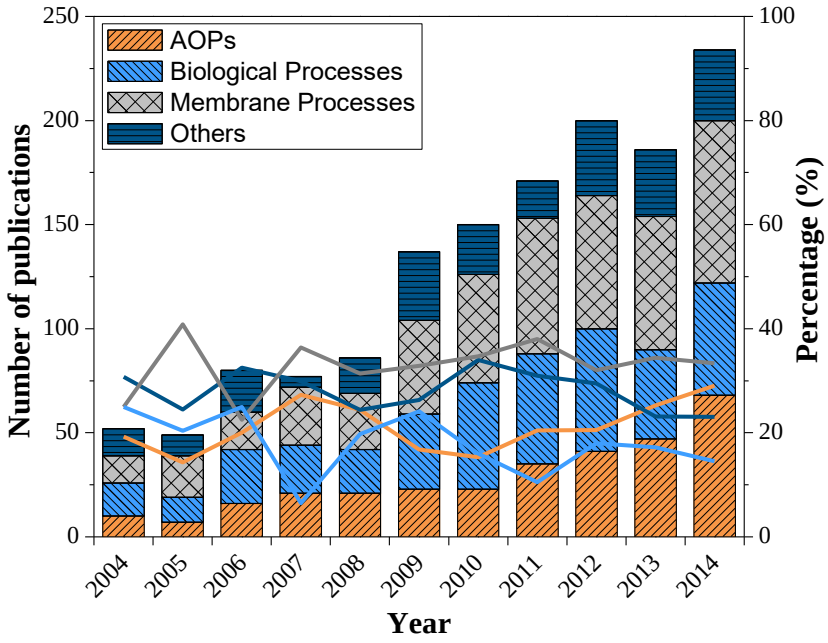

Figure 1.3. Numbers of research articles appearing on textile wastewater treatment technologies per year: search results in the period 2004-2014 with the SCOPUS (keyword "Textile Wastewater Treatment").

The combination of some factors, like a high presence of recalcitrant compounds [41], high volumes, high colour and the spatiotemporal dynamics of textile wastewater between and within industries [79] make the textile wastewater treatment a challenge. In literature there are many options for the treatment

of textile wastewater, all of them aiming at achieving a significant reduction in colour and concentration of organic matter [80-85]. While there are several highly effective treatment options available, some key factors must be considered in the selection of a waste treatment process, for example, the financial requirement for the initial outlay, maintenance costs, degree of specialization of operators, and the efficiency of care legislation, etc. Table 1.9 summarizes some of the main studies on the treatment of real textile wastewater.

Table 1.9. Summary of some main studies on the treatment of real textile wastewater.

Wastewater type	Treatment technology	Efficiencies (%)	Reference
Real textile wastewater	Sequential Batch Reactor	BOD_5 = 11 COD = 13 Colour = 19	[86]
Real textile wastewater	Sequencing batch biofilter granular reactor	COD = 80	[84]
Printing and dyeing processes	Anoxic filter bed and biological wriggle bed-ozone biological aerated filter	COD = 84	[87]
Dyeing and finishing processes	Sequencing batch biofilter granular reactor	COD = 80 Colour = 60	[88]
Real textile wastewater	Combination of aerobic Sequencing Batch Reactor and Fenton´s reaction	TOC = 92	[89]
Silk and silky fibres wastewater	Sequencing batch biofilter granular reactor	COD = 82	[79]
Real textile wastewater	Sequencing batch reactor coupled to photo-Fenton processes	COD = 97 TOC = 95	[52]
Real textile wastewater	Wetland system	BOD_5 = 77 COD = 79	[90]
Real textile wastewater	Membranes with physic-chemical treatment	COD = 50	[91]
Dyeing, bleaching and washing processes	Ultrafiltration and adsorption on activated carbon	COD = 80 Colour = 74	[92]
Real textile wastewater	Membrane fouling in an integrated membrane coagulation reactor	COD = 88	[93]
Real textile wastewater	Electrocoagulation	COD = 97	[94]
Real textile wastewater	Fenton´s reaction	BOD_5 = 60 COD = 45	[95]
Real textile wastewater	Fenton´s reaction	BOD_5 = 61 TOC = 64	[96]
Dry-spun acrylic fibre wastewater	Fenton´s reaction	COD = 47	[97]
Real textile wastewater	Photo-Fenton	DOC = 65	[31]
Bleaching of a cotton substrate	Photo-Fenton	TOC = 70	[98]
Polyester and acetate fibre dyeing wastewater	Advanced Oxidation Processes (O_3, UV/O_3, UV/H_2O_2, UV/O_3/H_2O_2, Fe^{2+}/H_2O_2)	COD = 90-99 Colour = 85-96	[99]
Real textile wastewater	Advanced Oxidation Processes (UV/H_2O_2, UV/Fe^{2+}/H_2O_2, UV/TiO_2, UV/TiO_2/H_2O_2)	DOC = 89 Colour = 98	[100]

Many biological methods result in incomplete degradation of compounds present in the textile wastewater, and a number of laboratories investigate the ability of bacteria, fungi, and algae in removing the colour of dyes. Santos et al., [80] covered the biological and non-biological processes for textile

wastewater decolourisation. A critical review is showed on the current technologies available for the decolourisation of textile wastewaters and effective and economically attractive alternatives are suggested. A special attention to the azo dyes was given, because according to the authors, they represent the largest class of dyes used in industries, and due to the broad literature available. Sarayu and Sandhya [101] presented a review about the current technologies for the biological treatment of textile wastewater. This work gave a significant emphasis to the difficulty in completing the treatment of textile wastewater by biological treatment systems only, mainly due to the constant presence of biocide and/or recalcitrant compounds in textile wastewater.

Verma et al., [26] put forward a review on chemical coagulation/flocculation technologies for the removal of colour from textile wastewaters. It was revealed in this study that coagulation/flocculation has been used for many years as a main treatment or pretreatment of dye-containing wastewaters due to its low capital cost. However, the major limitation of this process is the generation of sludge and the ineffective removal of some soluble dyes. Relative advantages and disadvantages of different physicochemical methods have been also briefly summarized, as Fenton´s reagent, their efficiency in the decolourisation of both soluble and insoluble dyes and consequent sludge generation and its handling.

Khandegar and Saroha [102] dedicated a review to catalogue some research about the use of electrocoagulation for the removal of different kinds of dyes and mixed dyes, and to summarize the most important factors affecting the reported varying removal efficiencies of electrocoagulation in the treatment of textile industry wastewater. For instance, it was reported that the efficiency of the electrocoagulation process depends on many operational parameters such as the conductivity of the solution, arrangement of the electrodes, electrode shape, type of power supply, pH of the solution, current density, distance between the electrodes, agitation speed, electrolysis time, initial pollutant concentration, retention time and passivation of the electrode.

Research studies in this field have usually focused on the development of the application of Advanced Oxidation Processes (AOPs) to treat wastewaters contaminated with components with high chemical stability and/or low biodegradability, such as textile wastewater. During recent years many of studies dealing with the combination of AOPs and biological treatments for industrial wastewater decontamination have been reported [52, 103-105]. For this reason, the following section will deal entirely with AOPs.

1.2.4 Current applications of AOPs for textile wastewater treatment

Advanced Oxidation Processes are efficient technologies for the treatment of a large variety of contaminated water and wastewater, through the formation of highly reactive chemical species that are able to degrade the more recalcitrant chemicals, making them biodegradable compounds [106]. Basically, AOPs are characterized by the production of hydroxyl radicals ($^{\bullet}OH$), non-selective oxidants capable to oxidize and to mineralize almost all organic molecules, producing as a result, CO_2, H_2O and inorganic ions [3]. The classification of AOPs can be divided as follows: i) chemical oxidation (O_3, O_3/H_2O_2, H_2O_2/Fe^{2+}), ii) photochemical (UV/O_3, UV/H_2O_2, $UV/H_2O_2/O_3$) and, iii) photocatalytic (UV/TiO_2, photo-Fenton) processes [107].

In order to increase competitiveness and, in consequence, to promote the AOPs industrial applicability, many researchers followed two lines of research: i) AOPs combination with other treatment processes, such as biological processes [2, 4, 108], or membrane processes [109, 110]; and ii) optimization of the use and source of the necessary energy, for example, solar energy or, more recently, a combination of solar and UV lamps energy [111]. In consequence, the AOPs relying on solar energy, UV lamps or both, such as photo-Fenton and UV/TiO_2, are considered the most promising and environmental friendly technologies [112].

Babuna et al., [113] investigated the effect of ozonation on the toxicity and biodegradability of a naphthalene sulphonic acid derivative commonly applied in textile mills. Ozonation experiments were conducted under the following conditions: 1200 mg O_3 h^{-1} and 2400 mg O_3 h^{-1} both at pH 5 and pH 11; 5325 mg O_3 h^{-1} at both pH 12 and at the original pH (pH = 5.5). The optimum operation conditions required the application of 5325 mg O_3 h^{-1} ozone for 30 min at original pH. Since the results related to the acute toxicity (in 50% v/v EC values) towards the marine algae *Phaeodactylum tricornutum* indicate that the toxicity was increased considerably, the researchers recommended new tests with other oxidants instead of ozone.

Arslan-Alaton and Alaton [44] studied the degradation of three xenobiotic compounds normally used on the fabrics preparation using ozonation and UVC/H_2O_2. The synthetic textile wastewater was composed by a non-ionic surfactant, the polyamide dyeing stage by synthetic tannin and an aqueous biocidal finishing. UVC/H_2O_2 treatment promoted partial oxidation (50% COD) and after both tested treatments, the inhibitory effect on activated sludge completely disappeared.

However, the achievement of detoxification and/or biodegradability improvement was accompanied with high electrical energy requirements. In another work of the same research group [45],

alkylpolyethylene ether-based surfactant (formulation commonly used in the textile preparation stage) in aqueous solution was treated with photochemical oxidation (UVC/H_2O_2) and/or biochemical treatment. Results emphasized that stand-alone photochemical and biological treatment should be preferred to a UVC/H_2O_2 + Activated sludge treatment combination, since a dramatic reduction in activated sludge treatment efficiency was obtained after UVC/H_2O_2 pre-treatment.

Shu [114] investigated the degradation of C.I. Direct Blue 199 also using processes of ozonation, UV/H_2O_2 and in sequence of ozonation with UV/H_2O_2. By ozonation alone, the colour removal was greater than 80% within 15 min and the reduction of total organic carbon (TOC) was about 60%. On the other hand, by UV/H_2O_2 alone (low pressure mercury arc UVC lamps with 35 W of power), the colour removal took longer time for obtaining the same removal efficiencies (30 min). Nevertheless, it was more effective than ozonation for TOC removal, about 75% in 30 min. The sequence process was designed to begin with ozonation to rapidly remove colour proficiently, following by UV/H_2O_2 in order to promptly and efficiently remove the remaining TOC. The successful sequence of ozonation with UV/H_2O_2 proved the significant improvement for the removal of both colour and TOC.

Degradation of a commercial textile biocide formulation containing a 2,4,4´-trichloro-2´-hydroxydiphenyl ether as the active ingredient, by different advanced oxidation processes (Fenton, photo-Fenton, UVA/TiO_2, UVA/TiO_2/H_2O_2) and ozone was studied by Arslan-Alaton [115]. The photocatalytic experiments (i.e. photo-Fenton, UVA/TiO_2 and UVA/TiO_2/H_2O_2), which were carried out using a 125 W black light lamp, yielded appreciably higher COD and DOC removal efficiencies. During ozonation of the textile biocide effluent, complete detoxification was found after continued ozonation for at least 30 min (corresponding to 400 mg O_3). The Fenton-based treatment experiments and particularly the dark Fenton reaction resulted in relatively poor degradation, de-aromatization and acute toxicity removals.

Textile wastewater treatment by solar-driven advanced oxidation processes was studied by Vilar et al., [100]. The authors tested different AOPs namely, UV/H_2O_2, UV/TiO_2, Fenton and photo-Fenton reaction, using solar light at pilot plant scale. Solar-photo-Fenton was the most efficient of all solar AOPs studied, for an optimum catalyst concentration of 100 mg Fe^{2+} L^{-1}, enhancing the biodegradability of the wastewater and making possible its combination with a biological oxidation process. Moreover, the optimum energy dose required to reach a biodegradable wastewater was 12 kJ_{UV} L^{-1}, consuming 52 mM of hydrogen peroxide (added in excess), as calculated from the kinetic studies, and leading to 55% mineralisation and 96% decolourisation.

Table 1.10 summarizes some information on the main AOPs. The characteristics and mechanism of these processes will not be discussed here. The photo-Fenton reaction, UV/TiO_2 and UVC/H_2O_2 are exceptions, as there are plenty of detailed studies regarding general and particular aspects of each technique or combination thereof [3, 4, 106, 107, 116].

Table 1.10. Summary of some information of the main AOPs.

Processes	Strengths	Drawbacks	References
O_3 and UV/O_3	i) ozone is effective over a wide pH range and rapidly reacts with bacteria, viruses, and protozoans; ii) has a very strong oxidizing power with a short reaction time; iii) the treatment process does not add chemicals to the water.	i) equipment and operational cost higher; ii) ozonation by-products are still being evaluated ii) ozone generation requires a large amount of and electrical energy; iii) potential fire hazards and toxicity issues associated with ozone generation.	[117-120]
O_3/H_2O_2 and UV/O_3/H_2O_2	i) the costs involved in the process are lower than the costs of a system utilizing only UV and ozone, because the addition of hydrogen peroxide allows the use of a smaller ozone generator and less oxidants; ii) the residence times needed to decrease the concentration of a contaminant to a certain level are lower.	i) each of the constituents in the process has dangers: ozone is explosive, toxic, hydrogen peroxide is an irritant, can cause chemical burns, and is an explosive hazard, and UV can burn unprotected skin and the mercury in UV lamps can damage the central nervous system; ii) the energy required for the process is high resulting in high costs.	[119, 121-123]
UV/H_2O_2	i) more advantageous compared with ozone, providing a cheap and safe source of radicals, eliminating this way the problem of the handling of ozone.	i) if the solution presents a strong absorbance this competes with hydrogen peroxide for this radiation, thus cloudy waters or containing compounds absorbing UV radiation can present problems at being treated by this method.	[124, 125]
Fenton	i) simplicity of its implementation, since the reaction occurs at ambient temperature and pressure; ii) requires no special equipment or reagent and; iii) applies to a wide variety of compounds.	i) need for acidification of the wastewater; ii) process stopped after total oxidation of Fe^{2+}; iii) some organic compounds are not oxidized in this process; iv) the resulting sludge requires appropriate treatment, which implies an increase in the cost of treatment.	[126-129]
Photo-Fenton	i) all the cited advantages of Fenton reaction; ii) alternating dark and illumination intervals has shown to reduce the necessary illumination time and makes the reaction rate faster.	i) need for acidification of the wastewater; ii) the resulting sludge requires appropriate treatment, which implies an increase in the cost of treatment.	[3, 15, 52, 130-133]
UV/TiO_2	i) TiO_2 is biologically and chemically inert, it is stable to photo- and chemical corrosion and inexpensive.	i) the catalyst separation from solution, as well as the fouling of the catalyst by the organic matter; ii) use the small percentage of the ultraviolet radiation coming from the sun.	[134-136]

1.2.4.1 Treatment by photo-Fenton

Homogeneous photocatalytic AOPs in aqueous phase are mainly based on the photo-Fenton reaction (Eqs. (1.1) and (1.2)) using Fe^{2+} salts and hydrogen peroxide in mildly acid solutions (pH between 2.5 and 5.0). These processes utilize the photoreduction of produced ferric ions (Fe^{3+}) and ferric complexes. In contrast to the Fenton reaction, without photo-activation, ferrous ion (Fe^{2+}) is recycled continuously by irradiation of Fe^{3+}-H_2O and therefore it is not depleted during the oxidation reaction [106].

$$Fe^{2+} + H_2O_2 \rightarrow HO^- + {}^{\bullet}OH + Fe^{3+} \quad (1.1)$$

$$Fe^{3+} + H_2O \xrightarrow{h\nu} Fe^{2+} + H^+ + {}^{\bullet}OH \quad (1.2)$$

A lot of works can be found in the literature using photo-Fenton process for dyes removal in aqueous solution [38]. Although not so numerous, some researches also have been devoted to treatment of textile wastewater using photo-Fenton [52]. Table 1.11 presents the optimal operating conditions and the removals achieved in other studies regarding the treatment of dye solutions or textile wastewaters by the photo-Fenton process.

Table 1.11. Studies on the treatability of dye solutions and textile wastewaters by photo-Fenton process.

Wastewater/ pollutant	Optimal Operating Conditions	Removal efficiencies (%)	Reference
Reactive Orange 4 dye solution	pH = 3 t = 40 min UVA radiation; P = 32 W [dye] = $5x10^{-4}$ mol L^{-1} [Fe^{2+}] = 2.8 mg L^{-1} [H_2O_2] = 340 mg L^{-1}	DOC = 65	[137]
Procion Red H-E7B dye solution	pH = 3 t = 120 min UVA radiation; P = 6 W [Fe^{2+}] = 10 mg L^{-1} [H_2O_2] = 100 mg L^{-1}	TOC = ~100 Colour = 81	[138]
Reactive Blue 19 dye solution	pH = 3 UVC radiation; P = 65 W [Fe^{2+}] = 32 mg L^{-1} [H_2O_2] = 150 mg L^{-1}	COD = 96 Colour = 100	[139]
Real textile wastewater	pH = 3.6 Solar radiation t_{30W} = 22.4 min Q_{UV} = 3.5 kJ_{UV} L^{-1} [Fe^{2+}] = 60 mg L^{-1} [H_2O_2] = 18.5 mM	DOC = 70	[104]
Synthetic textile wastewater	pH = 4 t = 30 min UVC radiation; P = 64 W [dye] = $5x10^{-4}$ mol L^{-1} [Fe^{2+}] = 20 mg L^{-1} [H_2O_2] = 100 mg L^{-1}	COD = 70 Colour = 93	[140]
Real textile wastewater	pH = 2.7 t = 50 min UVA radiation; P = 25 W T = 35ºC [Fe^{2+}] = 216 mg L^{-1} [H_2O_2] = 4950 mg L^{-1}	COD = 79 TOC = 75 Colour = 98	[52]
Synthetic textile wastewater	pH = 3 UVA radiation; P = 15W Q_{UV} = 23 kJ_{UV} L^{-1} [Fe^{2+}] = 0.12 g L^{-1} [H_2O_2] = 4.54 g L^{-1}	COD = 79 TOC = 79 Colour = 100	[141]

Chacón et al., [142] studied the solar photocatalytic degradation of the azo-dye Acid Orange 24 by a photo-Fenton reaction promoted by solar energy. The authors reported decolourisation higher than 85% after 50 kJ L^{-1} of accumulated energy. And, in the case of the best reaction conditions, a decolourisation of up to 95%, using concentrations of Fe^{2+} = 1.43×10^{-4} M and H_2O_2 = 5.2×10^{-3} M, which were determined as optimal concentrations for the photocatalytic process.

Modirshahla et al., [143] investigated the degradation of azo-dye Acid Yellow 23 (AY23) by photo-Fenton processes (UVC lamp with 30W of power). The effect of dye concentration, pH, initial H_2O_2 concentration, Fe^{2+} concentration and the UV light intensity were studied. Optimum conditions for the decolourisation of AY23 were achieved at pH = 3.0, with an initial Fe^{2+} concentration of 0.1 mM and an initial H_2O_2 concentration of 700 mg L^{-1} with a dye concentration of 40 mg L^{-1}.

Prato-Garcia and Buitrón [144] evaluated three reagent dosing strategies in a solar photo-Fenton process for the decolourisation of a mixture of sulphonated dyes (Acid Blue 113, Acid Orange 7 and Acid Red 151). In one strategy, the Fenton's reactants were dosed in a punctual mode, while in the other two strategies, the reactants were dosed continuously. Continuous addition of the reagents improved the aromatic content removal. This strategy substantially improved the effluent quality in two key areas: toxicity and biodegradability.

Hernández-Rodríguez et al., [141], working with simulated wastewaters from wool dyeing, investigated the decolourisation and mineralisation using a solar photo-Fenton process. The effect of H_2O_2 and Fe(II) dosage and fractional or initial addition of these reagents on the photo-mineralisation processes were studied and the optimal conditions were found. It was reported that, under optimal conditions, 100% of colour removal and no toxic effects on marine bacteria *Vibrio fischeri* were observed. TOC was reduced by 79% with 23 kJ L^{-1}, and HPLC analysis confirmed that the remaining organic carbon was due to the presence of sodium acetate.

Punzi et al., [145] compared the efficiencies of homogeneous and heterogeneous photo-Fenton oxidation for treatment of azo-dye containing synthetic textile wastewater. Irradiation was provided by an 18 W UVA–vis blue-lamp. For both treatments and for all dyes studied, the complete decolourisation was achieved. In terms of mineralisation, COD reductions of 96% and 93% in the homogenous and heterogeneous reactions were observed, respectively. Similar amounts of iron-containing sludge were produced in both processes, while the release of iron ions was reduced by 50% when using the heterogeneous photo-Fenton process.

Manenti et al., [103] integrated in batch mode the processes of electrocoagulation, photo-Fenton oxidation, and activated sludge biological degradation for treatment of real textile wastewater. The photo-Fenton step was carried out in a pilot plant with 0.91 m^2 of solar collectors. The authors assessed the influence of many reaction conditions, as iron concentration, solution pH, temperature and irradiance. It was observed a COD reduction of 65% for the optimal conditions of the photo-Fenton reaction (100 mg Fe^{2+} L^{-1}, pH 2.8, 12 mM H_2O_2, 6.9 kJ_{UV} L^{-1} accumulated energy). Optimum pH for the photo-Fenton reaction was 2.8 because not only the predominant iron species in solution is $FeOH^{2+}$, which is the most photoactive ferric ion-water complex, but also because iron precipitation is avoided. A recognized limitation of the photo-Fenton process applied to the treatment of textile wastewaters is related to their high alkalinity, associated to the presence of carbonates and bicarbonates, being necessary high volumes of acid for the acidification and further consumption of base for the neutralization. In addition, some works have showed the formation of stable complexes between ferric ions and organic constituents present in textile wastewaters, limiting the photoreduction of Fe^{3+}, decreasing the decomposition of H_2O_2 in the Fenton reaction and the overall efficiency of the photo-Fenton process [8, 9].

Formation of complexes between Fe^{3+} and carboxylate ions has been pointed out as the most viable way to overcome these drawbacks (Eq. (1.3)). In this way, the photo-Fenton process is enhanced because these ferricarboxylate complexes: i) have much higher quantum yields than ferric iron-water complexes; ii) can use a higher fraction of the solar radiation spectrum, up to 580 nm [146, 147]; iii) are photodecarboxylated under visible radiation; iv) provide a quicker pathway for Fe^{3+} regeneration accelerating thereby the process [9]; v) are more soluble than ferric iron-water complexes, allowing work at neutral pH values, increasing the applicability of this process at industrial scale, since costs and drawbacks of acidifying and the subsequent neutralization are eliminated; vi) are stronger and more stable complexes than ferric iron-sulphates, iron-chloride or iron-organic ligands complexes.

$$Fe^{III} - L \xrightarrow{h\nu} \left[Fe^{III} - L\right]^{\bullet} \rightarrow Fe^{II} + L^{\bullet} \tag{1.3}$$

Ferricarboxylate-mediated solar photo-Fenton has already been successfully applied to treat different wastewaters and specific pollutants, whereby carboxylate ions such as oxalate, citrate and EDDS (ethylenediamine-N, N'-disuccinic acid) were used to form complexes with Fe^{3+} (Eqs. (1.4), (1.5) and (1.6)) [111, 147].

$$Fe^{3+}(Oxa) \xrightarrow{h\nu} Fe^{2+} + {}^{\bullet}Oxa \tag{1.4}$$

$$Fe^{3+}(Cit) \xrightarrow{h\nu} Fe^{2+} + {}^{\bullet}Cit \quad (1.5)$$

$$Fe^{3+}(EDDS) \xrightarrow{h\nu} Fe^{2+} + {}^{\bullet}EDDS \quad (1.6)$$

Carneiro et al. [148] investigated the oxidation of C.I. Reactive Blue 4 (RB4) by the photo-Fenton process mediated by ferrioxalate under artificial (15 W UVA lamp) and solar irradiation. The best results were obtained using 1.0 mM ferrioxalate and 10 mM of hydrogen peroxide. Under these experimental conditions, 80% of TOC and 100% of colour removal were obtained for a 0.1 mM RB4 dye after 35 min of solar irradiation. Durán et al., [149] also applied solar photo-Fenton-ferrioxalate processes to the degradation of Reactive Blue 4 (RB4) solutions. These authors showed that, under optimum conditions, ($[H_2O_2]$ = 120 mg L^{-1}, [Fe(II)] = 7 mg L^{-1}, $[(COOH)_2]$ = 10 mg L^{-1}, pH 2.5), colour and COD were completely removed whereas TOC was reduced up to 66%.

Lucas and Peres [150] assessed the feasibility of employing different photoxidation systems, like UVC/Fe^{2+}/H_2O_2 and UVA-Vis/Fe^{2+}/H_2O_2/Oxalate in the decolourisation and mineralisation of Reactive Black 5 (RB5). The optimal operational conditions of the processes were investigated, as pH, H_2O_2 dosage, iron dosage, RB5 concentration and source of light. The experiments indicate that RB5 can be effectively decolourized by UVC/Fe^{2+}/H_2O_2 and UVA-Vis/Fe^{3+}/H_2O_2/Oxalate processes with a small difference between the two processes, 98.1% and 93.2%, respectively, after 30 min. Although there is a small difference in dye decolourisation, the authors state that significant increment in TOC removal was found with UVC/Fe^{2+}/H_2O_2 process (46.4% TOC removal) in relation to UVA-Vis/Fe^{3+}/H_2O_2/Oxalate process (29.6% TOC removal).

Manenti et al. [151] published a study regarding the treatment of a real textile wastewater by a conventional photo-Fenton reaction and mediated by different ferric–organic ligands complexes, performed in lab and pilot scale photoreactors irradiated by simulated and natural solar radiation. The conventional solar-photo-Fenton reaction showed limited efficiency in the mineralisation of the textile wastewater. The addition of organic ligands, such as oxalic acid, citric acid and EDDS, enhanced significantly the reaction, avoiding the formation of iron–organic pollutants complexes, and consequently increasing the quantum yield for ferrous ions´ production through the photodecarboxylation of ferric–organic ligands complexes. The catalytic activity of the iron–organic ligands complexes increased in the following order: Fe(III)–EDDS < Fe(III)–citrate < Fe(III)–oxalate. The researchers reported that all the tested processes mediated by ferric–organic ligands complexes contributed to an effective decolourisation and mineralisation, but the most efficient system was the photo-Fenton-ferrioxalate reaction with an optimum catalyst concentration of 100 mg Fe^{3+} L^{-1}, pH 2.8, temperature of 30ºC, which led to complete decolourisation and 69% mineralisation after less than

8.8 kJ_{UV} L^{-1}. Aside from textile treatments, the enhancement of the photo-Fenton reaction through the use of ferricarboxylate complexes, such as ferrioxalate, ferricitrate and ferrimaleate, can be seen in many publications. Table 1.12 shows some publications that have reported the enhancement of the photo-Fenton process for the treatment of different wastewaters and specific pollutants.

Table 1.12. Summary of some publications regarding the enhancement of the photo-Fenton process using ferricarboxylate complexes.

Ferric-organic ligands complexes	Wastewater/ pollutant	Operational conditions	Reference
Ferrioxalate	Synthetic phenolic wastewater	pH = 5.6; Iron/Oxalate mass ratio = 1:15; Fe^{3+} concentration = 20 mg L^{-1} and 50 mg L^{-1}; Using natural solar radiation;	[147]
	Azo dye Reactive Black 5	pH = between 1.0 and 8.0; Iron/Oxalate molar ratio = 1:60; Fe^{3+} concentration = 1.5x10^{-4} M; Using solar radiation or a low-pressure mercury vapour lamp;	[150]
	Winery wastewater	pH = 3.5; Oxalate concentration = 16.2 mg L^{-1} to 80.0 mg L^{-1}; Fe^{2+} concentration = 6.1 mg L^{-1} to 30.0 mg L^{-1}; Using natural solar radiation;	[152]
	Oxytetracycline	pH = 4.0 to 6.0; Iron/Oxalate molar ratio = 1:3; Fe^{3+} concentration = 1.0 mg L^{-1} to 5.0 mg L^{-1}; An air-cooled xenon arc lamp, a daylight filter and quartz filter with IR coating as well as natural solar radiation;	[153]
	indigo-dyed wastewaters	pH = 5.0 to 6.0; Iron/Oxalate mass ratio = 1:35; Fe^{2+} concentration = 1.87 mg L^{-1}; Using natural solar radiation;	[154]
Ferricitrate	3-Methylphenol	pH = 2.8 to 6.4; Iron/Citrate molar ratio = 1:1 and 1:2; Fe(III)-Citrate = 0.2 mM to 0.5 mM; With low pressure mercury UV lamp;	[155]
	Oxytetracycline	pH = 3.6 and 5.0; Iron/Citrate molar ratio = 1:1; Fe^{3+} concentration = 2.0 mg L^{-1}; An air-cooled xenon arc lamp, a daylight filter and quartz filter with IR coating as well as natural solar radiation;	[153]
	Herbicide tebuthiuron	pH = 2.5 and 7.5; Iron/Citrate molar ratio = 1:1; Fe:Cit concentration = 1.0 mM; Using natural solar radiation;	[156]
	Municipal wastewater treatment plant	pH = neutral pH; Iron/Citrate molar ratio = 1:0.5 to 1:5; Iron concentration = 0.1 mM and 0.2 mM; Using natural solar radiation;	[157]
	Ciprofloxacin	pH = 2.5 to 6.5; Iron/Citrate molar ratio = 1:1; Iron concentration = 0.16 mM; Using natural solar radiation;	[158]
ferric-EDDS	17β-estradiol	pH = between 3.1 and 8.0; Iron/EDDS molar ratio = 1:1; Fe-EDDS concentration = 5x10^{-5} M at 1x10^{-3} M; With fluorescent light bulb lamp (spectrum is 300-500 nm);	[159]

Table 1.12. Summary of some publications regarding the enhancement of the photo-Fenton process using ferricarboxylate complexes.

Ferric-organic ligands complexes	Wastewater/ pollutant	Operational conditions	Reference
ferric-EDDS	2,2-bis-(4-hydroxyphenyl) propane	pH = 3.7, 6.2 and 8.7; Iron/EDDS molar ratio = 1:1; Fe-EDDS concentration = 0.01 mM at 0.4 mM; With fluorescent light bulb lamp (spectrum is 300-500 nm);	[160]
	Municipal wastewater treatment plant	pH = 3.0 and neutral pH; EDDS concentration = 0.2 mM; Iron concentration = 5 mg L^{-1}; Using natural solar radiation;	[10]
	Municipal wastewater treatment plant	pH = neutral pH; Iron/EDDS molar ratio = 1:0.5 to 1:3; Iron concentration = 0.1 mM and 0.2 mM; Using natural solar radiation;	[157]
	Pharmaceuticals	pH = 5-6; Iron/EDDS molar ratio = 1:2; Iron concentration = 0.1 mM; Using natural solar radiation;	[130]

1.2.4.2 Treatment by UV/TiO_2

Heterogeneous photocatalysis using suspended TiO_2 is of special interest due to the chemical stability of the photocatalyst, low cost and ability of using the small percentage of ultraviolet radiation coming from the sun. TiO_2 is an n-type wide bandgap semiconductor and has three crystalline phases in nature, anatase (tetragonal), rutile (tetragonal) and brookite (orthorhombic). Rutile TiO_2 is the most stable form, whereas anatase and brookite phases are metastable and can be transformed to rutile phase when heated at high temperature (~750°C) [161].

For the last decades TiO_2 has been the most used and most efficient semiconductor in photocatalytic applications; other semiconductors commonly used are ZnO, SnO_2, etc. However, TiO_2 presents three main limitations: i) the threshold of absorption band does not allow visible light absorption, using only UV radiation which corresponds to 3-5% of the solar spectrum reaching the Earth; ii) the degradation process has low quantum yield; iii) the fast recombination of the charge carriers is in the order of nanoseconds [162]. In recent years, chemical and physical modification of the TiO_2 by doping metal and non-metal ions into the TiO_2 lattice, deposition of transition metals, dye photosensitization or coupling with other semiconductors have been used to overcome those TiO_2 limitations [163, 164].

The absorption by the TiO_2 (semiconductor) of incident photons of energy matching or exceeding the semiconductor band-gap energy produces conduction-band electrons e_{cb}^{-}(TiO_2) and valence-band holes h_{vb}^{+}(TiO_2), i.e. electron-hole pairs (Eq. (1.7)) [162]. Once at the surface of the semiconductor, the

presence of suitable acceptor (for e_{cb}^-) and donor (for h_{vb}^+) will avoid the near instantaneous and undesirable generated recombination. Molecular oxygen acts as electron acceptor, leading to the formation of hydroxyl ($HO^\bullet$) and superoxide ($O_2^{\bullet-}$) radicals (Eqs. (1.8), (1.9) and (1.10))[165].

$$TiO_2 \xrightarrow{hv} e_{cb}^- (TiO_2) + h_{vb}^+ (TiO_2) \quad (1.7)$$

$$h_{vb}^+ (TiO_2) + H_2O_{ads} \rightarrow OH^\bullet + H^+ \quad (1.8)$$

$$h_{vb}^+ (TiO_2) + H_2O^-_{ads} \rightarrow OH^\bullet \quad (1.9)$$

$$e_{cb}^- (TiO_2) + O_{2(ads)} \rightarrow OH^\bullet_{2(ads)} \quad (1.10)$$

If an organic molecule (RH) is adsorbed onto the semiconductor surface, the reaction with hydroxyl radical will occur, followed by structural breakdown into several intermediates until, eventually, total mineralisation (Eq. (1.11)) [166]. The photogenerated holes, due to their high oxidation potential, can also participate in the direct oxidation of the organic pollutants (Eq. (1.12)) [167].

Peroxide radical ($HOO^\bullet$) can also be generated from the protonation of $O_2^{\bullet-}$ radical and subsequently forms hydrogen peroxide (Eqs. (1.13) and (1.14)) [106].

$$RH + HO^\bullet \rightarrow RH^{\bullet+} + HO^- \rightarrow R^\bullet + H^+ + HO^- \quad (1.11)$$

$$h_{vb}^+ (TiO_2) + RH \rightarrow RH^{\bullet+} \rightarrow R^\bullet + H^+ \quad (1.12)$$

$$O_2^{\bullet-} + H^+ \rightarrow HOO^\bullet \quad (1.13)$$

$$O_2^{\bullet-} + HOO^\bullet + H^+ \rightarrow H_2O_2 + O_2 \quad (1.14)$$

Araña et al. [168] reported the use of Degussa P25 as received and doped with Fe (Fe–TiO_2) for the photocatalytic degradation (with four 15 W UVA lamps) of the commercial dye Lanaset Sun Yellow

180. With (Fe–TiO_2) catalyst, the formation of a photoactive complex was observed between the dye and Fe atoms of the catalyst surface that accelerated degradation. Toxicity analyses indicated that intermediates were not toxic. The researchers concluded that the photocatalytic method seem to be interesting for the decolourisation of wastewaters containing this dye.

Eskandarloo et al. [169] applied TiO_2/NiO coupled nanoparticles for the photocatalytic degradation of C. I. Basic Red 46 (BR46). The effect of operational variables was predicted and optimized using response surface methodology (RSM) and the obtained results showed that the predicted data from RSM was found to be in good agreement with the experimental results. A maximum degradation efficiency (91%) was achieved at the optimum operational conditions: initial dye concentration of 10.2 mg L^{-1}, catalyst dosage of 0.46 g L^{-1}, irradiation time of 30 min, and distance of the solution from UVC lamp (15W) of 3 cm. Table 1.13 presents the optimal operating conditions and the removals achieved in other studies regarding the treatment of dye solutions or textile wastewaters by UV/TiO_2.

Table 1.13. Studies on the treatability of dye solutions and textile wastewaters by UV/TiO_2.

Wastewater/ pollutant	Optimal Operating Conditions	Removal efficiencies (%)	Reference
Remazol Red RR dye solution	pH = 3.0 t = 30 min UVA radiation; P = 9 W [TiO_2] = 1.5 g L^{-1}	Colour = 96.7%	[170]
Acid Blue 80 dye solution	pH = 3.0 UVC radiation t = 30 min [TiO_2] = 0.5 g L^{-1}	Colour = 40%	[171]
Reactive Yellow 14 dye solution	pH = 5.5 Solar radiation t = 40 min [TiO_2] = 4 g L^{-1}	Colour = 82.1%	[172]
Real textile wastewater	pH = 4.5 Solar radiation Q_{UV} = 190 kJ_{UV} L^{-1} [TiO_2] = 200 mg L^{-1}	TOC = 36% Colour = 68%	[100]
Real textile wastewater	pH = 4.5 Solar radiation Q_{UV} = 39.5 kJ_{UV} L^{-1} [TiO_2] = 200 mg L^{-1}	TOC = 34.4%	[104]
Synthetic textile wastewater	pH = 7.0 t = 60 min UVA radiation; P = 60 W [TiO_2] = 1 g L^{-1}	TOC = 23% Colour = 86%	[173]
Synthetic textile wastewater	pH = 3.0 t = 60 min UVA radiation; P = 15 W [TiO_2] = 1 g L^{-1}	TOC = 12.5%	[174]

1.2.4.3 Treatment by UVC/H_2O_2

The combination of hydrogen peroxide and UVC radiation produces hydroxyl free radicals $^{\bullet}OH$ to enhance the degradation rate of organics in aqueous system. The photolysis of aqueous hydrogen peroxide (Eq. (1.15)) in the UVC range of the electromagnetic spectrum represents one of the easiest ways to produce sufficient amounts of hydroxyl radicals. However, the fate of $^{\bullet}OH$ radicals in aqueous solution is complex due to their high reactivity and short lifetime [106].

$$H_2O_2 \xrightarrow{h\nu} 2^{\bullet}OH \qquad (1.15)$$

The UVC/H_2O_2 process is relatively conventional and the most studied AOP, because of its powerful oxidation ability, no sludge production and simplicity of operation [175-177]. The use of UVC radiation involves the use of high concentrations of H_2O_2. As in all cases in which H_2O_2 is used, there must be a control of the system pH and temperature to prevent degradation of H_2O_2 (Eq. (1.16)).

$$2H_2O_2 \rightarrow 2H_2O + O_2 \qquad (1.16)$$

Several studies have reported about the successful application of the UVC/H_2O_2 process to many types of various organic pollutants, for the remediation of both ground and drinking waters [177-183]. More specifically, many authors investigated the decolourisation of various dyes by the UVC/H_2O_2 process and they found it efficient for laboratory prepared pure dye solutions [114, 184, 185], while it was seldom reported for industrial textile wastewaters [174].

Timchak and Gitis [186] investigated the inactivation of viruses (MS2, phi X 174 and T4), alone and jointly with the degradation of two fluorescent dyes, rhodamine B and fluorescein. Complex dye-virus experiments were performed in mixed suspensions of free floating and conjugated species. The studies were performed in collimated beam and in continuous-flow UVC reactors (UVC lamp of 43W power) and showed that the inactivation of viruses is not affected by the presence of dyes but can be improved by the addition of hydrogen peroxide. It was observed that the addition of 0.2 M H_2O_2 at 70 mJ cm^{-2} increased the inactivation of MS2 by two logs and had no effect on phi X 174 and T4. The bleaching of fluorescent dyes in the presence of viruses was decreased due to limited availability of hydroxyl radicals and their preferential participation in virus inactivation.

Kasiri and Khataee [187] used Response Surface Methodology (RSM) to study the effects of operational parameters on the photooxidative decolourisation of two dyes (C.I. Basic Blue 3 (BB3) and C.I. Acid Green 25 (AG25)) with different molecular structure under UVC light illumination (30 W) in the

presence of hydrogen peroxide (H_2O_2). Reaction variables were investigated, as the reaction time, dye and H_2O_2 initial concentrations and distance of UV lamp from the solution. Central Composite Design (CCD) was used for the optimization of photooxidative decolourisation process and results demonstrated that CCD methodology could efficiently optimize the photooxidative decolourisation of BB3 and AG25 using the UVC/H_2O_2 process. Under optimal value of process parameters, high colour removal (>95%) was obtained for dye solution containing BB3 or AG25.

Neamtu et al. [185] reported the use of laboratory-scale batch photoreactor equipped with an immersed low-pressure mercury lamp (15W) for the decolourisation and mineralisation of reactive azo dyes. Different doses of hydrogen peroxide, at constant initial concentration of the substrate (100 mg L^{-1}) were used. The obtained results showed that with a dose of 24.5 mmol L^{-1} H_2O_2 and a 60 min irradiation time the decolourisation was higher than 99.6% for all the three aqueous dye solutions. To use a hydrogen peroxide dosage higher than 24.5 mmol L^{-1} H_2O_2 was not cost effective. Researchers argued that the UVC/H_2O_2 process can be a suitable pre-treatment method for the complete decolourisation and detoxification of wastewaters from textile dyeing and finishing processes. They believe that the investigations should be continued in order to find the influence of other factors like textile auxiliaries, salts, surfactants and natural impurities on the mineralisation degree. Table 1.14 presents the optimal operating conditions and the removals achieved in other studies regarding the treatment of dye solutions or textile wastewaters by UVC/H_2O_2 system.

Table 1.14. Studies on the treatability of dye solutions and textile wastewaters by UVC/H_2O_2 system.

Wastewater/ pollutant	Optimal Operating Conditions	Removal efficiencies (%)	Reference
C. I. Acid Blue 113 dye solution	pH = 5.5 t = 20 min; P = 14 W [H_2O_2] = 46.53 mM	Colour = 97.2	[184]
C. I. Direct Blue 199 dye solution	pH = 6.8 t = 120 min; P = 35 W [H_2O_2] = 116.32 mM	TOC = 80 Colour = 95	[114]
Vat Green 01 dye solution	pH = 3.0 t = 120 min; P = 125 W [H_2O_2] = 1 g L^{-1}	Colour = 41	[188]
C. I. Reactive Black 5; C. I. Direct Yellow 12; C. I. Direct Red 28	pH = 7.0 t = 60 min; P = 16 W [H_2O_2] = 50 mM	Colour (RB5) = 99 Colour (DY12) = 98 Colour (DR28) = 40	[189]
Synthetic textile wastewater	pH = 3.0 t = 60 min; P = 25 W [H_2O_2] = 680 mg L^{-1}	TOC = 30.4 Colour = 87.0	[174]
Real textile wastewater	pH = 3.0 t = 120 min; P = 125 W [H_2O_2] = 1 g L^{-1}	COD = 69 Colour = 74	[188]

1.3 References

1. IPPC, I.P.P.a.C.-. *Reference Document on Best Available Techniques for the Textile Industry*. 2003, European Commission. p. 626.
2. Oller, I., S. Malato, and J.A. Sánchez-Pérez, *Combination of Advanced Oxidation Processes and biological treatments for wastewater decontamination—A review.* Science of The Total Environment, 2011. **409**(20): p. 4141-4166.
3. Malato, S., P. Fernández-Ibáñez, M.I. Maldonado, J. Blanco, and W. Gernjak, *Decontamination and disinfection of water by solar photocatalysis: Recent overview and trends.* Catalysis Today, 2009. **147**(1): p. 1-59.
4. Oller, I., S. Malato, J.A. Sánchez-Pérez, W. Gernjak, M.I. Maldonado, L.A. Pérez-Estrada, and C. Pulgarín, *A combined solar photocatalytic-biological field system for the mineralization of an industrial pollutant at pilot scale.* Catalysis Today, 2007. **122**(1–2): p. 150-159.
5. Nidheesh, P.V., R. Gandhimathi, and S.T. Ramesh, *Degradation of dyes from aqueous solution by Fenton processes: a review.* Environmental Science and Pollution Research, 2013. **20**(4): p. 2099-2132.
6. Faouzi, M., P. Cañizares, A. Gadri, J. Lobato, B. Nasr, R. Paz, M.A. Rodrigo, and C. Saez, *Advanced oxidation processes for the treatment of wastes polluted with azoic dyes.* Electrochimica Acta, 2006. **52**(1): p. 325-331.
7. Haji, S., B. Benstaali, and N. Al-Bastaki, *Degradation of methyl orange by UV/H_2O_2 advanced oxidation process.* Chemical Engineering Journal, 2011. **168**(1): p. 134-139.
8. Spuhler, D., J. Andrés Rengifo-Herrera, and C. Pulgarin, *The effect of Fe^{2+}, Fe^{3+}, H_2O_2 and the photo-Fenton reagent at near neutral pH on the solar disinfection (SODIS) at low temperatures of water containing Escherichia coli K12.* Applied Catalysis B: Environmental, 2010. **96**(1–2): p. 126-141.
9. De la Cruz, N., J. Giménez, S. Esplugas, D. Grandjean, L.F. de Alencastro, and C. Pulgarín, *Degradation of 32 emergent contaminants by UV and neutral photo-fenton in domestic wastewater effluent previously treated by activated sludge.* Water Research, 2012. **46**(6): p. 1947-1957.
10. Klamerth, N., S. Malato, A. Agüera, and A. Fernández-Alba, *Photo-Fenton and modified photo-Fenton at neutral pH for the treatment of emerging contaminants in wastewater treatment plant effluents: A comparison.* Water Research, 2013. **47**(2): p. 833-840.
11. Hai, F.I., K. Yamamoto, and K. Fukushi, *Hybrid Treatment Systems for Dye Wastewater.* Critical Reviews in Environmental Science and Technology, 2007. **37**(4): p. 315-377.
12. Sarria, V., S. Parra, N. Adler, P. Péringer, N. Benitez, and C. Pulgarin, *Recent developments in the coupling of photoassisted and aerobic biological processes for the treatment of biorecalcitrant compounds.* Catalysis Today, 2002. **76**(2–4): p. 301-315.
13. Mantzavinos, D. and E. Psillakis, *Enhancement of biodegradability of industrial wastewaters by chemical oxidation pre-treatment.* Journal of Chemical Technology & Biotechnology, 2004. **79**(5): p. 431-454.
14. Gaya, U.I. and A.H. Abdullah, *Heterogeneous photocatalytic degradation of organic contaminants over titanium dioxide: A review of fundamentals, progress and problems.* Journal of Photochemistry and Photobiology C: Photochemistry Reviews, 2008. **9**(1): p. 1-12.

15. Silva, T.F.C.V., M.E.F. Silva, A.C. Cunha-Queda, A. Fonseca, I. Saraiva, M.A. Sousa, C. Gonçalves, M.F. Alpendurada, R.A.R. Boaventura, and V.J.P. Vilar, *Multistage treatment system for raw leachate from sanitary landfill combining biological nitrification–denitrification/solar photo-Fenton/biological processes, at a scale close to industrial – Biodegradability enhancement and evolution profile of trace pollutants.* Water Research, 2013. **47**(16): p. 6167-6186.

16. Eurostat, *Statistics on the production of manufactured goods Value ANNUAL 2009*. 2013, European Commission.

17. Eurostat, *Statistics on the production of manufactured goods Value ANNUAL 2010*. 2013, European Commission.

18. Eurostat, *Statistics on the production of manufactured goods Value ANNUAL 2012*. 2014, European Commission.

19. Eurostat, *Statistics on the production of manufactured goods Value ANNUAL 2011*. 2014, European Commission.

20. Eurostat, *Statistics on the production of manufactured goods Value ANNUAL 2013*. 2015, European Commission.

21. Eurostat, *Statistics on the production of manufactured goods Value ANNUAL 2014*. 2015, European Commission.

22. Hasanbeigi, A. and L. Price, *A review of energy use and energy efficiency technologies for the textile industry.* Renewable and Sustainable Energy Reviews, 2012. **16**(6): p. 3648-3665.

23. Hasanbeigi, A., A. Hasanabadi, and M. Abdorrazaghi, *Comparison analysis of energy intensity for five major sub-sectors of the Textile Industry in Iran.* Journal of Cleaner Production, 2012. **23**(1): p. 186-194.

24. Kandilli, C. and A. Koclu, *Assessment of the optimum operation conditions of a plate heat exchanger for waste heat recovery in textile industry.* Renewable and Sustainable Energy Reviews, 2011. **15**(9): p. 4424-4431.

25. Lin, B. and M. Moubarak, *Decomposition analysis: Change of carbon dioxide emissions in the Chinese textile industry.* Renewable and Sustainable Energy Reviews, 2013. **26**: p. 389-396.

26. Verma, A.K., R.R. Dash, and P. Bhunia, *A review on chemical coagulation/flocculation technologies for removal of colour from textile wastewaters.* Journal of Environmental Management, 2012. **93**(1): p. 154-168.

27. Wang, L.K., Y.-T. Hung, H.H. Lo, and C. Yapijakis, *Handbook of industrial and hazardous wastes treatment*. 2004: CRC Press.

28. Correia, V.M., T. Stephenson, and S.J. Judd, *Characterisation of textile wastewaters - a review.* Environmental Technology, 1994. **15**(10): p. 917-929.

29. Bisschops, I. and H. Spanjers, *Literature review on textile wastewater characterisation.* Environmental Technology, 2003. **24**(11): p. 1399-1411.

30. Crini, G. and P.-M. Badot, *Application of chitosan, a natural aminopolysaccharide, for dye removal from aqueous solutions by adsorption processes using batch studies: A review of recent literature.* Progress in Polymer Science, 2008. **33**(4): p. 399-447.

31. Rodriguez, M., V. Sarria, S. Esplugas, and C. Pulgarin, *Photo-Fenton treatment of a biorecalcitrant wastewater generated in textile activities: biodegradability of the photo-treated solution.* Journal of Photochemistry and Photobiology A: Chemistry, 2002. **151**(1–3): p. 129-135.

32. Gregory, P., *Dyes and Dye Intermediates*, in *Kirk-Othmer Encyclopedia of Chemical Technology*. 2000, John Wiley & Sons, Inc.

33. Board, N., *The Complete Technology Book On Dyes & Dye Intermediates*. 2003: NIIR Project Consultancy Services.

34. Delée, W., C. O'Neill, F.R. Hawkes, and H.M. Pinheiro, *Anaerobic treatment of textile effluents: A review.* Journal of Chemical Technology & Biotechnology, 1998. **73**(4): p. 323-335.

35. Schönberger, H. and T. Schäfer, *Best Available Techniques in Textile Industry*, R.R. 329, Editor. 2003, Umweltbundesamt - Federal Environmental Agency: Berlin. p. 364.

36. Moore, S.B. and L.W. Ausley, *Systems thinking and green chemistry in the textile industry: concepts, technologies and benefits.* Journal of Cleaner Production, 2004. **12**(6): p. 585-601.

37. Demirbas, A., *Agricultural based activated carbons for the removal of dyes from aqueous solutions: A review.* Journal of Hazardous Materials, 2009. **167**(1–3): p. 1-9.

38. Forgacs, E., T. Cserháti, and G. Oros, *Removal of synthetic dyes from wastewaters: a review.* Environment International, 2004. **30**(7): p. 953-971.

39. Husain, Q., *Potential Applications of the Oxidoreductive Enzymes in the Decolorization and Detoxification of Textile and Other Synthetic Dyes from Polluted Water: A Review.* Critical Reviews in Biotechnology, 2006. **26**(4): p. 201-221.

40. Sun, Q. and L. Yang, *The adsorption of basic dyes from aqueous solution on modified peat–resin particle.* Water Research, 2003. **37**(7): p. 1535-1544.

41. Cristóvão, R.O., A.P.M. Tavares, A.I. Brígida, J.M. Loureiro, R.A.R. Boaventura, E.A. Macedo, and M.A.Z. Coelho, *Immobilization of commercial laccase onto green coconut fiber by adsorption and its application for reactive textile dyes degradation.* Journal of Molecular Catalysis B: Enzymatic, 2011. **72**(1–2): p. 6-12.

42. Gupta, V.K., R. Jain, and S. Varshney, *Electrochemical removal of the hazardous dye Reactofix Red 3 BFN from industrial effluents.* Journal of Colloid and Interface Science, 2007. **312**(2): p. 292-296.

43. Rieger, P.-G., H.-M. Meier, M. Gerle, U. Vogt, T. Groth, and H.-J. Knackmuss, *Xenobiotics in the environment: present and future strategies to obviate the problem of biological persistence.* Journal of Biotechnology, 2002. **94**(1): p. 101-123.

44. Arslan-Alaton, I. and I. Alaton, *Degradation of xenobiotics originating from the textile preparation, dyeing, and finishing industry using ozonation and advanced oxidation.* Ecotoxicology and Environmental Safety, 2007. **68**(1): p. 98-107.

45. Arslan-Alaton, I. and E. Erdinc, *Effect of photochemical treatment on the biocompatibility of a commercial nonionic surfactant used in the textile industry.* Water Research, 2006. **40**(18): p. 3409-3418.

46. Arslan Alaton, I., G. Insel, G. Eremektar, F. Germirli Babuna, and D. Orhon, *Effect of textile auxiliaries on the biodegradation of dyehouse effluent in activated sludge.* Chemosphere, 2006. **62**(9): p. 1549-1557.

47. Castillo, M. and D. Barceló, *Characterisation of organic pollutants in textile wastewaters and landfill leachate by using toxicity-based fractionation methods followed by liquid and gas chromatography coupled to mass spectrometric detection.* Analytica Chimica Acta, 2001. **426**(2): p. 253-264.

48. Manekar, P., G. Patkar, P. Aswale, M. Mahure, and T. Nandy, *Detoxifying of high strength textile effluent through chemical and bio-oxidation processes.* Bioresource Technology, 2014. **157**: p. 44-51.

49. Rodrigues, C.S.D., L.M. Madeira, and R.A.R. Boaventura, *Treatment of textile dye wastewaters using ferrous sulphate in a chemical coagulation/flocculation process.* Environmental Technology, 2012. **34**(6): p. 719-729.

50. Lotito, A.M., U. Fratino, G. Bergna, and C. Di Iaconi, *Integrated biological and ozone treatment of printing textile wastewater.* Chemical Engineering Journal, 2012. **195–196**: p. 261-269.

51. Aouni, A., C. Fersi, M. Ben Sik Ali, and M. Dhahbi, *Treatment of textile wastewater by a hybrid electrocoagulation/nanofiltration process.* Journal of Hazardous Materials, 2009. **168**(2–3): p. 868-874.

52. Blanco, J., F. Torrades, M. Morón, M. Brouta-Agnésa, and J. García-Montaño, *Photo-Fenton and sequencing batch reactor coupled to photo-Fenton processes for textile wastewater reclamation: Feasibility of reuse in dyeing processes.* Chemical Engineering Journal, 2014. **240**: p. 469-475.

53. Zhang, W., W. Liu, J. Zhang, H. Zhao, Y. Zhang, X. Quan, and Y. Jin, *Characterisation of acute toxicity, genotoxicity and oxidative stress posed by textile effluent on zebrafish.* Journal of Environmental Sciences, 2012. **24**(11): p. 2019-2027.

54. Prigione, V., V. Tigini, C. Pezzella, A. Anastasi, G. Sannia, and G.C. Varese, *Decolourisation and detoxification of textile effluents by fungal biosorption.* Water Research, 2008. **42**(12): p. 2911-2920.

55. Anastasi, A., B. Parato, F. Spina, V. Tigini, V. Prigione, and G.C. Varese, *Decolourisation and detoxification in the fungal treatment of textile wastewaters from dyeing processes.* New Biotechnology, 2011. **29**(1): p. 38-45.

56. Şen, S. and G.N. Demirer, *Anaerobic treatment of real textile wastewater with a fluidized bed reactor.* Water Research, 2003. **37**(8): p. 1868-1878.

57. Debik, E., G. Kaykioglu, A. Coban, and I. Koyuncu, *Reuse of anaerobically and aerobically pre-treated textile wastewater by UF and NF membranes.* Desalination, 2010. **256**(1–3): p. 174-180.

58. Soares, P., T.C.V. Silva, D. Manenti, S.A.G.U. Souza, R.R. Boaventura, and V.P. Vilar, *Insights into real cotton-textile dyeing wastewater treatment using solar advanced oxidation processes.* Environmental Science and Pollution Research, 2013: p. 1-14.

59. Yang, X., *Interior microelectrolysis oxidation of polyester wastewater and its treatment technology.* Journal of Hazardous Materials, 2009. **169**(1–3): p. 480-485.

60. Golob, V., A. Vinder, and M. Simonič, *Efficiency of the coagulation/flocculation method for the treatment of dyebath effluents.* Dyes and Pigments, 2005. **67**(2): p. 93-97.

61. Ghosh, P., A.N. Samanta, and S. Ray, *Reduction of COD and removal of Zn^{2+} from rayon industry wastewater by combined electro-Fenton treatment and chemical precipitation.* Desalination, 2011. **266**(1–3): p. 213-217.

62. Chowdhury, S. and R. Balasubramanian, *Graphene/semiconductor nanocomposites (GSNs) for heterogeneous photocatalytic decolorization of wastewaters contaminated with synthetic dyes: A review.* Applied Catalysis B: Environmental, 2014. **160**: p. 307-324.

63. Hessel, C., C. Allegre, M. Maisseu, F. Charbit, and P. Moulin, *Guidelines and legislation for dye house effluents.* Journal of environmental management, 2007. **83**(2): p. 171-180.

64. EPA, *Technical Support Document for the 2010 Effluent Guidelines Program Plan* E.P.A.-. EPA, Editor. 2011.

65. Earnhart, D. and D.R. Harrington, *Effect of audits on the extent of compliance with wastewater discharge limits.* Journal of Environmental Economics and Management, 2014. **68**(2): p. 243-261.

66. Government, U.S.A., *Title 40 - Protection of Environment*. 2012, Office of the Federal Register National Archives and Records Administration: Washington. p. 709.

67. Clesceri, L.S., A.E. Greenberg, and A.D. Eaton, *Standard Methods for Examination of Water & Wastewater*. 21 ed, ed. A.P.H.A. (APHA). 2005.

68. CONAMA, *Resolução n.357 de 17 de março de 2005*. 2005, Conselho Nacional do Meio Ambiente: Diário Oficial da União. p. 27.

69. CONAMA, *Resolução n.410 de 04 de Maio de 2009*. 2009, Conselho Nacional do Meio Ambiente: Diário Oficial da União. p. 1.

70. CONAMA, *Resolução n.430 de 13 de maio de 2011*. 2011, Conselho Nacional do Meio Ambiente: Diário Oficial da União. p. 9.

71. EEC, *Directive 91/271 Council directive of 21 May concerning urban waste water treatment*. 1991, European Commission: Brussels.

72. EEC, *Directive 98/15 Council directive of 27 February concerning urban waste water treatment.* 1998, European Commission: Brussels.

73. Parliament, E., *Regulation (EC) n. 1882/2003*. 2003, European Parliament and of the Council of the European Union: Brussels.

74. Wasserhaushaltsgesetz, *Gesetz zur Ordnung des Wasserhaushalts (Wasserhaushaltsgesetz – WHG)*, B. I, Editor. 2009, Bundesministerium der Justiz: Bundesrepublik Deutschland.

75. 7887, D.E.I., *DIN EN ISO 7887:2012-04, Wasserbeschaffenheit - Untersuchung und Bestimmung der Färbung*. 2012, Deutsches Institut für Normung - DIN.

76. Portugal, *Portaria nº423/97 de 25 de Junho, Diário da República-I Série*. 1997. p. 3111-3112.

77. Portugal, *Decreto-Lei nº.236/98*. 1998, Ministério do Ambiente: Diário da República. p. 47.

78. Abwasserverordnung, *Verordnung über Anforderungen an das Einleiten von Abwasser in Gewässer (Abwasserverordnung - AbwV)*, B. I, Editor. 2004, Bundesministerium der Justiz: Bundesrepublik Deutschland.

79. Lotito, A.M., M. De Sanctis, C. Di Iaconi, and G. Bergna, *Textile wastewater treatment: Aerobic granular sludge vs activated sludge systems.* Water Research, 2014. **54**: p. 337-346.

80. dos Santos, A.B., F.J. Cervantes, and J.B. van Lier, *Review paper on current technologies for decolourisation of textile wastewaters: Perspectives for anaerobic biotechnology.* Bioresource Technology, 2007. **98**(12): p. 2369-2385.

81. Srinivasan, A. and T. Viraraghavan, *Decolorization of dye wastewaters by biosorbents: A review.* Journal of Environmental Management, 2010. **91**(10): p. 1915-1929.

82. Blánquez, P., M. Sarrà, and T. Vicent, *Development of a continuous process to adapt the textile wastewater treatment by fungi to industrial conditions.* Process Biochemistry, 2008. **43**(1): p. 1-7.

83. Hai, F.I., K. Yamamoto, and K. Fukushi, *Development of a submerged membrane fungi reactor for textile wastewater treatment.* Desalination, 2006. **192**(1–3): p. 315-322.

84. Lotito, A.M., C. Di Iaconi, U. Fratino, A. Mancini, and G. Bergna, *Sequencing batch biofilter granular reactor for textile wastewater treatment.* New Biotechnology, 2011. **29**(1): p. 9-16.

85. Yu, R.-F., C.-H. Lin, H.-W. Chen, W.-P. Cheng, and M.-C. Kao, *Possible control approaches of the Electro-Fenton process for textile wastewater treatment using on-line monitoring of DO and ORP*. Chemical Engineering Journal, 2013. **218**: p. 341-349.

86. Sirianuntapiboon, S., K. Chairattanawan, and S. Jungphungsukpanich, *Some properties of a sequencing batch reactor system for removal of vat dyes.* Bioresource Technology, 2006. **97**(10): p. 1243-1252.

87. Fu, Z., Y. Zhang, and X. Wang, *Textiles wastewater treatment using anoxic filter bed and biological wriggle bed-ozone biological aerated filter.* Bioresource Technology, 2011. **102**(4): p. 3748-3753.

88. Lotito, A.M., U. Fratino, A. Mancini, G. Bergna, and C. Di Iaconi, *Effective aerobic granular sludge treatment of a real dyeing textile wastewater.* International Biodeterioration & Biodegradation, 2012. **69**: p. 62-68.

89. Blanco, J., F. Torrades, M. De la Varga, and J. García-Montaño, *Fenton and biological-Fenton coupled processes for textile wastewater treatment and reuse.* Desalination, 2012. **286**: p. 394-399.

90. Shehzadi, M., M. Afzal, E. Islam, A. Mobin, S. Anwar, and Q.M. Khan, *Enhanced degradation of textile effluent in constructed wetland system using Typha domingensis and textile effluent-degrading endophytic bacteria.* Water Research, 2014. **58**: p. 152-159.

91. Bes-Piá, A., J.A. Mendoza-Roca, M.I. Alcaina-Miranda, A. Iborra-Clar, and M.I. Iborra-Clar, *Reuse of wastewater of the textile industry after its treatment with a combination of physico-chemical treatment and membrane technologies.* Desalination, 2002. **149**(1–3): p. 169-174.

92. Harrelkas, F., A. Azizi, A. Yaacoubi, A. Benhammou, and M.N. Pons, *Treatment of textile dye effluents using coagulation–flocculation coupled with membrane processes or adsorption on powdered activated carbon.* Desalination, 2009. **235**(1–3): p. 330-339.

93. Li, J., D. Wang, D. Yu, P. Zhang, and Y. Li, *Performance and membrane fouling in an integrated membrane coagulation reactor (IMCR) treating textile wastewater.* Chemical Engineering Journal, 2014. **240**: p. 82-90.

94. Tezcan Un, U. and E. Aytac, *Electrocoagulation in a packed bed reactor-complete treatment of color and cod from real textile wastewater.* Journal of Environmental Management, 2013. **123**: p. 113-119.

95. Papadopoulos, A.E., D. Fatta, and M. Loizidou, *Development and optimization of dark Fenton oxidation for the treatment of textile wastewaters with high organic load.* Journal of Hazardous Materials, 2007. **146**(3): p. 558-563.

96. Karthikeyan, S., A. Titus, A. Gnanamani, A.B. Mandal, and G. Sekaran, *Treatment of textile wastewater by homogeneous and heterogeneous Fenton oxidation processes.* Desalination, 2011. **281**: p. 438-445.

97. Wei, J., Y. Song, X. Tu, L. Zhao, and E. Zhi, *Pretreatment of dry-spun acrylic fiber manufacturing wastewater by Fenton process: Optimization, kinetics and mechanisms.* Chemical Engineering Journal, 2013. **218**: p. 319-326.

98. Pérez, M., F. Torrades, X. Domènech, and J. Peral, *Fenton and photo-Fenton oxidation of textile effluents.* Water Research, 2002. **36**(11): p. 2703-2710.

99. Azbar, N., T. Yonar, and K. Kestioglu, *Comparison of various advanced oxidation processes and chemical treatment methods for COD and color removal from a polyester and acetate fiber dyeing effluent.* Chemosphere, 2004. **55**(1): p. 35-43.

100. Vilar, V.J.P., L.X. Pinho, A.M.A. Pintor, and R.A.R. Boaventura, *Treatment of textile wastewaters by solar-driven advanced oxidation processes.* Solar Energy, 2011. **85**(9): p. 1927-1934.

101. Sarayu, K. and S. Sandhya, *Current Technologies for Biological Treatment of Textile Wastewater–A Review.* Applied Biochemistry and Biotechnology, 2012. **167**(3): p. 645-661.

102. Khandegar, V. and A.K. Saroha, *Electrocoagulation for the treatment of textile industry effluent – A review.* Journal of Environmental Management, 2013. **128**: p. 949-963.

103. Manenti, D.R., A.N. Módenes, P.A. Soares, F.R. Espinoza-Quiñones, R.A.R. Boaventura, R. Bergamasco, and V.J.P. Vilar, *Assessment of a multistage system based on electrocoagulation, solar photo-Fenton and biological oxidation processes for real textile wastewater treatment.* Chemical Engineering Journal, 2014. **252**: p. 120-130.

104. Manenti, D.R., P.A. Soares, T.F. Silva, A.N. Módenes, F.R. Espinoza-Quiñones, R. Bergamasco, R.A. Boaventura, and V.J. Vilar, *Performance evaluation of different solar advanced oxidation processes applied to the treatment of a real textile dyeing wastewater.* Environmental Science and Pollution Research, 2015: p. 1-13.

105. Doumic, L.I., P.A. Soares, M.A. Ayude, M. Cassanello, R.A.R. Boaventura, and V.J.P. Vilar, *Enhancement of a solar photo-Fenton reaction by using ferrioxalate complexes for the treatment of a synthetic cotton-textile dyeing wastewater.* Chemical Engineering Journal, 2015. **277**: p. 86-96.

106. Oppenländer, T., *Photochemical Purification of Water and Air*, ed. W.-V. Verlag. 2003, Germany. 368.

107. Poyatos, J.M., M.M. Muñio, M.C. Almecija, J.C. Torres, E. Hontoria, and F. Osorio, *Advanced Oxidation Processes for Wastewater Treatment: State of the Art.* Water, Air, and Soil Pollution, 2010. **205**(1-4): p. 187-204.

108. Dhir, A., N. Prakash, and D. Sud, *Coupling of solar-assisted advanced oxidative and biological treatment for degradation of agro-residue-based soda bleaching effluent.* Environmental Science and Pollution Research, 2012. **19**(9): p. 3906-3913.

109. Senta, I., M. Matošić, H.K. Jakopović, S. Terzic, J. Ćurko, I. Mijatović, and M. Ahel, *Removal of antimicrobials using advanced wastewater treatment.* Journal of Hazardous Materials, 2011. **192**(1): p. 319-328.

110. Liu, P., H. Zhang, Y. Feng, F. Yang, and J. Zhang, *Removal of trace antibiotics from wastewater: A systematic study of nanofiltration combined with ozone-based advanced oxidation processes.* Chemical Engineering Journal, 2014. **240**: p. 211-220.

111. Monteagudo, J.M., A. Durán, I.S. Martín, and M. Aguirre, *Catalytic degradation of Orange II in a ferrioxalate-assisted photo-Fenton process using a combined UV-A/C–solar pilot-plant system.* Applied Catalysis B: Environmental, 2010. **95**(1–2): p. 120-129.

112. Muñoz, I., J. Peral, J. Antonio Ayllón, S. Malato, P. Passarinho, and X. Domènech, *Life cycle assessment of a coupled solar photocatalytic–biological process for wastewater treatment.* Water Research, 2006. **40**(19): p. 3533-3540.

113. Germirli Babuna, F., S. Camur, I.A. Alaton, O. Okay, and G. Iskender, *The application of ozonation for the detoxification and biodegradability improvement of a textile auxiliary: Naphtalene sulphonic acid.* Desalination, 2009. **249**(2): p. 682-686.

114. Shu, H.-Y., *Degradation of dyehouse effluent containing C.I. Direct Blue 199 by processes of ozonation, UV/H_2O_2 and in sequence of ozonation with UV/H_2O_2.* Journal of Hazardous Materials, 2006. **133**(1–3): p. 92-98.

115. Arslan-Alaton, I., *Degradation of a commercial textile biocide with advanced oxidation processes and ozone.* Journal of Environmental Management, 2007. **82**(2): p. 145-154.

116. Malato Rodríguez, S., J. Blanco Gálvez, M.I. Maldonado Rubio, P. Fernández Ibáñez, D. Alarcón Padilla, M. Collares Pereira, J. Farinha Mendes, and J. Correia de Oliveira, *Engineering of solar photocatalytic collectors.* Solar Energy, 2004. **77**(5): p. 513-524.

117. Benitez, F.J., J.L. Acero, J.F. Garcia-Reyes, F.J. Real, G. Roldan, E. Rodriguez, and A. Molina-Díaz, *Determination of the Reaction Rate Constants and Decomposition Mechanisms of Ozone with Two Model Emerging Contaminants: DEET and Nortriptyline.* Industrial & Engineering Chemistry Research, 2013. **52**(48): p. 17064-17073.

118. Papageorgiou, A., D. Voutsa, and N. Papadakis, *Occurrence and fate of ozonation by-products at a full-scale drinking water treatment plant.* Science of The Total Environment, 2014. **481**: p. 392-400.

119. Beltrán, F.J., J. Encinar, and J.F. González, *Industrial wastewater advanced oxidation. Part 2. Ozone combined with hydrogen peroxide or UV radiation.* Water Research, 1997. **31**(10): p. 2415-2428.

120. Garoma, T., M.D. Gurol, L. Thotakura, and O. Osibodu, *Degradation of tert-butyl formate and its intermediates by an ozone/UV process.* Chemosphere, 2008. **73**(11): p. 1708-1715.

121. Lekkerkerker-Teunissen, K., A.H. Knol, L.P. van Altena, C.J. Houtman, J.Q.J.C. Verberk, and J.C. van Dijk, *Serial ozone/peroxide/low pressure UV treatment for synergistic and effective organic micropollutant conversion.* Separation and Purification Technology, 2012. **100**: p. 22-29.

122. Kusic, H., N. Koprivanac, and A.L. Bozic, *Minimization of organic pollutant content in aqueous solution by means of AOPs: UV- and ozone-based technologies.* Chemical Engineering Journal, 2006. **123**(3): p. 127-137.

123. Tizaoui, C., L. Bouselmi, L. Mansouri, and A. Ghrabi, *Landfill leachate treatment with ozone and ozone/hydrogen peroxide systems.* Journal of Hazardous Materials, 2007. **140**(1–2): p. 316-324.

124. Audenaert, W.T.M., D. Vandierendonck, S.W.H. Van Hulle, and I. Nopens, *Comparison of ozone and HO induced conversion of effluent organic matter (EfOM) using ozonation and UV/H_2O_2 treatment.* Water Research, 2013. **47**(7): p. 2387-2398.

125. Ferhan, M., N. Tanguy, N. Yan, and M. Sain, *Comparison of Enzymatic, Alkaline, and UV/H_2O_2 Treatments for Extraction of Beetle-Infested Lodgepole Pine (BILP) and Aspen Bark Polyphenolic Extractives.* ACS Sustainable Chemistry & Engineering, 2013. **2**(2): p. 165-172.

126. Munoz, M., G. Pliego, Z.M. de Pedro, J.A. Casas, and J.J. Rodriguez, *Application of intensified Fenton oxidation to the treatment of sawmill wastewater.* Chemosphere, 2014. **109**: p. 34-41.

127. Gupta, A., R. Zhao, J.T. Novak, and C. Douglas Goldsmith, *Application of Fenton's reagent as a polishing step for removal of UV quenching organic constituents in biologically treated landfill leachates.* Chemosphere, 2014. **105**: p. 82-86.

128. Li, Y. and A. Zhang, *Removal of steroid estrogens from waste activated sludge using Fenton oxidation: Influencing factors and degradation intermediates.* Chemosphere, 2014. **105**: p. 24-30.

129. Yin, X., W. Liu, and J. Ni, *Removal of coexisting Cr(VI) and 4-chlorophenol through reduction and Fenton reaction in a single system.* Chemical Engineering Journal, 2014. **248**: p. 89-97.

130. Miralles-Cuevas, S., F. Audino, I. Oller, R. Sánchez-Moreno, J.A. Sánchez Pérez, and S. Malato, *Pharmaceuticals removal from natural water by nanofiltration combined with advanced tertiary treatments (solar photo-Fenton, photo-Fenton-like Fe(III)–EDDS complex and ozonation).* Separation and Purification Technology, 2014. **122**: p. 515-522.

131. Fernandes, L., M.S. Lucas, M.I. Maldonado, I. Oller, and A. Sampaio, *Treatment of pulp mill wastewater by Cryptococcus podzolicus and solar photo-Fenton: A case study.* Chemical Engineering Journal, 2014. **245**: p. 158-165.

132. Silva, T.F.C.V., M.E.F. Silva, A. Cristina Cunha-Queda, A. Fonseca, I. Saraiva, R.A.R. Boaventura, and V.J.P. Vilar, *Sanitary landfill leachate treatment using combined solar photo-Fenton and biological oxidation processes at pre-industrial scale.* Chemical Engineering Journal, 2013. **228**: p. 850-866.

133. Silva, T.F.C.V., A. Fonseca, I. Saraiva, V.J.P. Vilar, and R.A.R. Boaventura, *Biodegradability enhancement of a leachate after biological lagooning using a solar driven photo-Fenton reaction, and further combination with an activated sludge biological process, at pre-industrial scale.* Water Research, 2013. **47**(10): p. 3543-3557.

134. Pereira, J.H.O.S., V.J.P. Vilar, M.T. Borges, O. González, S. Esplugas, and R.A.R. Boaventura, *Photocatalytic degradation of oxytetracycline using TiO_2 under natural and simulated solar radiation.* Solar Energy, 2011. **85**(11): p. 2732-2740.

135. Sousa, M.A., C. Gonçalves, J.H.O.S. Pereira, V.J.P. Vilar, R.A.R. Boaventura, and M.F. Alpendurada, *Photolytic and TiO_2-assisted photocatalytic oxidation of the anxiolytic drug lorazepam (Lorenin® pills) under artificial UV light and natural sunlight: A comparative and comprehensive study.* Solar Energy, 2013. **87**: p. 219-228.

136. Pereira, J.H.O.S., A.C. Reis, D. Queirós, O.C. Nunes, M.T. Borges, V.J.P. Vilar, and R.A.R. Boaventura, *Insights into solar TiO_2-assisted photocatalytic oxidation of two antibiotics employed in aquatic animal production, oxolinic acid and oxytetracycline.* Science of The Total Environment, 2013. **463–464**: p. 274-283.

137. Muruganandham, M. and M. Swaminathan, *Decolourisation of Reactive Orange 4 by Fenton and photo-Fenton oxidation technology.* Dyes and Pigments, 2004. **63**(3): p. 315-321.

138. Torrades, F., J. Garcıa-Montano, J.A. Garcıa-Hortal, X. Domenech, and J. Peral, *Decolorization and mineralization of commercial reactive dyes under solar light assisted photo-Fenton conditions.* Solar Energy, 2004. **77**(5): p. 573-581.

139. Guimarães, J.R., M. Guedes Maniero, and R. Nogueira de Araújo, *A comparative study on the degradation of RB-19 dye in an aqueous medium by advanced oxidation processes.* Journal of Environmental Management, 2012. **110**: p. 33-39.

140. Kang, S.-F., C.-H. Liao, and S.-T. Po, *Decolorization of textile wastewater by photo-fenton oxidation technology.* Chemosphere, 2000. **41**(8): p. 1287-1294.

141. Hernández-Rodríguez, M.J., C. Fernández-Rodríguez, J.M. Doña-Rodríguez, O.M. González-Díaz, D. Zerbani, and J. Pérez Peña, *Treatment of effluents from wool dyeing process by photo-Fenton at solar pilot plant.* Journal of Environmental Chemical Engineering, 2014. **2**(1): p. 163-171.

142. Chacón, J.M., M. Teresa Leal, M. Sánchez, and E.R. Bandala, *Solar photocatalytic degradation of azo-dyes by photo-Fenton process.* Dyes and Pigments, 2006. **69**(3): p. 144-150.

143. Modirshahla, N., M.A. Behnajady, and F. Ghanbary, *Decolorization and mineralization of C.I. Acid Yellow 23 by Fenton and photo-Fenton processes.* Dyes and Pigments, 2007. **73**(3): p. 305-310.

144. Prato-Garcia, D. and G. Buitrón, *Evaluation of three reagent dosing strategies in a photo-Fenton process for the decolorization of azo dye mixtures.* Journal of Hazardous Materials, 2012. **217–218**: p. 293-300.

145. Punzi, M., B. Mattiasson, and M. Jonstrup, *Treatment of synthetic textile wastewater by homogeneous and heterogeneous photo-Fenton oxidation.* Journal of Photochemistry and Photobiology A: Chemistry, 2012. **248**: p. 30-35.

146. Pignatello, J.J., E. Oliveros, and A. MacKay, *Advanced Oxidation Processes for Organic Contaminant Destruction Based on the Fenton Reaction and Related Chemistry.* Critical Reviews in Environmental Science and Technology, 2006. **36**(1): p. 1-84.

147. Prato-Garcia, D., R. Vasquez-Medrano, and M. Hernandez-Esparza, *Solar photoassisted advanced oxidation of synthetic phenolic wastewaters using ferrioxalate complexes.* Solar Energy, 2009. **83**(3): p. 306-315.

148. Carneiro, P.A., R.F.P. Nogueira, and M.V.B. Zanoni, *Homogeneous photodegradation of C.I. Reactive Blue 4 using a photo-Fenton process under artificial and solar irradiation.* Dyes and Pigments, 2007. **74**(1): p. 127-132.

149. Durán, A., J.M. Monteagudo, and E. Amores, *Solar photo-Fenton degradation of Reactive Blue 4 in a CPC reactor.* Applied Catalysis B: Environmental, 2008. **80**(1–2): p. 42-50.

150. Lucas, M.S. and J.A. Peres, *Degradation of Reactive Black 5 by Fenton/UV-C and ferrioxalate/H_2O_2/solar light processes.* Dyes and Pigments, 2007. **74**(3): p. 622-629.

151. Manenti, D.R., P.A. Soares, A.N. Módenes, F.R. Espinoza-Quiñones, R.A.R. Boaventura, R. Bergamasco, and V.J.P. Vilar, *Insights into solar photo-Fenton process using iron(III)–organic ligand complexes applied to real textile wastewater treatment.* Chemical Engineering Journal, 2015. **266**: p. 203-212.

152. Monteagudo, J.M., A. Durán, J.M. Corral, A. Carnicer, J.M. Frades, and M.A. Alonso, *Ferrioxalate-induced solar photo-Fenton system for the treatment of winery wastewaters.* Chemical Engineering Journal, 2012. **181–182**: p. 281-288.

153. Pereira, J.H.O.S., D.B. Queirós, A.C. Reis, O.C. Nunes, M.T. Borges, R.A.R. Boaventura, and V.J.P. Vilar, *Process enhancement at near neutral pH of a homogeneous photo-Fenton reaction using ferricarboxylate complexes: Application to oxytetracycline degradation.* Chemical Engineering Journal, 2014. **253**: p. 217-228.

154. Vedrenne, M., R. Vasquez-Medrano, D. Prato-Garcia, B.A. Frontana-Uribe, M. Hernandez-Esparza, and J.M. de Andrés, *A ferrous oxalate mediated photo-Fenton system: Toward an increased biodegradability of indigo dyed wastewaters.* Journal of Hazardous Materials, 2012. **243**: p. 292-301.

155. Seraghni, N., S. Belattar, Y. Mameri, N. Debbache, and T. Sehil, *Fe(III)-Citrate-Complex-Induced Photooxidation of 3-Methylphenol in Aqueous Solution.* International Journal of Photoenergy, 2012. **2012**.

156. Silva, M.R.A., A.G. Trovó, and R.F.P. Nogueira, *Degradation of the herbicide tebuthiuron using solar photo-Fenton process and ferric citrate complex at circumneutral pH.* Journal of Photochemistry and Photobiology A: Chemistry, 2007. **191**(2–3): p. 187-192.

157. Miralles-Cuevas, S., I. Oller, J.A.S. Pérez, and S. Malato, *Removal of pharmaceuticals from MWTP effluent by nanofiltration and solar photo-Fenton using two different iron complexes at neutral pH.* Water Research, 2014. **64**: p. 23-31.

158. de Lima Perini, J.A., M. Perez-Moya, and R.F.P. Nogueira, *Photo-Fenton degradation kinetics of low ciprofloxacin concentration using different iron sources and pH.* Journal of Photochemistry and Photobiology A: Chemistry, 2013. **259**: p. 53-58.

159. Li, J., G. Mailhot, F. Wu, and N. Deng, *Photochemical efficiency of Fe(III)-EDDS complex: OH radical production and 17β-estradiol degradation.* Journal of Photochemistry and Photobiology A: Chemistry, 2010. **212**(1): p. 1-7.

160. Huang, W., M. Brigante, F. Wu, K. Hanna, and G. Mailhot, *Development of a new homogenous photo-Fenton process using Fe(III)-EDDS complexes.* Journal of Photochemistry and Photobiology A: Chemistry, 2012. **239**: p. 17-23.

161. Liao, Y., W. Que, Q. Jia, Y. He, J. Zhang, and P. Zhong, *Controllable synthesis of brookite/anatase/rutile TiO_2 nanocomposites and single-crystalline rutile nanorods array.* Journal of Materials Chemistry, 2012. **22**(16): p. 7937-7944.

162. Monteiro, R.A.R., S.M. Miranda, C. Rodrigues-Silva, J.L. Faria, A.M.T. Silva, R.A.R. Boaventura, and V.J.P. Vilar, *Gas phase oxidation of n-decane and PCE by photocatalysis using an annular photoreactor packed with a monolithic catalytic bed coated with P25 and PC500.* Applied Catalysis B: Environmental, 2015. **165**: p. 306-315.

163. Bellardita, M., M. Addamo, A. Di Paola, and L. Palmisano, *Photocatalytic behaviour of metal-loaded TiO_2 aqueous dispersions and films.* Chemical Physics, 2007. **339**(1–3): p. 94-103.

164. Wang, Y., Y. He, Q. Lai, and M. Fan, *Review of the progress in preparing nano TiO_2: An important environmental engineering material.* Journal of Environmental Sciences, 2014. **26**(11): p. 2139-2177.

165. Linsebigler, A.L., G. Lu, and J.T. Yates Jr, *Photocatalysis on TiO_2 surfaces: principles, mechanisms, and selected results.* Chemical reviews, 1995. **95**(3): p. 735-758.

166. Kolen'ko, Y.V., K.A. Kovnir, A.I. Gavrilov, A.V. Garshev, P.E. Meskin, B.R. Churagulov, M. Bouchard, C. Colbeau-Justin, O.I. Lebedev, and G. Van Tendeloo, *Structural, Textural, and Electronic Properties of a Nanosized Mesoporous Zn x Ti1-x O2-x Solid Solution Prepared by a Supercritical Drying Route.* The Journal of Physical Chemistry B, 2005. **109**(43): p. 20303-20309.

167. Benoit-Marquié, F., U. Wilkenhöner, V. Simon, A.M. Braun, E. Oliveros, and M.-T. Maurette, *VOC photodegradation at the gas–solid interface of a TiO_2 photocatalyst: Part I: 1-butanol and 1-butylamine.* Journal of Photochemistry and Photobiology A: Chemistry, 2000. **132**(3): p. 225-232.

168. Araña, J., D. Zerbani, J.H. Melián, D.G. Sousa, O.G. Díaz, and J.D. Rodríguez, *Effect of additives in photocatalytic degradation of commercial azo dye Lanaset Sun Yellow 180.* Photochemical & Photobiological Sciences, 2013. **12**(4): p. 703-708.

169. Eskandarloo, H., A. Badiei, and C. Haug, *Enhanced photocatalytic degradation of an azo textile dye by using TiO_2/NiO coupled nanoparticles: Optimization of synthesis and operational key factors.* Materials Science in Semiconductor Processing, 2014. **27**: p. 240-253.

170. Soutsas, K., V. Karayannis, I. Poulios, A. Riga, K. Ntampegliotis, X. Spiliotis, and G. Papapolymerou, *Decolorization and degradation of reactive azo dyes via heterogeneous photocatalytic processes.* Desalination, 2010. **250**(1): p. 345-350.

171. Kusvuran, E., O. Gulnaz, S. Irmak, O.M. Atanur, H. Ibrahim Yavuz, and O. Erbatur, *Comparison of several advanced oxidation processes for the decolorization of Reactive Red 120 azo dye in aqueous solution.* Journal of Hazardous Materials, 2004. **109**(1–3): p. 85-93.

172. Muruganandham, M. and M. Swaminathan, *Solar driven decolourisation of Reactive Yellow 14 by advanced oxidation processes in heterogeneous and homogeneous media.* Dyes and pigments, 2007. **72**(2): p. 137-143.

173. Arslan, İ., I.A. Balcioğlu, and D.W. Bahnemann, *Advanced chemical oxidation of reactive dyes in simulated dyehouse effluents by ferrioxalate-Fenton/UV-A and TiO_2/UV-A processes.* Dyes and Pigments, 2000. **47**(3): p. 207-218.

174. Alaton, I.A., I.A. Balcioglu, and D.W. Bahnemann, *Advanced oxidation of a reactive dyebath effluent: comparison of O_3, H_2O_2/UV-C and TiO_2/UV-A processes.* Water Research, 2002. **36**(5): p. 1143-1154.

175. Rosario-Ortiz, F.L., E.C. Wert, and S.A. Snyder, *Evaluation of UV/H_2O_2 treatment for the oxidation of pharmaceuticals in wastewater.* Water Research, 2010. **44**(5): p. 1440-1448.

176. He, X., M. Pelaez, J.A. Westrick, K.E. O'Shea, A. Hiskia, T. Triantis, T. Kaloudis, M.I. Stefan, A.A. de la Cruz, and D.D. Dionysiou, *Efficient removal of microcystin-LR by UV-C/H_2O_2 in synthetic and natural water samples.* Water Research, 2012. **46**(5): p. 1501-1510.

177. Jung, Y.J., W.G. Kim, Y. Yoon, J.-W. Kang, Y.M. Hong, and H.W. Kim, *Removal of amoxicillin by UV and UV/H_2O_2 processes.* Science of The Total Environment, 2012. **420**: p. 160-167.

178. Shah, N.S., X. He, H.M. Khan, J.A. Khan, K.E. O'Shea, D.L. Boccelli, and D.D. Dionysiou, *Efficient removal of endosulfan from aqueous solution by UV-C/peroxides: A comparative study.* Journal of Hazardous Materials, 2013. **263, Part 2**: p. 584-592.

179. Lopez, A., A. Bozzi, G. Mascolo, and J. Kiwi, *Kinetic investigation on UV and UV/H_2O_2 degradations of pharmaceutical intermediates in aqueous solution.* Journal of Photochemistry and Photobiology A: Chemistry, 2003. **156**(1–3): p. 121-126.

180. Rekab, K., C. Lepeytre, M. Dunand, F. Dappozze, J.-M. Herrmann, and C. Guillard, *H_2O_2 and/or photocatalysis under UV-C irradiation for the removal of EDTA, a chelating agent present in nuclear waste waters.* Applied Catalysis A: General, 2014. **488**: p. 103-110.

181. Khan, J.A., X. He, N.S. Shah, H.M. Khan, E. Hapeshi, D. Fatta-Kassinos, and D.D. Dionysiou, *Kinetic and mechanism investigation on the photochemical degradation of atrazine with activated H_2O_2, $S_2O_8^{2-}$ and HSO_5^-*. Chemical Engineering Journal, 2014. **252**: p. 393-403.

182. Karci, A., I. Arslan-Alaton, T. Olmez-Hanci, and M. Bekbolet, *Degradation and detoxification of industrially important phenol derivatives in water by direct UV-C photolysis and H_2O_2/UV-C process: A comparative study.* Chemical Engineering Journal, 2013. **224**: p. 4-9.

183. Karci, A., I. Arslan-Alaton, M. Bekbolet, G. Ozhan, and B. Alpertunga, *H_2O_2/UV-C and Photo-Fenton treatment of a nonylphenol polyethoxylate in synthetic freshwater: Follow-up of degradation products, acute toxicity and genotoxicity.* Chemical Engineering Journal, 2014. **241**: p. 43-51.

184. Shu, H.-Y., M.-C. Chang, and H.-J. Fan, *Effects of gap size and UV dosage on decolorization of C.I. Acid Blue 113 wastewater in the UV/H_2O_2 process.* Journal of Hazardous Materials, 2005. **118**(1–3): p. 205-211.

185. Neamtu, M., I. Siminiceanu, A. Yediler, and A. Kettrup, *Kinetics of decolorization and mineralization of reactive azo dyes in aqueous solution by the UV/H_2O_2 oxidation.* Dyes and Pigments, 2002. **53**(2): p. 93-99.

186. Timchak, E. and V. Gitis, *A combined degradation of dyes and inactivation of viruses by UV and UV/H_2O_2.* Chemical Engineering Journal, 2012. **192**: p. 164-170.

187. Kasiri, M.B. and A.R. Khataee, *Photooxidative decolorization of two organic dyes with different chemical structures by UV/H_2O_2 process: Experimental design.* Desalination, 2011. **270**(1–3): p. 151-159.

188. Schrank, S.G., J.N.R.d. Santos, D.S. Souza, and E.E.S. Souza, *Decolourisation effects of Vat Green 01 textile dye and textile wastewater using H_2O_2/UV process.* Journal of Photochemistry and Photobiology A: Chemistry, 2007. **186**(2–3): p. 125-129.

189. Bali, U., E. Çatalkaya, and F. Şengül, *Photodegradation of Reactive Black 5, Direct Red 28 and Direct Yellow 12 using UV, UV/H_2O_2 and UV/H_2O_2/Fe^{2+}: a comparative study.* Journal of Hazardous Materials, 2004. **114**(1–3): p. 159-166.

2 Materials and methods

This second chapter regards the preparation of synthetic textile dyeing wastewaters and the characterization of synthetic and real textile dyeing wastewaters. In addition, it presents an overview of all the chemicals and reagents used in this thesis, a detailed description of the experimental units used to perform all the assays. The employed analytical methods are also herein described.

2.1 Chemical and reagents

Hydrogen peroxide was purchased from Quimitécnica, S.A. (50% (w/v), 1.10 g cm^{-3}), iron sulphate heptahydrated was from Panreac and iron ferric chloride hexahydrated from Merck. Concentrated sulphuric acid and sodium hydroxide, both of analytical grade and used for pH adjustment, were supplied by Pronalab and Merck, respectively. (S,S)-ethylenediamine-N,N`disuccinic acid (EDDS) (35% w/v) was purchased from Aldrich, oxalic acid dihydrate (purity ≥ 98%) and citrate acid monohydrate (100%) were purchased from VWR Prolabo. Heterogeneous photocatalytic experiments used Degussa P-25 (80% anatase and 20% rutile) Titanium Dioxide (TiO_2).

Ultrapure and deionized water was produced by a Millipore® system (Direct-Q model) and a reverse osmosis system (Panice®), respectively. In the biodegradability tests, catalase 0.1 g L^{-1} (Sigma-Aldrich®, 2500 U mg^{-1} bovine liver) was employed for H_2O_2 elimination.

2.2 Analytical methods

All samples, before analysis, except for the determination of TSS, VSS, BOD_5 and COD, were filtered with 0.45μm Nylon filters purchased from Whatman. For the cotton-textile dyeing wastewater and acrylic-textile dyeing wastewater, before analysis, except for the determination of TSS, VSS, BOD_5 and COD, all samples were centrifuged in a HIMAC CT 6E centrifuge at 4000 rpm for 5 minutes. That procedure was necessary since, for these wastewaters, the filtration procedure retained uneven amounts of dyes, which could compromise the results.

2.2.1 Dissolved organic carbon (DOC) and Total dissolved nitrogen (TN)

Dissolved organic carbon (DOC) was measured by NDIR spectrometry in a TC-TOC-TN analyzer equipped with ASI-V auto sampler (Shimadzu, model TOC-VCSN) and calibrated with standard solutions of potassium hydrogen phthalate (total carbon) and a mixture of sodium hydrogen carbonate/sodium carbonate (inorganic carbon).

Total dissolved nitrogen was measured in the same TC-TOC-TN analyzer coupled with a TNM-1 unit (Shimadzu, model TOC-VCSN) by thermal decomposition and NO detection by chemiluminescence method, calibrated with standard solutions of potassium nitrate.

2.2.2 Low-molecular-weight carboxylate anions (LMWCA)

Carboxylic acids were measured by HPLC-DAD (VWR Hitachi ELITE Lachrom com DAD L-2455; Rezex^{TM} ROA-Organic Acid H+ (8%), LC Column 300 × 7.8 mm, Ea). The programme for carboxylic acids determination comprised a 25 min run with a sulfuric acid solution (0.005 N) as mobile phase delivered at a flow rate of 0.5 mL min^{-1}. The method allowed the concurrent detection of 17 carboxylic acids: oxalic, tartronic, maleic, citric, oxamic, tartaric, malic, malonic, glycolic, succinic, shikimic, formic, acetic, glutaric, fumaric, propionic and acrylic.

2.2.3 Inorganic Ions

Inorganic ions (choride, nitrate, nitrite, phosphate, sulphate, fluoride, bromide, lithium, sodium, ammonium, potassium, magnesium and calcium) were measured by ion chromatography (Dionex ICS-2100 and Dionex DX-120 for anions and cations, respectively), using a Dionex Ionpac (columns: AS9-HC/CS12A 4 mm × 250 mm; suppressor: ASRS®300/CSRS®300 4 mm, respectively for anions and cations). The programme for anions/cations determination comprises a 12 min run with 30 mM NaOH/20 mM methanesulfonic acid at a flow rate of 1.5/1.0 mL min^{-1}.

2.2.4 Biochemical oxygen demand (BOD_5) and chemical oxygen demand (COD)

COD concentration was measured by Merck Spectroquant kits (ref: 1.14541.0001). Biochemical oxygen demand (BOD_5) determination was carried out according to Standard Methods using an OXITOP# system (Method 5210 B) [1].

2.2.5 Alkalinity, pH, temperature and conductivity

The alkalinity was evaluated by titration with H_2SO_4 at pH 4.5 (Method 2320 D) [1]. pH, temperature and conductivity were measured using a pH meter HANNA HI 4522 or a pH meter VWR symphony - SB90M5.

2.2.6 Total suspended solids (TSS) and Volatile suspended solids (VSS)

Total suspended solids (TSS) and Volatile suspended solids (VSS) were determinated according to Method 2540 B and Method 2540 E [1], respetively.

2.2.7 Hydrogen peroxide and dissolved iron concentration

Evaluation of H_2O_2 concentration during experiments was performed by metavanadate method, based on the reaction of H_2O_2 with ammonium metavanadate in acid medium, which results in the formation of a red-orange colour peroxovanadium cation, with maximum absorbance at 450 nm [2]. Dissolved iron concentration was determined by colorimetry with 1,10-phenantroline according to ISO 6332 [3].

2.2.8 Colour

Two different methods were used for the colour measurement: i) absorbance at three wavelengths were observed (436, 525, and 620 nm) and then, DFZ_y calculation was made according to the Eq. (2.1), following the method DIN EN ISO 7887 [4]; and ii) platinum-cobalt (Pt-Co) method, at 400 nm wavelength [1]. Besides, in order to evaluate the compliance with the discharge limit as defined in Portuguese Ordinance nº 423/97 [5], for textile wastewaters, the samples were diluted 40 times and visually checked for the presence or absence of colour. And, for mixed wastewater that has two sources, textile wastewater and domestic sewage, the samples were diluted 20 times and visually checked for the presence or absence of colour, as defined in Portuguese Decree Law nº236/98 [6]. Such procedure (uncoloured at 1:20 dilution or 1:40 dilution) cannot be used for the experimental treatment monitoring because it is not a measure and does not have values that may be compared. In order to overcome this limitation, German textile wastewater discharge standards [7] were also considered, since it is used values of absorbance at three wavelengths, 436, 525, and 620 nm according to DIN EN ISO:7887 [4].

$$DFZ_y = 100 \times \left(\frac{E_y}{d} \right) \tag{2.1}$$

where E_y is absorbance at a y wavelength and d is the cell path length in cm.

2.2.9 UV spectra and photometric measurements

The spectrophotometric measurements to obtain the textile wastewaters' UV absortion spectra and to determine the concentration of dissolved iron and of H_2O_2 were carried out with a UNICAM Helios spectrophotometer or a Spectroquant® Pharo 100 (Merck) spectrophotometer.

Due to the textile wastewater´s absorption at the selected wavelengths, a blank/control sample (diluted as for the colorimetric analyses) was always prepared, and the absorbance measured at the same wavelength was used for correction.

2.2.10 Biodegradability tests

A 28 days biodegradability test (Zahn–Wellens test) was performed according to the EC protocol, Directive 88/303/EEC [3]. Activated sludge from a municipal WWTP of Porto, Portugal, previously centrifuged, and mineral nutrients (KH_2PO_4, K_2HPO_4, Na_2HPO_4, NH_4Cl, $CaCl_2$, $MgSO_4$ and $FeCl_3$) were added to the samples. The control and blank experiments were prepared using glucose and distilled water, respectively. The percentage of biodegradation (D_t) was determined by Eq.(2.2) [8]:

$$D_t = \left[1 - \frac{C_t - C_B}{C_A - C_{BA}}\right] \times 100 \tag{2.2}$$

where C_A and C_{BA} are the DOC (mg L^{-1}) in the sample and in the blank, measured 3 hours after the beginning of the experiment, C_t and C_B are the DOC (mg L^{-1}) in the sample and in the blank, measured at the sampling time *t*. The carbon oxidation state (*COS*) parameter was calculated by Eq. (2.3), which is used to evaluate the oxidation degree and effectiveness of the oxidative process [9].

$$COS = 4 - 1.5\frac{COD}{DOC_0} \tag{2.3}$$

where DOC_0 is the initial dissolved organic carbon on the solution (mg C L^{-1}), and *COD* is the chemical oxygen demand at time *t* (mg O_2 L^{-1}).

2.2.11 Photonic flux

The UVA lamp incident light flux was determined by 2-nitrobenzaldehyde (2-NB) actinometry method. The 2-NB actinometry was accomplished adapting the method proposed by Willett and Hites [10]. A 2.5 mM 2-NB solution was prepared using water/ethanol (10:90) as solvent and stored in the dark. A volume of 1250 mL of the above solution was added to the system and recirculated for 10 min in the dark. Then, the UVA lamp was switched on and samples were collected every 5 min from time zero during a total period of 30 min to follow 2-NB concentration. This concentration was determined by HPLC using a VWR Hitachi ELITE LaChrom (Merck-Hitachi, Tokyo, Japan) LC filled with a Merck

LiChrosorb® RP-18 (5 µm) LiChroCART® 125-4 column at 25 °C under isocratic operation. The mobile phase composed of 40:60 (v/v) acetonitrile/0.014 M oxalic acid was injected at a flow rate of 0.6 mL min^{-1}. Samples of 5 µL were injected into the LC and the DAD was set at λ = 258 nm.

The UVC lamps incident light flux was determined by hydrogen peroxide [11] actinometry method. A volume of 1000 mL of water was added to the system and recirculated for 10 min in the dark. A dose of hydrogen peroxide was added (50 mM H_2O_2), the mixture was well homogenized for 10 min and a sample was taken for H_2O_2 concentration control. Then, the UVC lamp was switched on and samples were collected every 5 min from time zero during a total period of 90 min to follow hydrogen peroxide concentration. This concentration was determined by the metavanadate method [2].

The incident flux of the UVA-Visible lamp (xenon arc lamp 1700 Watt air cooled) installed inside the solar radiation simulator (ATLAS, model SUNTEST XLS) was determined by potassium ferrioxalate actinometry method [12]. A volume of 1600 mL of water was added to the system and recirculated for 15 min in the dark. Afterwards, oxalic acid (30 mM) and iron chloride (6 mM) were added. After 15 min another sample was taken for iron concentration control, determined by colorimetry with 1,10-phenantroline according to ISO 6332 [3]. Then, the SUNTEST was turned on (the radiation intensity was set at 500 W m^{-2}) and samples were collected every 2 min from time zero during a total period of 30 min to follow iron concentration. For all actinometry tests, the concentrations-time (CT) plot thus obtained was fitted to a zero-order kinetics and Eq. (2.4) permitted to calculate F_0 (Einstein s^{-1}):

$$F_0 = -\frac{d[\mathrm{CT}]}{dt} \times \left(\frac{1}{\phi}\right) \times V \tag{2.4}$$

where d[CT]$/dt$ is the zero-order kinetics constant (mol L^{-1} s^{-1}), ϕ is the quantum yield of: i) 2-NB at the lamp wavelength (0.41 at 280-405 nm [13]); ii) hydrogen peroxide at the lamp wavelength (1.25 at 253.7 nm [11]) and; iii) ferrioxalate at the lamp wavelength (1.15 at 300-514 nm [12]), and V is the solution volume (L). Afterwards, in all actinometry tests the photonic flux was converted to J s^{-1} (pf) as:

$$pf = F_0 \times E \times N_A \tag{2.5}$$

where E is the energy (J) calculated from Plank's equation for: i) λ_{max} = 360 nm of the UVA lamp; ii) λ_{max} = 253.7 nm of the UVC lamps, and iii) $\lambda_{\bar{x}}$ = 407 nm of the UVA-Visible lamp, and N_A is Avogadro's number (6.022×10^{23} mol^{-1}).

2.2.12 Chemical equilibrium modelling

The molar fractions of the iron species were calculated by the chemical equilibrium modelling system MINEQL+ [14]. Table 2.1 shows oxalic acid ionization reactions, citric acid ionization reactions and EDDS ionization reactions, besides the Fe(III)-sulfate complexes, Fe(III)-hydroxy complexes, Fe(IIII)-chloride complexes and iron-ligand complexes that were also considered for the speciation diagrams.

Table 2.1. Equilibrium reactions and respective equilibrium constants (log K^*) and enthalpies (ΔH) used in the chemical equilibrium modelling system MINEQL+ [14] for speciation diagrams calculation (T = 25 ºC and ionic strength = 0 M[*]).

Reaction	log K^*	Reference	ΔH (kcal mol^{-1})	Reference
$H_2O \leftrightarrow OH^- + H^+$	-13.997	[14]	13.339	[14]
$H^+ + SO_4^{2-} \leftrightarrow HSO_4^-$	1.990	[14]	5.258	[14]
$Na^+ + SO_4^{2-} \leftrightarrow NaSO_4^-$	0.730	[14]	0.239	[14]
Fe(III)-hydroxy complexes				
$Fe^{3+} + H_2O \leftrightarrow FeOH^{2+} + H^+$	-2.187	[14]	9.993	[14]
$Fe^{3+} + 2H_2O \leftrightarrow Fe(OH)_2^+ + 2H^+$	-4.594	[14]	-	
$2Fe^{3+} + 2H_2O \leftrightarrow Fe_2(OH)_2^{4+} + 2H^+$	-2.854	[14]	13.771	[14]
$Fe^{3+} + 3H_2O \leftrightarrow Fe(OH)_{3\,(aq)} + 3H^+$	-12.560	[14]	24.809	[14]
$Fe^{3+} + 4H_2O \leftrightarrow Fe(OH)_4^- + 4H^+$	-21.588	[14]	-	
$3Fe^{3+} + 4H_2O \leftrightarrow Fe_3(OH)_4^{5+} + 4H^+$	-6.288	[14]	15.593	[14]
Fe(III)-sulfate complexes				
$Fe^{3+} + SO_4^{2-} \leftrightarrow FeSO_4^+$	4.050	[14]	5.975	[14]
$Fe^{3+} + 2SO_4^{2-} \leftrightarrow Fe(SO_4)_2^-$	5.380	[14]	4.589	[14]
Fe(IIII)-chloride complexes				
$Fe^{3+} + Cl^- \leftrightarrow FeCl^{2+}$	1.480	[14]	5.497	[14]
$Fe^{3+} + 2Cl^- \leftrightarrow FeCl_2^+$	2.130	[14]	-	
$Fe^{3+} + 3Cl^- \leftrightarrow FeCl_{3\,(aq)}$	1.130	[14]	-	
Oxalic acid protonation/deprotonation equilibria				
$C_2O_4^{2-} + H^+ \leftrightarrow HC_2O_4^-$	4.266	[15]	1.58	[15]
$C_2O_4^{2-} + 2H^+ \leftrightarrow H_2C_2O_4$	5.516	[15]	2.38	[15]
Fe(III)-oxalate complexes				
$Fe^{3+} + H^+ + C_2O_4^{2-} \leftrightarrow FeH(C_2O_4)^{2+}$	9.53	[16]	-	
$Fe^{3+} + C_2O_4^{2-} \leftrightarrow Fe(C_2O_4)^+$	9.40	[16]	1.30	[15]
$Fe^{3+} + 2C_2O_4^{2-} \leftrightarrow Fe(C_2O_4)_2^-$	16.20	[16]	0.70	[15]
$Fe^{3+} + 3C_2O_4^{2-} \leftrightarrow Fe(C_2O_4)_3^{3-}$	20.78	[16]	0.10	[15]
Citric acid protonation/deprotonation equilibria				
$cit^{3-} + H^+ \leftrightarrow Hcit^{2-}$	6.396	[14]	0.80	[14]
$cit^{3-} + 2H^+ \leftrightarrow H_2cit^-$	11.157	[14]	0.31	[14]
$cit^{3-} + 3H^+ \leftrightarrow H_3cit$	14.285	[14]	-0.66	[14]
Fe(III)-citrate complexes				
$Fe^{3+} + cit^{3-} \leftrightarrow Fecit$	13.10	[14]	-	
$Fe^{3+} + H^+ + cit^{3-} \leftrightarrow FeHcit^+$	14.40	[14]	-	
$Fe^{3+} + cit^{3-} \leftrightarrow FeOHcit^- + H^+$	10.33	[17]	-	
EDDS protonation/deprotonation equilibria				
$EDDS^{4-} + H^+ \leftrightarrow H(EDDS)^{3-}$	10.888	[18]	-	
$EDDS^{4-} + 2H^+ \leftrightarrow H_2(EDDS)^{2-}$	18.389	[18]	-	
$EDDS^{4-} + 3H^+ \leftrightarrow H_3(EDDS)^-$	22.690	[18]	-	
$EDDS^{4-} + 4H^+ \leftrightarrow H_4(EDDS)$	25.860	[18]	-	
Fe(III)-EDDS complexes			-	
$Fe^{3+} + EDDS^{4-} \leftrightarrow Fe(EDDS)^-$	24.645	[18]	-	

[*]log *K* values found in the literature at ionic strengths differing from zero were corrected to zero ionic strength using Davies equation [19];

2.2.13 Kinetic modelling

A pseudo-first-order kinetic model was fitted to the experimental data obtained from the kinetic studies by non-linear regression (sofware Fig.P for Windows from Fig.P Software Incorporated). The model parameters were obtained by minimizing the sum of the square deviations between the experimental and predicted values.

2.3 Textile dyeing Wastewaters

Textile manufacturing process, due to the wide range of dyes and chemicals involved, in addition to the different fabrics and colours according to fashion season, contributes to the high variability found in its wastewaters. Many rivers run with colours of the season as unfixed dyes wash off from textile facilities. In order to attend this peculiarity, this thesis focuses on the treatment of four different textile wastewaters. This part regards the preparation and characterization of two synthetic textile dyeing wastewaters as well as the characterization of two real textile dyeing wastewaters.

2.3.1 Synthetic textile dyeing wastewater

2.3.1.1 Synthetic acrylic-textile dyeing wastewater

The synthetic acrylic-textile wastewater was prepared according to the information provided by the dye-house, Erfoc-Acabamentos Têxteis 110 S.A. (Famalicão, Portugal), concerning the amounts of rejected products from dyeing acrylic fibres [20]. Samples of the auxiliary products and dye were kindly supplied by the same company and DyStar Anilinas Têxteis, Unip Ltd (Porto, Portugal). An azo dye denominated C.I. Basic blue 41 with commercial name Astrazon Blue FGGL 300% (Figure 2.1) was used.

Table 2.2 presents the characteristics of the dye and dyeing auxiliary products employed in the preparation of the synthetic textile wastewater. The auxiliary chemical Sera®Con N-VS, non-ionic, is used as acid donor for dyeing acrylic, wool and polyamide fibres. On the other hand, the chemical Sera®Tard A-AS, together with sodium sulphate, is used as a retarder for dyeing acrylic fibres and blends with cationic dyestuffs. The non-ionic dispersing agent Sera®Sperce M-IW is used in the polyacrylic yarn dyeing process with cationic dyestuffs. The auxiliary product Sera®Lube M-CF, non-ionic amides polymers in aqueous solution, is a crease inhibitor and lubricant for dyeing and scouring processes.

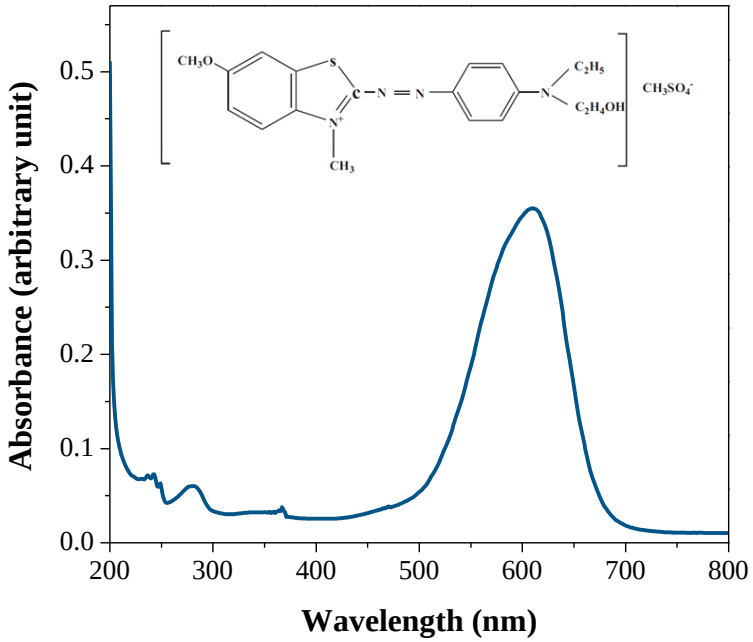

Figure 2.1. UV-Vis absorption spectra of the wastewater and the chemical structure of Astrazon Blue FGGL 300%.

The textile auxiliary products do not fix in the fibres, being 100% discharged with the wastewaters generated. The only exception is sodium sulphate, in which 90% of the total amount used is eliminated by the wastewater. Auxiliary chemicals Sera® Tard A-AS and Sera® Con N-VS are responsible for 30% and 26%, respectively, of the total dissolved organic carbon content in the acrylic-textile dyeing wastewater. The dye represents only 3.5% (10.4 mg C L^{-1}) of the total DOC.

Table 2.2. Characteristics of the dye and dyeing auxiliary products present in the synthetic acrylic-textile dyeing wastewater.

Dyeing Product	Chemical Characteristics	Wastewater Characteristics		
		Concentration	pH	DOC
Astrazon Blue FGGL 300%	Azo dye - Basic blue 41	0.03 g L^{-1}	8.3	10.4 mg C L^{-1}
Sera® Con N-VS	Acid carboxylic ester	0.13 mL L^{-1}	6.0	78.2 mg C L^{-1}
Sera® Tard A-AS	alkyl dimethyl benzyl ammonium chloride	0.33 mL L^{-1}	6.8	89.4 mg C L^{-1}
Sera® Sperse M-IW	alkyl polyglycol ether	0.19 mL L^{-1}	7.3	58.5 mg C L^{-1}
Sera® Lube M-CF	Polymeric amines	0.79 mL L^{-1}	6.2	50.4 mg C L^{-1}
Sodium Sulphate	Na_2SO_4	0.91 g L^{-1}	8.0	0.0 mg C L^{-1}

The acrylic-textile dyeing wastewater was prepared taking into account that in each particular case different volumes of water and chemicals are employed along the process, and the ratio between the amount of fibre to be dyed and the water used in the bath was assumed to be 1:10 (kg:L). Finally, the percentage of these products unfixed in the textile fibres (and therefore released into the water) should

be also taken into account. Figure 2.2 shows the temperature profiles of the respective dyeing process and the moment of addition of each component.

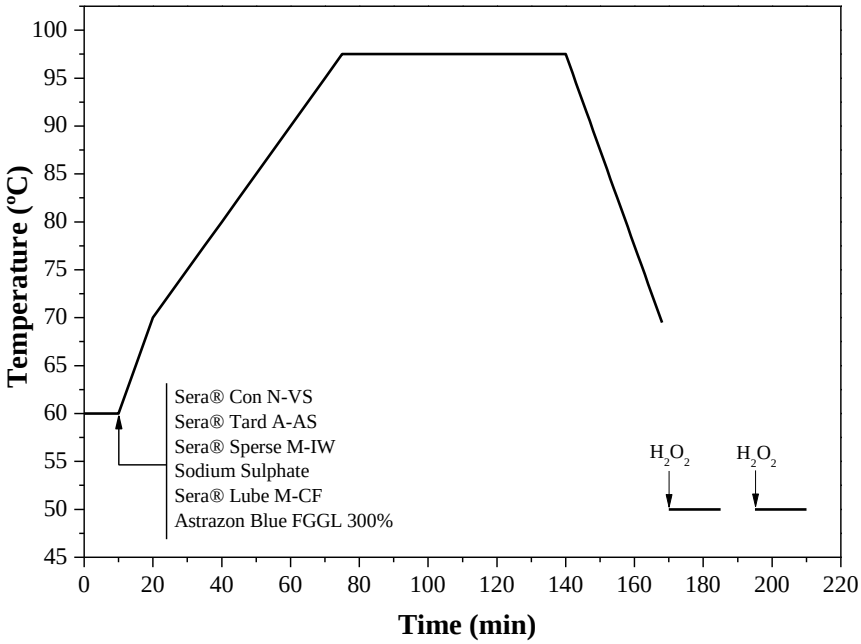

Figure 2.2. Scheme of acrylic fibres dyeing process.

Table 2.3 shows a brief characterisation of the synthetic acrylic-textile dyeing wastewater. The wastewater presents a blue colour, which is mainly related to the dye colour, originating a maximum absorbance peak at 610 nm. The wastewater presents a neutral pH value and moderated organic load, where more than 96.5% of DOC is related to the dyeing auxiliary products and 3.5% is due to the dye. The low BOD_5/COD ratio indicates low biodegradability of this textile wastewater, which was confirmed by the Zahn-Wellens test.

Table 2.3. Characteristics of the synthetic acrylic-textile dyeing wastewater.

Parameters		Units	Values
pH		Sorënsen scale	6.8
Conductivity		mS cm^{-1}	1.3
COD – Chemical oxygen demand		mg O_2 L^{-1}	836
BOD_5 – Biochemical oxygen demand		mg O_2 L^{-1}	30
BOD_5/COD ratio		-	0.03
DOC - Dissolved organic carbon		mg C L^{-1}	295
Biodegradability - Zahn-Wellens test		%	27
Absorbance at 254 nm		-	0.043
Colour	DFZ_{436nm}	m^{-1}	2.8
	DFZ_{525nm}	m^{-1}	10.1
	DFZ_{620nm}	m^{-1}	34.2
	Pt-Co Scale	mg L^{-1}	24

Table 2.3. Characteristics of the synthetic acrylic-textile dyeing wastewater.

Parameters	Units	Values
Visual colour dilution 1:40	-	visible
Formic Acid	mg CH_2O_2 L^{-1}	64
Chloride	mg Cl^- L^{-1}	41
Sulphate	mg SO_4^{2-} L^{-1}	593
Total Dissolved Nitrogen	mg N L^{-1}	20
Nitrate	mg N-NO_3^- L^{-1}	3.8
Nitrite	mg N-NO_2^- L^{-1}	0.8
Ammonia	mg N-NH_4^+ L^{-1}	0.1
Phosphate	mg P-PO_4^{3-} L^{-1}	0.8
Sodium	mg Na^+ L^{-1}	344
Magnesium	mg Mg^{2+} L^{-1}	6
Calcium	mg Ca^{2+} L^{-1}	34
Total suspended solids	mg TSS L^{-1}	55
Volatile suspended solids	mg VSS L^{-1}	45

2.3.1.2 Synthetic polyester-cotton dyeing textile wastewater

The synthetic polyester-cotton dyeing wastewater was prepared according to the information provided by DyStar Anilinas Têxteis, Unip Ltd (Porto, Portugal), concerning the amounts of rejected products from dyeing for both fibres. Samples of the auxiliary products and dye were also kindly supplied by the same company. Polyester and cotton wastewaters were singly prepared and after that, mixed based on the average Portuguese textile cotton/polyester mixture: 70% cotton dyeing wastewater and 30% polyester dyeing wastewater. The polyester-cotton dyeing wastewater was prepared taking into account that in each particular case different volumes of water and chemicals are employed along the process, and the ratio between the amount of fibre to be dyed and the water used in the bath was assumed to be 1:10 (kg:L). Finally, the percentage of these products unfixed in the textile fibres (and therefore released into the water) should be also taken into account. Two disperse dyes (Dianix Blue K-FBL and Dianix Orange K3G) were selected for the preparation of the synthetic polyester dyeing wastewater, as they are commonly used for dyeing polyester fibres (Figure 2.3). The selection of these dyes also took into account the rising of disperse dyes consumption in the world following the increase in demand for polyester fibres.

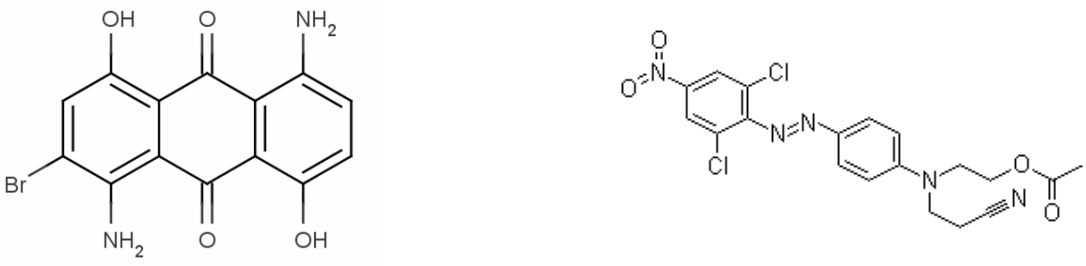

Figure 2.3. Chemical structure of dyes used in the preparation of the polyester dyeing wastewater: Dianix Blue KFBL (left) and Dianix Orange K3G (right).

Figure 2.4 shows the temperature profiles of the polyester dyeing, including the steps of the preparation of the dyebaths and the reduction cleaning process, as well as the moment of addition of each component. Table 2.4 presents the concentration and characteristics of the dyes and dyeing auxiliary products employed in the preparation of the synthetic polyester dyeing textile wastewater.

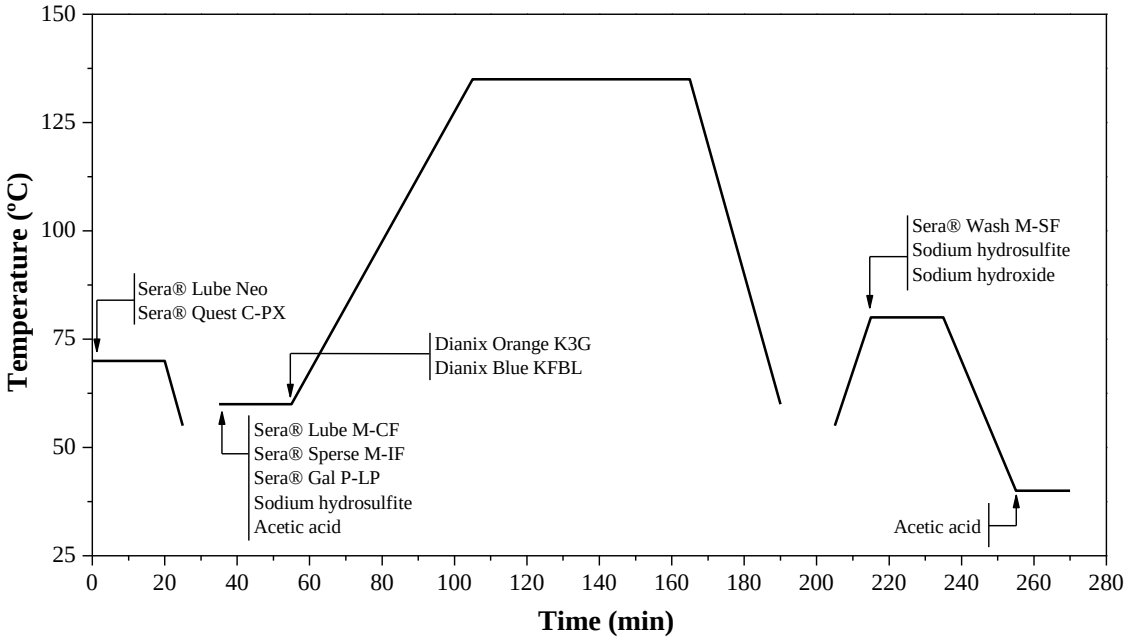

Figure 2.4. Scheme of polyester fibres dyeing process.

Two reactive (Procion Yellow H-EXL gran and Procion Deep Red HEXL gran) dyes were selected for the preparation of the synthetic cotton dyeing wastewater (its chemical structure is not available). These dyes were selected due to several aspects: i) the high consumption for dyeing fibres in Portugal; ii) the low degree of fixation on the fibres, and consequently high quantities are rejected and will be present in

the wastewater; iii) the majority of reactive dyes are not easily removed by conventional processes, such as biological treatment and coagulation/flocculation using inorganic coagulants.

Table 2.4. Characteristics of the dyes and dyeing auxiliary products present in the synthetic polyester dyeing textile wastewater.

Step	Dyeing Product	Chemical Characteristics	Wastewater Characteristics		
			Concentration	pH	DOC
Fibre preparation	Sera® Lube Neo	Creasing prevent	2.0 g L^{-1}	7.0	53.2 mg C L^{-1}
	Sera® Quest C-PX	Polymer combination; dispersing and sequestering agent	1.0 g L^{-1}	7.4	27.0 mg C L^{-1}
Dyeing	Sera® Lube M-CF	Polymeric amide; Lubricant and crease inhibitor	2.0 g L^{-1}	6.6	38.2 mg C L^{-1}
	Sera® Sperse M-IF	Sodium naphthalene sulfonate condensate; dispersing agent	1.5 g L^{-1}	6.8	187.6 mg C L^{-1}
	Sera® Gal P-LP	Alkyl polyglycol derivative; dispersing agent	2.0 g L^{-1}	6.6	183.3 mg C L^{-1}
	Sodium hydrosulphite	Sodium dithionite; reducing agent	3.0 g L^{-1}	3.1	0.0 mg C L^{-1}
	Acetic acid	$C_2H_4O_2$	150.0 mg L^{-1}	4.0	25.6 mg C L^{-1}
	Dianix Orange K3G	Disperse Orange 30	22.0 mg L^{-1}	6.4	5.7 mg C L^{-1}
	Dianix Blue KFBL	Disperse Blue 56	8.0 mg L^{-1}	6.5	2.3 mg C L^{-1}
Reduction cleaning	Sera® Wash M-SF	Non-foaming detergent	450.0 mg L^{-1}	6.8	66.5 mg C L^{-1}
	Sodium hydroxide	NaOH	5.0 g L^{-1}	13.5	0.0 mg C L^{-1}
	Acetic acid	$C_2H_4O_2$	150.0 mg L^{-1}	3.6	69.3 mg C L^{-1}
	Sodium hydrosulphite	Sodium dithionite; reducing agent	3.0 g L^{-1}	3.1	0.0 mg C L^{-1}

Figure 2.5 shows the temperature profiles of the cotton dyeing, the preparation of the dyebaths and the reduction cleaning process, as well as the moment of addition of each component. Table 2.5 presents the concentration and characteristics of the dyes and dyeing auxiliary products employed in the preparation of the synthetic cotton dyeing textile wastewater.

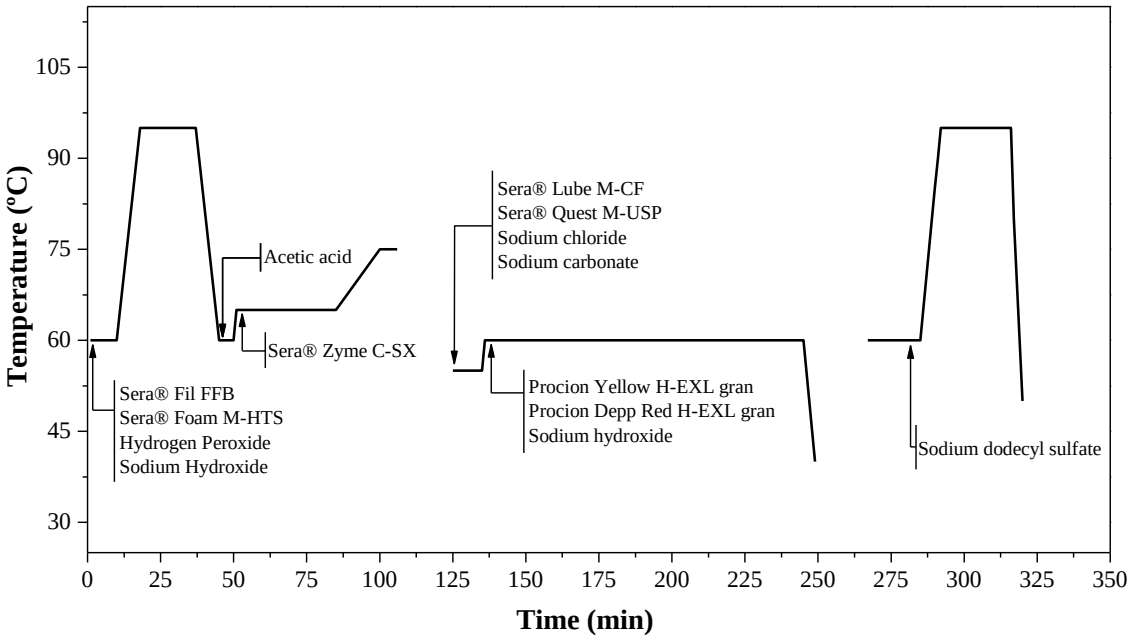

Figure 2.5. Scheme of cotton fibres dyeing process.

Table 2.5. Characteristics of the dyes and dyeing auxiliary products present in the synthetic cotton dyeing textile wastewater.

Step	Dyeing Product	Chemical Characteristics	Wastewater Characteristics		
			Concentration	pH	DOC
Fibre preparation	Sera® Foam M-HTS	Mineral oil; emulsifier	450.0 mg L^{-1}	6.5	56.3 mg C L^{-1}
	Sera® Fil FFB	Ethoxylate and phosphonated alcohol	450.0 mg L^{-1}	6.2	26.3 mg C L^{-1}
	Sera® Zyme C-SX	Aqueous enzyme;	1.8 g L^{-1}	6.4	2.4 mg C L^{-1}
	Acetic acid	$C_2H_4O_2$	250.0 mg L^{-1}	3.7	48.6 mg C L^{-1}
	Hydrogen peroxide	H_2O_2	1.3 g L^{-1}	3.0	0.0 mg C L^{-1}
	Sodium hydroxide	NaOH	1.2 g L^{-1}	13.5	0.0 mg C L^{-1}
Dyeing	Sera® Lube M-CF	Polymeric amide; Lubricant/crease inhibitor	2.0 g L^{-1}	6.6	38.2 mg C L^{-1}
	Sera® Quest M-USP	organophosphonic acid	1.0 g L^{-1}	6.6	4.4 mg C L^{-1}
	Sodium chloride	NaCl	20.0 g L^{-1}	7.0	0.0 mg C L^{-1}
	Sodium carbonate	Na_2CO_3	5.0 g L^{-1}	9.2	0.0 mg C L^{-1}
	Procion Yellow H-EXL gran	Reactive Yellow 138:1	5.0 mg L^{-1}	6.4	3.0 mg C L^{-1}
	Procion Red H-EXL gran	Azo dye	15.0 mg L^{-1}	6.4	5.6 mg C L^{-1}
	Sodium hydroxide	NaOH	1.2 g L^{-1}	13.5	0.0 mg C L^{-1}
Washing	Sodium dodecyl sulphate	$NaC_{12}H_{25}SO_4$	225.0 mg L^{-1}	6.6	51.6 mg C L^{-1}

Table 2.6 shows a brief characterisation of the synthetic polyester-cotton dyeing textile wastewater. The wastewater presents a red colour (Figure 2.6), and a neutral pH value and high organic load, where more than 97% of DOC is related to the dyeing auxiliary products and 3% is due to the dyes. The wastewater moderate biodegradability percentage, in large part, is related to the constituents of the cotton dyeing wastewater.

Table 2.6. Characteristics of the synthetic polyester and cotton textile dyeing wastewaters and their mixture.

Parameters		Units	Polyester	Cotton	Polyester-Cotton
pH		Sorënsen scale	7.4	10.1	8.4
Conductivity		mS cm^{-1}	3.7	5.0	4.5
COD – Chemical oxygen demand		mg O_2 L^{-1}	2530	1112	1450
BOD_5 – Biochemical oxygen demand		mg O_2 L^{-1}	700	350	440
BOD_5/COD ratio		-	0.28	0.31	0.30
DOC - Dissolved organic carbon		mg C L^{-1}	659	254	354
Biodegradability - Zahn-Wellens test		%	64	89	81
Absorbance at 254 nm		-	4.255	0.954	2.003
Colour	DFZ_{436nm}	m^{-1}	3.5	21.5	16.7
	DFZ_{525nm}	m^{-1}	1.7	20.4	17.5
	DFZ_{620nm}	m^{-1}	1.5	1.2	0.2
	Pt-Co Scale	mg L^{-1}	75	260	230
Visible colour dilution 1:40		-	not visible	visible	visible
Chloride		mg Cl^- L^{-1}	42	1900	1470
Sulphate		mg SO_4^{2-} L^{-1}	934	292	737
Total Dissolved Nitrogen		mg N L^{-1}	11	9	10
Nitrate		mg N-NO_3^- L^{-1}	7	7	7
Nitrite		mg N-NO_2^- L^{-1}	4	2	3
Ammonia		mg N-NH_4^+ L^{-1}	<0.5	<0.5	<0.5
Phosphate		mg P-PO_4^{3-} L^{-1}	6	<0.5	<0.5
Sodium		mg Na^+ L^{-1}	1723	1998	1772
Magnesium		mg Mg^{2+} L^{-1}	21	16	17
Calcium		mg Ca^{2+} L^{-1}	150	73	91
Total suspended solids		mg TSS L^{-1}	38	141	98
Volatile suspended solids		mg VSS L^{-1}	36	103	83

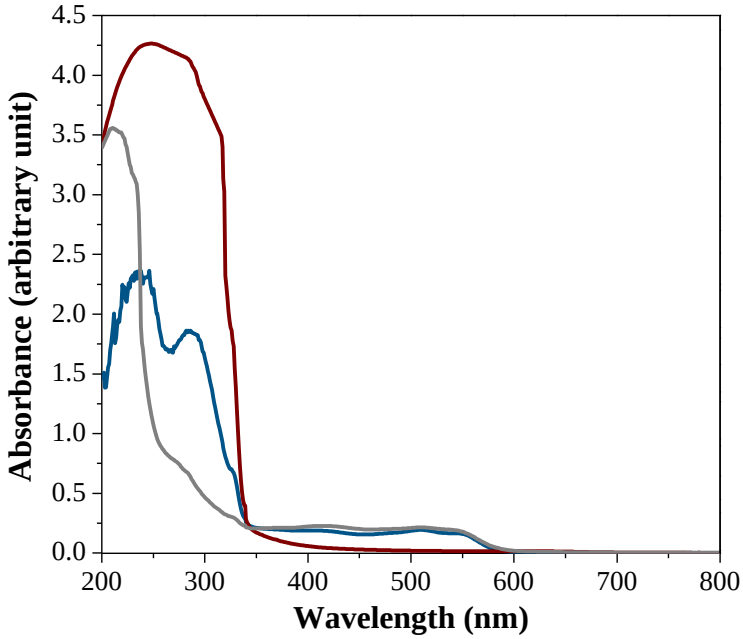

Figure 2.6. UV-Vis absorption spectra of (—) polyester-dyeing, (—) cotton-dyeing and (—) polyester-cotton dyeing textile wastewater.

2.3.2 Real textile wastewaters

Two different real textile-dyeing wastewaters were also used in this work. The first one, cotton-textile dyeing wastewater, was collected in a textile company located at the north of Portugal, before being subjected to any form of treatment. The wastewater selected is exclusively originating from the dyeing process of cotton fibres. The wastewater presents a lilac colour, resulting from the mixture of different reactive dyes, originating a maximum absorbance peak at 641 nm (Figure 2.7). The wastewater presents a relatively high pH value and temperature, and a moderate organic load (COD = 684 mg O_2 L^{-1} and DOC = 152 mg C L^{-1}). High values were found for total dissolved nitrogen and ammonia, 117 mg L^{-1} and 79 mg L^{-1}, respectively.

According to the Zahn-Wellens test, the wastewater presents a moderate biodegradability, mainly attributed to: i) presence of the textile biodegradable auxiliaries (e.g. acetic acid and others) used on cotton dyeing process and, ii) some organic compounds leached from the cotton fibres during the chemical washing (scouring process), which removes natural wax and non-fibrous impurities (e.g. the remains of seed fragments) from the fibres and any added soiling or dirt.

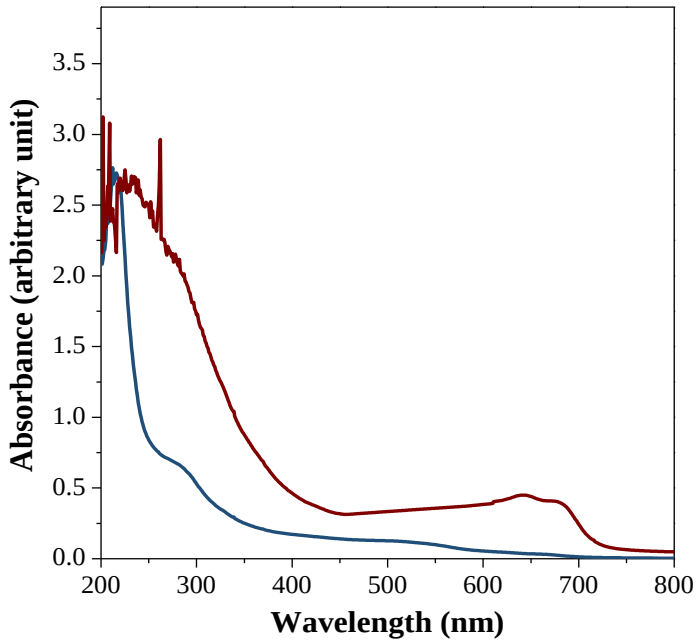

Figure 2.7. UV-Vis absorption spectra of (—) cotton-dyeing textile wastewater and (—) bio-treated textile wastewater.

Another textile wastewater sample was collected after the biological oxidation and filtration steps in a wastewater treatment plant (WWTP), located in northern Portugal. The raw wastewater that enters in the WWTP has two main sources: 70% textile wastewater and 30% domestic sewage. Before being discharged to the sewerage system and further diluted with the urban wastewaters, still in the textile facilities, the textile wastewater goes through a neutralization procedure, normally with CO_2 injection. The WWTP comprises the following treatment units: (i) equalization tanks; (ii) activated sludge reactors; (iii) sedimentation tanks; (iv) filtration columns and (v) ozonation system. Samples were collected at the outlet of filtration columns.

The bio-treated textile wastewater presents a near neutral pH value, a low organic load (COD = 107 mg O_2 L^{-1} and DOC = 32 mg C L^{-1}). High values were found for chloride and sodium ions, 613 mg Cl^- L^{-1} and 659 mg Na^+ L^{-1}, respectively. The wastewater shows a reddish colour, equivalent to 160 mg Pt-Co L^{-1}. Furthermore, it was observed a major absorbance on DFZ_{436nm} than DFZ_{525nm} and DFZ_{620nm}, which indicates high predominance of violet colour and weak presence of green and orange colours on the wastewater absorption spectra (Figure 2.7). Table 2.7 presents the main physicochemical characteristics for both real textile-dyeing wastewaters.

Table 2.7. Main physicochemical characteristics of real textile-dyeing wastewaters.

Parameters		Units	Cotton dyeing	WWTP
pH		Sorensen scale	8.2	7.8
Temperature		ºC	32.5	30.0
Conductivity		mS cm^{-1}	4.3	6.9
COD - Chemical oxygen demand		mg O_2 L^{-1}	684	107
BOD_5 - Biochemical oxygen demand		mg O_2 L^{-1}	255	-
BOD_5 /COD ratio		-	0.37	-
DOC – Dissolved organic carbon		mg C L^{-1}	152	32
Biodegradability - Zahn-Wellens test		%	40	-
Absorbance at 254 nm		-	2.459	0.841
Colour	DFZ_{436nm}	m^{-1}	34.1	14.5
	DFZ_{525nm}	m^{-1}	34.5	11.4
	DFZ_{620nm}	m^{-1}	41.3	4.5
	Pt-Co Scale	mg L^{-1}	500	160
Visual colour dilution 1:20		-	-	visible
Visual colour dilution 1:40		-	visible	-
Chloride		mg Cl^- L^{-1}	105	613
Sulphate		mg SO_4^{2-} L^{-1}	35	121
Total Dissolved Nitrogen		mg N L^{-1}	117	13
Nitrate		mg N-NO_3^- L^{-1}	<0.2	9.4
Nitrite		mg N-NO_2^- L^{-1}	5.3	2.7
Ammonia		mg N-NH_4^+ L^{-1}	79	0.8
Phosphate		mg P-PO_4^{3-} L^{-1}	6.7	<0.05
Sodium		mg Na^+ L^{-1}	495	659
Potassium		mg K^+ L^{-1}	42	<0.05
Magnesium		mg Mg^{2+} L^{-1}	11	27
Calcium		mg Ca^{2+} L^{-1}	20	61
Total suspended solids		mg TSS L^{-1}	193	9.6
Volatile suspended solids		mg VSS L^{-1}	171	6.0

2.4 Experimental units

The experiments were carried out in four different experimental units: i) a lab-scale sunlight simulator photoreactor; ii) a lab-scale lamp photoreactor; iii) a CPC solar pilot plant and iv) a lab-scale biological reactor. All experimental units have been installed at the Chemical Engineering Department of the Faculty of Engineering, University of Porto (FEUP), Portugal. The detailed description of all reactors and the corresponding experimental procedures can be seen below.

2.4.1 Lab-scale sunlight simulator photoreactor

The lab-scale sunlight simulator photoreactor (Figure 2.8) incorporates the following systems: i) a solar radiation simulator (ATLAS, model SUNTEST XLS) with 1100 cm^2 of exposition area, a 1700 Watt

air-cooled xenon arc lamp, a daylight filter and quartz filter with IR coating; ii) a compound parabolic collector (CPC) with 0.026 m^2 of illuminated area with anodized aluminum reflectors and a borosilicate tube (Schott-Duran type 3.3, Germany, cut-off at 280 nm, internal diameter 46.4 mm, length 161 mm and thickness 1.8 mm); iii) one glass vessel (capacity of 1.5 L) with a cooling jacket coupled to a refrigerated thermostatic bath (Lab. Companion, model RW-0525G) to ensure a constant temperature during the experiment; iv) a magnetic stirrer (Velp Scientifica, model ARE) to ensure complete homogenization of the solution inside the glass vessel; v) one gear pump (Ismatec, model BVP-Z) to recirculate the water between the CPC and the glass vessel; vi) pH and temperature meter (VWR symphony - SB90M5). All the systems are connected by Teflon tubing.

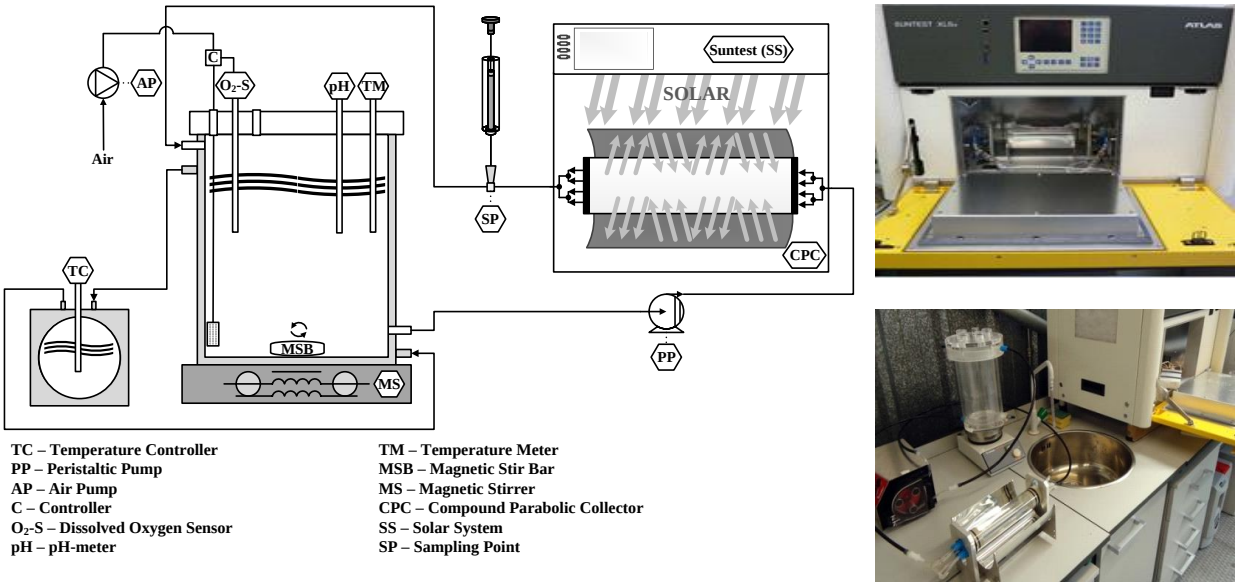

Figure 2.8. Schematic representation of the experimental set-up and views of the lab-scale sunlight simulator photoreactor.

For the set of experiments described in Chapters 3 and 4, the UV irradiance was measured by a broadband UV radiometer (Kipp & Zonen B.V., model CUV5), which was placed inside the sunlight simulator at the same level as that of the photoreactor center. The radiometer was plugged into a handheld display unit (Kipp & Zonen B.V., model Meteon) to record the incident irradiance (W_{UV} m^{-2}) in the wavelength range from 280 to 400 nm. The amount of accumulated UV energy ($Q_{UV,n}$ kJ L^{-1}) received on any surface in the same position with regard to the sun, per unit of volume of water inside the reactor, in the time interval Δt is calculated using the Eq. (2.6):

$$Q_{UV,n} = Q_{UV,n-1} + \Delta t_n \overline{UV}_{G,n} \frac{A_r}{1000 \times V_t}; \quad \Delta t_n = t_n - t_{n-1} \tag{2.6}$$

where t_n is the time corresponding to *n*-water sample (s), V_t the total reactor volume (L), A_r the illuminated collector surface area (m^2) and $\overline{UV}_{G,n}$ the average solar ultraviolet radiation (W m^{-2}) measured during the period Δt_n (s).

For the set of experiments described in Chapter 5 and 6, the UV radiance was determined by potassium ferrioxalate actinometry [12], considering that the radiation source used in the lab-scale sunlight simulator photoreactor is positioned in the external side. The radiation intensity was always set at 500 W m^{-2}, and the photonic flux reaching the reaction volume was 1.81 J_{UV} s^{-1}. The amount of accumulated UV energy ($Q_{UV,n}$, in kJ L^{-1}) inside the reactor in a time per unit of volume of solution was calculated from Eq. (2.7):

$$Q_{UV,n} = pf \frac{t_n}{V_t \times 1000} \tag{2.7}$$

where *pf* is the photonic flux reaching the system (J_{UV} s^{-1}), t_n is the time corresponding to the *n* sample (s), V_t is the solution volume (L) and 1000 is a conversion factor (J kJ^{-1}).

2.4.2 Lab-scale lamp photoreactor

The experiments regarding the use of UVC or UVA radiation were carried out in a lab-scale lamp photoreactor (Figure 2.9), consisting of: i) a gear pump (Ismatec, model BVP-Z); ii) a cylindrical glass vessel equipped with a cooling jacket coupled to a refrigerated thermostatic bath (Lab. Companion, model RW-0525G); iii) a magnetic stirrer (Velp Scientifica, model ARE); iv) a pH and temperature meter (VWR symphony - SB90M5); v) a borosilicate tube (Schott-Duran type 3.3, Germany, cut-off at 280 nm, internal diameter 70 mm, length 200 mm and thickness 1.8 mm) associated to a concentric inner quartz tube with 22 mm external diameter filled with a) a Philips TL 6W/08 fluorescent blacklight blue lamp (photonic flux = 0.65 J_{UV} s^{-1}); b) a Philips G6T5 6W UVC Germicidal Sterilamp (photonic flux = 0.65 J_{UV} s^{-1}); c) a Philips G5T5 4W UVC Germicidal Steriamp (photonic flux = 0.51 J_{UV} s^{-1}); d) a Philips G5 11W UVC Germicidal Steriamp (photonic flux = 1.22 J_{UV} s^{-1}).

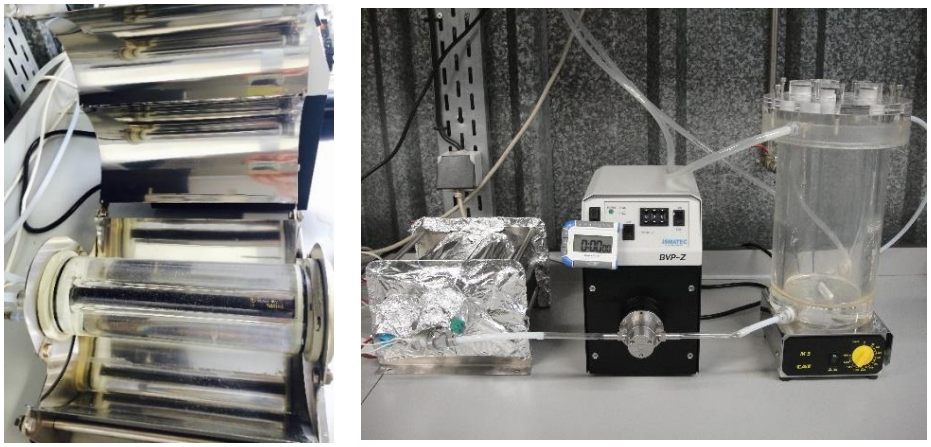

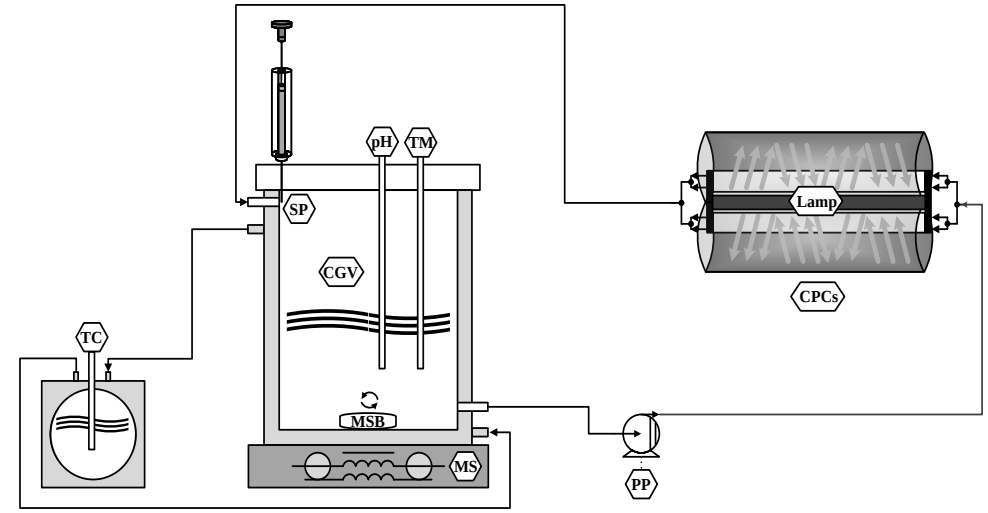

TC – Temperature Controller
SP – Sampling Point
pH – pH-meter
TM – Temperature Meter
CGV – Cylindrical Glass Vessel
MSB – Magnetic Stir Bar
MS – Magnetic Stirrer
PP – Peristaltic Pump
CPCs – Compound Parabolic Collectors Structure
UVA – UVC, UVA or Visible Lamp

Figure 2.9. Views of the lab-scale lamp photoreactor and the schematic representation of the experimental set-up.

Two polypropylene caps with four equidistant inlets and outlets ensured a better distribution of the feed stream throughout the photoreactor. The borosilicate tube was allocated in the focus of two stainless steel reflectors (double CPC), each one consisting of two truncated parabolas and exhibiting a total dimension of 19.5 cm × 21.0 cm, one at the bottom and another at the top, allowing illumination along the total tubular reactor perimeter and minimizing radiation losses. For the lab-scale lamp photoreactor, the radiation source is located inside the tubular reactor, provided by an UVC or UVA lamp. In this case the incident light flux was determined by hydrogen peroxide [11] (UVC lamps) and 2-nitrobenzaldehyde [21] (UVA lamp) actinometry methods. The amount of accumulated UV energy inside the reactor was calculated from Eq. (2.7).

2.4.3 CPC solar pilot plant

The solar driven AOPs experiments were carried out in a CPC solar pilot plant installed at the roof of the Chemical Engineering Department of the Faculty of Engineering, University of Porto (FEUP), Portugal (Figure 2.10 and Figure 2.11). The solar collector consists of a CPC unit (0.91 m^2) of four borosilicate (Duran) tubes (Schott–Duran type 3.3, Germany, cut-off at 280 nm, internal diameter 50 mm, length 1500 mm and width 1.8 mm) connected in series by polypropylene junctions, with their CPC mirrors in anodized aluminum, supported by a aluminum structure, oriented to south and tilted 41° (local latitude).

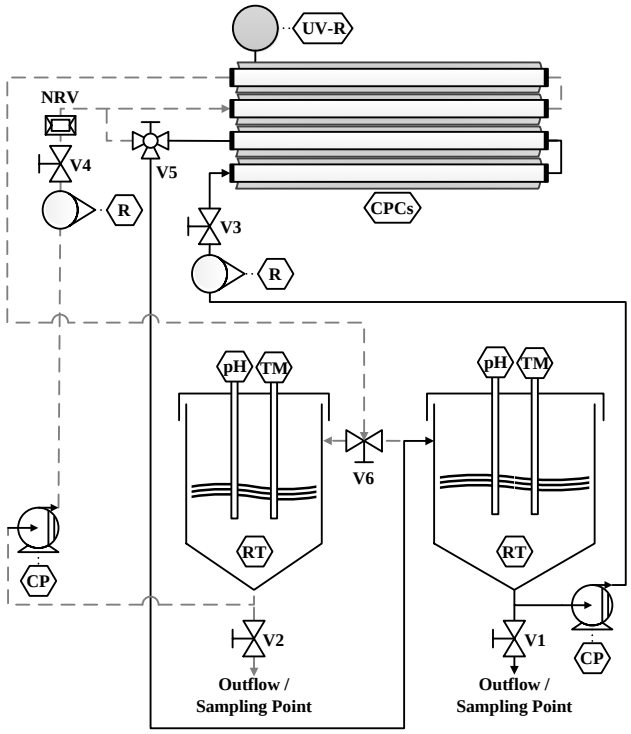

TM – Temperature meter; **pH** – pH-meter; **CPCs** – Compound Parabolic Collectors; **UV-R** – UV radiometer; **RT** - Recirculation tank; **CP** – Centrifugal pump; **R** – Rotameter; **NRV** – Non-return valve; **TC** – temperature controller; **PP** – peristaltic pump; **AP** – air pump; **C** – controller; **O_2-S** – dissolved oxygen sensor; **pH** – pH meter; **TM** – temperature meter; **CPC** – Compound Parabolic Collector; **SS** – Suntest System; **SP** – sampling point.

(——) Main path; (---) Alternative path.

Figure 2.10. Schematic representation of the CPC solar pilot plant.

The pilot plant has also two recirculation tanks (10 L and 20 L), two recirculation pumps (35 L min^{-1}), two flow meters, five polypropylene valves and an electric board for process control. The pilot plant can be operated in two ways: using the total CPCs area (0.91 m^2) or using 0.455 m^2 of CPCs area individually, giving the possibility of performing two different experiments at the same time and under the same solar radiation conditions. The intensity of solar UV radiation is measured by a global UV radiometer (ACADUS 85-PLS) mounted on the pilot plant with the same inclination, which provides data in terms of incident W_{UV} m^{-2}. The amount of accumulated UV energy ($Q_{UV,n}$ kJ L^{-1}) received on

any surface in the same position with regard to the sun, per unit of volume of water inside the reactor, in the time interval Δt is calculated using the Eq. (2.6).

Figure 2.11. Views of the CPC solar pilot plant.

2.4.4 Lab-scale biological reactor

The experimental set-up (Figure 2.12) used to carry out the biological experiments consists in: i) a cylindrical glass vessel (capacity of 3.0 L) equipped with a cooling jacket coupled to a refrigerated thermostatic bath (Lab. Companion, model RW-0525G); ii) a mechanical stirrer (VWR, VOS 14 overhead stirrer); iii) pH and temperature meter (VWR symphony - SB90M5); iv) an air pump to supply oxygen to the activate sludge, through air diffusers located on the bottom of the reactor.

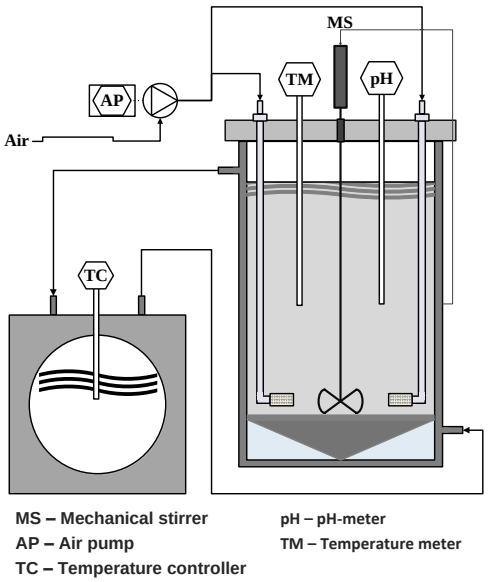

Figure 2.12. Schematic representation of the lab-scale biological reactor.

2.5 Experimental procedure

The experimental procedure varied according to the employed photocatalytic processes and experimental units. Therefore, the detailed description of the experimental procedures was separated according to the employed processes for each experimental unit. The range of operational conditions also can be seen here. However, each chapter presents the detailed operational conditions applied to each set of experiments.

2.5.1 Lab-scale sunlight simulator photoreactor

The lab-scale sunlight simulator photoreactor was used in the sets of experiments presented in Chapters 3, 4, 5 and 6. In this experimental unit, three experimental procedures were performed, namely: i) Fenton´s reaction, ii) UVA-Vis/Fe^{2+}/H_2O_2 and, iii) UVA-Vis/Fe^{3+}/H_2O_2/Organic ligands.

i) Fenton´s Reaction

The temperature set-point of the refrigerated thermostatic bath was controlled to keep the desired wastewater temperature (30ºC). The recirculation glass vessel was filled with 1.0 L of wastewater, which was pumped to the CPC unit and homogenized by recirculation in the closed system during 15 min. pH was adjusted to 2.8 using sulphuric acid and another sample was taken 15 min later to confirm the desired value. Afterwards, ferrous sulphate was added to obtain the desired iron concentration (60 mg L^{-1}), and another sample was taken after 15 min for iron concentration control.

Finally, H_2O_2 was added (500 mg L^{-1}/14.7 mM), and its concentration was maintained between 200 and 500 mg L^{-1} (5.9-14.7 mM), during the entire runs, through the addition of small amounts of hydrogen peroxide to compensate the consumption. Samples were taken at successive time intervals to evaluate the progress of the Fenton´s reaction and different analytical determinations were performed.

ii) UVA-Vis/Fe^{2+}/H_2O_2

In the photo-Fenton reactions, the recirculation glass vessel was filled with 1.0-1.5 L of wastewater, which was pumped to the CPC unit and homogenized by recirculation in the closed system. The temperature set-point of the refrigerated thermostatic bath was controlled to keep the desired wastewater temperature (between 10-50ºC). pH was adjusted using sulphuric acid (between 2.4-5.5) and another sample was taken 15 min later. Afterwards, ferrous sulphate was added to obtain the desired iron concentration (between 2-100 mg L^{-1}), and another sample was taken after 15 min for iron concentration

control. The SUNTEST was turned on and the first dose of hydrogen peroxide was added (between 24-500 mg L^{-1}/0.7-14.7 mM). The H_2O_2 concentration was maintained within the desired range along the reactions course (between 50-100 mg L^{-1}/1.5-2.9 mM, 100-200 mg L^{-1}/2.9-5.9 mM and 200-500 mg L^{-1}/5.9-14.7 mM), by replenishing the consumed amount. In some reactions, only one dose of H_2O_2 was added at the beginning and no more additions were performed. Samples were taken at pre-defined times to evaluate the degradation process.

iii) UVA-Vis/Fe^{3+}/H_2O_2/Organic ligand

A similar procedure was followed in the UV/Fe^{3+}/H_2O_2/Organic ligand reactions. The temperature set-point of the refrigerated thermostatic bath was controlled to keep the desired wastewater temperature (between 20-40ºC). The recirculation glass vessel was filled with 1.0-1.5 L of wastewater, which was pumped to the CPC unit and homogenized by recirculation in the closed system during 15 min in the darkness. Oxalic acid, citrate acid or EDDS was added at iron/organic ligand molar ratios of 1:3; 1:1 and 1:1, respectively, and another sample was taken 15 min later. Additional assays were carried out using different iron/oxalate molar ratios (between 1:3-1:10). pH was adjusted using sulphuric acid (between 2.8-5.5) and another sample was taken 15 min later.

Afterwards, ferrous sulphate was added to obtain the desired iron concentration (between 2-80 mg L^{-1}), and another sample was taken after 15 min for iron concentration control. The SUNTEST was turned on and, the first dose of hydrogen peroxide was added (between 71-2,319 mg L^{-1}/2.1-68.2 mM). The H_2O_2 concentration was maintained within intervals 50-100, 100-200 or 200-500 mg L^{-1} (1.5-2.9, 2.9-5.9 or 5.9-14.7 mM) along the reaction course, by replenishing the consumed amount. Samples were taken at pre-defined times to evaluate the degradation process.

2.5.2 Lab-scale lamp photoreactor

The lab-scale lamp photoreactor was used in the sets of experiments presented in Chapters 5 and 6. In this experimental unit, four experimental procedures were performed, namely: i) UVC photolysis, ii) H_2O_2, iii) UVC/H_2O_2 and iv) UVC or UVA/Fe^{2+}/H_2O_2.

i) UVC photolysis

In the UVC photolysis, the set-point of the refrigerated thermostatic bath was controlled to keep the desired wastewater temperature (30ºC) and the recirculation glass vessel was filled with 1.5 L of wastewater. pH was adjusted using sulphuric acid (2.8 and natural wastewater pH) and a sample was

taken 15 min later. The UVC lamp was turned on and samples were taken at pre-defined times to evaluate the degradation process.

ii) H_2O_2

The recirculation glass vessel was filled with 1.5 L of wastewater, which was pumped to CPC unit and homogenized by recirculation in the closed system. The set-point of the refrigerated thermostatic bath was controlled to keep the desired wastewater temperature (30ºC). pH was adjusted using sulphuric acid (2.8 and natural wastewater pH) and another sample was taken 15 min later. Then, only one dose of hydrogen peroxide was added (between 235-1,768 mg L^{-1}/6.9-52 mM). Samples were taken at pre-defined times to evaluate the decolourisation process.

iii) UVC/H_2O_2

In the UVC/H_2O_2 reactions, the recirculation glass vessel was filled with 1.5 L, which was pumped to the CPC unit and homogenized by recirculation in the closed system. The set-point of the refrigerated thermostatic bath was controlled to keep the desired wastewater temperature (between 15-45ºC). pH was adjusted using sulphuric acid (2.8; 5.0; 11.0 and natural wastewater pH) and another sample was taken 15 min later. The UVC lamp was turned on and, the first dose of hydrogen peroxide was added (between 24-340 mg L^{-1}/0.7-10 mM) and if necessary, other doses were added. Samples were taken at pre-defined times to evaluate the decolourisation process.

iv) UVC or UVA/Fe^{2+}/H_2O_2

In the UVC or UVA/Fe^{2+}/H_2O_2 reactions, a similar procedure was followed. The recirculation glass vessel was filled with 1.5 L, which was pumped to the CPC unit and homogenized by recirculation in the closed system. The set-point of the refrigerated thermostatic bath was controlled to keep the desired wastewater temperature (between 15-45ºC). pH was adjusted using sulphuric acid (pH 2.8) and a sample was taken 15 min later, and then ferrous sulphate was added to obtain the desired iron concentration (between 0.5-2.0 mg L^{-1}). After that, another sample was taken 15 min later. The lamp was turned on and, the first dose of hydrogen peroxide was added (between 24-340 mg L^{-1}/0.7-10 mM) and if necessary, other doses were added. Samples were taken at pre-defined times to evaluate the decolourisation process.

2.5.3 CPC solar pilot plant

The CPC solar pilot plant was used in the set of experiment presented in Chapters 3 and 4. In this experimental unit, five experimental procedures were performed, namely: i) UVA-Vis photolysis, ii) UVA-Vis/H_2O_2, iii) UVA-Vis/Fe^{2+}/H_2O_2, iv) UVA-Vis/Fe^{2+}/H_2O_2/Oxalic acid and, v) UVA-Vis/TiO_2.

i) UVA-Vis photolysis

A volume of 15 L of wastewater was added to the recirculation tank of the CPC units and homogenized by turbulent recirculation, during 15 min in darkness (a first control sample was taken for further characterization). Preliminary acidification of the textile wastewater to approximately pH 4.5 was performed, in order to eliminate the carbonates and bicarbonates, just before uncovering the CPCs. Samples were taken at successive time intervals to evaluate the progress of the oxidation.

ii) UVA-Vis/H_2O_2

A volume of 15 L of wastewater was added to the recirculation tank of the CPC units and homogenized by turbulent recirculation, during 15 min in darkness, and a control sample was taken. Preliminary acidification of the textile wastewater to approximately 4.5 was performed. The first dose of hydrogen peroxide (500 mg L^{-1}/14.7 mM) was added. The CPCs were uncovered and samples were taken at different time intervals to evaluate the degradation process. Hydrogen peroxide concentration was maintained between 200 and 500 mg L^{-1} (5.9-14.7 mM), during the entire runs, through the addition of small amounts of hydrogen peroxide to compensate the consumption.

iii) UVA-Vis/Fe^{2+}/H_2O_2

A volume of 15 L of wastewater was added to the recirculation tank of the CPC units and homogenized by turbulent recirculation, during 15 min in darkness (a first control sample was taken). pH was adjusted to 2.8 with sulfuric acid and another sample was taken 15 min later. Afterwards, iron salt (60 mg L^{-1}) was added, the mixture was well homogenized for 15 min and a sample was taken for iron concentration control. Finally, the first dose of hydrogen peroxide (500 mg L^{-1}/14.7 mM) was added, the CPCs were uncovered and samples were taken at different time intervals to evaluate the degradation process. Hydrogen peroxide concentration was maintained between 200 and 500 mg L^{-1} (5.9-14.7 mM), through the addition of small amounts of hydrogen peroxide to compensate the consumption.

iv) UVA-Vis/Fe^{3+}/H_2O_2/Oxalic acid

22 L of wastewater was added to the recirculation tank, which was pumped to the CPC unit and homogenized by recirculation in the closed system during 15 min in the darkness (a first control sample was taken for further characterization). Afterwards, oxalic acid (iron/oxalate molar ratio of 1:3) and ferric chloride (40 mg L^{-1}) were added. After 15 min another sample was taken for iron and oxalic concentrations control. Finally, H_2O_2 was added (200 mg L^{-1}/5.9 mM), the CPCs were uncovered and the reaction started.

Hydrogen peroxide concentration was maintained between 100 and 200 mg L^{-1} (2.9-5.9 mM), during the entire runs, through the addition of small amounts of hydrogen peroxide to compensate the consumption. In all cases, samples were taken at successive time intervals to evaluate the progress of the photo-Fenton reaction and different analytical determinations were performed.

v) UVA-Vis/TiO_2 and UVA-Vis/TiO_2/H_2O_2

A volume of 15 L of wastewater was added to the recirculation tank of the CPC units and homogenized by turbulent recirculation, during 15 min in darkness (a first control sample was taken). pH was adjusted to 4.5 with sulfuric acid and another sample was taken 15 min later. After taking the sample, titanium dioxide was added up to a concentration of 200 mg L^{-1} and the mixture recirculated for more than 15 min. For UVA-Vis/TiO_2 tests, a sample was collected just before uncovering the CPC units, in order to evaluate the pollutants adsorption onto the catalyst surface.

In the case of UVA-Vis/TiO_2/H_2O_2 experiments, a sample was as well collected and hydrogen peroxide (500 mg L^{-1}/14.7 mM) was added to the mixture TiO_2/wastewater, just before uncovering the CPCs. Hydrogen peroxide concentration was maintained between 200 and 500 mg L^{-1} (5.9-14.7 mM), during the entire runs, through the addition of small amounts of hydrogen peroxide to compensate the consumption. In both tests, samples were taken at successive time intervals to evaluate the progress of the photocatalytic oxidation.

2.5.4 Lab-scale biological reactor

The lab-scale biological reactor was used in the sets of experiments presented in Chapters 5 and 6. In the first cycle, the reactor was inoculated with 200 mL of well-settled activated sludge from a municipal wastewater treatment plant and mineral nutrients were added (KH_2PO_4, K_2HPO_4, Na_2HPO_4, NH_4Cl, $CaCl_2$, $MgSO_4$ and $FeCl_3$). Then, a volume of 2 L of textile wastewater was added to the aerobic

biological system and agitated for 5 days for acclimation of the microorganisms. In subsequent cycles, the reactor was fed with 1.5 L of wastewater to compensate the amount of treated wastewater discharged. The set-point of the refrigerated thermostatic bath was controlled to keep the desired wastewater temperature (30ºC). The pH was maintained between 6.5 and 8.0 and the dissolved oxygen in a 2–4 mg O_2 L^{-1} range. Samples were taken at successive time intervals to evaluate the progress of the biodegradation, until DOC values were constant, which happened, in average, approximately after 44 h (0.5 h feeding, 40 h reaction, 3 h sedimentation, 0.5 h discharge).

2.6 References

1. Clesceri, L.S., A.E. Greenberg, and A.D. Eaton, *Standard Methods for Examination of Water & Wastewater*. 21 ed, ed. A.P.H.A. (APHA). 2005.
2. Nogueira, R.F.P., M.C. Oliveira, and W.C. Paterlini, *Simple and fast spectrophotometric determination of H_2O_2 in photo-Fenton reactions using metavanadate.* Talanta, 2005. **66**(1): p. 86-91.
3. OECD, *OECD Guidelines for the Testing of Chemicals. Test Nº. 302B: Inherent Biodegradability: Zahn–Wellens/ EMPA*. 1992, OECD Publishing.
4. 7887, D.E.I., *DIN EN ISO 7887:2012-04, Wasserbeschaffenheit - Untersuchung und Bestimmung der Färbung*. 2012, Deutsches Institut für Normung - DIN.
5. Portugal, *Portaria nº423/97 de 25 de Junho, Diário da República-I Série*. 1997. p. 3111-3112.
6. Portugal, *Decreto-Lei nº.236/98*. 1998, Ministério do Ambiente: Diário da República. p. 47.
7. Abwasserverordnung, *Verordnung über Anforderungen an das Einleiten von Abwasser in Gewässer (Abwasserverordnung - AbwV)*, B. I, Editor. 2004, Bundesministerium der Justiz: Bundesrepublik Deutschland.
8. EPA, *US Environmental Protection Agency, Prevention Pesticides and Toxic Substances (7101)*, in *Fates, Transport and Transformation Test Guidelines OPPTS 835.3200 Zahn–wellens/EMPA Test*. 1996, EPA: Washington, DC.
9. Amat, A.M., A. Arques, F. Galindo, M.A. Miranda, L. Santos-Juanes, R.F. Vercher, and R. Vicente, *Acridine yellow as solar photocatalyst for enhancing biodegradability and eliminating ferulic acid as model pollutant.* Applied Catalysis B: Environmental, 2007. **73**(3–4): p. 220-226.
10. Willett, K.L. and R.A. Hites, *Chemical Actinometry: Using o-Nitrobenzaldehyde to Measure Lamp Intensity in Photochemical Experiments.* Journal of Chemical Education, 2000. **77**(7): p. 900.
11. Nicole, I., J. De Laat, M. Dore, J. Duguet, and C. Bonnel, *Utilisation du rayonnement ultraviolet dans le traitement des eaux: mesure du flux photonique par actinométrie chimique au peroxyde d'hydrogène.* Water Research, 1990. **24**(2): p. 157-168.
12. Kuhn, H., S. Braslavsky, and R. Schmidt, *Chemical actinometry (IUPAC technical report).* Pure and Applied Chemistry, 2004. **76**(12): p. 2105-2146.
13. Galbavy, E.S., K. Ram, and C. Anastasio, *2-Nitrobenzaldehyde as a chemical actinometer for solution and ice photochemistry.* Journal of Photochemistry and Photobiology A: Chemistry, 2010. **209**(2–3): p. 186-192.
14. Schecher, W.D. and D.C. McAvoy, *MINEQL+: A Chemical Equilibrium Modeling System, Version 4.6 for Windows*. 2007, Environmental Research Software: Hallowell, Maine, United States.
15. Smith, R.M. and A.E. Martell, *NIST Critically Selected Stability Constants of Metal Complexes Database, Version 8.0 for Windows*. 2004, Texas A&M University: United States.
16. Vincze, L. and S. Papp, *Individual quantum yields of $Fe^{3+}OX_n^{2-}H_m^{+}$ complexes in aqueous acidic solutions ($OX^{2-} \equiv C_2O_4^{2-}$, n = 1 – 3, m = 0,1).* Journal of Photochemistry, 1987. **36**(3): p. 289-296.

17. Field, T.B., J.L. McCourt, and W.A.E. McBryde, *Composition and Stability of Iron and Copper Citrate Complexes in Aqueous Solution.* Canadian Journal of Chemistry, 1974. **52**(17): p. 3119-3124.

18. Orama, M., H. Hyvonen, H. Saarinen, and R. Aksela, *Complexation of [S,S] and mixed stereoisomers of N,N[prime or minute]-ethylenediaminedisuccinic acid (EDDS) with Fe(iii), Cu(ii), Zn(ii) and Mn(ii) ions in aqueous solution.* Journal of the Chemical Society, Dalton Transactions, 2002(24): p. 4644-4648.

19. Sawyer, C.N., P.L. McCarty, and G.F. Parkin, *Chemistry for Environmental Engineering and Science, fifth ed.* Vol. 5th edition. 2003, New York, United States: McGraw-Hill.

20. Rodrigues, C.S.D., L.M. Madeira, and R.A.R. Boaventura, *Synthetic textile dyeing wastewater treatment by integration of advanced oxidation and biological processes – Performance analysis with costs reduction.* Journal of Environmental Chemical Engineering, 2014. **2**(2): p. 1027-1039.

21. Moreira, F.C., S. Garcia-Segura, R.A.R. Boaventura, E. Brillas, and V.J.P. Vilar, *Degradation of the antibiotic trimethoprim by electrochemical advanced oxidation processes using a carbon-PTFE air-diffusion cathode and a boron-doped diamond or platinum anode.* Applied Catalysis B: Environmental, 2014. **160–161**: p. 492-505.

3 Insights into Real Cotton-Textile Dyeing Wastewater Treatment using Solar Advanced Oxidation Processes[1]

Different advanced oxidation processes (AOPs) were applied to the treatment of a real cotton-textile dyeing wastewater as a pre-oxidation step to enhance the biodegradability of recalcitrant compounds, which can be further oxidized by a biological process. Tests were conducted on a lab-scale prototype using artificial solar radiation and at pilot scale with compound parabolic collectors using natural solar radiation. The efficiency of the photo-Fenton reaction was evaluated for different process variables such as iron concentration, pH, temperature and irradiance.

[1]This Chapter is based on the research article: "Soares, P., Silva, T.C.V., Manenti, D., Souza, S.A.G.U., Boaventura, R.R., and Vilar V.P., *Insights into real cotton-textile dyeing wastewater treatment using solar advanced oxidation processes.* Environmental Science and Pollution Research, 2014. 21(2): p. 932-945."

3.1 Introduction

The Portuguese textile industry is an important economic pillar representing 21% of all exports from this country [1]. The textile industry is one of the largest consumers of water in the world, and consequently, one of the largest producers of wastewaters (until 300 L kg^{-1} material) [2]. Textile wastewaters resulting mainly from dyeing and finishing processes, present different dyes with a complex organic structure, surfactants, detergents and inorganic salts, which constitutes a risk for the environment and ecosystems when unloaded improperly in the environment [3]. During the last years, publications regarding textile wastewaters treatment rose continuously. Although biological treatments present competitive costs they are usually ineffective in degradation of complex organic dye molecules. Scientific community research interests have been focused in biological, membrane and advanced oxidation processes (AOPs) technologies for the treatment of textile wastewaters (Figure 1.3). Other processes, such as, coagulation/flocculation, activated carbon adsorption and membrane separation can only transfer the contaminants from one phase to another leaving the problem essentially unsolved [4]. Therefore, much attention has been paid to the development of wastewater treatment techniques that lead to the complete destruction of the dye molecules into CO_2, H_2O and mineral acids or transforming them into biodegradable compounds that can be easily eliminated by biological oxidation. In this context, advanced oxidation processes (AOPs) are recognized by their effectiveness in the treatment of recalcitrant wastewaters through the formation of highly reactive and non-selective hydroxyl radicals [5, 6]. Several studies propose the use of AOPs for the treatment of textile wastewater: UVA-Vis/H_2O_2 [7]; UVA-Vis/TiO_2 [8, 9]; UVA-Vis/TiO_2/H_2O_2 [10]; Fe^{2+}/H_2O_2 [5, 11, 12]; UVA-Vis/Fe^{2+}/H_2O_2 [13].

However, the costs involved with the energy requirements and chemicals, especially when the goal is the complete mineralisation, are high and eventually make these technologies non-competitive [6]. An alternative is the use of solar radiation, as UV-Vis photon source [14] and applies the chemical oxidation as a pre-treatment to enhance the biodegradability through the degradation of the most persistent organic compounds [15, 16]. The photo-Fenton reaction was found to be the best solar driven AOP in the treatment of different recalcitrant wastewaters [17, 18], including real textile wastewaters, which is related to the higher light sensitivity up to 580 nm, corresponding to 35% of solar radiation spectrum. Therefore, this work compares the efficiency of different AOPs in the treatment of a real cotton-textile dyeing wastewater at pilot scale under natural sunlight and evaluates the influence of the main photo-Fenton reaction variables, such as iron concentration, pH, temperature and irradiance, in a lab-scale prototype under controlled conditions using artificial solar radiation.

3.2 Material and Methods

All the chemicals and reagents used in this work, the detailed description of the lab-scale and pilot-plant scale experimental units, along with the corresponding experimental procedures followed, and, finally, the employed methods can be consulted in Chapter 2. The detailed operational conditions of the assays performed in this chapter are shown in Table 3.1.

Table 3.1. Operational conditions of the assays performed.

	Experiments	I	TDI	T	pH
Natural sunlight	UVA-Vis	19.0[a]	-	17.7[c]	4.51[d]
	UVA-Vis/H_2O_2	25.0[a]	-	25.2[c]	4.47[d]
	UVA-Vis/TiO_2	17.0[a]	-	25.8[c]	4.46[d]
	UVA-Vis/TiO_2/H_2O_2	22.1[a]	-	22.3[c]	4.45[d]
	UVA-Vis/Fe^{2+}/H_2O_2	26.0[a]	47.1[b]	40.7[c]	2.80[d]
Artificial sunlight	UVA-Vis/Fe^{2+}/H_2O_2	44	20 40 60 80 100	30	2.8
	UVA-Vis/Fe^{2+}/H_2O_2	44	60	30	2.4 2.8 3.2 3.6 4.5
	UVA-Vis/Fe^{2+}/H_2O_2	44	60	10 20 30 40 50	2.8
	UVA-Vis/Fe^{2+}/H_2O_2	22 44 68	60	30	2.8

[a]Average irradiation intensity (W m^{-2}); [b]Average total dissolved iron (mg L^{-1}); [c]Average liquid temperature (ºC); [d]Average pH.

3.3 Results and discussion

3.3.1 Cotton-textile dyeing wastewater characterization

Table 2.7 (Materials and methods – Chapter 2) shows a brief characterization of the cotton-textile dyeing wastewater used in this study, which was collected in a textile company located at the north of Portugal, before being subjected to any form of treatment. The wastewater selected is exclusively originating from the dyeing process of cotton fibres. The wastewater presents a lilac colour, resulting from the mixture of different reactive dyes, originating a maximum absorbance peak at 641 nm. The wastewater presents a relatively high pH value (8.2) and temperature (32.5ºC), and a moderate organic load (COD = 684 mg O_2 L^{-1} and DOC = 152 mg C L^{-1}).

High values were found for total dissolved nitrogen and ammonia, 117 mg L^{-1} and 79 mg L^{-1}, respectively. The concentration of chloride and sulphate ions is relatively small when compared with other textile wastewaters [19, 20]. According to the Zahn-Wellens test, the wastewater presents a moderate biodegradability, mainly attributed to presence of the textile biodegradable auxiliaries (e.g. acetic acid and others) used on cotton dyeing process. Besides, organic compounds leached from the cotton fibres during the chemical washing (scouring process) also can enhance the content of biodegradable organic matter in the wastewater.

3.3.2 Solar Driven AOPs

Preliminary treatment studies at CPC solar pilot plant (Figure 2.10, Materials and methods – Chapter 2) were performed in order to compare the efficiency of different advanced oxidation processes (UVA-Vis; UVA-Vis/TiO_2; UVA-Vis/H_2O_2; UVA-Vis/TiO_2/H_2O_2 and UVA-Vis/Fe^{2+}/H_2O_2) under natural solar conditions. Figure 3.1 shows the mineralisation profiles for all the solar driven AOPs tested and Table 3.1 presents the operational conditions.

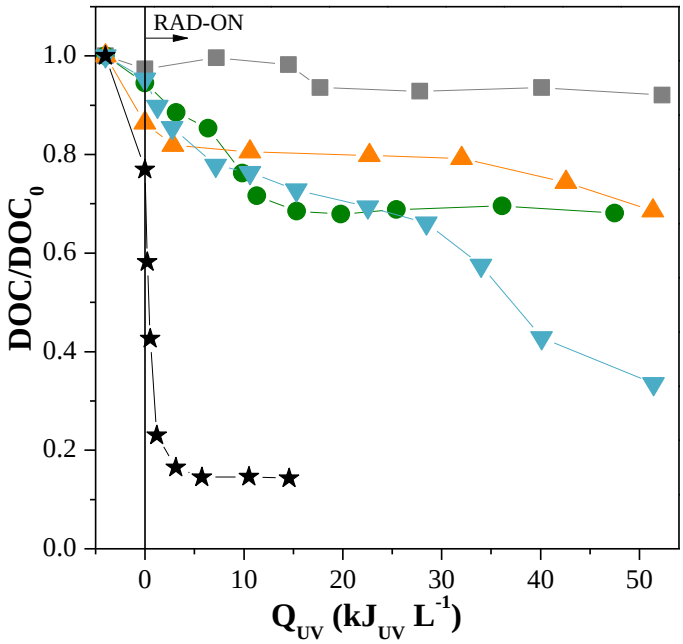

Figure 3.1. Mineralisation of the cotton-textile dyeing wastewater: comparison between the different AOPs evaluated. ■ – UVA-Vis process; ● – UVA-Vis/TiO_2; ▲ – UVA-Vis/H_2O_2; ▼ - UVA-Vis/TiO_2/H_2O_2; ★ – UVA-Vis/Fe^{2+}/H_2O_2.

Preliminary acidification of the textile wastewater to approximately pH 4.5 was performed for all tests, with exception of photo-Fenton (pH = 2.8), in order to eliminate the carbonates and bicarbonates, which act as $^{\bullet}OH$ scavengers, leading to formation of less reactive species [21]. The acidification procedure to pH 4.5 or 2.8 (photo-Fenton reaction) resulted in a DOC abatement of approximately 13% and 23%, attributed to the formation of small amount of foam (which can retain a certain amount of organic matter) and precipitation of some organic compounds as observed by the sludge formation.

Table 3.2 shows clearly that the solar photo-Fenton process is the most efficient of all solar AOPs studied, achieving 85.5% mineralisation after 5.8 kJ_{UV} L^{-1} and consuming 68.4 mM of H_2O_2. The initial reaction rate of the photo-Fenton reaction, considering a pseudo-first-order reaction kinetics, is more than 47 times higher than that of the UVA-Vis/TiO_2/H_2O_2 system. Similar results have been also reported by Vilar et al., [19] for the treatment of a real textile wastewater.

Table 3.2. Operational conditions and pseudo-first-order kinetic constants of the assays performed.

	Experiments	I	TDI	T	pH	Kinetic parameters			
						DOC degradation		H_2O_2 consumption	
						k^e	R^2	$k_H{}^f$	R^2
Natural sunlight	UVA-Vis	19.0[a]	-	17.7[c]	4.51[d]	0.0010 ± 0.0001	0.995	-	-
	UVA-Vis/H_2O_2	25.0[a]	-	25.2[c]	4.47[d]	0.0050 ± 0.0004	0.999	0.20 ± 0.01	0.999
	UVA-Vis/TiO_2	17.0[a]	-	25.8[c]	4.46[d]	0.014 ± 0.002	0.993	-	-
	UVA-Vis/TiO_2/H_2O_2	22.1[a]	-	22.3[c]	4.45[d]	0.020 ± 0.002	0.995	1.20 ± 0.08	0.994
	UVA-Vis/Fe^{2+}/H_2O_2	26.0[a]	47.1[b]	40.7[c]	2.80[d]	1.0 ± 0.6	0.997	9 ± 2	0.984
Artificial sunlight	UVA-Vis/Fe^{2+}/H_2O_2	44	20	30	2.8	0.081 ± 0.009	0.999	2.6 ± 0.3	0.997
			40			0.11 ± 0.02	0.997	3.9 ± 0.2	0.999
			60			0.26 ± 0.04	0.992	5 ± 1	0.983
			80			0.25 ± 0.05	0.991	7 ± 2	0.994
			100			0.30 ± 0.03	0.996	7 ± 3	0.979
	UVA-Vis/Fe^{2+}/H_2O_2	44	60	30	2.4	0.13 ± 0.01	0.994	5.1 ± 0.5	0.994
					2.8	0.26 ± 0.04	0.992	5 ± 1	0.983
					3.2	0.26 ± 0.04	0.997	6.6 ± 0.9	0.990
					3.6	0.24 ± 0.01	0.999	6.6 ± 0.8	0.996
					4.5	-	-	2.1 ± 0.1	0.999
	UVA-Vis/Fe^{2+}/H_2O_2	44	60	10	2.8	0.029 ± 0.008	0.960	1.5 ± 0.1	0.994
				20		0.043 ± 0.007	0.988	3.8 ± 0.1	0.999
				30		0.26 ± 0.04	0.992	5 ± 1	0.983
				40		0.28 ± 0.02	0.999	7 ± 2	0.988
				50		0.49 ± 0.04	0.996	9 ± 2	0.980
	UVA-Vis/Fe^{2+}/H_2O_2	22	60	30	2.8	0.32 ± 0.06	0.990	7.9 ± 0.9	0.996
		44				0.26 ± 0.04	0.992	5 ± 1	0.983
		68				0.4 ± 0.2	0.999	6 ± 2	0.988

[a]Average irradiation intensity (W m^{-2}); [b]Average total dissolved iron (mg L^{-1}); [c]Average liquid temperature (ºC); [d]Average pH; [e]Pseudo-first-order kinetic constant (L kJ^{-1}); [f]H_2O_2 consumption rate (mmol kJ^{-1});.

3.3.3 Photo-Fenton reaction: Processes variables and their influence

As the photo-Fenton reaction showed the highest efficiency in the treatment of the cotton-textile wastewater, considering all the AOPs applied, the influence of the main reaction variables, such as, iron concentration, pH, temperature and radiation intensity, was evaluated under controlled conditions in a lab-scale photoreactor with a sunlight simulator (Figure 2.8, Materials and methods – Chapter 2). Table 3.2 presents the photo-Fenton reaction conditions used in all sets of experiments and pseudo-first-order kinetic constants.

3.3.3.1 Iron concentration

Malato Rodríguez et al. [22] reported that the optimum iron concentration for the solar photo-Fenton reactions, using CPCs with borosilicate tubes with an internal diameter of 46.4 mm, is between 0.2 and 0.5 mM (amount of iron necessary to absorb all the UV-Vis photons). However, if there are other light-absorbing species present in solution, especially in coloured wastewaters, such as textile effluent (dyes presents an aromatic structure that absorbs UV and visible light), this decreases the number of photons that can be absorbed by the iron complexes, being necessary higher iron concentrations (above 1 mM) to achieve the desired reaction rates [23]. Therefore, the optimum iron concentration must be optimized for each particular application, aiming at cost reduction and reaction rate maximization.

Figure 3.2 presents the textile wastewater mineralisation profiles for five different initial iron concentrations (TDI) (20, 40, 60, 80 and 100 mg Fe^{2+} L^{-1}), at a constant temperature of approximately 30ºC, similar to the real cotton-textile wastewater conditions, and pH 2.8. A similar DOC abatement (15%) was observed after pH adjustment to pH 2.8 due to the formation of foam and sludge (possible precipitation of some compounds at low pH).

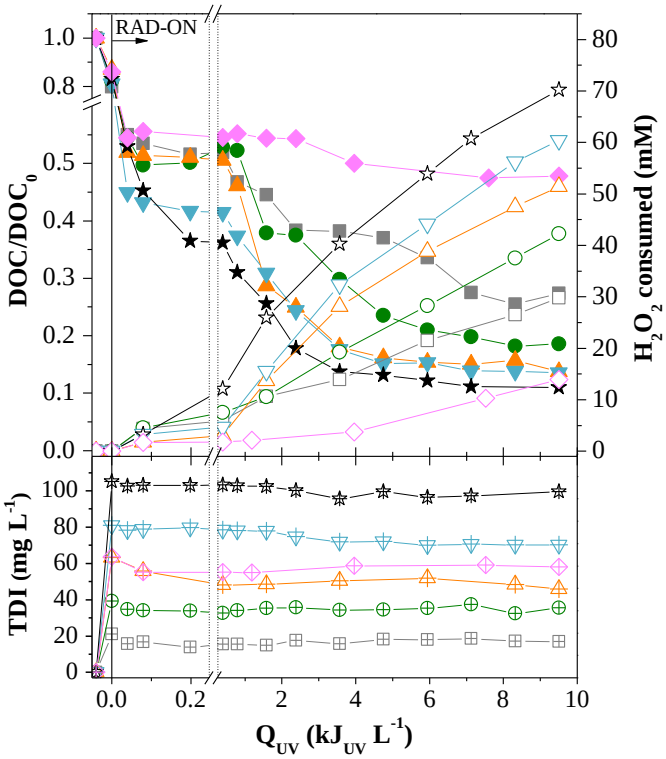

Figure 3.2. Textile wastewater treatment by photo-Fenton reaction at different concentrations of dissolved total iron, as well as the Fenton´s reaction. Photo-Fenton´s operation conditions: pH = 2.8; T = 30ºC; I = 44 W m^{-2}; solid symbols – DOC; open symbols – H_2O_2 consumed; cross symbols – Total dissolved Iron (TDI). ■ □ ⊞ - [Fe^{2+}] = 20 mg L^{-1}; ● ○ ⊕ - [Fe^{2+}] = 40 mg L^{-1}; ▲ △ ⧋ - [Fe^{2+}] = 60 mg L^{-1}; ▼ ▽ ⧩ - [Fe^{2+}] = 80 mg L^{-1}; ★ ☆ ✯ - [Fe^{2+}] = 100 mg L^{-1}. Fenton´s operation conditions: pH = 2.8; T = 30 ºC; [Fe^{2+}] = 60 mg L^{-1}; ◆ ◇ ⊕.

Afterwards, it can be observed a small induction period (up to 0.4 kJ_{UV} L^{-1}), characterized by low mineralisation and low hydrogen peroxide consumption (which is more visible in the experiment with the lowest iron dose). However, decolourisation is very fast suggesting a fast breaking down of the dyes molecules. Fenton tests were performed (only data for 60 mg Fe^{2+} L^{-1}), and it was observed the same mineralisation in the same period according to the amount of iron added, and afterwards the reaction almost stopped, achieving a constant DOC concentration. This suggests that after the first iron oxidation in the presence of hydrogen peroxide, the limiting step of the reaction is the availability of radiation for the regeneration of ferrous ions (reduction of Fe^{3+} to Fe^{2+})[24], as absorption of photons by other light absorbing species (inner filter effects), such as, dyes and its initial degradation molecules with aromatic structure, decreases the number of photons absorbed by the iron complexes.

Normally the direct photolysis of dyes has a low quantum yield, and consequently originates a loss of the photons absorbed [25]. The higher the iron concentration the smaller is the induction period, being almost eliminated for the highest iron concentration tested, which means that a high catalyst concentration is needed to compete efficiently for the photons with the other absorbing species present in the dark solution.

After this induction time, the mineralisation profile follows a pseudo-first-order kinetic model. Although the kinetic constants increase with iron concentration, the increment is very small for concentrations higher than 60 mg L^{-1}, being necessary higher amounts of H_2O_2. After approximately 4 kJ_{UV} L^{-1}, a very small mineralisation rate is observed, principally for iron concentrations above 60 mg L^{-1}, indicating the formation of iron complexes with some low molecular weight carboxylic acids, which are very stable and are not photodecarboxylated (e.g., ferrioxalate and ferricitrate complexes are easily photodecarboxylated), being necessary high energy doses for their complete mineralisation.

3.3.3.2 pH

Different authors reported that the optimum pH value for the photo-Fenton reaction is 2.8 mainly due to the fact that the predominant iron species in solution is $FeOH^{2+}$, which is the most photoactive ferric ion-water complex, but also because it avoids ferric hydroxide precipitation [26]. However, the need for acidification in the photo-Fenton process is often outlined as one of its major drawbacks, due to the additional cost associated to acidification and subsequent neutralization. Figure 3.3 presents the mineralisation of the textile wastewater at five different initial pHs values (2.4, 2.8, 3.2, 3.6 and 4.5) using the same initial iron concentration (60 mg L^{-1}).

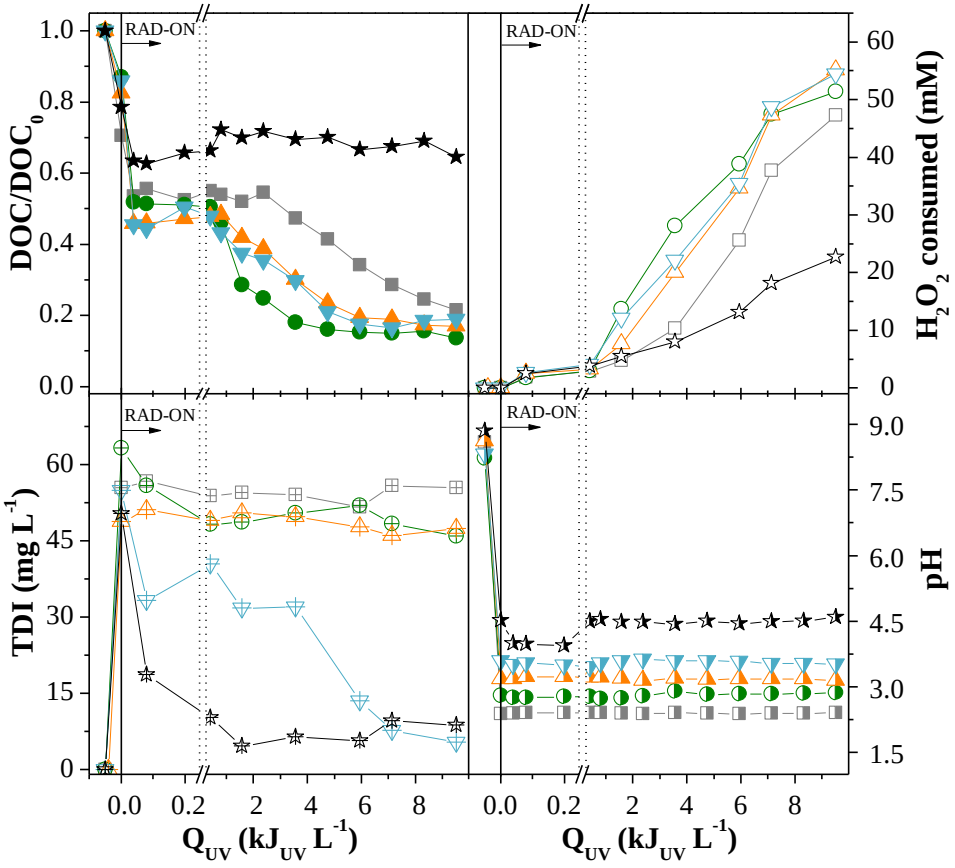

Figure 3.3. Textile wastewater treatment by photo-Fenton reaction at different pHs. Operation conditions: $[Fe^{2+}]$ = 60 mg L^{-1}; I = 44 W m^{-2}; T= 30ºC. Solid symbols – DOC; open symbols – H_2O_2 consumed; cross symbols – Total dissolved Iron (TDI); half-painted symbols - pHs. ■ □ ⊞ ◨ – pH = 2.4; ● ○ ⊕ ◑ - pH = 2.8; ▲ △ ◬ ◭ - pH = 3.2; ▼ ▽ ▿ ▾ - pH = 3.6; ★ ☆ ✯ ✰ - pH = 4.5.

For an initial pH value of 4.5, after the first oxidation of ferrous ions to ferric ions caused by hydrogen peroxide, it is observed a fast decay of dissolved iron concentration for values lower than 5 mg L^{-1}. The formation of the hydroxyl radicals during the first oxidation leads to a small initial oxidation and after that DOC remained approximately constant. The iron precipitation can be explained by theoretical speciation diagrams, which were made taking into account the importance of the type of iron complexes formed during the photo-Fenton reaction. The ferric speciation diagrams showed the formation of $Fe(OH)_3(s)$ and consequent iron precipitation at pHs higher than 3.5 (Table 3.3 and Figure 3.4).

For the reaction at an initial pH value of 3.6, after the first oxidation of ferrous ions with H_2O_2, the dissolved iron concentration decreased to about 35 mg L^{-1} until 3.0 kJ_{UV} L^{-1}, and then started to precipitate leading to dissolved iron concentrations below 5 mg L^{-1}. The DOC abatement for the experiment at pH 3.2 is similar to that obtained at pH 3.6, although dissolved iron concentration remained near 50 mg L^{-1} during the entire run. These behaviours are not in concordance with the theoretical speciation diagrams shown in Figure 3.6, which demonstrated that large part of iron would

precipitate at these pHs under these assay conditions. However, it is important to take into account that the information provided by the speciation diagrams must be used carefully and cannot be taken for granted, since this type of wastewater is composed by many compounds and its degradation can originate much more, which can also affect the type of iron complex formed. With this in mind, the high iron concentration that remained in the reactions can be associated with the formation of stable iron complexes with some organic compounds that were not considered in the speciation diagrams construction, e.g. ferricarboxylate complexes. The observed iron precipitation during reaction at pH 3.6, after an accumulated UV energy of 3 kJ_{UV} L^{-1}, can be associated with the photodecarboxylation of ferricarboxylates complexes formed and corroborates with explanation provided above.

Table 3.3. Theoretical molar fraction of Fe^{3+} species, associated to pH value in different assays.

pH	Iron Species Percentage (%)					
	Fe^{3+}	**$FeOH^{2+}$**	**$Fe(OH)_2^+$**	**$FeSO_4^+$**	**$Fe(SO_4)_2^-$**	**$Fe(OH_3)_{(S)}$**
2.4	6.7	2.7	1.6	79.8	9.2	0.0
2.8	5.2	7.1	5.3	75.3	7.1	0.0
3.2	0.0	3.5	3.3	13.1	1.4	78.8
3.6	0.0	2.6	0.0	0.0	0.0	97.4
4.5	0.0	0.0	0.0	0.0	0.0	100.0

It is observed a faster kinetic rate for the experiment at an initial pH 2.8 than pH 2.4, although the amount of dissolved iron during the experiments was very similar. Considering the analysis of the Figure 3.3 along with the data provided by speciation diagrams shown in the Table 3.3, for acid conditions pH range 2.4-2.8, it is possible to observe a directly proportional relation between the photo-Fenton reaction constant and the theoretical amount of $FeOH^{2+}$ species (the most photoactive complex). This suggests that the photo-Fenton reaction efficiency is mostly affected by the concentration of $FeOH^{2+}$ in solution, since this species is an additional source of hydroxyl radicals. Besides, it is worth mentioning that the concentration of H^+ rises in acidic medium, which can also have negative effects on the reaction (see Figure 3.3), since it can react with H_2O_2 (Eq.(3.1)), yielding the peroxonium ion ($H_3O_2^+$), therefore decreasing substantially its reactivity with Fe^{2+} ions, and working as a scavenger of the $^{\bullet}OH$ (Eq.(3.2)) [27, 28].

$$H_2O_2 + H^+ \rightarrow H_3O_2^+ \quad (3.1)$$

$$^{\bullet}OH + H^+ + e^- \rightarrow H_2O \quad (3.2)$$

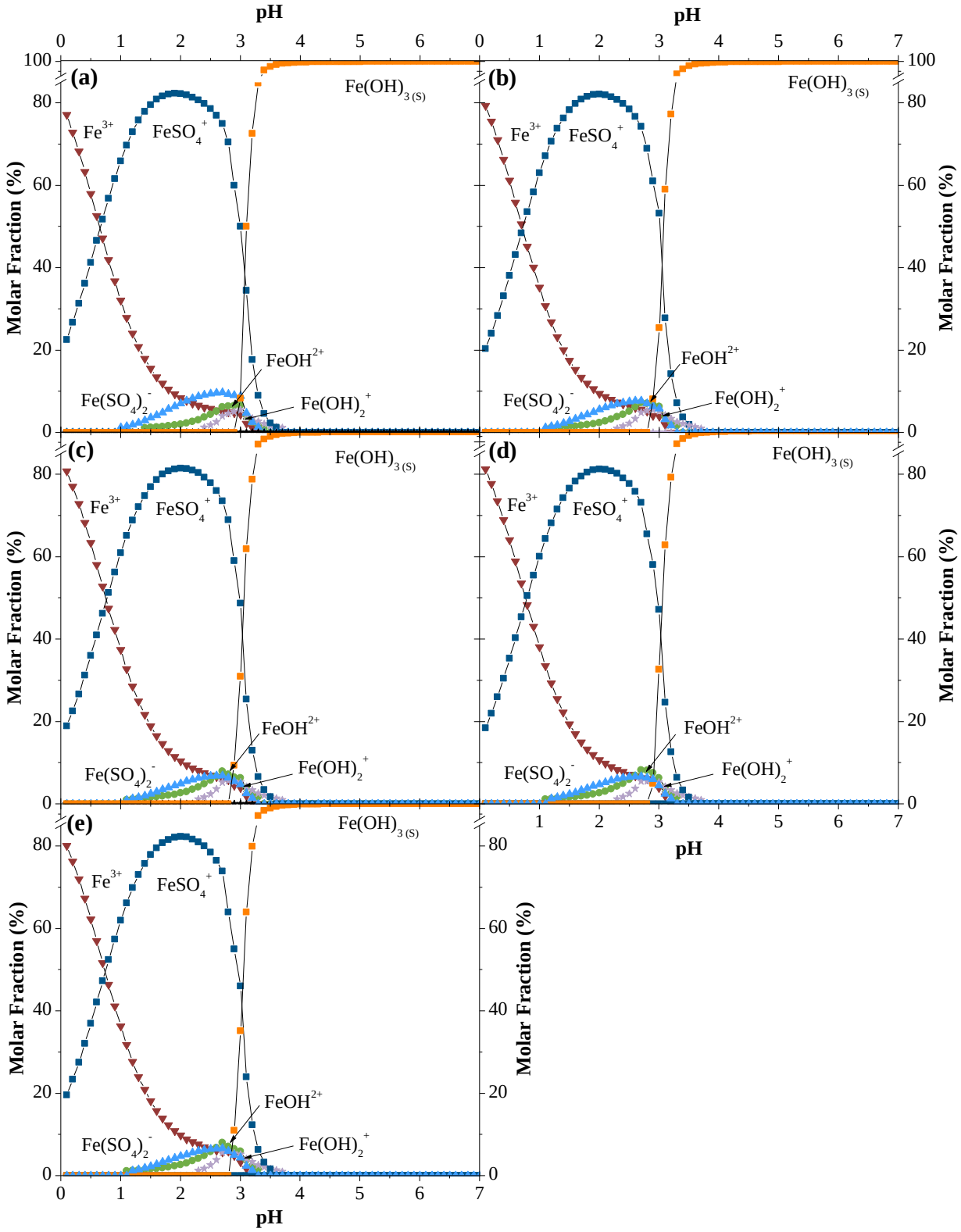

Figure 3.4. Speciation diagrams for ferric complexes as a function of pH, for a solution containing $Fe^{3+}/SO_4^{2-}/Cl^-$ in the conditions of the experiments performed at temperature of 30ºC and at different pH values: (a) pH 2.4: Ionic strength = 0.06 M; $[Fe^{3+}]$ = 1.1 mM; $[SO_4^{2-}]$ = 18.1 mM; $[Cl^-]$ = 3.0 mM; (b) pH 2.8: Ionic strength = 0.05 M; $[Fe^{3+}]$ = 1.1 mM; $[SO_4^{2-}]$ = 14 mM; $[Cl^-]$ = 3.0 mM; (c) pH 3.2: Ionic strength = 0.05 M; $[Fe^{3+}]$ = 1.1 mM; $[SO_4^{2-}]$ = 12.8 mM; $[Cl^-]$ = 3.0 mM; (d) pH 3.6: Ionic strength = 0.05 M; $[Fe^{3+}]$ = 1.1 mM; $[SO_4^{2-}]$ = 12.4 mM; $[Cl^-]$ = 3.0 mM; (e) pH 4.5: Ionic strength = 0.04 M; $[SO_4^{2-}]$ = 11.6 mM; $[Cl^-]$ = 3.0 mM.

3.3.3.3 Influence of temperature

Typical textile wastewaters present temperatures higher than 30ºC [29]. The oxygen solubility decreases with the increase of temperature, promoting algal growth, fish mortality and a decrease in water biodiversity. However, high temperatures (until 40-50ºC) favour the solar photo-Fenton reaction, which is an advantage when applied to the treatment of textile wastewaters [23].

Figure 3.5 shows the mineralisation of the textile wastewater at different temperatures (10°C, 20°C, 30°C, 40°C and 50°C), using an iron concentration of 60 mg L^{-1} and a pH value of 2.8. For temperatures between 10ºC and 20ºC the kinetics rates were extremely low achieving a mineralisation efficiency of about 60% after 9 kJ_{UV} L^{-1}. However, the consumption of H_2O_2 doubled when increasing the temperature from 10ºC to 20ºC (Table 3.2).

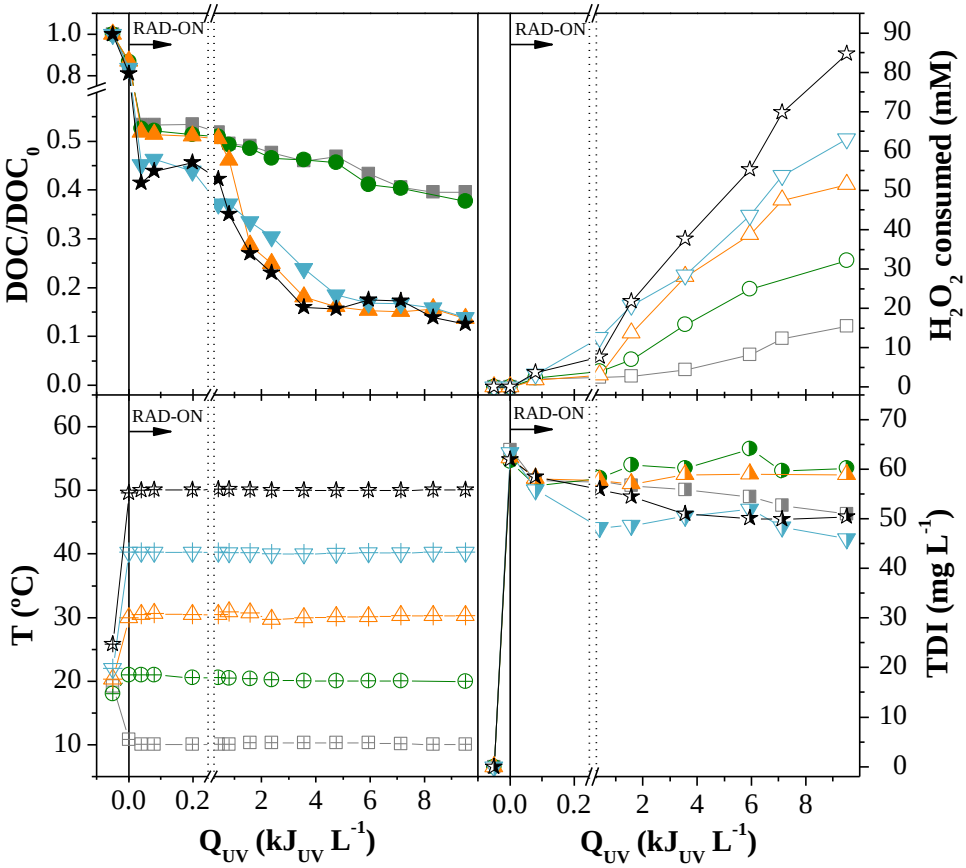

Figure 3.5. Textile wastewater treatment by photo-Fenton reaction at different temperatures. Operation conditions: pH = 2.8; [Fe^{2+}] = 60 mg L^{-1}; I = 44 W m^{-2}; solid symbols – DOC; open symbols – H_2O_2 consumed; cross symbols – temperature; half-painted symbols - Total dissolved Iron (TDI). ■ □ ⊞ ◨ - T = 10 ºC; ● ○ ⊕ ◑ - T = 20 ºC; ▲ △ ◬ ◭ - T = 30 ºC; ▼ ▽ ▽ ▽ - T = 40 ºC; ★ ☆ ☆ ★ - - T = 50 ºC.

As can be seen in the Figure 3.5, the increase of temperature improves the reaction rate, especially when is compared the reactions at 10ºC/20ºC with reaction at 30ºC. The molar fractions of the iron species

were calculated by the chemical equilibrium modelling system MINEQL+ [30] under the initial conditions in the presence of Fe^{3+}, SO_4^{2-} and Cl^-. According to the theoretical iron speciation diagrams at different temperatures, the molar fraction of the $FeOH^{2+}$ species increases with temperature (see Figure 3.6), achieving values of 4.5%, 6.3%, 7.1%, 8.3 and 9.5% respectively for the temperatures between 10ºC and 50ºC. Hence, the influence of temperature in photo-Fenton reactions at pH near 2.8 can be associated with the presence of different amounts of photoactive species ($FeOH^{2+}$) [31]. Besides, the increase of the reaction rate at high temperatures also can be related with the thermal reactions involved in the reduction of ferric ion, particularly Eqs. (3.3), (3.4) and (3.5), which use radiation of wavelengths higher than 500 nm.

$$Fe^{3+} + H_2O_2 \leftrightarrow Fe^{2+} + HO_2^{\bullet} + H^+ \quad (3.3)$$

$$Fe^{3+} + HO_2^{\bullet} \leftrightarrow Fe^{2+} + O_2 + H^+ \quad (3.4)$$

$$Fe^{3+} + O_2^{\bullet -} \leftrightarrow Fe^{2+} + O_2 \quad (3.5)$$

However, the increase from 30ºC to 50°C did not affect so much the mineralisation, approximately 85% after 5 kJ_{UV} L^{-1}, although the H_2O_2 consumption increased by a factor of 1.6 due to two mains factors: i) the inefficient H_2O_2 decomposition through the thermal reactions (Eqs. (3.3), (3.4) and (3.5)) involved in the Fe^{3+} reduction, with the formation of less reactive species, ii) the quicker thermal decomposition of H_2O_2 into H_2O and O_2 (inactive species), the rate of decomposition of hydrogen peroxide doubles every time the temperature rises by 10ºC.

For the experiments at 40ºC/50ºC, the iron concentration decreased slightly to values below 50 mg L^{-1}, indicating that some ferric-organic complexes with low solubility are formed. Iron speciation diagrams (Figure 3.6) clearly show the formation of $Fe(OH)_3$(s) and consequent iron precipitation at lower pH values due to increase of reaction temperature.

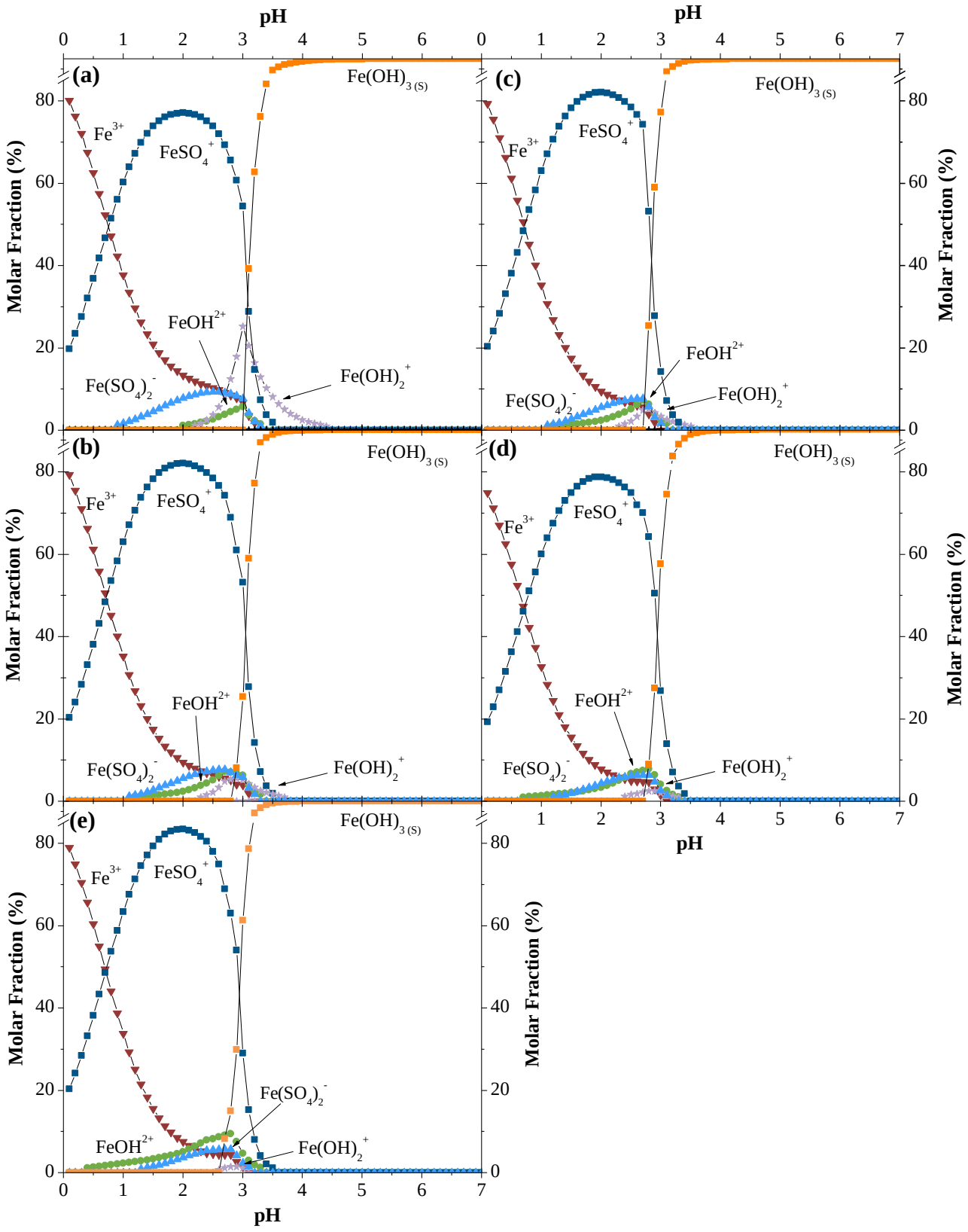

Figure 3.6. Speciation diagrams for ferric complexes as a function of pH for a solution containing $Fe^{3+}/SO_4^{2-}/Cl^-$ at different temperatures: (a) T = 10ºC; (b) T = 20ºC; (c) T = 30ºC; (d) T = 40ºC; (e) T = 50ºC. Ionic strength = 0.05 M; $[Fe^{3+}]$ = 1.1 mM; $[SO_4^{2-}]$ = 14 mM; $[Cl^-]$ = 3.0 mM.

3.3.3.4 *Influence of radiation intensity*

In northern Portugal, UV radiation power can achieve maximum values of around ~50 W m^{-2} between 12:00 and 16:00 hours and an average daily intensity of ~20 W m^{-2} in spring and summer seasons. Considering the irradiation intensity variation during the day, location and season and, high radiation intensities are associated to higher temperatures, assays were performed at different radiation intensities: 22, 44 and 68 W_{UV} m^{-2}, within the limits of the SUNTEST equipment (Figure 3.7).

Kinetic profiles show a slight improvement in the mineralisation with the increase of radiation intensity in terms of accumulated energy, with similar hydrogen peroxide consumption (Table 3.2). This means that the reaction rate remains approximately constant within the range of radiation intensities studied, which proves that the photo-Fenton reaction can be used efficiently during all the year. Considering the reaction velocity as a function of time, higher radiation intensities allow the same mineralisation rates in less time, since more photons per unit of time are available for the production of hydroxyl radicals.

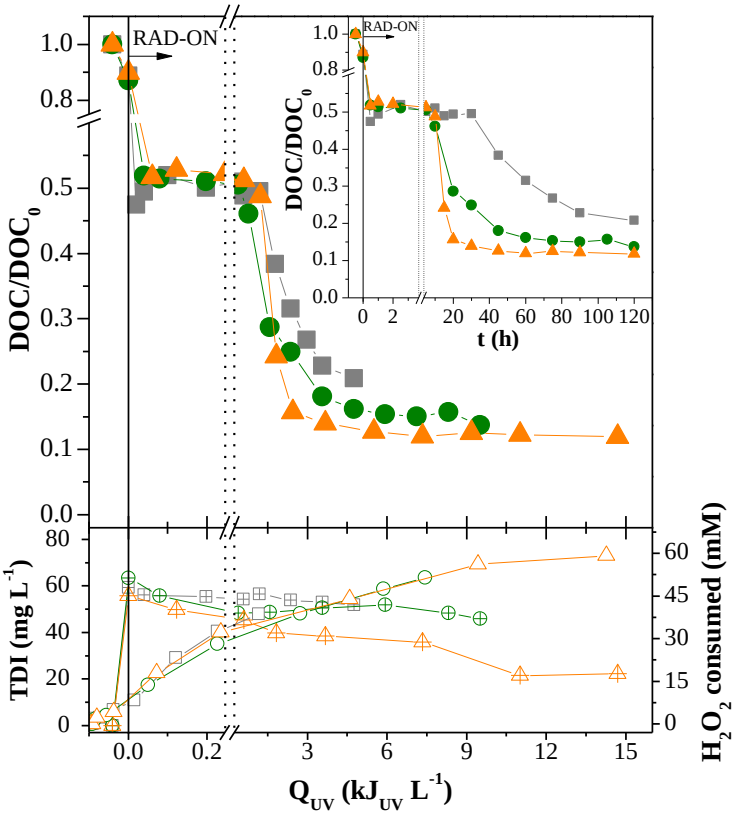

Figure 3.7. Textile wastewater treatment by photo-Fenton reaction at different radiation intensities. Operation conditions: $[Fe^{2+}]$ = 60 mg L^{-1}; pH = 2.8; T= 30ºC. Solid symbols – DOC; open symbols – H_2O_2 consumed; cross symbols – TDI. ■ □ ⊞ – I = 22 W m^{-2}; ● ○ ⊕ – I = 44 W m^{-2}; ▲ △ ⧋ – I = 68 W m^{-2}.

3.3.3.5 Biodegradability assays

A Zahn–Wellens test was carried out to evaluate the wastewater biodegradability at different stages of the solar-photo-Fenton treatment, in order to determine the optimum phototreatment time for coupling with a biological process. To collect pre-treated samples for this test, the previous solar-photo-Fenton experiment at pilot scale under natural solar conditions was repeated (pH= 2.8; $[Fe^{2+}]$ =60 mg L^{-1}), adding small amounts of hydrogen peroxide, and after total H_2O_2 consumption, a sample was taken for bioassays and another amount of H_2O_2 was added. This process was very important not only to prevent any reaction under dark conditions after sample collection but also to prevent the inhibition of microorganisms in bioassays due to the presence of residual H_2O_2. Besides the biodegradability test, some other analyses, such as COD, BOD_5, total nitrogen and low-molecular-weight carboxylate anions were also performed for a more thorough analysis of each step of the photo treatment.

The COD and DOC concentration decreased 63% and 67%, respectively, showing a strong oxidation of the organics, which is well correlated with the COS parameter as it increased from -2.8, indicating the presence of some reduced organic compounds, to +1.5 after 19.6 mM of H_2O_2 consumption, meaning strong mineralisation and generation of highly oxidized intermediates (Figure 3.8). Analysing the different process phases, more oxidized organic intermediates were formed at the beginning of the process, with substantial mineralisation, principally during the Fenton oxidation, which is corroborated by fast COD and DOC decrease until H_2O_2 consumption of 2.3 mM. To achieve almost complete decolourisation, 93% (Pt-Co method), 94% ($DFZ_{436\ nm}$); 95% ($DFZ_{525\ nm}$) and 93% ($DFZ_{525\ nm}$), it was necessary less than 8 mM of H_2O_2, following the same trend of the mineralisation process and in agreement with the kinetic tests conducted, both at lab and pilot scale photoreactors, showing that the photo-Fenton process is efficient in the decolourisation.

Figure 3.8 shows also a fast increase of the DOC corresponding to low-molecular-weight carboxylate anions (LMWCA/DOC ratio) after the beginning of the photo-Fenton reaction, achieving maximum values of 20.5% (considering the LMWCA analysed) at 7.5 mM H_2O_2 consumed (sample 4) (6.6, 2.8 and 1.5 mg C L^{-1} for propionate, malonate and oxalate respectively), followed by a fast decrease, since those acids correspond to the last oxidation products.

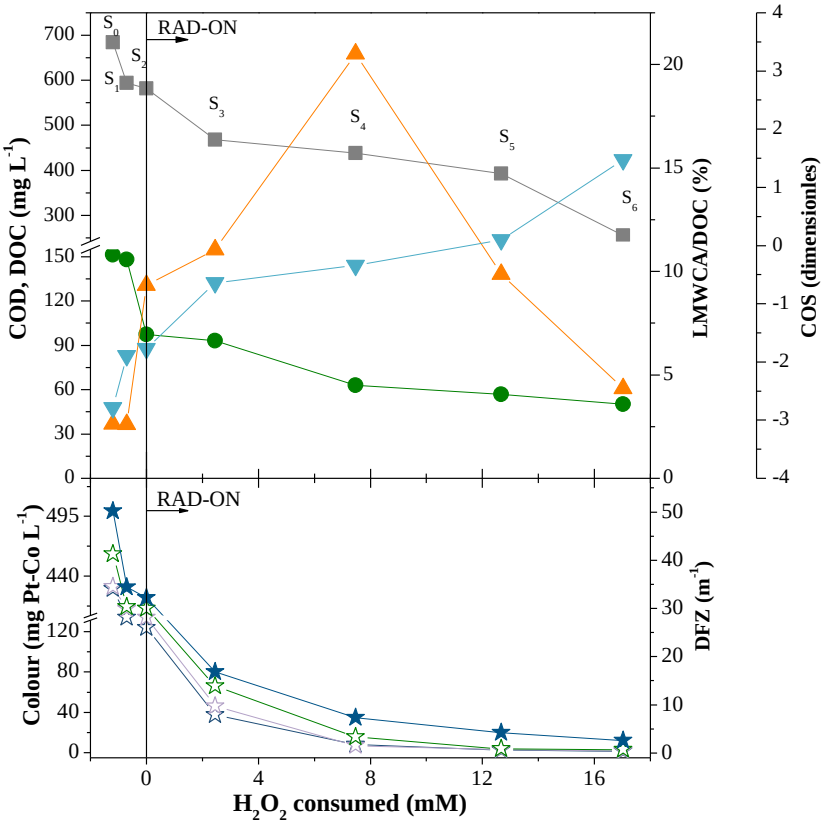

Figure 3.8. Solar-photo-Fenton treatment of the cotton-textile dyeing wastewater. ■ – COD; ● – DOC; ▲ – LMWCA/DOC ratio; ▼ – COS; ★ - Pt-Co scale; ☆ - DFZ_{436nm}; ☆ - DFZ_{525nm}; ☆ - DFZ_{620nm}.

According to the Zahn-Wellens test (Figure 3.9) the cotton-textile dyeing wastewater presents a moderate biodegradability of 40% related to the aspects reported above. The biodegradability remained approximately constant for the sample that suffered the acidification process until pH 2.8.

However, it decreased by 32% for the sample after the addition of iron, which can be attributed to the sedimentation of some biodegradable compounds. This is associated with the precipitation of iron phosphate, which is in agreement with the decrease of phosphates concentration from 6.7 mg L^{-1} to values lower than the detection limit of the analytical method, and dissolved iron concentration reduction from 60.0 to 48.7 mg L^{-1}. However, as expected, the biodegradability of the textile wastewater was enhanced during the photo-Fenton treatment, obtaining values of 38%, 40%, 48% and 58%, corresponding to 2.5, 7.5, 12.7 and 17.0 mM of H_2O_2 consumed (samples 3, 4, 5 and 6), respectively.

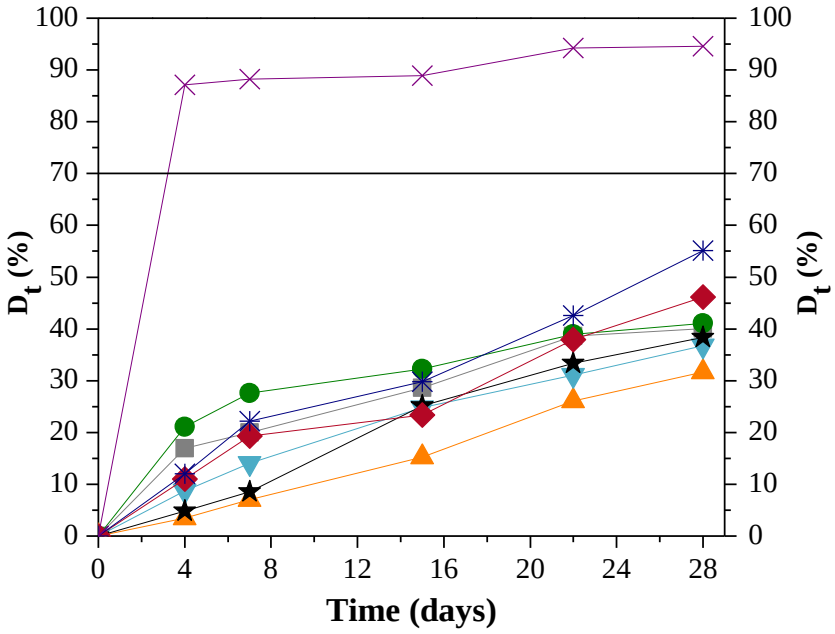

Figure 3.9. Zahn–Wellens test for selected samples during the solar-photo-Fenton treatment: ■ – S_0, DOC = 151.2 mg L^{-1}; ● – S_1, DOC = 148.0 mg L^{-1}; ▲ – S_2, DOC = 97.4 mg L^{-1}; ▼ – S_3, DOC = 93.1 mg L^{-1}; ★ – S_4, DOC = 62.9 mg L^{-1}; ◆ – S_5, DOC = 56.9 mg L^{-1}; ✳ – S_6, DOC = 50.1 mg L^{-1}; ✕ – reference, DOC = 107.6 mg L^{-1}.

Taking into consideration three main factors: a) higher LMWCA/DOC ratio; b) Zahn-Wellens results and c) UV energy and H_2O_2 savings; sample 4 can be considered the best point to stop the pre-oxidation process to achieve a COD < 250 mg O_2 L^{-1} (discharge limit into water bodies imposed by the Portuguese Legislation-Portaria nº423/97 of 25 June 1997) after the 28 days of the Zahn-Wellens test.

Considering the combination of a photo-Fenton reaction with a biological oxidation process in order to reach a final COD below 250 mg O_2 L^{-1}, the energy dose required for the photo-Fenton reaction is 0.5 kJ_{UV} L^{-1} ($\bar{T}$ = 30.7 ºC; $\overline{pH}$ = 2.80; $\overline{UV}_{G,n}$ = 13 W m^{-2}) consuming 7.5 mM of hydrogen peroxide (added in excess), as calculated from the kinetic studies performed at pilot plant under natural solar radiation, and leading to 58.4% mineralisation (DOC_f = 62.9 mg C L^{-1}). Throughout the treatment, the total nitrogen concentration remained approximately constant (113-117 mg N L^{-1}). Nitrite concentration decreased from 5.3 to 1.9 N-NO_2^- L^{-1} principally after the acidification process, although no nitrates were detected. On the other hand, ammonia increased from 79 to 91 mg N-NH_4^+ L^{-1} mainly due to the oxidation of the organic nitrogen. Sulphates increased from 34 to 1600 mg L^{-1} as the result of the addition of sulphuric acid for the acidification and iron sulphate. Chloride concentration remained at around 108 mg Cl^- L^{-1}.

3.4 Conclusions

Cotton-textile dyeing wastewaters presents a moderate organic load and low to moderate biodegradability mainly due to the presence of a mixture of recalcitrant dyes used in the dyeing process, which must be removed before discharging into the water bodies. The solar-photo-Fenton treatment was the most efficient of all solar AOPs studied, enhancing the biodegradability of the effluent and making possible its combination with a biological oxidation process, being possible to achieve a wastewater with a COD below 250 mg O_2 L^{-1}. The minimum iron concentration needed to compete efficiently for the photons with the other absorbing species in solution, leading to the highest reaction efficiency, is 60 mg L^{-1}. Although the better results with photo-Fenton reaction were obtained at pH 2.8, the efficiency remained approximately constant until pH of 3.6, decreasing the costs associated with acid and base consumption. The photo-Fenton efficiency increased greatly with the temperature, principally from 10 to 30ºC, mainly due to increase of the molar fraction of the photoactive species ($FeOH^{2+}$) as well as to the thermal reactions involved in the reduction of ferric ions, which use radiation of wavelengths higher than 500 nm. This condition is favourable, because the textile wastewater normally presents temperatures higher than 30ºC. The reaction rate remained approximately constant within the range of radiation intensities studied, which proves that the photo-Fenton reaction can be used efficiently during all the year or in regions with lower solar radiation intensities. Finally, considering the combination of a photo-Fenton reaction with a biological oxidation system for the treatment of the textile wastewater in order to reach a COD below 250 mg O_2 L^{-1}, the energy dose required for the photo-Fenton reaction is 0.5 kJ_{UV} L^{-1} (T = 30ºC; pH = 2.8) consuming 7.5 mM of hydrogen peroxide and leading to 58.4% mineralisation (DOC_f = 62.9 mg C L^{-1}).

3.5 References

1. Serra, F., J. Pointon, and H. Abdou, *Factors influencing the propensity to export: A study of UK and Portuguese textile firms.* International Business Review, 2012. **21**(2): p. 210-224.
2. El-Dein, A.M., J. Libra, and U. Wiesmann, *Cost analysis for the degradation of highly concentrated textile dye wastewater with chemical oxidation H_2O_2/UV and biological treatment.* Journal of Chemical Technology & Biotechnology, 2006. **81**(7): p. 1239-1245.
3. Prigione, V., V. Tigini, C. Pezzella, A. Anastasi, G. Sannia, and G.C. Varese, *Decolourisation and detoxification of textile effluents by fungal biosorption.* Water Research, 2008. **42**(12): p. 2911-2920.
4. Torrades, F., J. García-Montaño, J. Antonio García-Hortal, X. Domènech, and J. Peral, *Decolorization and mineralization of commercial reactive dyes under solar light assisted photo-Fenton conditions.* Solar Energy, 2004. **77**(5): p. 573-581.
5. Blanco, J., F. Torrades, M. De la Varga, and J. García-Montaño, *Fenton and biological-Fenton coupled processes for textile wastewater treatment and reuse.* Desalination, 2012. **286**: p. 394-399.
6. Oller, I., S. Malato, and J.A. Sánchez-Pérez, *Combination of Advanced Oxidation Processes and biological treatments for wastewater decontamination—A review.* Science of The Total Environment, 2011. **409**(20): p. 4141-4166.
7. Schrank, S.G., J.N.R.d. Santos, D.S. Souza, and E.E.S. Souza, *Decolourisation effects of Vat Green 01 textile dye and textile wastewater using H_2O_2/UV process.* Journal of Photochemistry and Photobiology A: Chemistry, 2007. **186**(2–3): p. 125-129.
8. Pekakis, P.A., N.P. Xekoukoulotakis, and D. Mantzavinos, *Treatment of textile dyehouse wastewater by TiO_2 photocatalysis.* Water Research, 2006. **40**(6): p. 1276-1286.
9. Byberg, R., J. Cobb, L.D. Martin, R.W. Thompson, T.A. Camesano, O. Zahraa, and M.N. Pons, *Comparison of photocatalytic degradation of dyes in relation to their structure.* Environmental Science and Pollution Research, 2013. **20**(6): p. 3570-3581.
10. Garcia, J.C., J.L. Oliveira, A.E.C. Silva, C.C. Oliveira, J. Nozaki, and N.E. de Souza, *Comparative study of the degradation of real textile effluents by photocatalytic reactions involving UV/TiO_2/H_2O_2 and UV/Fe^{2+}/H_2O_2 systems.* Journal of Hazardous Materials, 2007. **147**(1–2): p. 105-110.
11. Karthikeyan, S., A. Titus, A. Gnanamani, A.B. Mandal, and G. Sekaran, *Treatment of textile wastewater by homogeneous and heterogeneous Fenton oxidation processes.* Desalination, 2011. **281**: p. 438-445.
12. Nidheesh, P., R. Gandhimathi, and S. Ramesh, *Degradation of dyes from aqueous solution by Fenton processes: a review.* Environmental Science and Pollution Research, 2013. **20**(4): p. 2099-2132.
13. Módenes, A.N., F.R. Espinoza-Quiñones, D.R. Manenti, F.H. Borba, S.M. Palácio, and A. Colombo, *Performance evaluation of a photo-Fenton process applied to pollutant removal from textile effluents in a batch system.* Journal of Environmental Management, 2012. **104**: p. 1-8.
14. Malato, S., J. Blanco, D.C. Alarcón, M.I. Maldonado, P. Fernández-Ibáñez, and W. Gernjak, *Photocatalytic decontamination and disinfection of water with solar collectors.* Catalysis Today, 2007. **122**(1–2): p. 137-149.

15. Dhir, A., N. Prakash, and D. Sud, *Coupling of solar-assisted advanced oxidative and biological treatment for degradation of agro-residue-based soda bleaching effluent.* Environmental Science and Pollution Research, 2012. **19**(9): p. 3906-3913.

16. Aytar, P., S. Gedikli, M. Sam, B. Farizoğlu, and A. Çabuk, *Sequential treatment of olive oil mill wastewater with adsorption and biological and photo-Fenton oxidation.* Environmental Science and Pollution Research, 2013. **20**(5): p. 3060-3067.

17. Renou, S., J.G. Givaudan, S. Poulain, F. Dirassouyan, and P. Moulin, *Landfill leachate treatment: Review and opportunity.* Journal of Hazardous Materials, 2008. **150**(3): p. 468-493.

18. de Morais, J.L. and P.P. Zamora, *Use of advanced oxidation processes to improve the biodegradability of mature landfill leachates.* Journal of Hazardous Materials, 2005. **123**(1–3): p. 181-186.

19. Vilar, V.J.P., L.X. Pinho, A.M.A. Pintor, and R.A.R. Boaventura, *Treatment of textile wastewaters by solar-driven advanced oxidation processes.* Solar Energy, 2011. **85**(9): p. 1927-1934.

20. Somensi, C.A., E.L. Simionatto, S.L. Bertoli, A. Wisniewski Jr, and C.M. Radetski, *Use of ozone in a pilot-scale plant for textile wastewater pre-treatment: Physico-chemical efficiency, degradation by-products identification and environmental toxicity of treated wastewater.* Journal of Hazardous Materials, 2010. **175**(1–3): p. 235-240.

21. Kormann, C., D.W. Bahnemann, and M.R. Hoffmann, *Photolysis of chloroform and other organic molecules in aqueous TiO_2 suspensions.* Environ. Sci. Technol, 1991. **25**: p. 494-500.

22. Malato Rodríguez, S., J. Blanco Gálvez, M.I. Maldonado Rubio, P. Fernández Ibáñez, D. Alarcón Padilla, M. Collares Pereira, J. Farinha Mendes, and J. Correia de Oliveira, *Engineering of solar photocatalytic collectors.* Solar Energy, 2004. **77**(5): p. 513-524.

23. Malato, S., P. Fernández-Ibáñez, M.I. Maldonado, J. Blanco, and W. Gernjak, *Decontamination and disinfection of water by solar photocatalysis: Recent overview and trends.* Catalysis Today, 2009. **147**(1): p. 1-59.

24. Silva, M.R.A., A.G. Trovó, and R.F.P. Nogueira, *Degradation of the herbicide tebuthiuron using solar photo-Fenton process and ferric citrate complex at circumneutral pH.* Journal of Photochemistry and Photobiology A: Chemistry, 2007. **191**(2–3): p. 187-192.

25. Feng, W., D. Nansheng, and Z. Yuegang, *Discoloration of dye solutions induced by solar photolysis of ferrioxalate in aqueous solutions.* Chemosphere, 1999. **39**(12): p. 2079-2085.

26. Pignatello, J.J., E. Oliveros, and A. MacKay, *Advanced oxidation processes for organic contaminant destruction based on the fenton reaction and related chemistry.* Critical Reviews in Environmental Science and Technology, 2006. **36**: p. 1-84.

27. El-Ghenymy, A., S. Garcia-Segura, R.M. Rodríguez, E. Brillas, M.S. El Begrani, and B.A. Abdelouahid, *Optimization of the electro-Fenton and solar photoelectro-Fenton treatments of sulfanilic acid solutions using a pre-pilot flow plant by response surface methodology.* Journal of hazardous materials, 2012. **221**: p. 288-297.

28. Ghoneim, M.M., H.S. El-Desoky, and N.M. Zidan, *Electro-Fenton oxidation of Sunset Yellow FCF azo-dye in aqueous solutions.* Desalination, 2011. **274**(1): p. 22-30.

29. Ali, N., A. Hameed, and S. Ahmed, *Physicochemical characterization and Bioremediation perspective of textile effluent, dyes and metals by indigenous Bacteria.* Journal of Hazardous Materials, 2009. **164**(1): p. 322-328.

30. Schecher, W.D. and D.C. McAvoy, *MINEQL+: A Chemical Equilibrium Modeling System, Version 4.6 for Windows*. 2007, Environmental Research Software: Hallowell, Maine, United States.

31. Moreira, F.C., R.A.R. Boaventura, E. Brillas, and V.J.P. Vilar, *Degradation of trimethoprim antibiotic by UVA photoelectro-Fenton process mediated by Fe(III)–carboxylate complexes.* Applied Catalysis B: Environmental, 2015. **162**: p. 34-44.

4 Enhancement of a Solar Photo-Fenton Reaction with Ferric-Organic Ligands for the Treatment of Acrylic-Textile Dyeing Wastewater[2]

This chapter reports on the enhancement of a solar photo-Fenton reaction through the use of different ferric-organic ligands applied to the treatment of a simulated acrylic-textile dyeing wastewater, as a pre-oxidation step to increase its biodegradability. The degradation efficiency by the photo-Fenton reaction of different textile dyeing auxiliary products used in the preparation of the synthetic wastewater was also individually assessed. Different design parameters such as iron concentration, pH, temperature, flow conditions, UV irradiance and H_2O_2 addition strategy and dose were evaluated.

[2]This Chapter is based on the research article: "Soares, P.A., Batalha, M., Souza, Selene M. A. Guelli U., Boaventura, Rui A. R., Vilar, Vítor J. P., *Enhancement of a solar photo-Fenton reaction with ferric-organic ligands for the treatment of acrylic-textile dyeing wastewater*. Journal of Environmental Management, 2015. 152: p. 120-131."

4.1 Introduction

Textile industries are among the biggest users of water and complex chemicals, such as dyes, surfactants, soaps, fats, waxes, oils, solvents and salts. During textile processing stages, a high fraction of those organic and inorganic chemicals used is discharged into the wastewater stream, constituting a big environmental concern [1-3]. The dyeing process, perhaps the most studied step in textile processing, generates wastewaters with an intense colour, related to the mixture of different types of dyes and auxiliary products, such as organic acids, fixing agents, reducing agents, and diluents. The amount and composition of these wastewaters depend on various factors, including the processed fabrics, the process type and the chemicals used.

Some of the dyes commonly used in industry are considered to be electron-deficient xenobiotic compounds. For example, the azo-dyes have the azo (N=N) electron-withdrawing group, generating electron deficiency in the molecule and making the compound less susceptible to oxidative catabolism by bacteria [4]. Other synthetic organic chemicals are used as additives in different stages of textile manufacturing, with a wide range of functions (e.g.: sequestering agents, stabilizers, colour fixers, dispersants, etc.). They comprise substances which are used as auxiliary products in textile production, and are categorized under the term ‘‘xenobiotic’’ due to their biological persistence, i.e. their recalcitrant and even toxic nature [5, 6]. The recalcitrant feature of the textile wastewaters requires advanced treatment technologies, such as advanced oxidation processes (AOPs). Successful applications of AOPs to dyes solutions and textile wastewaters have been reported in the literature [7-9]. However, little attention has been paid to the treatability of textile dyeing auxiliary products [10].

The photo-Fenton process is among the most applied AOPs in the treatment of industrial wastewaters [11]. The optimum pH for the photo-Fenton reaction is 2.8, not only because the predominant iron species in solution is $FeOH^{2+}$, the most photoactive ferric ion-water complex, but also because iron precipitation is avoided. The major drawbacks of the photo-Fenton process when applied to the treatment of textile wastewaters are: i) the formation of stable complexes between ferric ions and organic constituents present in textile wastewaters, limiting the photoreduction of Fe^{3+}, decreasing the decomposition of H_2O_2 in the Fenton reaction and the overall efficiency of the photo-Fenton process [12, 13]; ii) the high alkalinity of the wastewater due to the presence of carbonates and bicarbonates, requiring high quantities of acid for the acidification process, increasing the concentration of sulphates in solution (H_2SO_4 is the most commonly used acid); they form stable

complexes with ferric ions, such as $FeSO_4^+$ and $Fe(SO_4)_2^-$, which are much less photoactive than $FeOH^{2+}$, and also lead to the formation of less oxidant species $SO_4^{\bullet-}$ when compared with $HO^\bullet$ radicals; iii) high chloride content generates soluble complexes with iron, such as $FeCl^+$, $FeCl^{2+}$ and $FeCl_2^+$, which are much less photoactive than $FeOH^{2+}$ and also leads to the formation of less oxidant species as $Cl^\bullet$, $Cl_2^{\bullet-}$ when compared with $HO^\bullet$ radicals. The enhancement of the photo-Fenton reaction can be achieved through the use of ferricarboxylate complexes, such as ferrioxalate, ferricitrate and ferrimaleate [14-19], which i) have much higher quantum yields than ferric iron-water complexes; ii) can use a higher fraction of the solar radiation spectrum, up to 580 nm [19, 20]; iii) are photodecarboxylated under visible radiation; iv) provide a quicker pathway for Fe^{3+} regeneration accelerating thereby the process [12]; v) are more soluble than ferric iron-water complexes, allowing to work at neutral pH values, increasing the applicability of this process on an industrial scale, since costs and drawbacks of acidification and the subsequent neutralisation are eliminated; vi) are more stable and strong complexes than ferric iron-sulphates, iron-chloride or iron-organic ligands complexes.

This chapter reports on treatment of a synthetic acrylic-textile dyeing wastewater using a photo-Fenton process enhanced by ferric-organic ligands (oxalic acid, citrate acid and EDDS-Ethylenediamine-N,N'-disuccinic acid), in a lab-scale prototype under controlled conditions, using artificial solar radiation and in a pilot scale under natural sunlight. The influence of the main ferrioxalate-solar-photo-Fenton reaction variables, such as iron concentration, pH, temperature, UV irradiance and H_2O_2 concentration and dosage strategy was investigated. The effect of hydrodynamics on the reactors performance was also assessed both in the dark and light parts of the system. The degradation efficiency by the photo-Fenton reaction of different textile dyeing auxiliary products used in the preparation of the synthetic wastewater was also individually assessed. For the first time, light intensity was correlated to the needs of iron in order to avoid the loss of photons.

4.2 Material and Methods

The detailed operational conditions of the assays performed in this chapter are shown in Table 4.1 (lab-scale sunlight simulator photoreactor) and in Table 4.2 (CPC solar pilot plant). All the chemicals and reagents used in this chapter, along with the corresponding experimental procedures followed, and, finally, the employed methods can be consulted in Chapter 2.

Table 4.1. Operational conditions with artificial sunlight.

System	I[a]	TDI[b]	T[c]	pH	Range of H_2O_2
Fe^{2+}/H_2O_2	-	60.0	30.0	2.8	200 - 500
UVA-Vis/Fe^{2+}/H_2O_2	41.6				
UVA-Vis/Fe^{2+}/H_2O_2[1]	41.6	40.0	30.0	2.8	200 - 500
UVA-Vis/Fe^{2+}/H_2O_2[2]					
UVA-Vis/Fe^{2+}/H_2O_2[3]					
UVA-Vis/Fe^{2+}/H_2O_2[4]					
UVA-Vis/Fe^{2+}/H_2O_2[5]					
UVA-Vis/Fe^{3+}/H_2O_2/Oxalic acid	41.6	60.0	30.0	2.8	200 - 500
UVA-Vis/Fe^{3+}/H_2O_2/EDDS					
UVA-Vis/Fe^{3+}/H_2O_2/Citric acid					
UVA-Vis/Fe^{3+}/H_2O_2/Oxalic acid	20.6	40.0	30.0	2.8	200-500
		60.0			
		80.0			
UVA-Vis/Fe^{3+}/H_2O_2/Oxalic acid	41.6	20.0	30.0	2.8	200-500
		40.0			
		60.0			
		80.0			
UVA-Vis/Fe^{3+}/H_2O_2/Oxalic acid	59.2	40.0	30.0	2.8	200-500
		60.0			
		80.0			
UVA-Vis/Fe^{3+}/H_2O_2/Oxalic acid	41.6	40.0	20.0	2.8	200 - 500
			30.0		
			40.0		
UVA-Vis/Fe^{3+}/H_2O_2/Oxalic acid	41.6	40.0	30.0	2.8	200 - 500
				3.5	
				4.0	
				4.5	
				5.0	
UVA-Vis/Fe^{3+}/H_2O_2/Oxalic acid	41.6	40.0	30.0	2.8	50 – 100
					100 – 200
					200 – 500
					68.2[d]

[a]Irradiation intensity (W m^{-2}); [b]Dissolved iron concentration (mg L^{-1}); [c]Liquid temperature (ºC); [d] dosage at the reaction start. Treated matrix: [1]dye; [2]Sera®Sperse; [3]Sera®Con; [4]Sera®Lube; [5]Sera®Tard.

Table 4.2. Operational conditions for solar driven photo-Fenton reactions.

System	Q^a	V_i^b	V_i/V_t^c	t_i^d	t_{dark}^e	Re^f
UVA-Vis/Fe^{3+}/H_2O_2/oxalic acid[1]	2	5.1	0.23	2.6	8.5	1027
	2[g]			2.6	8.5	1027
	9			0.6	1.9	4622
	20			0.3	0.9	10271
	35			0.2	0.5	17974

[a](L min^{-1}); [b]illuminated volume (L); [c]illuminated volume divided by the total volume; [d]illumination time (min); [e]time in the dark (min); [f]Reynolds number; [g]mechanically stirred dark phase; [1]Operation conditions: pH = 2.8; [Fe^{3+}] = 40 mg L^{-1}; iron/oxalate molar ratio of 1:3.

4.3 Results and discussion

4.3.1 Acrylic-textile dyeing wastewater characterization

Table 2.3 (Materials and methods – Chapter 2) shows a brief characterisation of the synthetic acrylic-textile dyeing wastewater used in this chapter. The wastewater presents a blue colour, which is mainly related to the dye colour, originating a maximum absorbance peak at 610 nm. The wastewater presents a neutral pH value, low alkalinity and moderated organic load, where more than 96.5% of DOC is related to the dyeing auxiliary products and 3.5% is due to the dye. The low BOD_5/COD ratio indicates low biodegradability of this textile wastewater, which was confirmed by the Zahn-Wallens test.

The low biodegradability of acrylic-textile dyeing wastewater is mainly associated with the presence of the dispersing agent Sera® Sperse M-IW and the surfactant auxiliary product Sera® Tard A-AS. The first is composed of polyglycol ethers used in acrylic yarn dyeing with cationic dyes. These chemicals are reported in the literature as highly water soluble, causing low turbidity, toxic, recalcitrant and are often referred to as xenobiotic [21-24]. The second is basically composed of alkyl dimethyl benzyl ammonium chloride, used as a retarder for dyeing acrylic fibers and in blends with cationic dyestuffs. This chemical compound, used in the textile industry, is also found in disinfectants and highly efficient cleaning products, cosmetics, food and in marine antifouling paints, personal care products, mainly because of its biocide characteristic [10, 24]. The biodegradability of these surfactants seems to increase with increasing water affinity and depends also on the length of alkyl chain, the number of ethoxylate groups and the total molecular weight [23].

A high concentration of formic acid was also detected in the textile wastewater, which was attributed to the textile auxiliary Sera® Con N-VS. Formic acid is highly biodegradable and represents 21% of the biodegradable organic fraction of the synthetic textile wastewater. The constituents of the auxiliary Sera® Con N-VS, acid carboxylic esters, correspond to 27% of the total organic carbon, which is correlated to the biodegradability index.

The wastewater presents also a high conductivity associated mainly to the high concentration of sulphates (593 mg SO_4^{2-} L^{-1}) and sodium (344 mg Na^+ L^{-1}) ions. Sulphate concentration corresponds to the amount of sodium sulphate added. On the other hand, sodium concentration is only 75% related with the sodium sulphate added and the remaining 25% must be originated from the other dyeing

auxiliary products. The wastewater presents total dissolved nitrogen of 20 mg N L^{-1} which is mainly derived from the two textile auxiliary products used, namely Sera®Lube M-CF, composed of polymeric amines, and Sera®Tard A-AS, a surfactant, mainly composed of alkyl dimethyl benzyl ammonium chloride.

4.3.2 Fenton and Photo-Fenton reactions

Figure 4.1 shows the textile wastewater mineralisation profiles using conventional Fenton and photo-Fenton reactions, at pH = 2.8, T = 30ºC, [Fe^{2+}] = 60 mg L^{-1} and irradiance of 41.6 W_{UV} m^{-2} (only for the photo-Fenton reaction). Mineralisation was negligible using the Fenton reaction, which is in agreement with the low hydrogen peroxide consumption and a high decrease of dissolved iron concentration to values lower than 15 mg L^{-1}.

For the photo-Fenton reaction it is observed an induction reaction period (low mineralisation and low hydrogen peroxide consumption) of ~6 kJ_{UV} L^{-1} (~100 min), mainly related to the formation of iron complexes with the dissolved organic matter (DOM) present in solution, decreasing substantially the photoreduction of Fe^{3+} (Eq. (4.1)), leading to a low H_2O_2 consumption. The reaction rate is very slow indicating that these iron complexes have a low photo-activity.

$$Fe^{III}(DOM)_n \xrightarrow{h\nu} Fe^{II}(DOM)_{n-1} + DOM^* \quad (4.1)$$

After this initial induction period, the reaction rate increases significantly, associated to the increase of dissolved iron concentration and consumption of H_2O_2, meaning that the iron-organic complexes initially formed were destroyed. Additional photo-Fenton reactions were carried using pure solutions of dye and dyeing auxiliary products, individually, in order to evaluate the influence of each organic constituent in the acrylic-textile wastewater treatment.

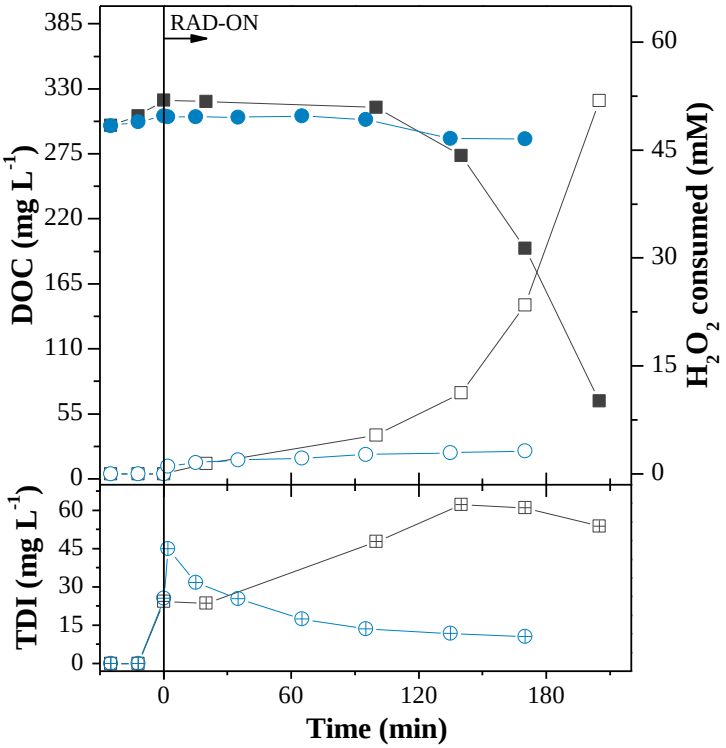

Figure 4.1. Evolution of the DOC concentration, H_2O_2 consumed and total dissolved iron during the Fenton and photo-Fenton reactions. Operation conditions: pH = 2.8; *T* = 30ºC; $[Fe^{2+}]$ = 60 mg L^{-1}; *I* = 41.6 W_{UV} m^{-2} (only for the photo-Fenton). Solid symbols – DOC; open symbols – H_2O_2 consumed; cross symbols – total dissolved iron (TDI). ■ □ ⊞ – UVA-Vis/Fe^{2+}/H_2O_2; ● ○ ⊕ - Fe^{2+}/H_2O_2.

Figure 4.2 shows a high decrease of dissolved iron for all the experiments performed with the dyeing auxiliary chemicals, which indicates that these compounds form stable complexes with iron, limiting the photo-Fenton reaction rate (Table 4.3).

The iron-dyes complexes are less relevant, confirmed by the higher values of dissolved iron concentration, leading to mineralisation rates of the pure dye solution higher than that observed for the synthetic wastewater and for all dyeing auxiliary products. The reverse situation was reported by Arana et al. [2], considering the photocatalytic degradation of the commercial dye Lanaset Sun Yellow 180, in the presence and absence of different additives (citric acid, alkyl amine polyglycol ether sulphate, sodium sulphate, sodium acetate and a special detergent composed of water, iso-propanol and a mixture of ethoxylates and sulphated aliphatic alcohols), where a high complexation between iron species and dye was observed.

Table 4.3. Operational conditions and pseudo-first-order kinetic constants with artificial sunlight.

System	I[a]	TDI[b]	T[c]	pH	Range of H_2O_2	Kinetic parameters			
						DOC degradation		H_2O_2 consumption	
						k^d	R^2	k_H[e]	R^2
Fe^{2+}/H_2O_2	-	60.0	30.0	2.8	200 - 500	0.005±0.001	0.889	0.19±0.02	0.940
UVA-Vis/Fe^{2+}/H_2O_2	41.6					0.05±0.02	0.900	3.0±0.7	0.799
UVA-Vis/Fe^{2+}/H_2O_2[1]						0.5±0.1	0.926	2.8±0.4	0.969
UVA-Vis/Fe^{2+}/H_2O_2[2]						0.05±0.02	0.882	1.1±0.2	0.913
UVA-Vis/Fe^{2+}/H_2O_2[3]	41.6	40.0	30.0	2.8	200 - 500	0.45±0.04	0.981	3.8±0.3	0.980
UVA-Vis/Fe^{2+}/H_2O_2[4]						0.4±0.1	0.912	3.1±0.3	0.960
UVA-Vis/Fe^{2+}/H_2O_2[5]						0.19±0.02	0.970	3.1±0.6	0.907
UVA-Vis/Fe^{3+}/H_2O_2/Oxalic acid						0.34±0.02	0.994	9±1	0.940
UVA-Vis/Fe^{3+}/H_2O_2/EDDS	41.6	60.0	30.0	2.8	200 - 500	0.18±0.02	0.978	5.7±0.7	0.921
UVA-Vis/Fe^{3+}/H_2O_2/Citric acid						0.28±0.03	0.964	10±1	0.933
UVA-Vis/Fe^{3+}/H_2O_2/Oxalic acid	20.6	40.0	30.0	2.8	200-500	0.26±0.01	0.968	7.8±0.9	0.989
		60.0				0.28±0.06	0.994	19±1	0.999
		80.0				0.49±0.05	0.994	21±2	0.996
UVA-Vis/Fe^{3+}/H_2O_2/Oxalic acid	41.6	20.0	30.0	2.8	200-500	0.106±0.007	0.925	1.12±0.07	0.981
		40.0				0.27±0.03	0.964	6.5±0.3	0.993
		60.0				0.34±0.02	0.994	14±2	0.940
		80.0				0.61±0.02	0.997	23.2±0.2	0.999
UVA-Vis/Fe^{3+}/H_2O_2/Oxalic acid	59.2	40.0	30.0	2.8	200-500	0.148±0.009	0.984	4.2±0.3	0.979
		60.0				0.35±0.04	0.957	11.3±0.7	0.980
		80.0				0.55±0.01	0.993	16±3	0.988
UVA-Vis/Fe^{3+}/H_2O_2/Oxalic acid	41.6	40.0	20.0	2.8	200 - 500	0.106±0.009	0.941	2.3±0.1	0.992
			30.0			0.27±0.03	0.964	6.5±0.3	0.993
			40.0			0.29±0.02	0.987	11.6±0.5	0.995
UVA-Vis/Fe^{3+}/H_2O_2/Oxalic acid	41.6	40.0	30.0	2.8	200 - 500	0.27±0.03	0.964	6.5±0.3	0.993
				3.5		0.24±0.02	0.991	9.0±0.4	0.991
				4.0		0.25±0.02	0.980	8.4±0.7	0.980
				4.5		0.28±0.04	0.961	7.5±0.4	0.993
				5.0		0.20±0.03	0.946	5.2±0.5	0.972
UVA-Vis/Fe^{3+}/H_2O_2/Oxalic acid	41.6	40.0	30.0	2.8	50 – 100	0.12±0.01	0.953	2.2±0.1	0.990
					100 – 200	0.205±0.009	0.993	5.9±0.2	0.996
					200 – 500	0.27±0.03	0.964	6.5±0.2	0.993
					68.2[f]	0.156±0.009	0.978	5.6±0.6	0.962

[a]Irradiation intensity (W m^{-2}); [b]Dissolved iron concentration (mg L^{-1}); [c]Liquid temperature (ºC); [d]Pseudo-first-order kinetic constant (L kJ^{-1}); [e]H_2O_2 consumption rate (mmol kJ^{-1}); [f] dosage at the reaction start. Treated matrix: [1]dye; [2]Sera®Sperse; [3]Sera®Con; [4]Sera®Lube; [5]Sera®Tard.

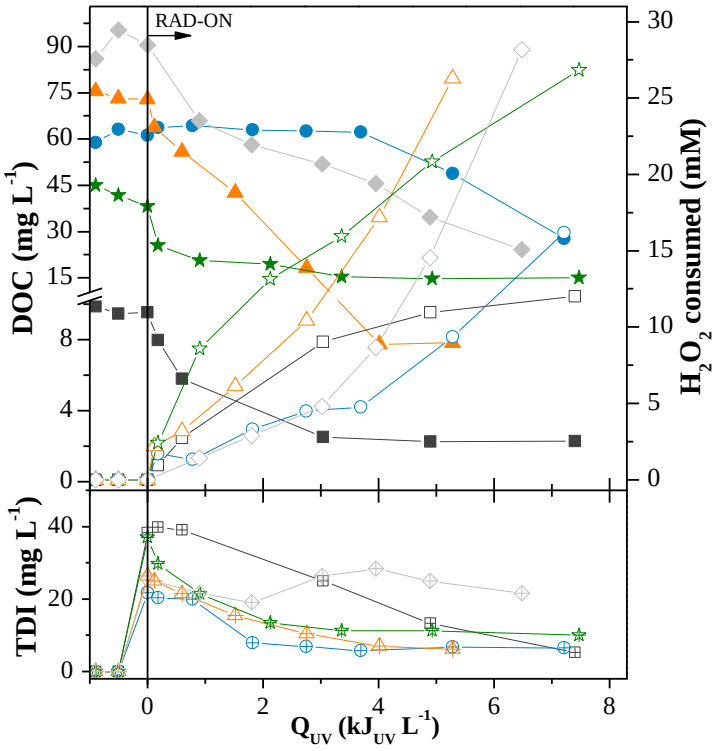

Figure 4.2. Mineralisation of individual solutions of dyeing auxiliary products and dye using a photo-Fenton reaction. Operation conditions: pH = 2.8; T = 30ºC; [Fe^{2+}] = 40 mg L^{-1}; I = 41.6 W_{UV} m^{-2}. Solid symbols - DOC; open symbols - H_2O_2 consumed; cross symbols - total dissolved iron (TDI). ■ □ ⊞ – Dye; ● ○ ⊕ – Sera Sperse M-IW; ▲ △ ⧋ – Sera Con N-VS; ★ ☆ ✯ – Sera Lube M-CF; ◆ ◇ ⌖ – Sera Tard A-AS.

According to the obtained results, the dispersing agent Sera® Sperse M-IW, with a non-ionic nature, and the cationic surfactant Sera® Tard A-AS, are the main causes for the induction reaction period in the photo-Fenton reaction applied to the synthetic textile wastewater. This can be attributed to the chemical structure of these organic compounds as also to the iron-organic complexes, since the dissolved iron concentration decreased in average 85% and 40%, for the assay with Sera® Sperse M-IW and Sera® Tard A-AS, respectively.

Figure 4.2 also shows that after a certain reaction time the photo-Fenton reaction almost stops, which can be associated with two main factors: i) the formation of low-molecular-weight carboxylic acids and their respective complexes with ferric ions, which present low photoactivity and recalcitrant characteristic to further mineralisation by hydroxyl radical attack [25, 26] and ii) the low mineralisation rate of the dyeing auxiliary products which present a short-chain aliphatic structure (alcohols, carboxylic acids, etc.) [27, 28].

4.3.3 Ferric-organic ligands complexes

Different studies report the photochemistry/chemistry of ferric and ferrous complexes in the presence of oxalic acid [18, 19, 29, 30], citric acid [31-33] and EDDS [16, 17, 34]. Ferric ions form stable and strong complexes with oxalic acid (Eq. (4.2)), citric acid (Eq. (4.3)), and/or EDDS (Eq. (4.4)), avoiding the undesired interactions with other organic ligands and at same time providing a quicker pathway for ferric iron regeneration in the presence of UV-visible light.

$$Fe^{3+}(Oxa) \xleftrightarrow{h\nu} Fe^{2+} + {}^{\bullet}Oxa \quad (4.2)$$

$$Fe^{3+}(Cit) \xleftrightarrow{h\nu} Fe^{2+} + {}^{\bullet}Cit \quad (4.3)$$

$$Fe^{3+}(EDDS) \xleftrightarrow{h\nu} Fe^{2+} + {}^{\bullet}EDDS \quad (4.4)$$

The enhancement of the photo-Fenton reaction through the use of ferric-organic ligands complexes, such as ferrioxalate, ferricitrate and ferric-EDDS, was evaluated in the treatment of the synthetic acrylic-textile dyeing wastewater, in order to avoid the formation of low photoactive complexes between ferric ions and auxiliary dyeing products present in the wastewater.

4.3.3.1 Oxalic Acid

The most stable ferric-oxalate complex results from the binding of three oxalate ions with one ferric ion [20, 35] which corresponds to a stoichiometric iron/oxalate molar ratio of 1:3. For lower molar ratios, insufficient oxalate is available to form the complex, decreasing the quantum yield for ferrous production. On the other hand, an excess of oxalate cannot complex totally with ferric ions in solution, and oxalate can act as an additional organic carbon source, competing for hydroxyl radicals with the target pollutant, then decreasing the reaction rate.

As expected, the addition of oxalic acid resulted in an increase of the dissolved organic carbon concentration (54 mg C L^{-1}). The DOC profile (Figure 4.3), after the addition of hydrogen peroxide in the presence of solar light, shows a fast decay until an accumulated UV energy of ~3.7 kJ_{UV} L^{-1}, following pseudo-first-order kinetics (k = 0.34 ± 0.02 L^{-1} kJ) (Table 4.3).

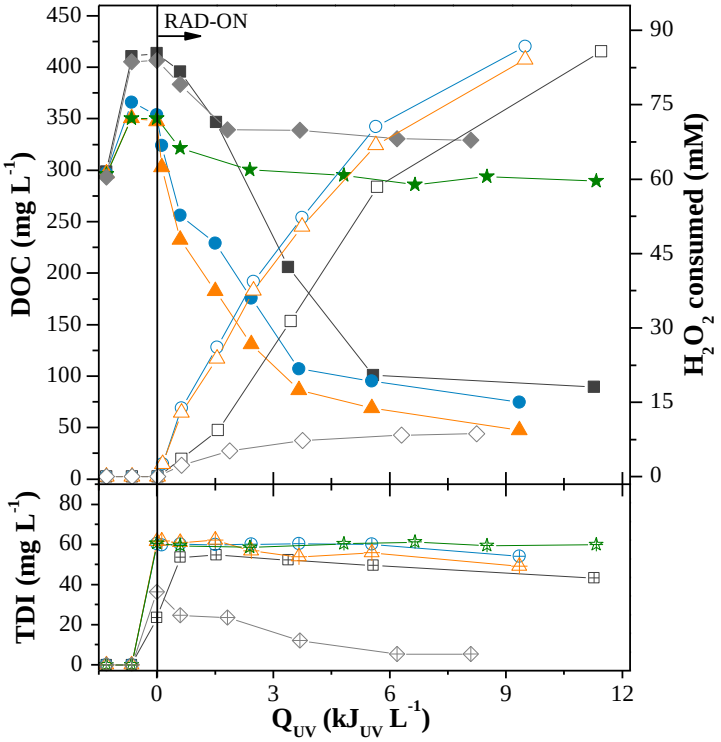

Figure 4.3. Mineralisation of the textile wastewater using a photo-Fenton reaction mediated by different ferric-organic ligand complexes. Operation conditions: pH = 2.8; T = 30ºC; [Fe^{3+}] = 60 mg L^{-1}; I = 41.6 W_{UV} m^{-2}. Solid symbols – DOC; open symbols – H_2O_2 consumed; cross symbols – total dissolved iron (TDI). ■ □ ⊞ – UVA-Vis/Fe^{3+}/H_2O_2/EDDS; ◆ ◇ ⊕ – UVA-Vis/Fe^{3+}/H_2O_2/EDDS (pH 6.8); ● ○ ⊕ - UVA-Vis/Fe^{3+}/H_2O_2/CIT; ▲ △ ⊞ - UVA-Vis/Fe^{3+}/H_2O_2/OXA; ★ ☆ ☆ - UVA-Vis/Fe^{3+}/OXA.

According to the ferric speciation diagram (Figure 4.4A), in the absence of oxalic acid, a molar fraction of only 15% for $FeOH^{2+}$ species at pH 2.8 is obtained, against a molar fraction of 38% for $FeSO_4^+$ species, which are less photoactive species when compared to $FeOH^{2+}$, and also can lead to the formation of less oxidant species $SO_4^{\bullet-}$ when compared to $^{\bullet}OH$ radicals. However, in the presence of oxalic acid (iron/oxalic molar ratio of 1:3), for the same pH value (Figure 4.4C), the predominant species in solution are $Fe(C_2O_4)_2^-$ (50%) and $Fe(C_2O_4)_3^{3-}$ (49%), which allow fast mineralisation kinetics, as therefore reducing significantly the formation of ferric-dyeing auxiliary products, ferric-sulphates and ferric-chloride complexes. Besides, ferrioxalate complexes are photodecarboxylated in the presence of UV-visible radiation (Eqs. (4.5)-(4.8)), enhancing the quantum yield for ferrous production and consequently the reaction rates [36].

$$Fe(C_2O_4)_2^- \xrightarrow{h\nu} Fe^{2+}(C_2O_2) + C_2O_4^{\bullet-} \qquad (4.5)$$

$$Fe(C_2O_4)_3^{3-} \xrightarrow{hv} Fe^{2+} 2C_2O_4^{2-} + C_2O_4^{\bullet-} \quad (4.6)$$

$$C_2O_4^{\bullet-} \rightarrow CO_2^{\bullet-} + CO_2 \quad (4.7)$$

$$CO_2^{\bullet-} + Fe(C_2O_4)_3^{3-} \rightarrow Fe^{2+} + CO_2 + 3C_2O_4^{2-} \quad (4.8)$$

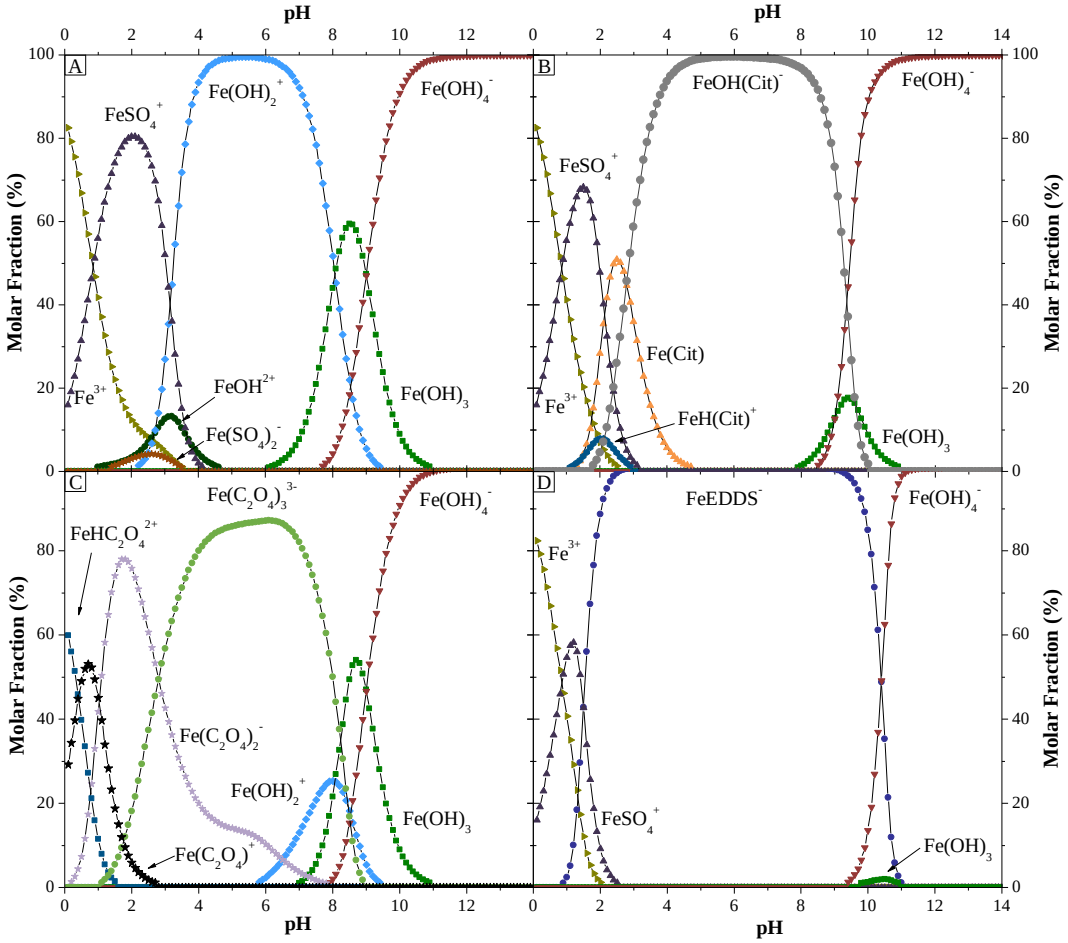

Figure 4.4. Speciation diagrams for ferric complexes as a function of pH for a solution containing: (A) $Fe^{3+}/SO_4^{2-}/Cl^-$; (B) $Fe^{3+}/SO_4^{2-}/Cl^-$/Citric acid; (C) $Fe^{3+}/SO_4^{2-}/Cl^-$/Oxalic acid; (D) $Fe^{3+}/SO_4^{2-}/Cl^-$/EDDS. Ionic strength=0.02 M; Temperature=30ºC; $[Fe^{3+}]=7.16\times10^{-1}$ mM (40 mg Fe^{3+} L^{-1}); [Citrate acid]$=7.16\times10^{-1}$ mM; [Oxalic acid]=2.15 mM; [EDDS]$=7.16\times10^{-1}$ mM; $[SO_4^{2-}]=6.17\times10^{-3}$ mM; $[Cl^-]=1.16\times10^{-3}$ mM. The formation of the solid iron phase $Fe(OH)_{3\,(s)}$ was excluded in the calculation.

Another interesting characteristic of the photo-Fenton reaction mediated by ferrioxalate complexes is the capacity of *in situ* generation of hydrogen peroxide, according to (Eqs. (4.9)-(4.12)). The photodecarboxylation of ferrioxalate complexes leads to the formation of carboxylate radical anion

($C_2O_4^{\bullet-}$), which decomposes into carbon dioxide radical anion ($CO_2^{\bullet-}$). Those radicals in the presence of oxygen form the oxygen and/or peroxide radicals and further reaction with ferrous ions promotes the formation of H_2O_2 [37].

$$CO_2^{\bullet-} + O_2 \rightarrow CO_2 + O_2^{\bullet-} \quad (4.9)$$

$$O_2^{\bullet-} + H^+ \rightarrow HO_2^{\bullet} \quad (4.10)$$

$$Fe^{2+} + O_2^{\bullet-} + 2H^+ \rightarrow Fe^{3+} + H_2O_2 \quad (4.11)$$

$$Fe^{2+} + HO_2^{\bullet} + H^+ \rightarrow Fe^{3+} + H_2O_2 \quad (4.12)$$

A photo-Fenton reaction mediated by ferrioxalate complexes without the addition of hydrogen peroxide was also performed and the results showed a low mineralisation, which can be associated with the insufficient *in situ* generation of H_2O_2 necessary to fuel the reaction.

4.3.3.2 Citric Acid

Although the effect of Fe(III) to citrate molar ratio on the photodegradation of different organic compounds has been discussed by several authors [32, 38, 39], the best iron-citrate molar ratio seems to be far from a consensus. However, 1:1 stoichiometry for the Fe(III) and citrate binding is recognized for the mononuclear complexes formation [32]. Considering the formation of mononuclear complexes and that the supplement of citrate consists in additional organic carbon source, 1:1 stoichiometry molar ratio of ferric-citrate was used.

The dissolved iron concentration remained also constant along the reaction, indicating that the ferricitrate complexes are stronger than ferric-dyeing auxiliary products, allowing a quicker photoreduction of ferric ions, and consequently leading to an enhancement of the photo-Fenton process. Although the addition of citric acid (68 mg C L^{-1}) leads to a higher increase on DOC than with the addition of oxalic acid, similar reaction rates were observed (0.28 ± 0.03 L^{-1} kJ), when compared to the reaction with oxalic acid, which suggests a high quantum yield of the Fe(Cit) (86%) species for Fe^{2+} formation (Figure 4.4B).

4.3.3.3 EDDS

Zhang [40], using a starting solution of Fe(III) (0.3 mM), additions of EDDS showed the complex formation through the increase of absorption. The complex absorption investigated at 340 nm showed a maximum at 0.3 mM of EDDS reaching a plateau up to 1 mM demonstrating that EDDS (hexadentate ligand) forms a 1 to 1 stable complex with Fe(III). The addition of EDDS led to a substantial increase of dissolved organic carbon (112 mg C L^{-1}), significantly higher when compared with contribution of citric and oxalic acids (Figure 4.3).

The addition of EDDS, as organic ligand of ferric ions, enhanced significantly the photo-Fenton reaction, when compared to the conventional one, achieving a pseudo-first-order kinetic constant of 0.18 ± 0.02 L^{-1} kJ, mostly due to two main factors: i) the $[Fe(EDDS)]^-$ complex enhances the dissolution and stability of iron in aqueous solution, which leads to higher activity of iron in solution (Figure 4.4D) [41]; ii) the $[Fe(EDDS)]^-$ complex is stable and photochemically efficient leading to a higher quantum yield for the formation of $^{\bullet}OH$ ($\phi_{\bullet OH} \approx 2.5 \times 10^{-3}$ at pH = 3.0) [34, 42].

Another photo-Fenton reaction with the ferric-EDDS complex was performed at the neutral wastewater pH value. Figure 4.3 shows an initial mineralisation profile similar to that obtained at pH 2.8 and afterwards the reaction stopped. According to the ferric speciation diagram, iron precipitation in the form of $Fe(OH)_{3(s)}$ starts to occur after pH 7 (Figure 4.5D). However, according to Figure 4.3, iron starts to precipitate at the beginning of the reaction indicating that other ferric-organic complexes with low solubility are formed at these pH values, which present a higher stability constant than the soluble $[Fe(EDDS)]^-$ complexes.

The catalytic activity of the organic ligands toward the ferrous-catalysed system followed this order: Fe(III)-Oxalate > Fe(III)-Citrate > Fe(III)-EDDS. For all tested organic ligands, the dissolved iron concentration remained almost constant during the entire reaction, which indicates that the formation of ferric-dyeing auxiliary products was avoided in the presence of the organic ligands. Therefore, the low photo-Fenton reaction rates can be mainly attributed to the formation of ferric complexes with the dissolved organic matter present in solution (for example: auxiliary products), reducing the quantum yield of ferrous formation.

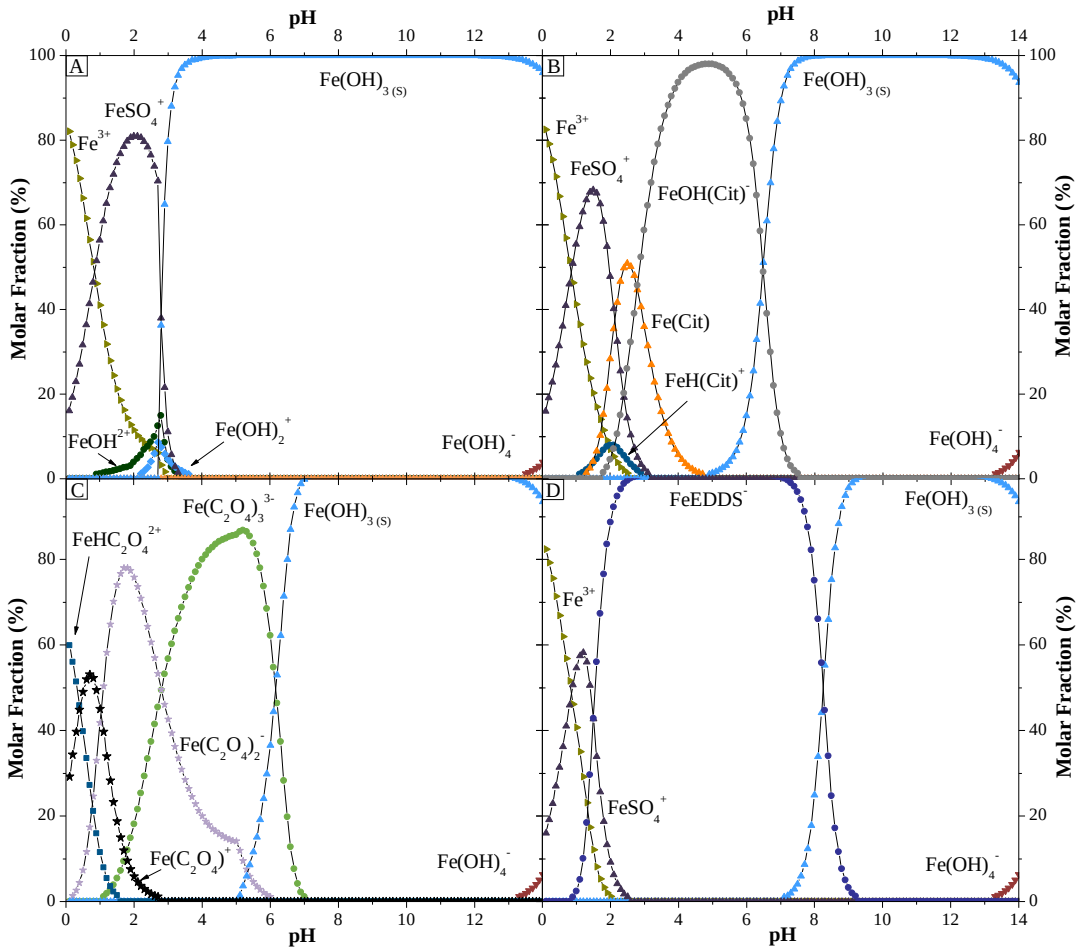

Figure 4.5. Speciation diagrams for ferric complexes as a function of pH for a solution containing: (A) $Fe^{3+}/SO_4^{2-}/Cl^-$; (B) $Fe^{3+}/SO_4^{2-}/Cl^-$/Citric acid; (C) $Fe^{3+}/SO_4^{2-}/Cl^-$/Oxalic acid; (D) $Fe^{3+}/SO_4^{2-}/Cl^-$/EDDS. Ionic strength=0.02 M; Temperature=30ºC; $[Fe^{3+}]=7.16\times10^{-1}$ mM (40 mg Fe^{3+} L^{-1}); [Citrate acid]=7.16×10^{-1} mM; [Oxalic acid]=2.15 mM; [EDDS]=7.16×10^{-1} mM; $[SO_4^{2-}]=6.17\times10^{-3}$ mM; $[Cl^-]=1.16\times10^{-3}$ mM. The formation of the solid iron phase $Fe(OH)_{3\,(s)}$ was included in the calculation.

4.3.4 Effect of different reaction variables of the photo-Fenton process enhanced by ferrioxalate

Further studies regarding the photo-Fenton reaction mediated by ferrioxalate were performed, in order to evaluate the effect of different reaction variables, such as iron concentration, temperature, irradiance, pH and hydrogen peroxide concentration and dosage strategy. The effect of flow rate in the photo-Fenton reaction was also evaluated in order to know the best hydrodynamic regime to achieve the higher reaction rate.

4.3.4.1 Effect of iron concentration

Figure 4.6 shows the influence of the iron concentration on the textile wastewater treatment using the photo-Fenton reaction mediated by ferrioxalate. Dissolved iron concentration remained almost constant during the entire experiment and very similar to the amount added initially. This indicates that the ferrioxalate complexes lifetime, considering an iron/oxalate molar ratio of 1:3, was sufficient to destroy all the dissolved organic matter responsible for the formation of unwanted low photoactive iron complexes.

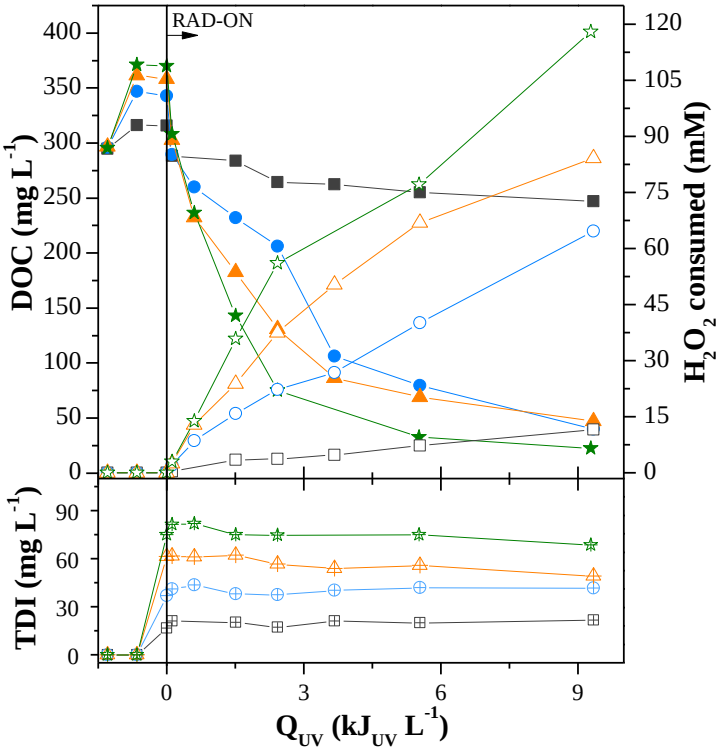

Figure 4.6. Photo-Fenton reaction mediated by ferrioxalate at different iron concentrations. Operation conditions: pH = 2.8; T = 30ºC; I = 41.6 W_{UV} m^{-2}. Solid symbols – DOC; open symbols – H_2O_2 consumed; cross symbols – total dissolved iron (TDI). ■ □ ⊞ – [Fe^{3+}] = 20 mg L^{-1}; ● ○ ⊕ - [Fe^{3+}] = 40 mg L^{-1}; ▲ △ ⧋ - [Fe^{3+}] = 60 mg L^{-1}; ★ ☆ ✯- [Fe^{3+}] = 80 mg L^{-1}.

The reaction rate increased substantially with the increase of iron concentration, principally between 20 and 40 mg L^{-1}. For concentrations higher than 40 mg L^{-1}, the increment in the reaction rate is small. This indicates that a concentration of 40 mg Fe^{3+} L^{-1} is enough to maximise the absorption of UV-visible photons, overcoming the presence of other light-absorbing species in solution (e.g.: dye) [43]. Higher iron concentrations require higher amounts of oxalic acid to be added in order to maintain the iron/oxalate molar ratio of 1:3. Moreover, oxalate can act as an additional organic carbon source,

competing with the target pollutant for hydroxyl radicals, and increasing the H_2O_2 consumption. This explains the increment in H_2O_2 consumption by a factor of 1.8 when total iron dissolved was changed from 40 to 80 mg L^{-1}.

4.3.4.2 Effect of solution temperature

Figure 4.7 shows the mineralisation of the textile wastewater at different temperatures (20°C, 30°C, and 40ºC) for an iron concentration of 40 mg L^{-1}, iron/oxalate molar ratio of 1:3, pH value of 2.8 and irradiance equal to 41.6 W_{UV} m^{-2}.

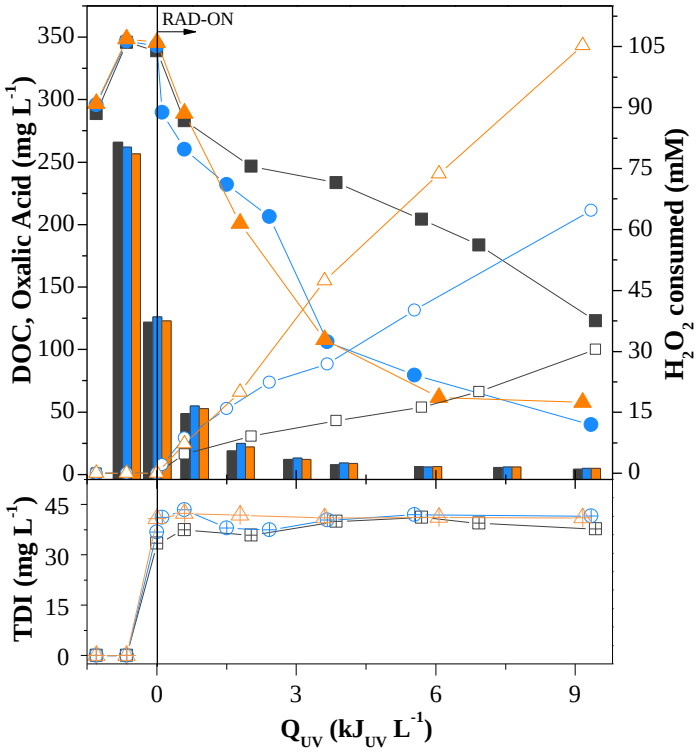

Figure 4.7. Evolution of the DOC concentration, H_2O_2 consumed and total dissolved iron during the photo-Fenton reaction mediated by ferrioxalate at different temperatures. Solid symbols – DOC; open symbols – H_2O_2 consumed; cross symbols – total dissolved iron (TDI); columns – oxalic acid concentration. ■ □ ⊞ – T=20ºC; ● ○ ⊕ – T = 30ºC; ▲ △ ⧋ – T = 40ºC.

The kinetic rate for the experiment performed at 20ºC was extremely low achieving a mineralisation efficiency of about 57% after 9 kJ_{UV} L^{-1}. The increase of the solution temperature from 20ºC to 30ºC improved significantly the reaction, achieving a mineralisation efficiency of 87% after 9 kJ_{UV} L^{-1}, consuming 64 mM H_2O_2. At the first moment, the observed mineralisation increase can be attributed

to a higher Fe^{3+} reduction through Fenton's thermal reactions [44]. But, a more careful analysis of the iron species in solution can reveal important considerations about this phenomenon.

The molar fractions of the iron species were calculated by the chemical equilibrium modelling system MINEQL+ [45] under the initial conditions in the presence of oxalate, Fe^{3+}, SO_4^{2-} and Cl^- and under the same settings but in the absence of oxalate ion (Figure 4.8), which corresponds to the system after photodecarboxylation of Fe(III)-oxalate complexes. According to the iron speciation diagrams at different temperatures, considering the starting conditions in terms of iron and oxalic acid concentration, quite similar molar fractions of $Fe(C_2O_4)_2^-$ and $Fe(C_2O_4)_3^{3-}$ were obtained for all the temperatures at pH 2.8 (see Figure 4.8D; Figure 4.8E and Figure 4.8F). However, in the absence of oxalic acid, the molar fraction of the $FeOH^{2+}$ species increases with temperature (see Figure 4.8A; Figure 4.8B and Figure 4.8C), achieving values of 9%, 15% and 16%, respectively for the temperatures of 20°C, 30°C, and 40ºC. So, after photodecarboxylation of ferrioxalate complexes, the beneficial effect of temperature on the reaction rates can be associated with two main factors [46]: i) presence of different amounts of photoactive species ($FeOH^{2+}$), and ii) higher Fe^{3+} reduction through Fenton's thermal reactions.

The increase of the solution temperature from 30ºC to 40ºC showed a negligible influence on the reaction rate, but increased significantly the H_2O_2 consumption mainly attributed to two main factors: i) thermal ferric ion reduction reactions without hydroxyl radicals production in contrast with the photo reduction pathway, where H_2O_2 is not necessary and leads to the production of more hydroxyl radicals and ii) hydrogen peroxide decomposition into H_2O and O_2 (inactive species) and the formation of radicals with smaller oxidation potential at high temperatures [30, 47] (the rate of decomposition of hydrogen peroxide doubles every time the temperature rises by 10ºC).

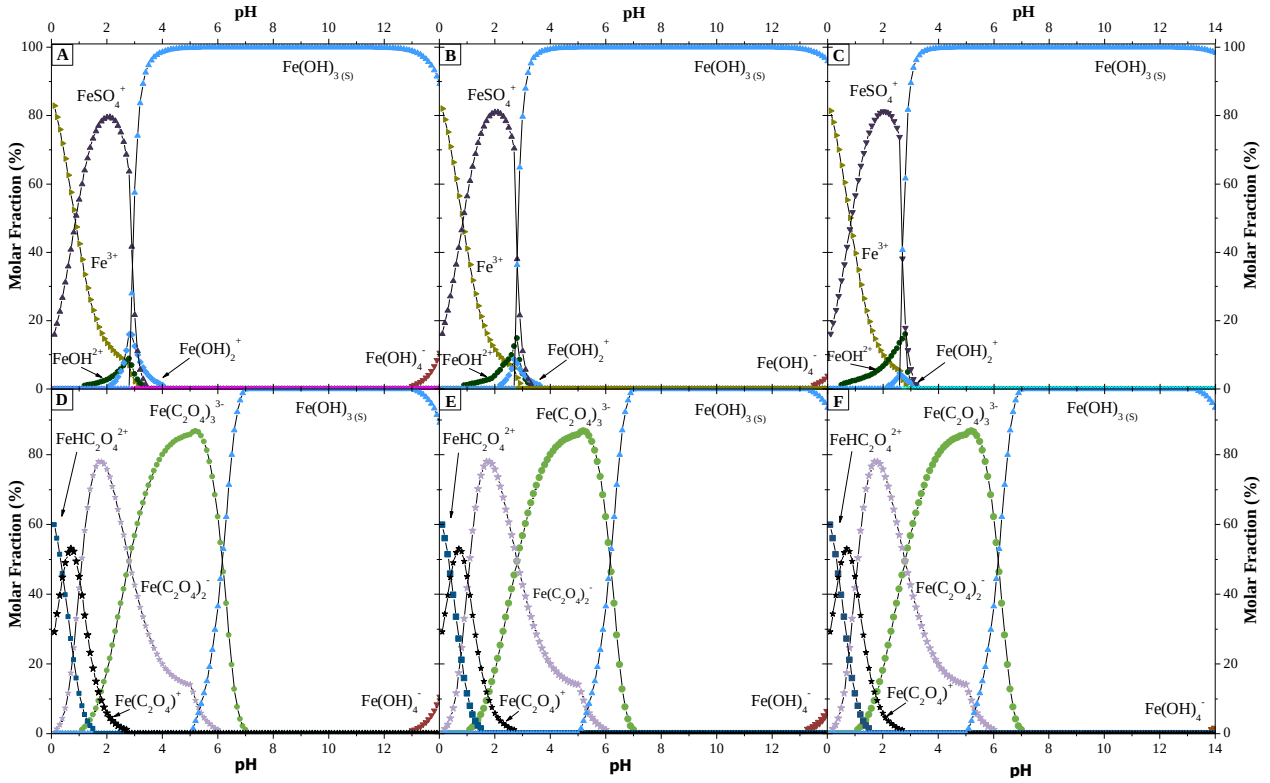

Figure 4.8. Speciation diagrams for ferric complexes as a function of pH for different temperatures, for a solution containing: $Fe^{3+}/SO_4^{2-}/Cl^-$: (A)-(T=20ºC); (B)-(T=30ºC); (C)-(T=40ºC). $Fe^{3+}/SO_4^{2-}/Cl^-$/Oxalic acid: (D)-(T=20ºC); (E)-(T=30ºC); (F)-(T=40ºC). Ionic strength=0.02 M; $[Fe^{3+}]=7.16\times10^{-1}$ mM (40 mg Fe^{3+} L^{-1}); [Oxalic acid]=2.15 mM; $[SO_4^{2-}]=6.17\times10^{-3}$ mM; $[Cl^-]=1.16\times10^{-3}$ mM. The formation of the solid iron phase $Fe(OH)_{3\,(s)}$ was included in the calculation.

4.3.4.3 Effect of UV irradiance

The solar light irradiance changes during the day, over the year, and according to the climatic conditions and local, e. g. latitude, seasons of the year or cloud cover, etc. Therefore, in this work it was evaluated the effect of solar light irradiance in the photo-Fenton reaction mediated by ferrioxalate process, using different weather conditions normally found in the north of Portugal - 20.6 W_{UV} m^{-2} (average daily irradiance in spring and summer), 41.6 W_{UV} m^{-2} (sunny midday in spring) and 59.2 W_{UV} m^{-2} (peak values in sunny midday in summer). Figure 4.9 shows the mineralisation of the textile wastewater at different solar light irradiances for different iron concentrations as a function of accumulated UV energy (kJ_{UV} L^{-1}).

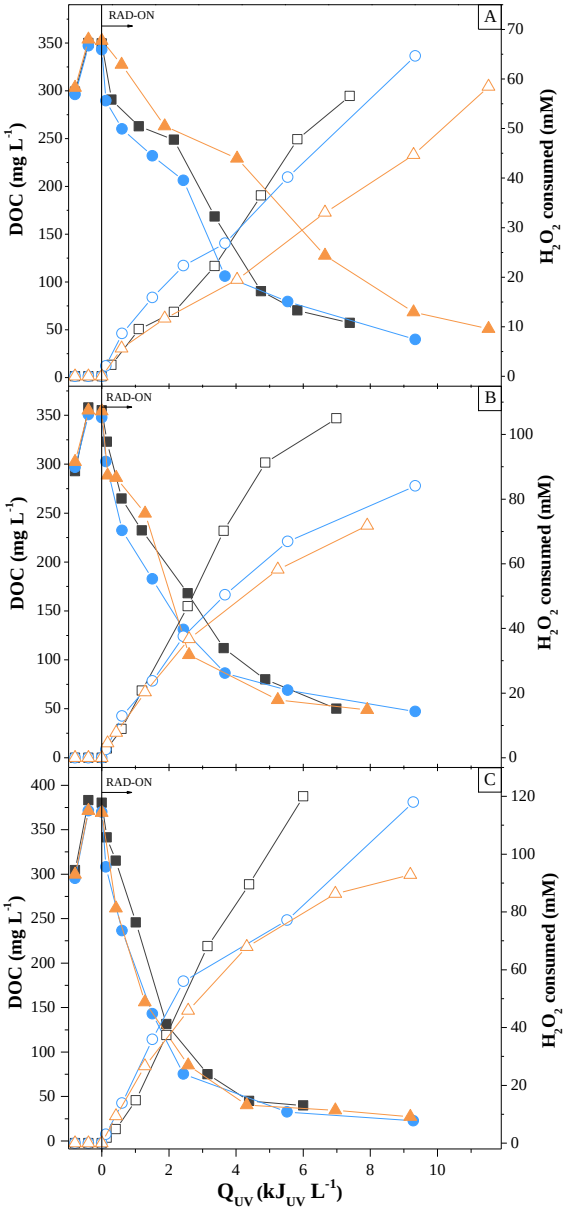

Figure 4.9. Mineralisation of the textile wastewater using a photo-Fenton reaction mediated by ferrioxalate at different UV irradiances and different iron concentrations. (a) $[Fe^{3+}]$ = 40 mg L^{-1}; (b) $[Fe^{3+}]$ = 60 mg L^{-1}; (c) $[Fe^{3+}]$ = 80 mg L^{-1}. Operation conditions: pH = 2.8; T = 30ºC. Solid symbols – DOC; open symbols – H_2O_2 consumed. ■ □ – I = 20.6 W_{UV} m^{-2}; ● ○ – I = 41.6 W_{UV} m^{-2}; ▲ △ – I = 59.2 W_{UV} m^{-2}.

According to the mineralisation values obtained, when iron concentration was 60-80 mg Fe^{3+} L^{-1}, for all three tested irradiance conditions, similar behaviour was found. However, when only 40 mg Fe^{3+} L^{-1} was used, for 59.2 W_{UV} m^{-2} of irradiance, it was observed a loss in the reaction efficiency. This means that considering the optical length of the reactor (borosilicate glass tube with 46.4 mm internal diameter), in order to avoid the loss of photons for irradiances of 59.2 W_{UV} m^{-2}, higher doses of iron are required to absorb all the photons. This indicates that the optimum iron concentration must be evaluated taking into account the variability on the UV irradiance (amount of photons available for the reaction).

4.3.4.4 Effect of H_2O_2 concentration range and dosage strategy

The hydrogen peroxide concentration plays an important role in the oxidation of organic compounds, since the decomposition of H_2O_2 catalysed by Fe(II), leads to the generation of the highly reactive hydroxyl radicals. A set of experiments were performed trying to explain the best strategy for the H_2O_2 supply, aiming high reaction rates and low H_2O_2 consumption (Figure 4.10). In the first three assays, hydrogen peroxide was supplied in multiple small doses, keeping always the desired H_2O_2 concentration between: i) 50-100 mg L^{-1}; ii) 100-200 mg L^{-1} and iii) 200-500 mg L^{-1}. Another experiment was performed adding all required H_2O_2 at the beginning of the reaction (2.3 g L^{-1}; 68.2 mM).

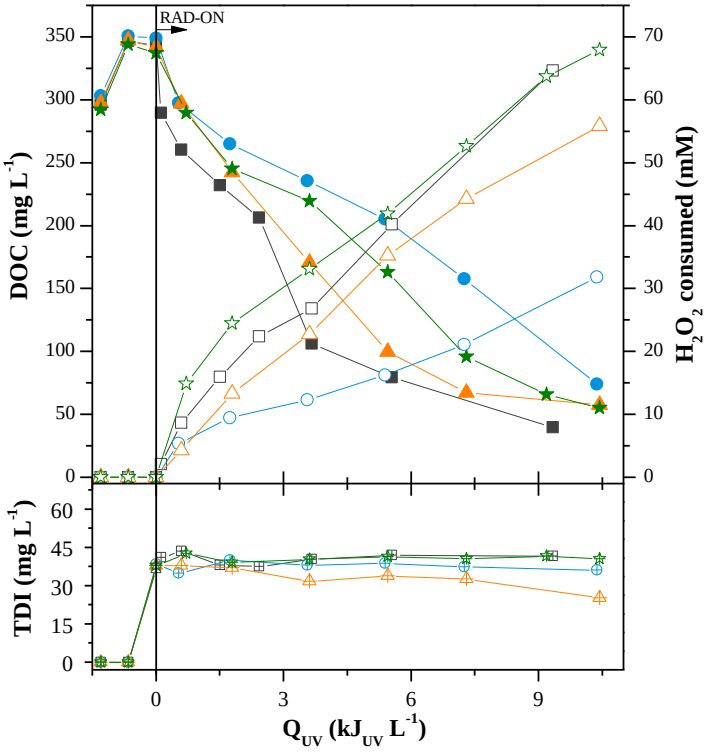

Figure 4.10. Mineralisation of the textile wastewater using a photo-Fenton reaction mediated by ferrioxalate using different hydrogen peroxide addition strategies and concentrations. Operation conditions: pH = 2.8; T = 30ºC; [Fe^{3+}] = 40 mg L^{-1}; I = 41.6 W_{UV} m^{-2}. Solid symbols – DOC; open symbols – H_2O_2 consumed; cross symbols – total dissolved iron (TDI). ■ □ ⊞ – [H_2O_2] = 200-500 mg L^{-1}; ▲ △ ⊞ – [H_2O_2] = 100-200 mg L^{-1}; ● ○ ⊕ – [H_2O_2] = 50-100 mg L^{-1}; ★ ☆ ☆ – one dose of H_2O_2 at the start of the reaction (68.2 mM).

Figure 4.10 shows that the strategy of adding small amounts of H_2O_2 during the photo-Fenton reaction improves the mineralisation rates, as also minimizes the consumption rate of H_2O_2. However, the mineralisation rate increases with the availability of H_2O_2, up to an optimal hydrogen peroxide concentration range between 100-200 mg L^{-1}. Further increase in the H_2O_2 concentration had negligible effect in the mineralisation, but higher amounts of H_2O_2 are required to achieve the same

mineralisation mainly associated with the well-known scavenger effect [48]. Although other radicals (e.g., $HO_2^{\bullet}$) are produced (Eq. (4.13)), their oxidation potential is much smaller than that of the hydroxyl radicals [18, 34, 49]. Furthermore, the decomposition of hydrogen peroxide to form water and oxygen is also favoured (Eq. (4.14)) [30].

$$H_2O_2 + {}^{\bullet}OH \rightarrow H_2O + HO_2^{\bullet} \quad (4.13)$$

$$2H_2O_2 \rightarrow 2H_2O + O_2 \quad (4.14)$$

4.3.4.5 Effect of solution pH

The high alkalinity of textile wastewaters constitutes a limitation for the application of the photo-Fenton reaction, since high amounts of acid are required to achieve the optimum pH (2.8) for the traditional photo-Fenton reaction. Beyond that, high amounts of base are also required to proceed with the correction of the pH until neutral pH conditions, to comply with the discharge limits established by authorities [1, 7]. Most of the photo-Fenton studies are performed under acidic conditions ($2.5 < pH < 3.5$) to avoid ferric precipitation [16, 20, 43] and since the predominant species in solution is $FeOH^{2+}$, the most photoactive ferric ion-water complex [50]. One of the main advantages on the use of ferric-organic ligands, such as ferrioxalate, is the high solubility of the ferrioxalate complexes, more soluble than ferric iron-water complexes, allowing to work at neutral pH values.

In order to evaluate the behaviour of the photo-Fenton reaction mediated by ferrioxalate complexes at near neutral pH conditions, assays were performed at different controlled pH values (2.8; 3.5; 4.0; 4.5 and 5.0). Figure 4.11 shows that higher initial doses of oxalic acid were required to achieve the same mineralisation profiles at higher pH values (pH 2.8 (1:3), pH 3.5 and pH 4.0 (1:7.5), pH 4.5 and 5.0 (1:10)).

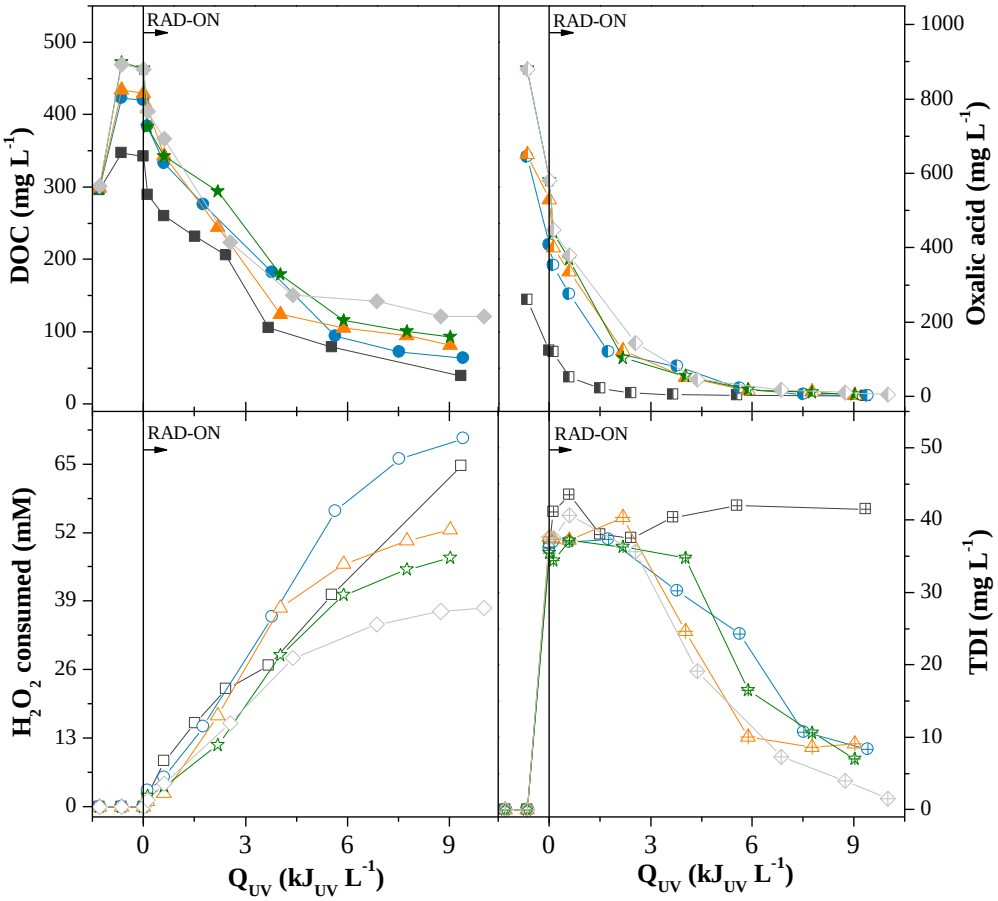

Figure 4.11. Mineralisation of the textile wastewater using a photo-Fenton reaction mediated by ferrioxalate at different pH values. Operation conditions: T = 30ºC; [Fe^{3+}] = 40 mg L^{-1}; I = 41.6 W_{UV} m^{-2}. Solid symbols – DOC; open symbols – H_2O_2 consumed; cross symbols – total dissolved iron (TDI); half painted symbols – oxalic acid concentration. ■ □ ⊞ ◧ – pH 2.8 and iron/oxalate molar ratio of 1:3; ● ○ ⊕ ◐ – pH 3.5 and iron/oxalate molar ratio of 1:7.5; ▲ △ ◬ ◭ – pH 4.0 and iron/oxalate molar ratio of 1:7.5; ★ ☆ ✯ ✭ – pH 4.5 and iron/oxalate molar ratio of 1:10; ◆ ◇ ⊕ ◈ - pH 5.0 and iron/oxalate molar ratio of 1:10.

From the oxalic acid concentration profiles, it can be seen that the lifetime of ferrioxalate complexes is very short. This indicates that higher doses of oxalic acid are necessary to avoid the precipitation of ferric hydroxides at higher pH values during the reaction time, enough to achieve the mineralisation of the recalcitrant textile organic compounds. For 1:1, 1:2, 1:3, 1:75 and 1:10 iron/oxalate molar ratios (Figure 4.12), the precipitation of $Fe(OH)_{3(s)}$ only starts for pH values higher than 3.1, 3.9, 5.1, 6.6 and 6.8. Figure 4.11 shows that, regardless of the initial oxalic acid concentration and solution pH, the precipitation of iron was only observed when the iron/oxalate molar ratio was lower than 1:1, since normally the formation of $Fe(OH)_{3(s)}$ is a slow reaction.

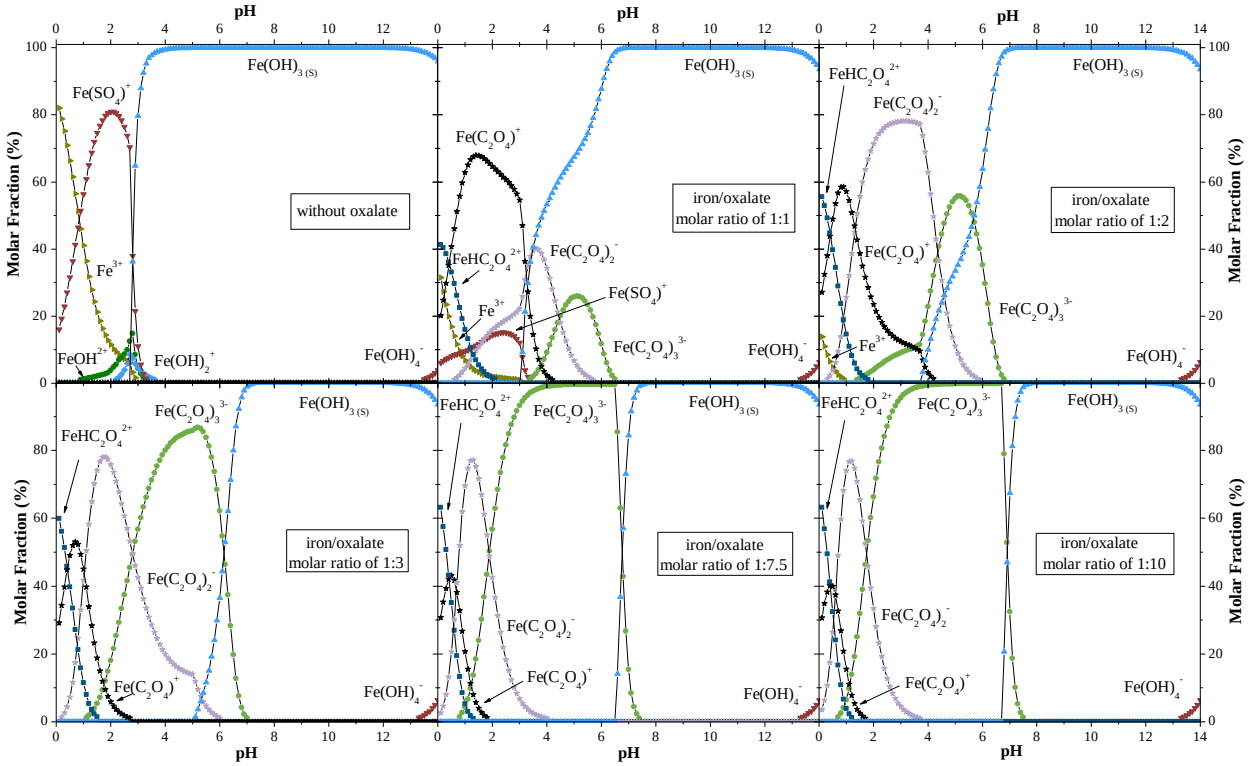

Figure 4.12. Speciation diagrams for ferric complexes as a function of pH for a solution containing 7.16×10^{-1} mM (40 mg Fe^{3+} L^{-1}) ferric ions, with different iron/oxalate molar ratios 1:1, 1:2, 1:3; 1:7.5; 1:10 and without oxalate. The formation of the solid iron phase $Fe(OH)_3$ was included in the calculation. Ionic strength = 0.02 M; Temperature = 30ºC; $[SO_4^{2-}] = 6.17\times10^{-3}$ mM; $[Cl^-] = 1.16\times10^{-3}$ mM.

It was also observed that the increase of oxalic acid concentration, needed for the reactions at higher pH values, decreases the H_2O_2 consumption. This indicates that the ferrous ions regeneration catalysed by the ferrioxalate complexes is more significant than the thermal Fenton reaction, at higher pH values [19], as also the possible generation of H_2O_2 due to photodecarboxylation of ferrioxalate complexes.

4.3.4.6 Effect of flow-rate

Several studies reported that if the catalyst is used in suspension, such as TiO_2 nanoparticles, a turbulent flow regime must be ensured to guarantee adequate fluid mixture and to avoid potential catalyst settlement along the hydraulic circuit. Therefore, the absorption of the UV photons by the photocatalyst is maximised and the mass transfer limitations between organic pollutants and the catalyst surface is reduced [51].

Figure 4.13 shows the photo-Fenton mineralisation profiles for the textile wastewater obtained in the lab-scale photoreactor prototype using simulated solar radiation at a flow-rate of 0.63 L min^{-1} (Re = 324, laminar regime), and in a pilot plant (natural sunlight) at different flow-rates: 2 L min^{-1} with and without mechanically stirred dark phase (Re = 1027; laminar regime); 9 L min^{-1} (Re = 4622; turbulent regime); 20 L min^{-1} (Re = 10271; turbulent regime); and 35 L min^{-1} (Re = 17974, turbulent regime) (Table 4.4).

The mineralisation profile obtained in the lab-scale prototype (laminar regime) is similar to the ones obtained in the pilot plant in turbulent regime (Re > 4000). In both plants, the hydraulic circuit is composed by a recirculation tank/vessel, connection tubing and borosilicate tubes (illuminated part). The glass vessel of the lab-scale prototype is magnetic stirred, allowing for a perfect mixture of the wastewater in the dark phase. On the other hand, in the pilot plant, the mixture inside the recirculation tank is only the one produced by the entrance of the wastewater, consequently a small mixture is obtained when low recirculation rates are used.

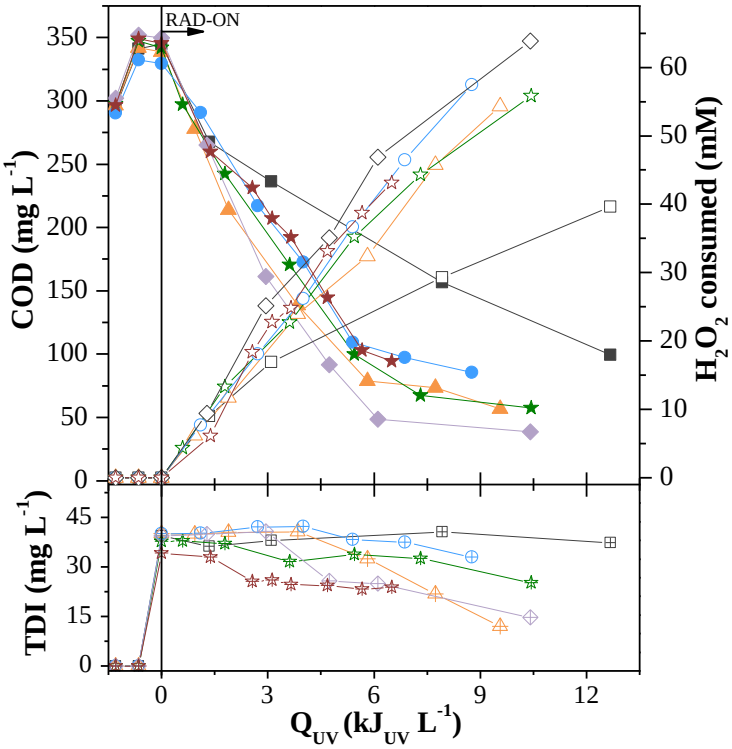

Figure 4.13. Mineralisation of the textile wastewater using a photo-Fenton reaction mediated by ferrioxalate (iron/oxalate molar ratio of 1:3) at different flow-rates. Operation conditions: pH = 2.8; [Fe^{3+}] = 40 mg L^{-1}. Pilot plant: ■ □ ⊞ – 2 L min^{-1}; ◆ ◇ ⊕ – 2 L min^{-1} with mechanically stirred dark phase; ★ ☆ ✯ – 9 L min^{-1}; ● ○ ⊕ – 20 L min^{-1}; ▲ △ ⧋ – 35 L min^{-1}. Lab-scale photoreactor: ★ ☆ ✯ - 0.63 L min^{-1}.

A low reaction rate can be observed for the experiment at a flow-rate of 2 L min^{-1} in the pilot plant, in agreement with the low H_2O_2 consumption profile and low dissolved iron concentrations. These results are explained by the low mixture in the recirculation tank (dark phase), as also the laminar flow inside the tubular photoreactors (illuminated phase). An additional experiment was performed at 2 L min^{-1} and the wastewater present in the recirculation tank was mechanically stirred. In these conditions, a faster reaction rate was observed, similar to the ones performed using a turbulent regime in the photoreactors. The design of a CPC plant must therefore take into account not only the need of a turbulent regime inside the tubular photoreactors, but also the mixing of the wastewater in the recirculation tank.

Table 4.4. Operational conditions and pseudo-first-order kinetic constants for solar driven photo-Fenton reactions.

System	Q^a	V_i^b	V_i/V_t^c	t_i^d	t_{dark}^e	Re^f	Kinetic parameters			
							DOC degradation		H_2O_2 consumption	
							k^g	R^2	k_H^h	R^2
UVA-Vis/Fe^{3+}/H_2O_2/oxalic acid[1]	2	5.1	0.23	2.6	8.5	1027	0.08±0.02	0.991	3±1	0.962
	2[i]			2.6	8.5	1027	0.32±0.09	0.986	7.6±0.4	0.994
	9			0.6	1.9	4622	0.17±0.02	0.961	6.7±0.9	0.996
	20			0.3	0.9	10271	0.20±0.01	0.978	6.0±0.1	0.999
	35			0.2	0.5	17974	0.23±0.01	0.992	5.8±0.2	0.997

[a](L min^{-1}); [b]illuminated volume (L); [c]illuminated volume divided by the total volume; [d]illumination time (min); [e]time in the dark (min); [f]Reynolds number; [g]Pseudo-first-order kinetic constant (L kJ^{-1}); [h]H_2O_2 consumption rate (mmol kJ^{-1}); [i]mechanically stirred dark phase; [1]Operation conditions: pH = 2.8; [Fe^{3+}] = 40 mg L^{-1}; iron/oxalate molar ratio of 1:3.

4.3.5 Integration of the photo-Fenton reaction with a biological oxidation process

The use of the photo-Fenton process should be considered when the wastewater presents toxic and/or non-biodegradable organic pollutants and therefore, not treatable by conventional biological processes [43]. In order to optimise the treatment process, reducing operation and capital costs, integrated system is becoming more frequent, combining the photo-Fenton reaction, as pre-oxidation step to enhance the biodegradability of the wastewater, with a biological oxidation process [11]. Therefore, a photo-Fenton reaction mediated by ferrioxalate, using the optimum conditions optimised at a lab-scale prototype (pH = 2.8; iron/oxalate molar ratio of 1:3; [Fe^{3+}] = 40 mg L^{-1}; flow-rate = 35 L min^{-1}), was conducted in a solar pilot plant (Figure 4.14), to evaluate the optimal phototreatment time to achieve a higher biological degradation efficiency. Various samples at

different phototreatment times were collected and a detailed characterisation was performed, including DOC, COD, BOD_5, low-molecular-weight carboxylic acids and the Zahn-Wellens test.

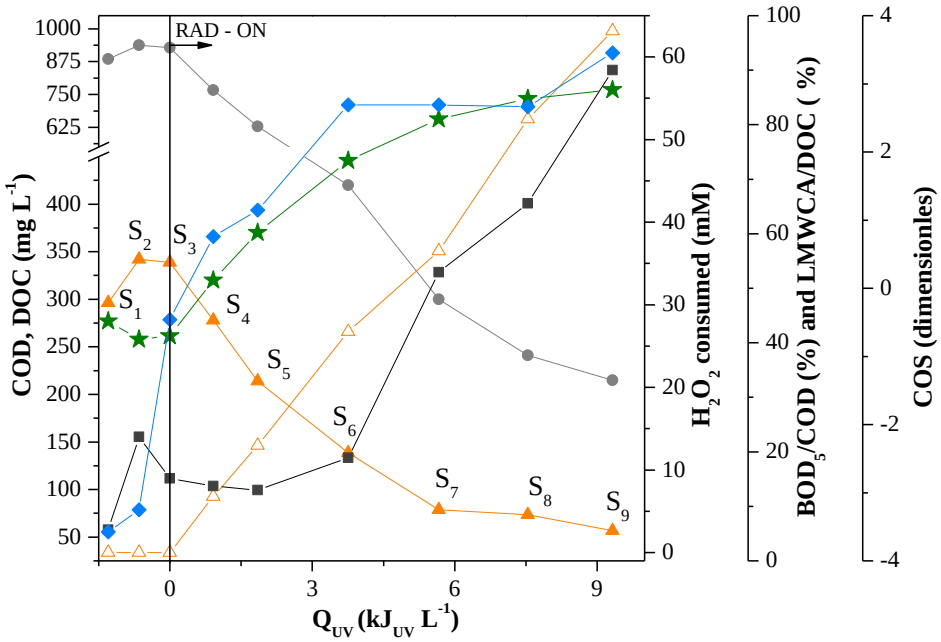

Figure 4.14. Evaluation of the solar photo-Fenton mediated by ferrioxalate (iron/oxalate molar ratio of 1:3) in the textile dyeing wastewater treatment: ● - COD, ▲ - DOC, ★ - COS, ■ - LMWCA/DOC ratio, △ - H_2O_2 consumed and ◆ - BOD_5/COD ratio. Operation conditions: pH = 2.8; $[Fe^{3+}]$ = 40 mg L^{-1}; $\overline{T}$ = 33ºC; $\bar{I}$ = 45 W m^{-2}.

Figure 4.14 shows a strong oxidation of the organics, with 66% and 73% COD and DOC decrease, respectively, after 5.7 kJ_{UV} L^{-1}. This behaviour is well related to the COS parameter, which showed a significant increase from -0.5 to 2.5 for the same energy dosage, suggesting the generation of highly oxidized intermediates. Additionally, the BOD_5/COD ratio increased significantly up to 83% after 3.85 kJ_{UV} L^{-1} only, corresponding to sample 6, which indicates a high enhancement of the textile wastewater biodegradability. Figure 4.14 also shows an increase of the DOC corresponding to low-molecular-weight carboxylate anions (LMWCA/DOC ratio), achieving maximum values of 90% (considering the analysed LMWCA) at 54.3 mM H_2O_2 consumed. Whilst the concentrations of oxalic acid (added) and formic acid decreased during the treatment, glutaric and acetic acid substantially increased after sample 5 (Table 4.5), achieving values of 56 mg $C_5H_8O_4$ L^{-1} and 86 mg $C_2H_4O_2$ L^{-1} at the end of the reaction.

Acetate ions form a stable complex with ferric ions which present a low photoactivity under UV-visible light and acetic acid presents a recalcitrant characteristic to further mineralisation by hydroxyl

radical attack [28, 52]. The presence of this complex can be associated with the low mineralisation rates observed after 5.7 kJ_{UV} L^{-1}.

Table 4.5. Concentration of carboxylic acids during the solar-photo-Fenton treatment.

Samples	Concentration of carboxylic acids (mg L^{-1})					
	Oxalic Acid	Formic Acid	Glutaric Acid	Tartaric Acid	Fumaric Acid	Acetic Acid
S_1	<0.04	64	<0.4	<0.05	<0.03	<0.5
S_2	231	62	<0.4	<0.05	<0.03	<0.5
S_3	130	64	<0.4	<0.05	<0.03	<0.5
S_4	101	43	<0.4	<0.05	<0.03	<0.5
S_5	29	43	11	<0.05	<0.03	15
S_6	12	11	24	<0.05	<0.03	34
S_7	6	<0.6	47	1.8	0.2	67
S_8	8	<0.6	54	2.1	0.3	77
S_9	7	<0.6	56	2.2	0.4	86

The photo-Fenton reaction mediated by ferrioxalate also indicated high decolourisation efficiency (Figure 4.15). Maximum values of colour reduction were 92% (Pt-Co method), 96% ($DFZ_{436\,nm}$), 96% ($DFZ_{525\,nm}$) and 97% (DFZ_{620nm}) consuming 32.4 mM H_2O_2 and 5.7 kJ_{UV} L^{-1}.

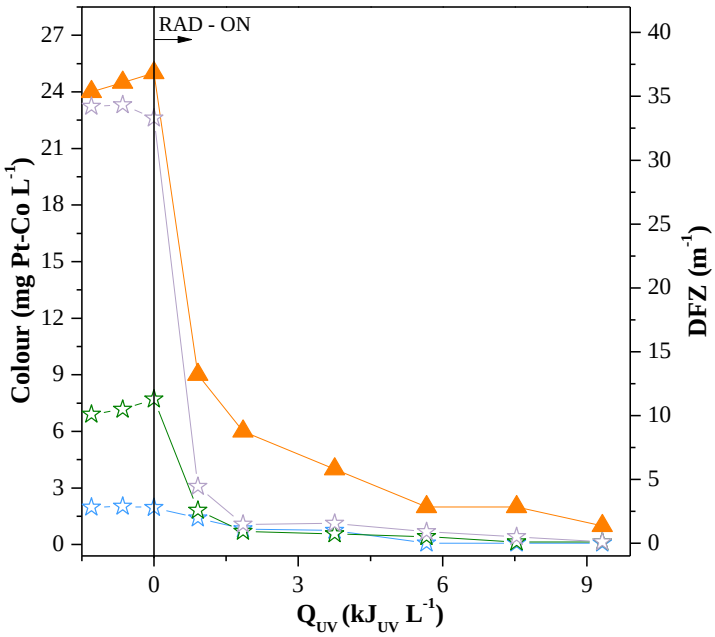

Figure 4.15. Cotton-textile dyeing wastewater decolourisation using Solar-photo-Fenton treatment mediated by ferrioxalate (iron/oxalate molar ratio of 1:3). ▲ - Pt-Co scale; ☆ - DFZ_{436nm}; ☆ - DFZ_{525nm}; ☆ - DFZ_{620nm}.

According to the Zahn-Wellens test (Figure 4.16), the textile dyeing wastewater presents a low biodegradability of 27% after 28 days of test. This value is mainly related to the presence of formic

acid (64 mg CH_2O_2 L^{-1}), resulting from the addition of the auxiliary textile Sera® Con N-VS in the dyeing process.

After the addition of iron and oxalate acid, the biodegradability reaches approximately 52%, which is related to the content of oxalic acid (231 mg $H_2C_2O_4$ L^{-1}) (Table 4.5). As expected, the biodegradability of the textile wastewater was significantly enhanced during the photo-Fenton treatment, achieving value of 73% corresponding to 32.4 mM of H_2O_2 consumed and 5.7 kJ_{UV} L^{-1} of energy dose. Over than 50% of the biodegradable organic fraction was in the form of low-molecular-weight carboxylic acids (the most representative: Glutaric Acid (27%) and Acetic Acid (23%)).

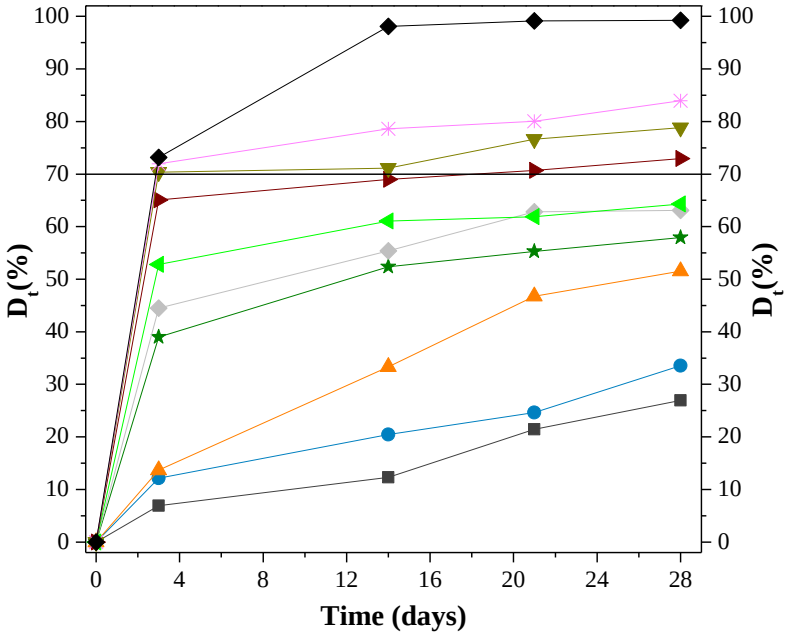

Figure 4.16. Zahn–Wellens test for selected samples at different photo-treatment times using a solar photo-Fenton reaction mediated by ferrioxalate (iron/oxalate molar ratio of 1:3): ■ – S_1, DOC = 295 mg L^{-1}; ● – S_2, DOC = 342 mg L^{-1}; ▲ – S_3, DOC = 339 mg L^{-1}; ★ – S_4, DOC = 278 mg L^{-1}; ◆ – S_5, DOC = 214 mg L^{-1}; ◀ – S_6, DOC = 139 mg L^{-1}; ▶ – S_7, DOC = 79 mg L^{-1}; ▼ – S_8, DOC = 74 mg L^{-1}; ✳ – S_9, DOC = 57 mg L^{-1}; ◆ – reference, DOC = 400 mg L^{-1}.

Throughout the treatment, successive additions of small dosages of sulphuric acid were responsible for the increment on the sulphate concentration (593-718 mg SO_4^{2-} L^{-1}). The chloride concentration increased from 41 to 100 mg Cl^- L^{-1} after ferric chloride dosing and remained constant during the whole phototreatment time. The concentration of sodium, magnesium, calcium and total nitrogen remained approximately constant during all reaction time. On the other hand, the phosphates concentration decreased from 0.8 mg PO_4^{3-} L^{-1} to values below the detection limit (0.1 mg PO_4^{3-} L^{-1}) during the reaction. This can be associated with the formation of Strengite ($FePO_4.2H_2O_{(s)}$) and

consequently precipitation of iron. Considering all the studied indicators and the current Portuguese Legislation (Decree-Law nº 236/98), the phototreatment must be performed until achieving the conditions of sample 7 before subsequent coupling with a biological treatment.

4.4 Conclusions

The acrylic-textile wastewater presents a moderate organic load with very low biodegradability associated with the presence of different recalcitrant dyeing auxiliary products. The traditional solar-photo-Fenton process showed limited efficiency in the mineralisation of the acrylic-textile wastewater, mainly attributed to the iron complexation with the dyeing auxiliaries, which presented a low photoactivity, almost stopping the photo-Fenton reaction.

The addition of organic ligands, such as oxalic acid, citric acid and EDDS, enhanced the photo-Fenton reaction significantly, minimising the formation of ferric complexes with the dyeing auxiliary products, and consequently increasing the quantum yield for ferrous ions production. The catalytic activity of the organic ligands toward the ferrous catalysed system followed the order: Fe(III)-Oxalate>Fe(III)-Citrate>Fe(III)-EDDS.

The optimum values for the acrylic-dyeing textile wastewater treatment variables using a photo-Fenton reaction mediated by ferrioxalate shall consider the following: i) the iron concentration must be selected taking into account the available UV irradiance; ii) the addition of small doses of H_2O_2 during the photo-Fenton reaction improves the mineralisation rates, while reducing the H_2O_2 consumption; iii) the mineralisation rate increases with the availability of H_2O_2 up to an optimal concentration range between 100-200 mg L^{-1}; iii) higher temperatures enhance the photo-Fenton reaction due to molar fraction increment of the photoactive species ($FeOH^{2+}$) and higher Fe^{3+} reduction rates through Fenton's thermal reactions; iv) hydrodynamic conditions in the dark phase (recirculation tank) and illuminated phase (tubular photoreactors) must be evaluated in order to achieve a complete mixing and turbulent regimes to minimise the mass transfer resistances as well as the catalyst sedimentation; vi) high doses of oxalic acid are required to work at near neutral pH conditions; vii) the photo-Fenton reaction mediated by ferrioxalate substantially enhances the textile wastewater biodegradability, mainly associated with low-molecular-weight carboxylic acids formation (acetic and glutaric acids), being possible to couple this process with a biological oxidation system minimizing the operation costs; viii) acetic acid forms a stable complex with ferric ions which has a low photoactivity under UVA-visible light and is very resistant to the attack of hydroxyl and other reactive oxygen species, almost stopping the photo-Fenton reaction.

4.5 References

1. Verma, A.K., R.R. Dash, and P. Bhunia, *A review on chemical coagulation/flocculation technologies for removal of colour from textile wastewaters.* Journal of Environmental Management, 2012. **93**(1): p. 154-168.
2. Arana, J., D. Zerbani, J.A. Herrera Melian, D. Garzon Sousa, O. Gonzalez Diaz, and J.M. Dona Rodriguez, *Effect of additives in photocatalytic degradation of commercial azo dye Lanaset Sun Yellow 180.* Photochemical & Photobiological Sciences, 2013. **12**(4): p. 703-708.
3. Moore, S.B. and L.W. Ausley, *Systems thinking and green chemistry in the textile industry: concepts, technologies and benefits.* Journal of Cleaner Production, 2004. **12**(6): p. 585-601.
4. Barragán, B.E., C. Costa, and M. Carmen Marquez, *Biodegradation of azo dyes by bacteria inoculated on solid media.* Dyes and pigments, 2007. **75**(1): p. 73-81.
5. Castillo, M. and D. Barceló, *Characterisation of organic pollutants in textile wastewaters and landfill leachate by using toxicity-based fractionation methods followed by liquid and gas chromatography coupled to mass spectrometric detection.* Analytica Chimica Acta, 2001. **426**(2): p. 253-264.
6. Rieger, P.-G., H.-M. Meier, M. Gerle, U. Vogt, T. Groth, and H.-J. Knackmuss, *Xenobiotics in the environment: present and future strategies to obviate the problem of biological persistence.* Journal of Biotechnology, 2002. **94**(1): p. 101-123.
7. Soares, P., T.C.V. Silva, D. Manenti, S.A.G.U. Souza, R.R. Boaventura, and V.P. Vilar, *Insights into real cotton-textile dyeing wastewater treatment using solar advanced oxidation processes.* Environmental Science and Pollution Research, 2013: p. 1-14.
8. Byberg, R., J. Cobb, L.D. Martin, R.W. Thompson, T.A. Camesano, O. Zahraa, and M.N. Pons, *Comparison of photocatalytic degradation of dyes in relation to their structure.* Environmental Science and Pollution Research, 2013. **20**(6): p. 3570-3581.
9. Nidheesh, P., R. Gandhimathi, and S. Ramesh, *Degradation of dyes from aqueous solution by Fenton processes: a review.* Environmental Science and Pollution Research, 2013. **20**(4): p. 2099-2132.
10. Arslan-Alaton, I., *Degradation of a commercial textile biocide with advanced oxidation processes and ozone.* Journal of Environmental Management, 2007. **82**(2): p. 145-154.
11. Oller, I., S. Malato, and J.A. Sánchez-Pérez, *Combination of Advanced Oxidation Processes and biological treatments for wastewater decontamination—A review.* Science of The Total Environment, 2011. **409**(20): p. 4141-4166.
12. De la Cruz, N., J. Giménez, S. Esplugas, D. Grandjean, L.F. de Alencastro, and C. Pulgarín, *Degradation of 32 emergent contaminants by UV and neutral photo-fenton in domestic wastewater effluent previously treated by activated sludge.* Water Research, 2012. **46**(6): p. 1947-1957.
13. Spuhler, D., J. Andrés Rengifo-Herrera, and C. Pulgarin, *The effect of Fe^{2+}, Fe^{3+}, H_2O_2 and the photo-Fenton reagent at near neutral pH on the solar disinfection (SODIS) at low temperatures of water containing Escherichia coli K12.* Applied Catalysis B: Environmental, 2010. **96**(1–2): p. 126-141.
14. Moncayo-Lasso, A., L.E. Mora-Arismendi, J.A. Rengifo-Herrera, J. Sanabria, N. Benitez, and C. Pulgarin, *The detrimental influence of bacteria (E. coli, Shigella and Salmonella) on the degradation of organic compounds (and vice versa) in TiO_2 photocatalysis and near-neutral*

photo-Fenton processes under simulated solar light. Photochemical & Photobiological Sciences, 2012. **11**(5): p. 821-827.

15. Ruales-Lonfat, C., J.F. Barona, A. Sienkiewicz, J. Vélez, L.N. Benítez, and C. Pulgarín, *Bacterial inactivation with iron citrate complex: A new source of dissolved iron in solar photo-Fenton process at near-neutral and alkaline pH.* Applied Catalysis B: Environmental, 2016. **180**: p. 379-390.
16. Klamerth, N., S. Malato, A. Aguera, and A. Fernandez-Alba, *Photo-Fenton and modified photo-Fenton at neutral pH for the treatment of emerging contaminants in wastewater treatment plant effluents: a comparison.* Water Research, 2013. **47**(2): p. 833-840.
17. Kwan, C.Y. and W. Chu, *The role of organic ligands in ferrous-induced photochemical degradation of 2,4-dichlorophenoxyacetic acid.* Chemosphere, 2007. **67**(8): p. 1601-1611.
18. Lucas, M.S. and J.A. Peres, *Degradation of Reactive Black 5 by Fenton/UV-C and ferrioxalate/H_2O_2/solar light processes.* Dyes and Pigments, 2007. **74**(3): p. 622-629.
19. Prato-Garcia, D., R. Vasquez-Medrano, and M. Hernandez-Esparza, *Solar photoassisted advanced oxidation of synthetic phenolic wastewaters using ferrioxalate complexes.* Solar Energy, 2009. **83**(3): p. 306-315.
20. Pignatello, J.J., E. Oliveros, and A. MacKay, *Advanced Oxidation Processes for Organic Contaminant Destruction Based on the Fenton Reaction and Related Chemistry.* Critical Reviews in Environmental Science and Technology, 2006. **36**(1): p. 1-84.
21. Poole, A.J., *Treatment of biorefractory organic compounds in wool scour effluent by hydroxyl radical oxidation.* Water Research, 2004. **38**(14–15): p. 3458-3464.
22. Liwarska-Bizukojc, E., K. Miksch, A. Malachowska-Jutsz, and J. Kalka, *Acute toxicity and genotoxicity of five selected anionic and nonionic surfactants.* Chemosphere, 2005. **58**(9): p. 1249-1253.
23. Ying, G.G., *Fate, behavior and effects of surfactants and their degradation products in the environment.* Environ Int, 2006. **32**(3): p. 417-31.
24. Pehlivanoglu-Mantas, E., G. Insel, O. Karahan, E.U. Cokgor, and D. Orhon, *Case Studies from Turkey: Xenobiotic-containing Industries, Wastewater Treatment and Modeling.* Water, Air, & Soil Pollution: Focus, 2008. **8**(5-6): p. 519-528.
25. Rodríguez, E.M., B. Núñez, G. Fernández, and F.J. Beltrán, *Effects of some carboxylic acids on the Fe(III)/UVA photocatalytic oxidation of muconic acid in water.* Applied Catalysis B: Environmental, 2009. **89**(1–2): p. 214-222.
26. Guinea, E., F. Centellas, J.A. Garrido, R.M. Rodríguez, C. Arias, P.-L. Cabot, and E. Brillas, *Solar photoassisted anodic oxidation of carboxylic acids in presence of Fe^{3+} using a boron-doped diamond electrode.* Applied Catalysis B: Environmental, 2009. **89**(3–4): p. 459-468.
27. Arslan-Alaton, I. and E. Erdinc, *Effect of photochemical treatment on the biocompatibility of a commercial nonionic surfactant used in the textile industry.* Water Research, 2006. **40**(18): p. 3409-3418.
28. Sinha, A., S. Chakrabarti, B. Chaudhuri, S. Bhattacharjee, P. Ray, and S.B. Roy, *Oxidative Degradation of Strong Acetic Acid Liquor in Wastewater Emanating from Hazardous Industries.* Industrial & Engineering Chemistry Research, 2007. **46**(10): p. 3101-3107.
29. Weller, C., S. Horn, and H. Herrmann, *Effects of Fe(III)-concentration, speciation, excitation-wavelength and light intensity on the quantum yield of iron(III)-oxalato complex photolysis.* Journal of Photochemistry and Photobiology A: Chemistry, 2013. **255**: p. 41-49.

30. Monteagudo, J.M., A. Durán, J.M. Corral, A. Carnicer, J.M. Frades, and M.A. Alonso, *Ferrioxalate-induced solar photo-Fenton system for the treatment of winery wastewaters.* Chemical Engineering Journal, 2012. **181–182**: p. 281-288.

31. Abrahamson, H.B., A.B. Rezvani, and J.G. Brushmiller, *Photochemical and spectroscopic studies of complexes, of iron(III) with citric acid and other carboxylic acids.* Inorganica Chimica Acta, 1994. **226**(1–2): p. 117-127.

32. Seraghni, N., S. Belattar, Y. Mameri, N. Debbache, and T. Sehil, *Fe(III)-Citrate-Complex-Induced Photooxidation of 3-Methylphenol in Aqueous Solution.* International Journal of Photoenergy, 2012. **2012**.

33. Ito, H., M. Fujii, Y. Masago, C. Yoshimura, T.D. Waite, and T. Omura, *Mechanism and kinetics of ligand exchange between ferric citrate and desferrioxamine B.* J Phys Chem A, 2011. **115**(21): p. 5371-9.

34. Huang, W., M. Brigante, F. Wu, K. Hanna, and G. Mailhot, *Development of a new homogenous photo-Fenton process using Fe(III)-EDDS complexes.* Journal of Photochemistry and Photobiology A: Chemistry, 2012. **239**: p. 17-23.

35. Monteagudo, J.M., A. Durán, M. Aguirre, and I.S. Martín, *Photodegradation of Reactive Blue 4 solutions under ferrioxalate-assisted UV/solar photo-Fenton system with continuous addition of H_2O_2 and air injection.* Chemical Engineering Journal, 2010. **162**(2): p. 702-709.

36. Safarzadeh-Amiri, A., J.R. Bolton, and S.R. Cater, *Ferrioxalate-mediated photodegradation of organic pollutants in contaminated water.* Water Research, 1997. **31**(4): p. 787-798.

37. Jeong, J. and J. Yoon, *Dual roles of CO_2^- for degrading synthetic organic chemicals in the photo/ferrioxalate system.* Water Research, 2004. **38**(16): p. 3531-3540.

38. Nansheng, D., W. Feng, L. Fan, and X. Mei, *Ferric citrate-induced photodegradation of dyes in aqueous solutions.* Chemosphere, 1998. **36**(15): p. 3101-3112.

39. Ou, X., X. Quan, S. Chen, F. Zhang, and Y. Zhao, *Photocatalytic reaction by Fe(III)–citrate complex and its effect on the photodegradation of atrazine in aqueous solution.* Journal of Photochemistry and Photobiology A: Chemistry, 2008. **197**(2–3): p. 382-388.

40. Zhang, C., *Photodegradation of Organic Pollutants Induced by Iron-carboxylate Complexes in Aqueous Solutions*, in *Department of Chemistry*. 2009, University Blaise Pascal.

41. Orama, M., H. Hyvonen, H. Saarinen, and R. Aksela, *Complexation of [S,S] and mixed stereoisomers of N,N[prime or minute]-ethylenediaminedisuccinic acid (EDDS) with Fe(iii), Cu(ii), Zn(ii) and Mn(ii) ions in aqueous solution.* Journal of the Chemical Society, Dalton Transactions, 2002(24): p. 4644-4648.

42. Li, J., G. Mailhot, F. Wu, and N. Deng, *Photochemical efficiency of Fe(III)-EDDS complex: OH radical production and 17β-estradiol degradation.* Journal of Photochemistry and Photobiology A: Chemistry, 2010. **212**(1): p. 1-7.

43. Malato, S., P. Fernández-Ibáñez, M.I. Maldonado, J. Blanco, and W. Gernjak, *Decontamination and disinfection of water by solar photocatalysis: Recent overview and trends.* Catalysis Today, 2009. **147**(1): p. 1-59.

44. Moreira, F.C., S. Garcia-Segura, V.J.P. Vilar, R.A.R. Boaventura, and E. Brillas, *Decolorization and mineralization of Sunset Yellow FCF azo dye by anodic oxidation, electro-Fenton, UVA photoelectro-Fenton and solar photoelectro-Fenton processes.* Applied Catalysis B: Environmental, 2013. **142–143**: p. 877-890.

45. Schecher, W.D. and D.C. McAvoy, *MINEQL+: A Chemical Equilibrium Modeling System, Version 4.6 for Windows*. 2007, Environmental Research Software: Hallowell, Maine, United States.

46. Moreira, F.C., R.A.R. Boaventura, EnricBrillas, and V.J.P. Vilar, *Degradation of trimethoprim antibiotic by UVA photoelectro-Fenton processmediated by Fe(III)-carboxylate complexes.* Applied Catalysis B: Environmental, 2015. **162**: p. 34-44.

47. Santos, A., P. Yustos, S. Rodriguez, E. Simon, and F. Garcia-Ochoa, *Abatement of phenolic mixtures by catalytic wet oxidation enhanced by Fenton's pretreatment: Effect of H_2O_2 dosage and temperature.* Journal of Hazardous Materials, 2007. **146**(3): p. 595-601.

48. Pupo Nogueira, R.F. and J.R. Guimarães, *Photodegradation of dichloroacetic acid and 2,4-dichlorophenol by ferrioxalate/H_2O_2 system.* Water Research, 2000. **34**(3): p. 895-901.

49. Bacardit, J., I. Oller, M.I. Maldonado, E. Chamarro, S. Malato, and S. Esplugas, *Simple Models for the Control of Photo-Fenton by Monitoring H_2O_2.* Journal of Advanced Oxidation Technologies, 2007. **10**(2): p. 219-228.

50. Feng, W. and D. Nansheng, *Photochemistry of hydrolytic iron (III) species and photoinduced degradation of organic compounds. A minireview.* Chemosphere, 2000. **41**(8): p. 1137-1147.

51. Malato, S., J. Blanco, A. Campos, J. Cáceres, C. Guillard, J.M. Herrmann, and A.R. Fernández-Alba, *Effect of operating parameters on the testing of new industrial titania catalysts at solar pilot plant scale.* Applied Catalysis B: Environmental, 2003. **42**(4): p. 349-357.

52. Irawaty, W., D. Friedmann, J. Scott, and R. Amal, *Relationship between mineralization kinetics and mechanistic pathway during malic acid photodegradation.* Journal of Molecular Catalysis A: Chemical, 2011. **335**(1–2): p. 151-157.

5 Remediation of Textile Wastewater from Polyester-Cotton Dyeing Combining Biological and Photochemical Oxidation Processes[3]

This chapter regards an integrated treatment strategy for synthetic polyester-cotton dyeing wastewater, combining biological and photochemical oxidation processes. The characterization of chemicals used as additives in different stages of cotton and polyester textile manufacturing was carried out. The synthetic wastewater was firstly subject to a biological oxidation with objective to remove the biodegradable matter. Thus, UVC/H_2O_2 and photo-Fenton oxidation processes were used as a polishing step for the decolourisation of bio-treated textile wastewater. The effect of hydrogen peroxide dosage, lamp power, solution pH and temperature on the UVC/H_2O_2 system was evaluated.

[3]This Chapter is based on the research article: "Petrick A. Soares, Renata Souza, Juan S. Escoda, Tânia F. C. V. Silva, Selene M. A. Guelli U. Souza, Rui A. R. Boaventura, Vítor J. P. Vilar, *Remediation of Textile Wastewater from Polyester-Cotton Dyeing Combining Biological and Photochemical Oxidation Processes.* Submitted.

5.1 Introduction

Textile industry is a major consumer of water and chemicals and consequently, one of the largest groups of industries causing intense water pollution. The amount and composition of the generated wastewater depends on many different factors such as processed fabric, type of fibres, the season of the year and others. In addition, textile manufacturing employs a variety of chemicals (one kilogram of these substances is used for each kilogram of fabric) during the different processing steps with many functions, depending on the nature of the raw material and product [1, 2]. The main chemicals usually used during the textile dyeing processes are composed by a mixture of different types of dyes and different auxiliary products, such as organic acids, fixing agents, reducing agents, oxidizing agents and others [3]. This leads to the generation of wastewaters with an intense colour, which are characterized by a moderate organic content, moderate biodegradability, variable pH values, usually in the alkaline range [4].

Generally, biological processes are the preferred choice for textile wastewater treatment due to their low cost and non-toxic products generation [5]. Furthermore, biological oxidation shows good results for the mineralisation of the non-recalcitrant fraction of textile wastewater [6]. However, conventional biological processes do not always provide satisfactory results, especially when the wastewater shows high concentration of synthetic organic chemicals, some categorized under the term ‘‘xenobiotic’’ due to their biological persistence [2, 7].

Many chemical and physical processes have been proposed for the treatment of textile wastewaters, such as adsorption, coagulation and oxidation by hypochlorite. These methods can be expensive and, in some cases, they also may not eliminate completely the colour [8]. Therefore, it has been increasingly accepted that the only feasible treatment for biologically persistent wastewater is the use of advanced technologies based on chemical oxidation, such as the Advanced Oxidation Processes - AOPs [9]. In addition, many studies have already demonstrated the high potential of AOPs for textile wastewater decolourisation [10-12]. However, the application of AOPs is limited and the costs involved are high given the energy and chemicals requirements, especially when the goal is the complete mineralisation, making these technologies non-competitive [13].

In order to overcome drawbacks on textile wastewater treatment, some researchers have demonstrated the suitability of AOPs as pre-treatment and post-treatment steps [6, 9, 14, 15]. Oller et al. [9] describe the application of chemical oxidation processes as pre-treatment to convert the initially persistent organic compounds into more biodegradable intermediates, which could be then treated by biological oxidation processes at considerably lower cost. Besides, some works have described real cases in which the

combination strategy is in the opposite direction, first eliminating the highly biodegradable part of the wastewater and then degrading the recalcitrant contaminants by an AOP post-treatment [6, 16].

The aim of this work was to optimize an integrated treatment strategy for textile wastewater from polyester-cotton dyeing combining biological activated sludge and chemical oxidation processes. The biodegradability of all constituents present in the synthetic wastewater was first evaluated by a Zahn-Wellens test. The biodegradable fraction of the wastewater was initially eliminated using a biological oxidation system. The UVC/H_2O_2, UVC/Fe^{2+}/H_2O_2 and UVC/Fe^{3+}/H_2O_2/Oxalic acid chemical oxidation systems were used as polishing step, regarding the wastewater decolourisation. Additionally, the effect of pH value, H_2O_2 dosage, temperature and lamp power was assessed for the UVC/H_2O_2 system.

5.2 Material and Methods

All the chemicals and reagents used in this chapter, the detailed description of the lab-scale lamp photoreactor experimental unit, along with the corresponding experimental procedures followed, and, finally, the employed methods can be consulted in Chapter 2. The detailed operational conditions of the assays performed in this chapter are shown in Table 5.1 (lab-scale lamp photoreactor).

Table 5.1. Operational conditions for reactions under UVC radiation.

System	P[a] (W)	T (ºC)	pH	Dosage of H_2O_2 (mM)
H_2O_2	-	30	8.4[(d)]	42
UVC	6			-
UVC/H_2O_2				42
UVC/Fe^{2+}/H_2O_2[(b)]			3.0	
UVC/Fe^{3+}/H_2O_2/Oxalic acid[(c)]			3.0	3
			5.0	
UVC/H_2O_2	4	30	8.4[(d)]	10
				20
				30
				42
				54
	6	30	8.4[(d)]	10
				20
				30
				42
				54
	11	30	8.4[(d)]	10
				20
				30
				42
				54
	6	30	3.0	42
			5.0	
			8.4[(d)]	
			11.0	
	6	15	8.4[(d)]	42
		30		
		45		

[a]Lamp Power; [b]$[Fe^{2+}]$ = 2 mg L^{-1}; [c]$[Fe^{3+}]$ = 2 mg L^{-1}; [d]natural bio-treated textile wastewater pH.

5.3 Results and discussion

5.3.1 Characteristics of the textile wastewater

The synthetic textile wastewater from polyester-cotton dyeing presents a neutral pH value and high organic load, being 97% of DOC related to dyeing auxiliary products and only 3% due to dyes (Table 2.6 - Materials and methods – Chapter 2). The wastewater presents a high concentration of sulphates (737 mg SO_4^{2-} L^{-1}) and sodium (1772 mg Na^+ L^{-1}) ions. Sulphates can be associated, in large part, with the addition of the sodium hydrosulphite, commonly used as reducing agent [17] in the polyester dyeing and reduction cleaning processes. Besides, the sodium hydrosulphite, along with sodium hydroxide (reduction cleaning processes – polyester and fibre preparation - cotton), sodium chloride and sodium carbonate (dyeing process – cotton) and sodium dodecyl sulphate (washing process – cotton) are the main sources of sodium in the wastewater. High concentration of chloride (1470 mg Cl^- L^{-1}) is also observed and can be related to the high dosage of sodium chloride added, a retardant agent often used in reactive dyeing during the cotton dyeing process [17].

The mixture of different dyes resulted in a polyester-cotton dyeing textile wastewater with a red colour, mainly associated with Procion Red H-EXL gran, an azo dye frequently used in the cotton dyeing process. Azo dyes are non-biodegradable under aerobic conditions, and therefore the discharge of azo dyes-containing wastewaters can cause several problems to the aquatic life [18]. On the other hand, as observed from the colour data (DFZs and Pt-Co scale), the polyester dyeing process almost does not contribute to the colour found in the final wastewater (mixture of polyester and cotton wastewaters) because this fibre dyeing processes include a reduction cleaning process as final step, which largely eliminates the wastewater colour.

According to the results obtained in the Zahn-Wellens test, both wastewaters present a high biodegradability (64-89%). Table 5.2 and Table 5.3 present the biodegradability of the textile auxiliaries and dyes used in both dyeing processes. Considering that some of textile auxiliaries show low DOC values, 50 mg C L^{-1} was adopted as standard concentration for all samples during the Zahn-Wellens test. The dispersing agent Sera® Sperse M-IF and the dispersing and sequestering agent Sera® Quest C-PX, used in the polyester dyeing process, present a low biodegradability (6% to 9%, respectively). Sera® Sperse M-IF, as many dispersant agents, has polyglycol ethers in its composition. These chemicals are reported in the literature as highly water soluble, toxic, recalcitrant and are often referred as xenobiotic [19-22]. The non-ionic dispersing and sequestering agent Sera® Quest C-PX is a polymer often applied

as sequestering agents of calcium and magnesium ions from hard waters used in the dyeing process. The two disperse dyes, Dianix Blue K-FBL and Dianix Orange K3G, show 0% of biodegradability.

Table 5.2. Characteristics of the dyes and dyeing auxiliary products present in the synthetic polyester dyeing textile wastewater.

Step	Dyeing Product	Chemical Characteristics/main function	Wastewater Characteristics		
			Concentration ($g\ L^{-1}$)	DOC ($mg\ C\ L^{-1}$)	Biodegradability (%)
Fibre preparation	Sera® Lube Neo	Polymeric amines/Creasing prevent	2.000	53.2	100
	Sera® Quest C-PX	Polymer combination/ dispersing and sequestering agent	1.000	27.0	9
Dyeing	Sera® Lube M-CF	Polymeric amides/ Lubricant and crease inhibitor	2.000	38.2	66
	Sera® Sperse M-IF	Sodium naphthalene sulfonate condensate/ dispersing agent	1.500	187.6	6
	Sera® Gal P-LP	Alkyl polyglycol derivative/ dispersing agent	2.000	183.3	91
	Sodium hydrosulphite	Sodium dithionite/ reducing agent	3.000	0.0	-
	Acetic acid	$C_2H_4O_2$/fixer	0.150	25.6	100
	Dianix Orange K3G	Disperse Orange 30/dye	0.022	5.7	0
	Dianix Blue KFBL	Disperse Blue 56/dye	0.008	2.3	0
Reduction cleaning	Sera® Wash M-SF	Non-foaming detergent	0.450	66.5	93
	Sodium hydroxide	NaOH/mercerization	5.000	0.0	-
	Acetic acid	$C_2H_4O_2$/acid generator	0.150	69.3	100
	Sodium hydrosulphite	Sodium dithionite/ reducing agent	3.000	0.0	-

The high biodegradability of cotton textile dyeing wastewater is associated with the textile auxiliary products. The only exceptions are a polymeric amide, used as lubricant and crease inhibitor, denominated Sera® Lube M-CF, and dyes. Procion Yellow H-EXL gran and Procion Red H-EXL gran present 0% and 1% of biodegradability, respectively and the polymeric amide shows 66% of biodegradability after the 28 days of Zahn-Wellens test.

Considering the Portuguese discharge regulations into water bodies [23] and the wastewater characteristics presented in Table 2.6, the treatment strategy adopted for the textile wastewater included: i) an activated sludge biological oxidation process, able to eliminate the biodegradable organic fraction of the wastewater; ii) a chemical oxidation process, as polishing step, for the degradation of the recalcitrant organic fraction, targeting colour removal.

Table 5.3. Characteristics of the dyes and dyeing auxiliary products present in the synthetic cotton dyeing textile wastewater.

Step	Dyeing Product	Chemical Characteristics/main function	Wastewater Characteristics		
			Concentration (g L^{-1})	DOC (mg C L^{-1})	Biodegradability (%)
Fibre preparation	Sera® Foam M-HTS	Mineral oil/emulsifier	0.450	56.3	100
	Sera® Fil FFB	Ethoxylate and phosphonated alcohol/wetting agent	0.450	26.3	90
	Sera® Zyme C-SX	Aqueous enzyme preparation/bleaching	1.800	2.4	96
	Acetic acid	$C_2H_4O_2$/acid generator	0.250	48.6	100
	Hydrogen peroxide	H_2O_2/oxidizing	1.300	0.0	-
	Sodium hydroxide	NaOH/alkaline system	1.200	0.0	-
Dyeing	Sera® Lube M-CF	Polymeric amide/ lubricant and crease inhibitor	2.000	38.2	66
	Sera® Quest M-USP	Organophosphonic acid/ dispersing and sequestering agent	1.000	4.4	0
	Sodium chloride	NaCl/retardant	20.000	0.0	-
	Sodium carbonate	Na_2CO_3/alkaline system	5.000	0.0	-
	Procion Yellow H-EXL gran	Reactive Yellow 138:1/dye	0.005	3.0	0
	Procion Red H-EXL gran	Azo dye	0.015	5.6	1
	Sodium hydroxide	NaOH/alkaline system	1.200	0.0	-
Washing	Sodium dodecyl sulphate	$NaC_{12}H_{25}SO_4$/surfactant, detergent	0.225	51.6	100

5.3.2 Biological oxidation

Figure 5.1 shows a fast decay of the DOC profile during the first 5 hours of operation, corresponding to the removal of the easily biodegradable organic fraction, achieving 38% mineralisation at a kinetic rate of 12±2 mg DOC g^{-1} VSS h^{-1}. The slow biodegradable organic fraction was almost totally removed after 48 hours, at a kinetic rate of 1.5±0.1 mg DOC g^{-1} VSS h^{-1}, leading to a final mineralisation of 76%, in agreement with the Zahn-Wellens results.

The remaining organic carbon fraction can be considered recalcitrant (84 mg C L^{-1}; 24% of the initial DOC), mainly attributed to the dispersing agent Sera® Sperse M-IF and the dispersing and sequestering agent Sera® Quest C-PX, used in the polyester dyeing process, as well as, the presence of the dyes used in both dyeing process.

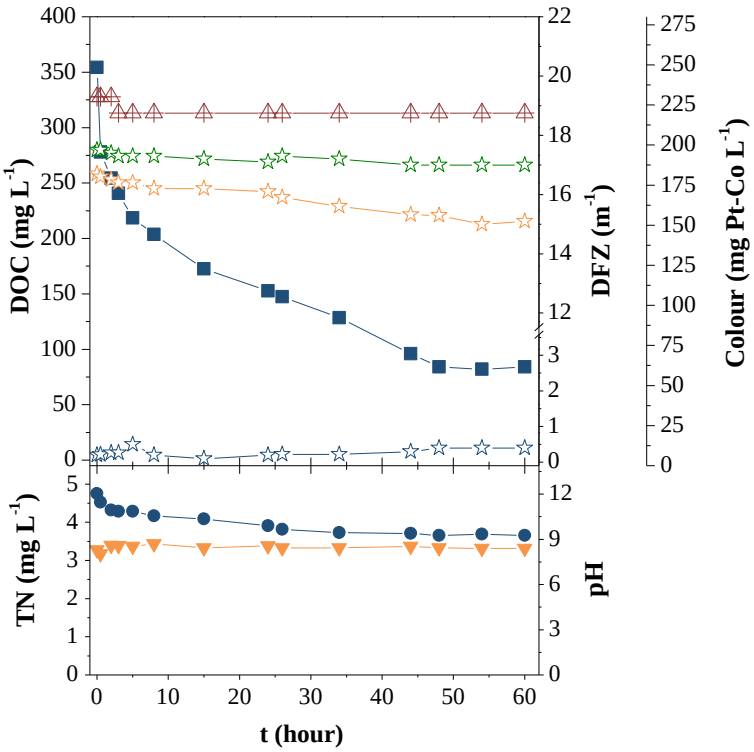

Figure 5.1. Biological oxidation of the textile wastewater from polyester-cotton dyeing: ■ - DOC; ☆ - DFZ_{436nm}; ☆ - DFZ_{525nm}; ☆ - DFZ_{620nm}; ⧋ - Pt-Co scale; ● - TN and ▼ - pH.

Sludge volume index (SVI) can be considered a good indicator of sludge settling properties [24, 25]. The SVI obtained during biological treatment was 103 mL g^{-1}. In general, SVI can vary from 30 to 400 mL g^{-1}, but a value lesser than 100-150 mL g^{-1} indicates good settling properties of the sludge [25, 26]. Another important operational parameter of activated sludge systems is the food-to-microorganism ratio (F/M ratio). The F/M ratio achieved was 0.119 g BOD g^{-1} VSS d^{-1}, a typical value for extended aeration processes [25].

According to the Zahn-Wellens results, in this preliminary biological pre-treatment, the organic contribution of Sera® Lube Neo, Sera® Gal P-LP and Sera® Wash M-SF, used in polyester dyeing and Sera® Foam M-HTS, Sera® Fil FFB, Sera® Zyme C-SX and sodium dodecyl sulphate, used in cotton dyeing, and acetic acid, used in both dyeing processes, was totally eliminated. The presence of those compounds have been previously correlated with lower mineralisation rates using chemical oxidation processes, due to the formation of undesired iron organic complexes, with low or null photoactivity [27, 28]. Furthermore, it is known that acetic acid molecule is very recalcitrant to hydroxyl radicals attack and that soluble ferric–acetate complexes have a low photoactivity [29, 30]. So, the biological oxidation of these organic compounds, as a low cost process, is essential to avoid negative interferences in the chemical oxidation system.

Nevertheless, the biological oxidation system was inefficient in wastewater decolourisation, being the colour visible after a dilution of 1:40. Pt-Co scale [31] and DFZ-*DurchsichtFarbZahl* (Visual colour number in German) [32] indicators were used as a quantitative colour measurement. To achieve a final wastewater in agreement with the discharge limits imposed by the Portuguese legislation must be obtained.

Considering the quantitative colour indicators, the efficiency of the biological oxidation process was less than 5% (Pt-Co scale), 9% (DFZ_{436nm}), 3% (DFZ_{525nm}) and 0% (DFZ_{620nm}), and consequently a further polishing treatment is necessary. Such inability to degrade textile dyes by biological oxidation is in agreement with other published works [33-35] and it was confirmed by the low biodegradability values obtained in the Zahn-Wellens test.

5.3.3 Photochemical oxidation

Different photochemical oxidation processes using UVC radiation (UVC/H_2O_2, UVC/Fe^{2+}/H_2O_2 and UVC/Fe^{3+}/H_2O_2/Oxalic acid) were applied as a polishing step of the bio-treated textile wastewater, targeting colour removal (Table 5.4 and Figure 5.2). All reactions were carried out with a 6 W UVC lamp (T = 30ºC). In the photo-Fenton reactions, an iron concentration of 2 mg L^{-1} (TDI) was used, which is the legal discharge limit for total iron according to the Portuguese legislation [36].

All photo-Fenton reactions enhanced by oxalic acid were carried out using an iron/organic ligand molar ratio of 1:3, which is reported in literature as the most stable ferric-oxalate complex [37]. Pt-Co, DFZ_{436nm} and DFZ_{525nm} measurements were used as quantitative colour indicators during the photochemical oxidation experiments, presenting a good agreement with visual observations. DFZ_{620nm} colour indicator was not displayed due to the low values obtained for the bio-treated wastewater.

UVC or H_2O_2 alone were not efficient in the decolourisation of the bio-treated wastewater, considering the UVC and H_2O_2 dose used. The UVC photolysis of the bio-treated wastewater resulted in a small increment on the colour indicators, Pt-Co and DFZ_{436nm}. The UV-visible spectra show a decline of the absorbance at wavelengths below 300 nm and an increase of the absorbance at wavelengths between 300 and 500 nm. This can be associated with the bathochromic shift of the dyes molecules [38-41] under irradiation, wherein the displacement of the absorption to longer wavelengths occurs.

Table 5.4. Operational conditions and pseudo-first-order kinetic constants for reaction under UVC radiation.

System	P[a] (W)	T (°C)	pH	Dosage of H_2O_2 (mM)	Kinetic parameters			
					Decolourisation[b]		H_2O_2 consumption	
					k[c] (L kJ^{-1})	R^2	k[d] (L kJ^{-1})	R^2
H_2O_2	-			42	-	-	2.5±0.6	0.969
UVC			8.4[g]	-	-	-	-	-
UVC/H_2O_2				42	0.50±0.01	0.995	5.5±0.7	0.981
UVC/Fe^{2+}/H_2O_2[e]	6	30	3.0		-	-	0.10±0.02	0.979
UVC/Fe^{3+}/H_2O_2/Oxalic acid[f]			3.0	3	-	-	0.11±0.02	0.962
			5.0		-	-	0.8±0.2	0.979
UVC/H_2O_2	4	30	8.4[g]	10	0.120±0.006	0.981	0.7±0.2	0.963
				20	0.199±0.006	0.988	2.2±0.5	0.952
				30	0.357±0.005	0.998	2.0±0.7	0.919
				42	0.459±0.001	0.998	5.2±0.8	0.984
				54	0.489±0.009	0.998	6.1±0.9	0.982
	6	30	8.4[g]	10	0.066±0.003	0.948	0.9±0.2	0.932
				20	0.189±0.001	0.998	2.3±0.7	0.912
				30	0.29±0.01	0.961	3.4±0.6	0.957
				42	0.50±0.01	0.995	5.5±0.7	0.981
				54	0.54±0.02	0.992	6.9±0.4	0.995
	11	30	8.4[g]	10	0.055±0.003	0.900	0.5±0.1	0.950
				20	0.099±0.001	0.998	1.2±0.3	0.937
				30	0.173±0.006	0.982	1.4±0.4	0.910
				42	0.309±0.006	0.996	2.4±0.5	0.951
				54	0.35±0.02	0.986	3.6±0.5	0.976
	6	30	3.0	42	0.189±0.002	0.998	3.4±0.5	0.980
			5.0		0.47±0.02	0.971	3.5±0.7	0.950
			8.4[g]		0.50±0.01	0.995	5.5±0.7	0.981
			11.0		0.35±0.01	0.989	9.5±2	0.955
	6	15	8.4[g]	42	0.256±0.004	0.997	3.3±0.4	0.984
		30			0.50±0.01	0.995	5.5±0.7	0.981
		45			0.595±0.007	0.998	6.2±0.7	0.987

[a]Lamp Power; [b]Platinum-Cobalt method; [c]Pseudo-first-order kinetic constant; [d]H_2O_2 consumption rate; [e]$[Fe^{2+}]$ = 2 mg L^{-1}; [f]$[Fe^{3+}]$ = 2 mg L^{-1}; [g]natural bio-treated textile wastewater pH.

For the photo-Fenton reaction, a colour reduction after acidification was obtained, i.e. 9% (Pt-Co scale), 20% (DFZ_{436nm}), and 11% (DFZ_{525nm}). A DOC decrease of 25% was also observed after pH adjustment, which may have occurred due to the precipitation of some organic compounds (sludge formation) as also retention in the generated foam (Figure 5.3) [42]. For the reaction at pH 5, the colour reduction observed after the acidification step was negligible.

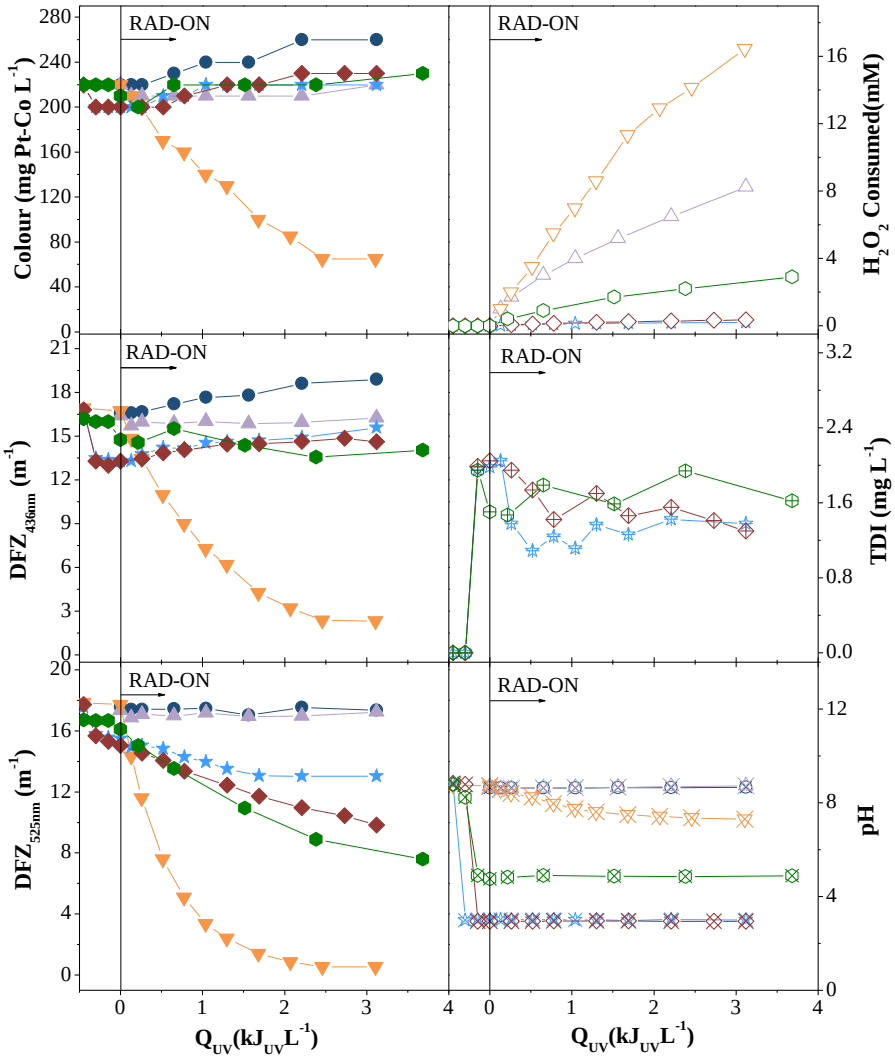

Figure 5.2. Bio-treated textile wastewater decolourisation using different AOPs. Operation conditions: T = 30ºC; 6W UVC lamp. Solid symbols – colour indicators; open symbols – H_2O_2 consumed; cross symbols – TDI concentration; "x" within symbols – pH. ● ○ ⊕ ⊗ – UVC (pH 8.4); ▲ △ ⍋ ⍋ – H_2O_2 (pH 8.4; [H_2O_2] = 42 mM); ▼ ▽ ⍒ ⍒ – UVC/H_2O_2 reaction (pH 8.4; [H_2O_2] = 42 mM); ★ ☆ ✡ ✡ – UVC/Fe^{2+}/H_2O_2 (pH 3.0; [H_2O_2] = 3 mM; [Fe^{2+}] = 2 mg L^{-1}); ◆ ◇ ⊕ ⊗ - UVC/Fe^{3+}/H_2O_2/Oxalic acid (pH 3.0; [H_2O_2] = 3 mM; [Fe^{3+}] = 2 mg L^{-1}; iron/oxalate molar ratio of 1:3); ⬢ ⬡ ⊕ ⊗ - UVC/Fe^{3+}/H_2O_2/Oxalic acid (pH 5.0; [H_2O_2] = 3 mM; [Fe^{3+}] = 2 mg L^{-1}; iron/oxalate molar ratio of 1:3).

Considering the wastewater colour removal measured by Pt-Co and DFZ_{436nm} indicators, the photo-Fenton reaction was an ineffective decolourisation method. The low efficiency of the photo-Fenton reaction on the wastewater decolourisation can be due to two possible effects: i) the presence of organic and inorganic species (e.g., auxiliary products) in the textile wastewater and their respective complexes with ferric ions, with a low photoactivity and recalcitrant characteristic to further mineralisation by hydroxyl radical attack [43, 44]; ii) the low iron concentration used is not able to suppress the inner filter effects related to other light-absorbing species present in the solution, namely dyes [13].

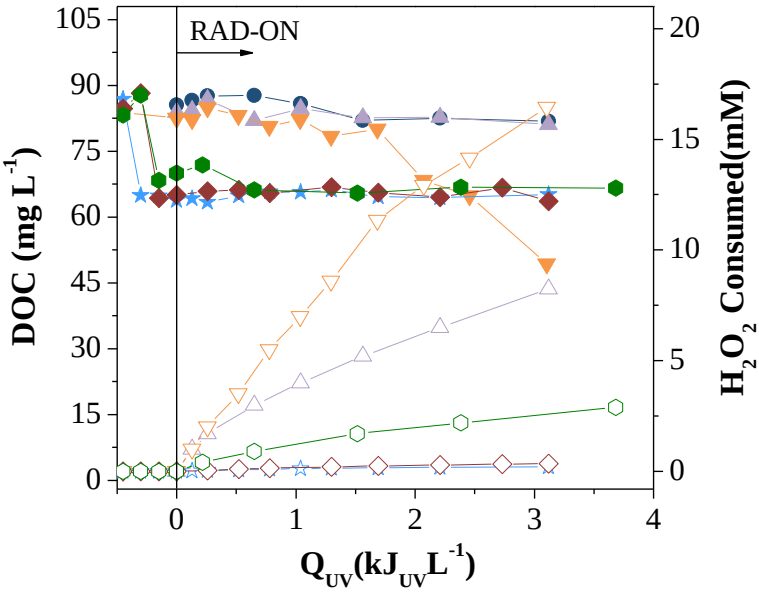

Figure 5.3. Textile wastewater mineralisation using different AOPs. Operation conditions: *T* = 30ºC and 6W UVC lamp. Solid symbols – DOC; open symbols – H_2O_2 consumed. ● ○ – UVC (pH 8.4); ▲ △ – H_2O_2 (pH 8.4; [H_2O_2] = 42 mM); ▼ ▽ – UVC/H_2O_2 reaction (pH 8.4; [H_2O_2] = 42 mM); ★ ☆ – UVC/Fe^{2+}/H_2O_2 (pH 3.0; [H_2O_2] = 3 mM; [Fe^{2+}] = 2 mg L^{-1}); ◆ ◇ - UVC/Fe^{3+}/H_2O_2/Oxalic acid (pH 3.0; [H_2O_2] = 3 mM; [Fe^{3+}] = 2 mg L^{-1}; iron/oxalate molar ratio of 1:3); ⬢ ⬡ - UVC/Fe^{3+}/H_2O_2/Oxalic acid (pH 5.0; [H_2O_2] = 3 mM; [Fe^{3+}] = 2 mg L^{-1}; iron/oxalate molar ratio of 1:3).

It is widely known that ferric ions form stable and strong complexes with oxalic acid, avoiding the undesired interactions with other organic and inorganic species [27, 37, 45-47]. Figure 5.2 shows that the photo-Fenton reaction mediated by ferrioxalate complexes showed also negligible wastewater decolourisation efficiency, in terms of Pt-Co units and DFZ_{436nm}. However, a small improvement on colour removal was observed for DFZ_{525nm} indicator. The total dissolved iron was similar for the reactions with and without oxalic acid.

The photolysis of hydrogen peroxide using UVC radiation was the most effective method for the decolourisation of the bio-treated textile wastewater. This indicates the high contribution of $^{\bullet}OH$ generated from H_2O_2 cleavage under UVC radiation (Eq. (5.1)).

$$H_2O_2 \xrightarrow{h\nu} 2^{\bullet}OH \qquad (5.1)$$

Maximum values of colour reduction were 71% (Pt-Co scale), 86% (DFZ_{436nm}) and 97% (DFZ_{525nm}) consuming 14.1 mM H_2O_2 and 2.5 kJ_{UVC} L^{-1}. It must be underlined that the photo-Fenton reactions were performed with much lower H_2O_2 concentrations when compared with the UVC/H_2O_2 system. Further UVC/H_2O_2 reactions were performed in order to evaluate the effect of different reaction variables, such as H_2O_2 dosage, lamp power, wastewater pH and temperature.

5.3.3.1 Effect of H_2O_2 dosage

The decolourisation of the bio-treated textile wastewater was evaluated through the UVC/H_2O_2 method using different initial H_2O_2 dosages (10, 20, 30, 42 and 54 mM) and UVC lamps (4, 6 and 11 W). Figure 5.4 shows that the decolourisation rates increase significantly with the availability of hydrogen peroxide, being almost six times higher for the initial H_2O_2 dose of 42 mM when compared with 10 mM. For H_2O_2 dosages higher than 42 mM the reaction rates remain almost unchanged.

Shu et al. [48] reported that when the equilibrium between the $^{\bullet}OH$ radicals and H_2O_2 concentrations is achieved, any increase on the hydrogen peroxide concentration cannot enhance the free radical concentration. Besides, higher H_2O_2 concentrations could inhibit the reaction rate because H_2O_2 acts as $^{\bullet}OH$ scavenger (Eq. (5.2)) [49-51]. Additionally, hydroxyl radicals generated at high concentration, dimerize to H_2O_2 (Eq. (5.3)). The peroxy radicals produced, as a result of Eq. (5.2), can also enter in other reaction pathways (Eq. (5.4)-(5.6)) [52-55].

$$H_2O_2 + {}^{\bullet}OH \rightarrow H_2O + HO_2^{\bullet} \quad (5.2)$$

$$^{\bullet}OH + {}^{\bullet}OH \rightarrow H_2O_2 \quad (5.3)$$

$$HO_2^{\bullet} + H_2O_2 \rightarrow {}^{\bullet}OH + H_2O + O_2 \quad (5.4)$$

$$2HO_2^{\bullet} \rightarrow H_2O_2 + O_2 \quad (5.5)$$

$$HO_2^{\bullet} + {}^{\bullet}OH \rightarrow H_2O + O_2 \quad (5.6)$$

Although the decolourisation rates increase significantly with the H_2O_2 dosage, higher amounts of H_2O_2 are consumed. In addition, higher residual H_2O_2 concentrations are obtained at the end of the experiments when using high H_2O_2 dosages (Figure 5.4), making necessary a subsequent system to achieve the complete decomposition of H_2O_2 present in the wastewater before its discharge to the aquatic environment.

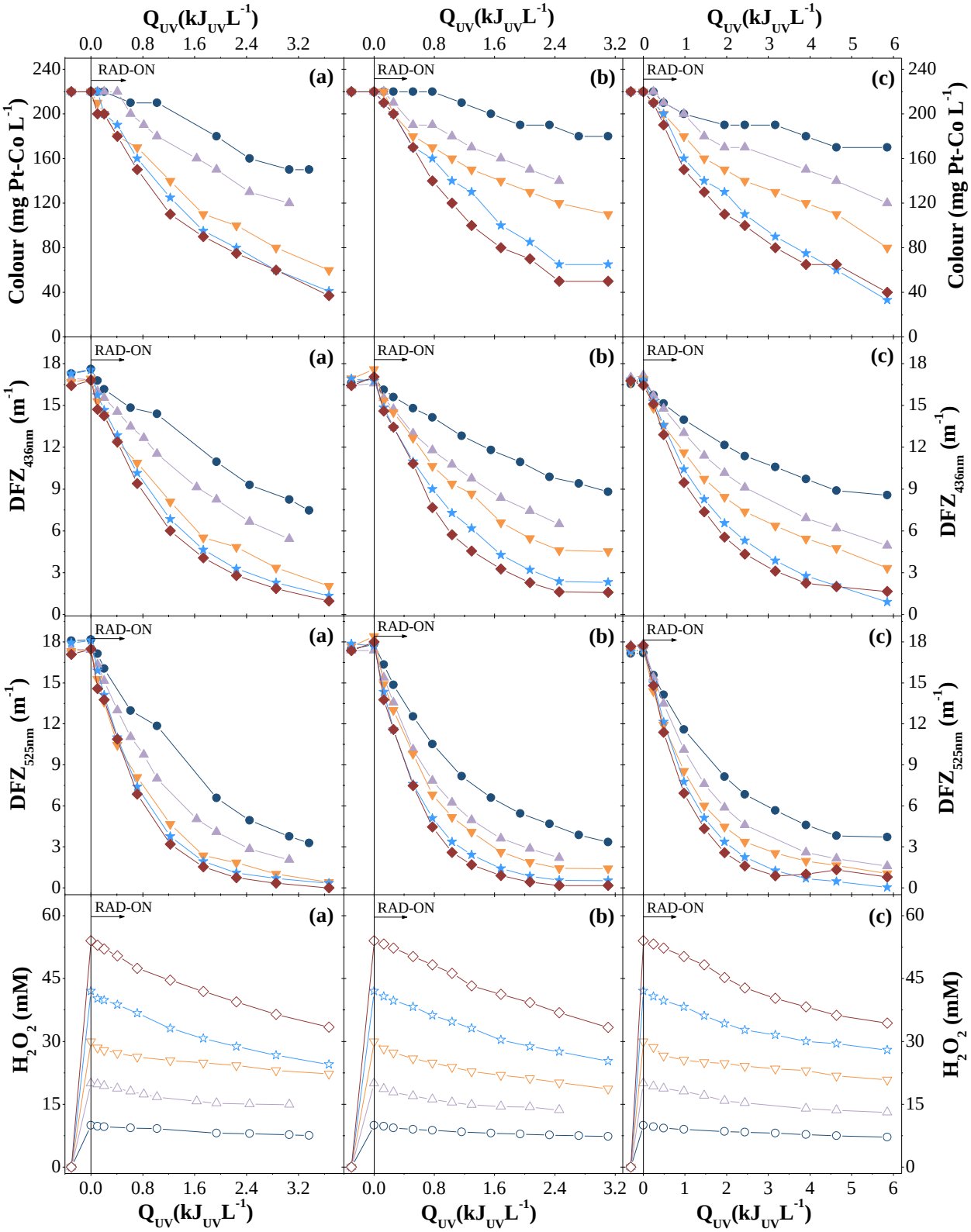

Figure 5.4. Decolourisation of the bio-treated textile wastewater using the UVC/H_2O_2 system at different H_2O_2 dosage. (a) 4W UVC lamp; (b) 6W UVC lamp; (c) 11W UVC lamp. Operation conditions: pH 8.4; T = 30ºC. Solid symbols – colour indicators; open symbols – H_2O_2 consumed. ● ○ - [H_2O_2] = 10 mM; ▲ △ - [H_2O_2] = 20 mM; ▼ ▽ - [H_2O_2] = 30 mM; ★ ☆ – [H_2O_2] = 42 mM; ◆ ◇ - [H_2O_2] = 54 mM.

Several authors reported that the UVC/H_2O_2 oxidation system is able to mineralise different organic pollutants, such as azo and reactive dyes [56, 57]. For the bio-treated textile wastewater, the UVC/H_2O_2 system showed negligible mineralisation values using H_2O_2 concentrations below 42 mM (Figure 5.5). However, DOC mineralisation around 40% was observed for a H_2O_2 dose of 54 mM (11W UVC lamp). This indicates that high doses of H_2O_2 are necessary to break the dyes molecules and other auxiliary products into smaller molecules and further conversion into carbon dioxide, water and inorganic acids.

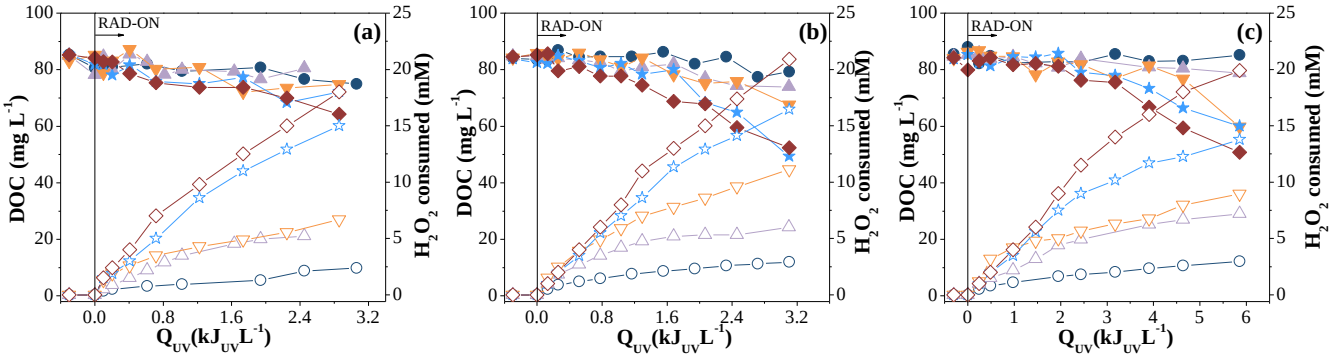

Figure 5.5. Textile wastewater mineralisation using UVC/H_2O_2 reaction at different H_2O_2 dosage. (a) 4W UVC lamp; (b) 6W UVC lamp; (c) 11W UVC lamp. Operation conditions: pH 8.4; *T* = 30ºC. Solid symbols – DOC; open symbols – H_2O_2 consumed. ● ○ - [H_2O_2] = 10 mM; ▲ △ - [H_2O_2] = 20 mM; ▼ ▽ - [H_2O_2] = 30 mM; ★ ☆ – [H_2O_2] = 42 mM; ◆ ◇ - [H_2O_2] = 54 mM.

5.3.3.2 Effect of lamp power

The pseudo-first-order kinetic constants obtained from the Pt-Co profiles, as a function of the H_2O_2 concentration, are plotted in Figure 5.6 (see also Table 5.4), considering three different UVC lamp powers. For the hydrogen peroxide dosage interval studied, it is possible to observe two different behaviours: i) for the interval between 10 and 30 H_2O_2 mM, the decolourisation rate obtained with a 4W UVC lamp is higher than those obtained with 6W and 11W UVC lamps; and ii) for the range between 42 and 54 H_2O_2 mM, the decolourisation rate achieved with 6W UVC lamp is higher. For all H_2O_2 doses tested, the decolourisation rates as a function of accumulated UVC energy, for the 11W UVC lamp are lower than for 4 and 6 W UVC lamps.

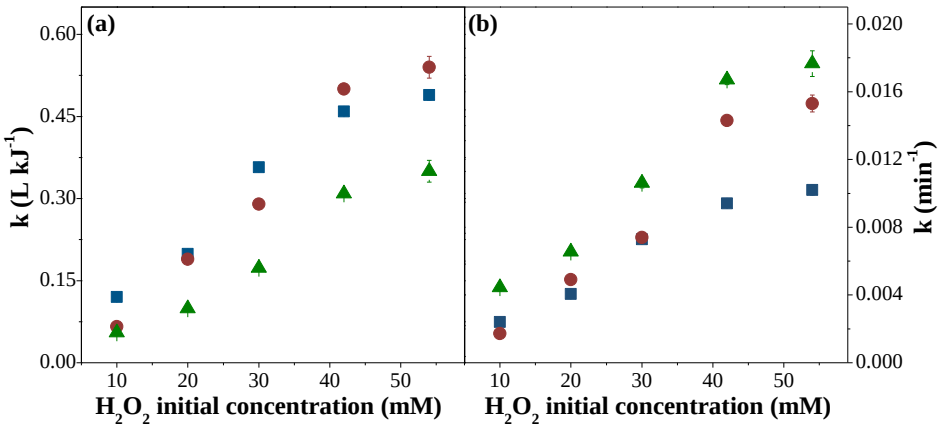

Figure 5.6. Pseudo-first-order kinetic constants vs. hydrogen peroxide dosage for UVC/H_2O_2 reactions using different UVC lamps. (a) – kinetic constants as a function of accumulated UVC energy; (b) - kinetic constant as a function of time. ■ – 4W UVC lamp; ● – 6W UVC lamp; ▲ – 11W UVC lamp.

This indicates that an excess of UVC photons emitted by the 11W UVC lamp is not properly used in the reaction according to the reactor pathlength. On the other hand, kinetic profiles show a slight improvement in the decolourisation with the radiation intensity increasing along time (see Figure 5.7), since more photons per unit of time are available for the production of hydroxyl radicals.

Finally, it is demonstrated that a detailed study considering the optical length of the reactor and linking the lamp power to the peroxide dosage should always be done in order to avoid unnecessary expenses with reagents and energy. Considering the presented results, the H_2O_2 dosage of 42 mM and 6W UVC lamp were used for further studies.

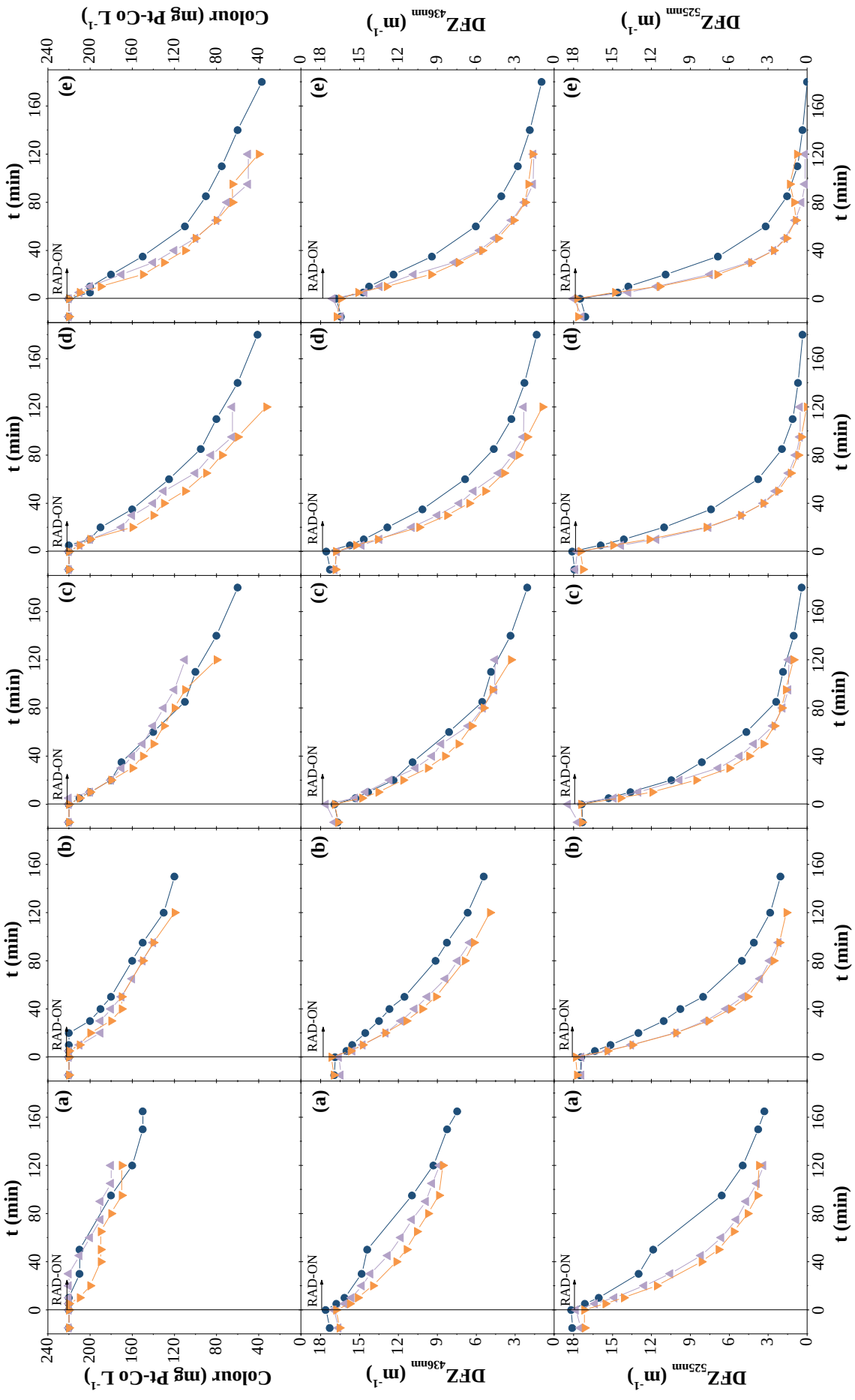

Figure 5.7. Decolourisation of the bio-treated textile wastewater using the UVC/H_2O_2 system at different H_2O_2 dosage. (a) $[H_2O_2]$ = 10 mM; (b) $[H_2O_2]$ = 20 mM; (c) $[H_2O_2]$ = 30 mM; (d) $[H_2O_2]$ = 42 mM; (e) $[H_2O_2]$ = 54 mM. Operation conditions: pH 8.4; T = 30°C. Solid symbols – colour indicators; open symbols – H_2O_2 consumed. ●○ - 4W UVC lamp; ▲△-6W UVC lamp; ▶▽ - 11W UVC lamp.

5.3.3.3 *Effect of wastewater pH*

Figure 5.8 shows the decolourisation kinetic profiles for the bio-treated textile wastewater using the UVC/H_2O_2 system at different initial pH values (3.0, 5.0, 8.4 and 11.0). Increasing the wastewater pH to 11 through the addition of NaOH, DFZ_{436nm} value increases ~24%, DFZ_{525nm} value decreases ~10%, while the value of Pt-Co indicator did not change (DOC remained constant). The wastewater pH affects the chemical speciation of the dyes and other organic and inorganic species, affecting the absorption properties of the wastewater (Figure 5.9) [58-62].

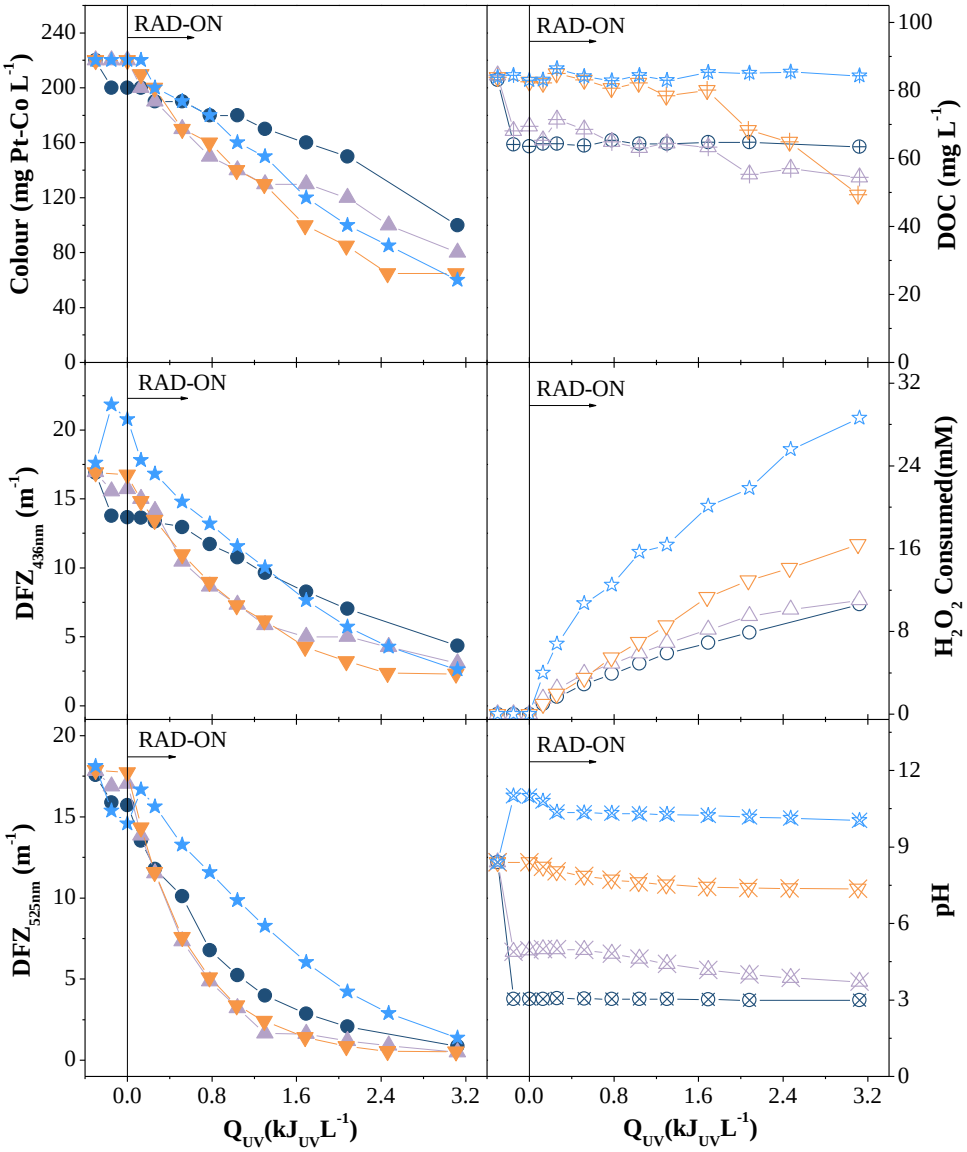

Figure 5.8. Bio-treated textile wastewater decolourisation using UVC/H_2O_2 reaction at different pH values. Operation conditions: T = 30ºC; [H_2O_2] = 42 mM and 6W UVC lamp. Solid symbols –colour indicators; cross symbols – DOC; open symbols – H_2O_2 consumed; "x" within symbols – pH. ● ⊕ ○ ⊗ – pH 3.0; ▲ ⧋ △ ⧊ – pH 5.0; ▼ ⧩ ▽ ⧨ – pH 8.4; ★ ✯ ☆ ✰ – pH 11.0.

After radiation was turned on, the reaction at natural wastewater pH (pH 8.4) showed better results than reactions at acidic and basic pH. The reaction rate at pH 5.0 was very similar to that observed at natural pH. However, the kinetic rates decreased by a factor of 2.6 when the pH decreased from 8.4 to 3.0, respectively.

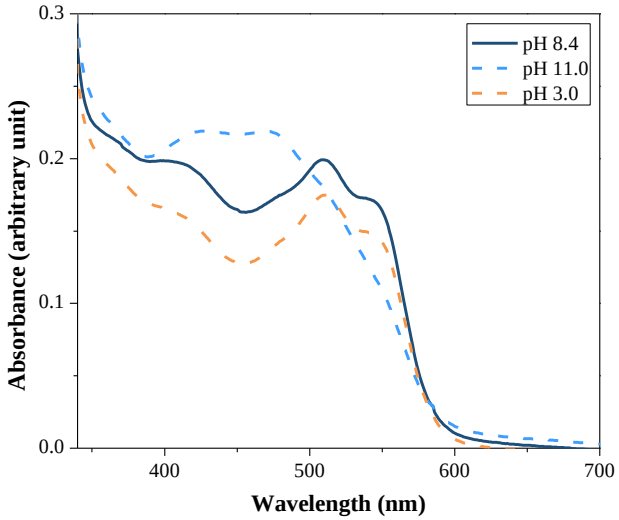

Figure 5.9. Variation of the UV-vis absorption spectra for the bio-treated textile wastewater as a function of pH.

The poor decolourisation results at low pH can be related to the presence of HSO_4^- at acid pH (as demonstrated on the Figure 5.10) [63], which is known to be a strong hydroxyl free radical scavenger (Eq. (5.7)) [52, 56, 64].

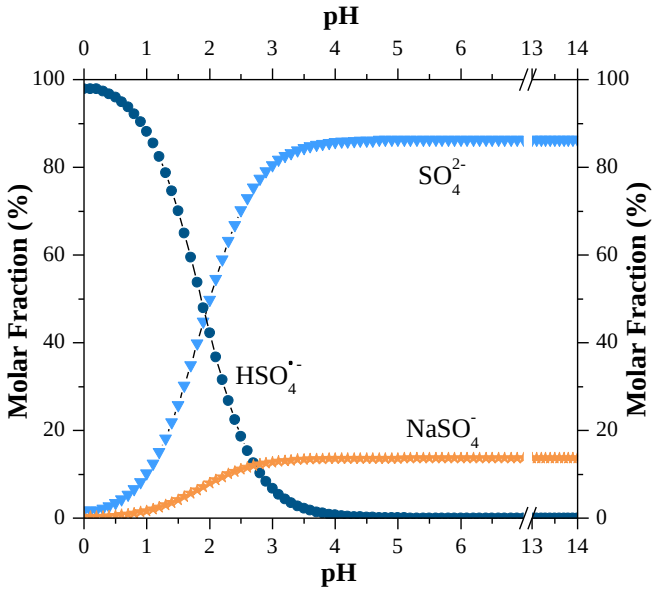

Figure 5.10. Speciation diagrams for SO_4^{2-} complexes as a function of pH for the bio-treated textile wastewater. Ionic strength = 0.08 M; Temperature = 30ºC; $[SO_4^{2-}]$ = 7.67 mM; $[Na^+]$ = 7.71×10^1 mM.

Depending on the operating conditions, the sulphate radical can oxidise some reactive oxygen species, including H_2O_2 (Eq. (5.8)-(5.12)). Beyond that, even being a strong oxidant, this species is slightly less reactive and more selective compared to $^{\bullet}OH$ [65, 66], affecting the organic compounds oxidation rates [67, 68].

$$HSO_4^- + {}^{\bullet}OH \rightarrow SO_4^{\bullet-} + H_2O \qquad k = 3.5\ 10^5\ M^{-1}\ s^{-1} \qquad (5.7)$$

$$SO_4^{\bullet-} + H_2O \rightarrow H^+ + SO_4^{2-} + {}^{\bullet}OH \qquad k = 6.6\ 10^2\ s^{-1} \qquad (5.8)$$

$$SO_4^{\bullet-} + HO^- \rightarrow SO_4^{2-} + {}^{\bullet}OH \qquad k = 1.4\ 10^7\ M^{-1}\ s^{-1} \qquad (5.9)$$

$$SO_4^{\bullet-} + H_2O_2 \rightarrow SO_4^{2-} + H^+ + HO_2^{\bullet} \qquad k = 1.2\ 10^7\ M^{-1}\ s^{-1} \qquad (5.10)$$

$$SO_4^{\bullet-} + HO_2^{\bullet} \rightarrow SO_4^{2-} + H^+ + O_2 \qquad k = 3.5\ 10^9\ M^{-1}\ s^{-1} \qquad (5.11)$$

$$SO_4^{\bullet-} + SO_2^{\bullet-} \rightarrow S_2O_8^{2-} \qquad k = 2.7\ 10^8\ M^{-1}\ s^{-1} \qquad (5.12)$$

Furthermore, in acidic medium, the concentration of H^+ rises, which can also have negative effects on the reaction, since it can react with H_2O_2 (Eq. (5.13)), yielding the peroxonium ion ($H_3O_2^+$), and acting as a scavenger of $^{\bullet}OH$ (Eq. (5.14)) [63].

$$H_2O_2 + H^+ \rightarrow H_3O_2^+ \qquad (5.13)$$

$${}^{\bullet}OH + H^+ + e^- \rightarrow H_2O \qquad (5.14)$$

Similar inhibition of the colour reduction was observed at pH 11. However, the H_2O_2 consumption rate is almost 2.0 times higher at pH 11 when compared with the reaction at natural wastewater pH. This can be attributed to two main factors: (i) in alkaline medium, the H_2O_2 becomes highly unstable and self-decomposition occurs, which is strongly pH dependent [69]. The self-decomposition will rapidly break down the H_2O_2 molecules into water and oxygen and they lose their characteristics as an oxidant, and most importantly as source of hydroxyl radicals (Eq. (5.15)); (ii) previous works described that under alkaline conditions, hydrogen peroxide deprotonates until achieving an equilibrium between H_2O_2 and HO_2^- species (pK_a =11.55 at 30ºC) (Figure 5.11) [52, 57, 64, 70].

The HO_2^- species reacts with $^{\bullet}OH$ (Eq. (5.16)) [71-73], which leads to dioxygen and water, instead of producing hydroxyl radicals under UVC radiation. Therefore, the instantaneous concentration of $^{\bullet}OH$

is lower than expected. Furthermore, the deactivation of $^{\bullet}OH$ is more important at basic pH values. The reaction of $^{\bullet}OH$ with HO_2^- is approximately 100 times faster than with H_2O_2 [64].

$$2H_2O_2 \rightarrow 2H_2O + O_2 \quad (5.15)$$

$$^{\bullet}OH + HO_2^- \rightarrow H_2O + O_2^- \qquad k = 7.5 \times 10^9\ M^{-1}\ s^{-1} \quad (5.16)$$

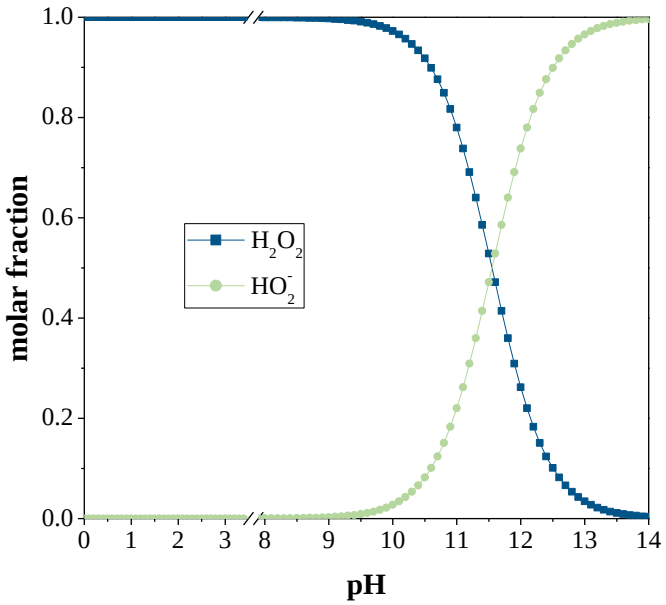

Figure 5.11. Distribution diagram of the molar fractions of hydrogen peroxide and hydroperoxy anion as a function of pH. (pK_a =11.55 at 30ºC) [70].

5.3.3.4 Effect of wastewater temperature

Figure 5.12 shows the effect of the bio-treated wastewater temperature on the decolourisation efficiency using the UVC/H_2O_2 system. Decolourisation and mineralisation rates are favoured at higher temperatures, especially when the temperature raises from 15 to 30ºC. This suggest that the generation of $^{\bullet}OH$ radicals through H_2O_2 photolysis is enhanced by the increase of the solution temperature [74]. Even though a slight increase in reaction efficiency was observed, increasing the temperature from 30 to 45ºC did not result in a considerable increase on the mineralisation and decolourisation. For the reaction at 15ºC, after 3.2 $kJ_{UV}\,L^{-1}$ of energy, only 7% of initial DOC was removed, in contrast with nearly 41% removal at 30ºC. Besides, the increase of the wastewater temperature from 30ºC to 45ºC did not promoted the H_2O_2 consumption rate. These results reinforce other ones from a similar work [75], where higher H_2O_2 consumption was observed only at higher temperatures than those tested here

(>50ºC), as a result of hydrogen peroxide decomposition into H_2O and O_2 (inactive species) and the formation of radicals with lesser oxidation potential [37].

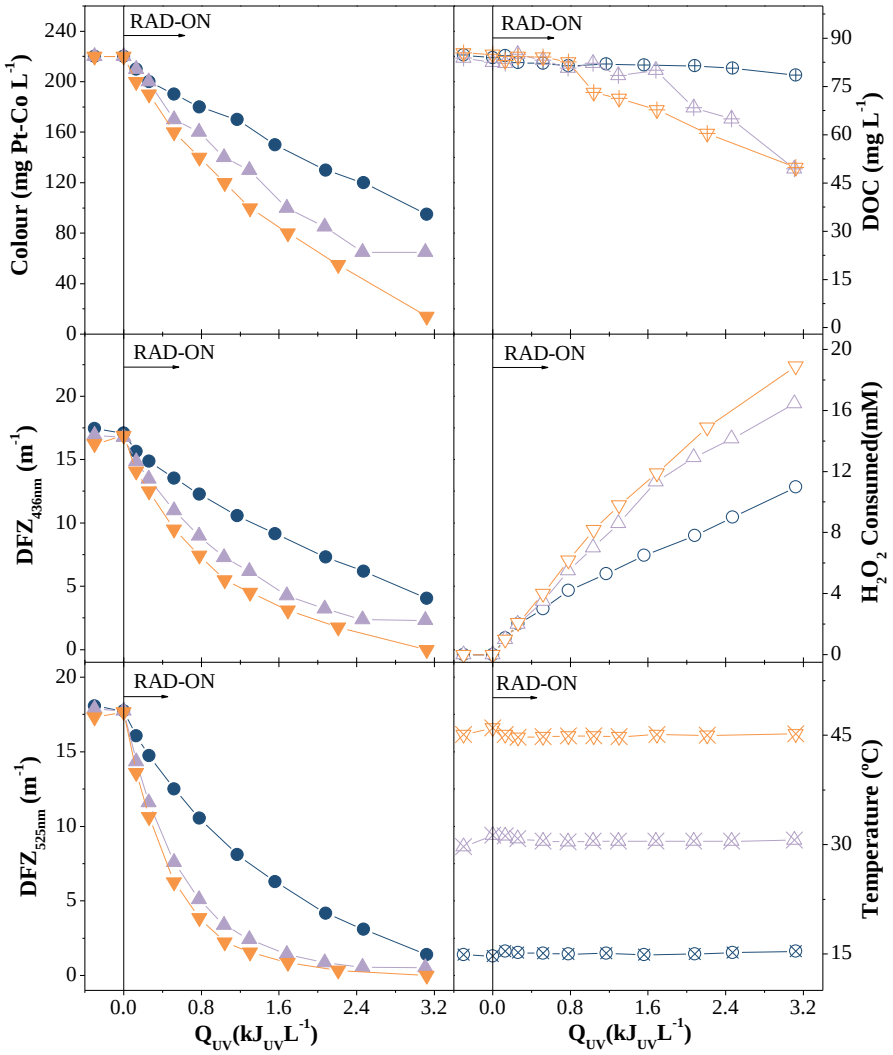

Figure 5.12. Decolourisation of the bio-treated textile wastewater using UVC/H_2O_2 reaction at different temperatures. Operation conditions: pH 8.4; [H_2O_2] = 42 mM and 6W UVC lamp. Solid symbols – colour indicators; cross symbols – DOC; open symbols – H_2O_2 consumed; "x" within symbols – Temperature. ● ⊕ ○ ⊗ – T = 15ºC; ▲ ⧋ △ ⧊ - T = 30ºC; ▼ ⧩ ▽ ⧨ - T = 45ºC.

5.3.3.5 *Evaluation of inorganic ions and low-molecular-weight carboxylate anions (LMWCA)*

Throughout the UVC/H_2O_2 reaction, the concentration of all measured inorganic ions remained approximately constant. As an example, Figure 5.13 shows that chloride and sulphate ions concentration remained at around 1465 mg Cl^- L^{-1} and 730 mg SO_4^{2-} L^{-1}, respectively. Figure 5.13 also shows an increase of the DOC corresponding to low-molecular-weight carboxylate anions (LMWCA/DOC ratio) after 0.8 kJ_{UV} L^{-1} of energy dosage, achieving maximum values of 20% (considering the LMWCA analysed). Previous works have reported that the oxidative cleavage of aromatic compounds can lead to

ring opening products, consisting of simpler organic acids including acetic, formic, glyoxylic and oxalic acids [73, 76].

It is noteworthy that, the carboxylic acids have emerged exactly after the induction period in DOC abatement (0.8 kJ_{UV} L^{-1}). After that, the mineralisation increases substantially associated with the conversion of carboxylic acids (final products of an oxidative reaction) to CO_2, H_2O and mineral acids [77]. According to the LMWCA analysis, only oxalic, maleic and tartaric acids were detected. Maleic acid, which can compete for the free radicals [30], was detected in very low concentrations (<0.18 mg L^{-1}). In contrast, the tartaric acid was accumulated in a larger extent up to 21.4 mg L^{-1}. Finally, oxalic acid, which is regarded as one of the ultimate carboxylic acids because it is directly oxidized to carbon dioxide [78] and is a common short-chain carboxylic acid resulting from the treatment process under study [79], was formed after 1 kJ_{UV} L^{-1} radiation and probably results from the degradation of the benzenic moieties of aromatic intermediates [80].

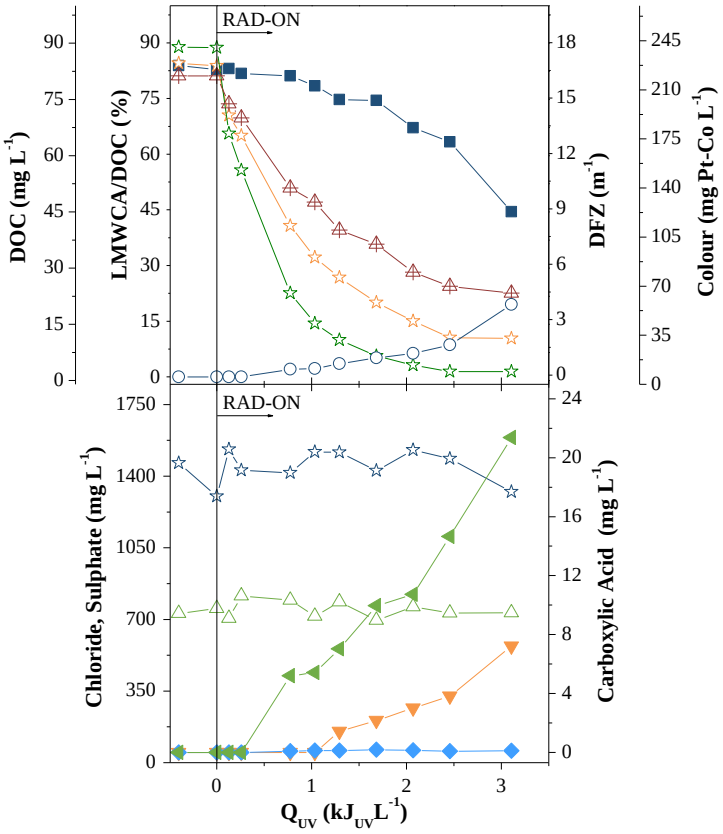

Figure 5.13. Detailed assessment of the bio-treated textile wastewater oxidation using the UVC/H_2O_2 system: ■ - DOC; ○ - LMWCA/DOC; ☆ - DFZ_{436nm}; ☆ - DFZ_{525nm}; ⧋ - Pt-Co scale; ☆ - Chloride; △ - Sulphate; ▼ - Oxalic acid; ◆ - Maleic acid; ◀ - Tartaric acid.

5.4 Conclusions

The textile wastewater from polyester-cotton dyeing exhibited a moderate biodegradability and, as a consequence, a significant DOC removal above 76% was achieved by biological oxidation. However, no significant decolourisation was detected during the biological oxidation, being the colour visible after 1:40 dilution. So, different AOPs were applied as a polishing step, regarding colour removal. UVC and H_2O_2 alone showed negligible decolourisation efficiencies. The UVC/Fe^{2+}/H_2O_2 process showed limited efficiency in the decolourisation of the bio-treated textile wastewater, mainly attributed to the low iron content able to be used, since the total iron discharge limit is 2 mg L^{-1}. In these conditions, the low iron concentration used is not able to suppress the inner filter effects related to other light-absorbing species present in the solution. Beyond that, ferric ions complexes with the organic and inorganic species (e.g., auxiliary products) present in the textile wastewater, which present low photoactivity and recalcitrant characteristic to further mineralisation by hydroxyl radical attack. The addition of oxalic acid, as a ferric ions ligand, did not lead to an increase of the wastewater decolourisation.

Although the UVC/H_2O_2 system showed to be effective in the decolourisation of the bio-treated textile wastewater, H_2O_2 in excess is requested. Higher wastewater temperature showed to have a positive effect on the UVC/H_2O_2 reaction. Alkaline and acidic wastewaters inhibited the decolourisation of the bio-treated wastewater using the UVC/H_2O_2 system. Besides, it was shown that the UVC/H_2O_2 reaction efficiency is mostly affected by the relation between the H_2O_2 dosage and lamp power. Finally, the integrated treatment strategy for the textile wastewater, combining biological and UVC/H_2O_2 oxidation processes, was able to meet with the legal discharge limits.

5.5 References

1. IPPC, I.P.P.a.C.-. *Reference Document on Best Available Techniques for the Textile Industry*. 2003, European Commission. p. 626.
2. Arslan-Alaton, I. and I. Alaton, *Degradation of xenobiotics originating from the textile preparation, dyeing, and finishing industry using ozonation and advanced oxidation.* Ecotoxicology and Environmental Safety, 2007. **68**(1): p. 98-107.
3. Delée, W., C. O'Neill, F.R. Hawkes, and H.M. Pinheiro, *Anaerobic treatment of textile effluents: A review.* Journal of Chemical Technology & Biotechnology, 1998. **73**(4): p. 323-335.
4. Correia, V.M., T. Stephenson, and S.J. Judd, *Characterisation of textile wastewaters - a review.* Environmental Technology, 1994. **15**(10): p. 917-929.
5. Pearce, C., J. Lloyd, and J. Guthrie, *The removal of colour from textile wastewater using whole bacterial cells: a review.* Dyes and pigments, 2003. **58**(3): p. 179-196.
6. Doumic, L.I., P.A. Soares, M.A. Ayude, M. Cassanello, R.A.R. Boaventura, and V.J.P. Vilar, *Enhancement of a solar photo-Fenton reaction by using ferrioxalate complexes for the treatment of a synthetic cotton-textile dyeing wastewater.* Chemical Engineering Journal, 2015. **277**: p. 86-96.
7. Arslan Alaton, I., G. Insel, G. Eremektar, F. Germirli Babuna, and D. Orhon, *Effect of textile auxiliaries on the biodegradation of dyehouse effluent in activated sludge.* Chemosphere, 2006. **62**(9): p. 1549-1557.
8. Konstantinou, I.K. and T.A. Albanis, *TiO_2-assisted photocatalytic degradation of azo dyes in aqueous solution: kinetic and mechanistic investigations: a review.* Applied Catalysis B: Environmental, 2004. **49**(1): p. 1-14.
9. Oller, I., S. Malato, and J.A. Sánchez-Pérez, *Combination of Advanced Oxidation Processes and biological treatments for wastewater decontamination—A review.* Science of The Total Environment, 2011. **409**(20): p. 4141-4166.
10. Nidheesh, P.V., R. Gandhimathi, and S.T. Ramesh, *Degradation of dyes from aqueous solution by Fenton processes: a review.* Environmental Science and Pollution Research, 2013. **20**(4): p. 2099-2132.
11. Faouzi, M., P. Cañizares, A. Gadri, J. Lobato, B. Nasr, R. Paz, M.A. Rodrigo, and C. Saez, *Advanced oxidation processes for the treatment of wastes polluted with azoic dyes.* Electrochimica Acta, 2006. **52**(1): p. 325-331.
12. Haji, S., B. Benstaali, and N. Al-Bastaki, *Degradation of methyl orange by UV/H_2O_2 advanced oxidation process.* Chemical Engineering Journal, 2011. **168**(1): p. 134-139.
13. Malato, S., P. Fernández-Ibáñez, M.I. Maldonado, J. Blanco, and W. Gernjak, *Decontamination and disinfection of water by solar photocatalysis: Recent overview and trends.* Catalysis Today, 2009. **147**(1): p. 1-59.
14. Miralles-Cuevas, S., F. Audino, I. Oller, R. Sánchez-Moreno, J.A. Sánchez Pérez, and S. Malato, *Pharmaceuticals removal from natural water by nanofiltration combined with advanced tertiary treatments (solar photo-Fenton, photo-Fenton-like Fe(III)–EDDS complex and ozonation).* Separation and Purification Technology, 2014. **122**: p. 515-522.

15. Oller, I., S. Malato, J.A. Sánchez-Pérez, W. Gernjak, M.I. Maldonado, L.A. Pérez-Estrada, and C. Pulgarín, *A combined solar photocatalytic-biological field system for the mineralization of an industrial pollutant at pilot scale.* Catalysis Today, 2007. **122**(1–2): p. 150-159.

16. Silva, T.F.C.V., M.E.F. Silva, A.C. Cunha-Queda, A. Fonseca, I. Saraiva, M.A. Sousa, C. Gonçalves, M.F. Alpendurada, R.A.R. Boaventura, and V.J.P. Vilar, *Multistage treatment system for raw leachate from sanitary landfill combining biological nitrification–denitrification/solar photo-Fenton/biological processes, at a scale close to industrial – Biodegradability enhancement and evolution profile of trace pollutants.* Water Research, 2013. **47**(16): p. 6167-6186.

17. Bisschops, I. and H. Spanjers, *Literature review on textile wastewater characterisation.* Environmental Technology, 2003. **24**(11): p. 1399-1411.

18. Wang, S., *A comparative study of Fenton and Fenton-like reaction kinetics in decolourisation of wastewater.* Dyes and Pigments, 2008. **76**(3): p. 714-720.

19. Liwarska-Bizukojc, E., K. Miksch, A. Malachowska-Jutsz, and J. Kalka, *Acute toxicity and genotoxicity of five selected anionic and nonionic surfactants.* Chemosphere, 2005. **58**(9): p. 1249-1253.

20. Pehlivanoglu-Mantas, E., G. Insel, O. Karahan, E.U. Cokgor, and D. Orhon, *Case Studies from Turkey: Xenobiotic-containing Industries, Wastewater Treatment and Modeling.* Water, Air, & Soil Pollution: Focus, 2008. **8**(5-6): p. 519-528.

21. Poole, A.J., *Treatment of biorefractory organic compounds in wool scour effluent by hydroxyl radical oxidation.* Water Research, 2004. **38**(14–15): p. 3458-3464.

22. Ying, G.G., *Fate, behavior and effects of surfactants and their degradation products in the environment.* Environ Int, 2006. **32**(3): p. 417-31.

23. Portugal, *Portaria nº423/97 de 25 de Junho, Diário da República-I Série*. 1997. p. 3111-3112.

24. Ranade, V.V. and V.M. Bhandari, *Industrial Wastewater Treatment, Recycling, and Reuse*. 2014, Oxford, UK. 577.

25. Eddy, M., *Wastewater Engineering: Treatment and Reuse*. 4th Edition. 2005: McGraw Hill Higher Education. 1408.

26. Palm, J.C., D. Jenkins, and D.S. Parker, *Relationship between Organic Loading, Dissolved Oxygen Concentration and Sludge Settleability in the Completely-Mixed Activated Sludge Process.* Journal (Water Pollution Control Federation), 1980. **52**(10): p. 2484-2506.

27. Soares, P.A., M. Batalha, S.M.A.G.U. Souza, R.A.R. Boaventura, and V.J.P. Vilar, *Enhancement of a solar photo-Fenton reaction with ferric-organic ligands for the treatment of acrylic-textile dyeing wastewater.* Journal of Environmental Management, 2015. **152**: p. 120-131.

28. Arslan-Alaton, I. and E. Erdinc, *Effect of photochemical treatment on the biocompatibility of a commercial nonionic surfactant used in the textile industry.* Water Research, 2006. **40**(18): p. 3409-3418.

29. Guinea, E., F. Centellas, J.A. Garrido, R.M. Rodríguez, C. Arias, P.-L. Cabot, and E. Brillas, *Solar photoassisted anodic oxidation of carboxylic acids in presence of Fe^{3+} using a boron-doped diamond electrode.* Applied Catalysis B: Environmental, 2009. **89**(3): p. 459-468.

30. Rodríguez, E.M., B. Núñez, G. Fernández, and F.J. Beltrán, *Effects of some carboxylic acids on the Fe (III)/UVA photocatalytic oxidation of muconic acid in water.* Applied Catalysis B: Environmental, 2009. **89**(1): p. 214-222.

31. Clesceri, L.S., A.E. Greenberg, and A.D. Eaton, *Standard Methods for Examination of Water & Wastewater*. 21 ed, ed. A.P.H.A. (APHA). 2005.

32. *DIN EN ISO 7887:2012-04, Wasserbeschaffenheit - Untersuchung und Bestimmung der Färbung*. 2012, Deutsches Institut für Normung - DIN.

33. Barragán, B.E., C. Costa, and M. Carmen Marquez, *Biodegradation of azo dyes by bacteria inoculated on solid media.* Dyes and pigments, 2007. **75**(1): p. 73-81.

34. Araña, J., D. Zerbani, J.H. Melián, D.G. Sousa, O.G. Díaz, and J.D. Rodríguez, *Effect of additives in photocatalytic degradation of commercial azo dye Lanaset Sun Yellow 180.* Photochemical & Photobiological Sciences, 2013. **12**(4): p. 703-708.

35. Kandelbauer, A. and G.M. Guebitz, *Bioremediation for the Decolorization of Textile Dyes — A Review*, in *Environmental Chemistry*, E. Lichtfouse, J. Schwarzbauer, and D. Robert, Editors. 2005, Springer Berlin Heidelberg. p. 269-288.

36. Portugal, *Decreto-Lei nº.236/98*. 1998, Ministério do Ambiente: Diário da República. p. 47.

37. Monteagudo, J.M., A. Durán, J.M. Corral, A. Carnicer, J.M. Frades, and M.A. Alonso, *Ferrioxalate-induced solar photo-Fenton system for the treatment of winery wastewaters.* Chemical Engineering Journal, 2012. **181–182**: p. 281-288.

38. Tehrani Bagha, A.R., H. Bahrami, B. Movassagh, M. Arami, and F.M. Menger, *Interactions of gemini cationic surfactants with anionic azo dyes and their inhibited effects on dyeability of cotton fabric.* Dyes and Pigments, 2007. **72**(3): p. 331-338.

39. Oliveira, M.M., C. Moustrou, L.M. Carvalho, J.A.C. Silva, A. Samat, R. Guglielmetti, R. Dubest, J. Aubard, and A.M.F. Oliveira-Campos, *Synthesis and photochromic behaviour under flash photolysis and continuous irradiation of novel 2H-chromenes derived from hydroxydibenzothiophenes.* Tetrahedron, 2002. **58**(9): p. 1709-1718.

40. Irie, M., *Diarylethenes for Memories and Switches.* Chemical Reviews, 2000. **100**(5): p. 1685-1716.

41. Queiroz, M.-J.R.P., R. Dubest, J. Aubard, R. Faure, and R. Guglielmetti, *Synthesis of photochromic thieno-2H-chromene derivatives.* Dyes and Pigments, 2000. **47**(3): p. 219-229.

42. Soares, P., T.C.V. Silva, D. Manenti, S.A.G.U. Souza, R.R. Boaventura, and V.P. Vilar, *Insights into real cotton-textile dyeing wastewater treatment using solar advanced oxidation processes.* Environmental Science and Pollution Research, 2014. **21**(2): p. 932-945.

43. Rodríguez, E.M., B. Núñez, G. Fernández, and F.J. Beltrán, *Effects of some carboxylic acids on the Fe(III)/UVA photocatalytic oxidation of muconic acid in water.* Applied Catalysis B: Environmental, 2009. **89**(1–2): p. 214-222.

44. Guinea, E., F. Centellas, J.A. Garrido, R.M. Rodríguez, C. Arias, P.-L. Cabot, and E. Brillas, *Solar photoassisted anodic oxidation of carboxylic acids in presence of Fe^{3+} using a boron-doped diamond electrode.* Applied Catalysis B: Environmental, 2009. **89**(3–4): p. 459-468.

45. Manenti, D.R., P.A. Soares, A.N. Módenes, F.R. Espinoza-Quiñones, R.A.R. Boaventura, R. Bergamasco, and V.J.P. Vilar, *Insights into solar photo-Fenton process using iron(III)–organic ligand complexes applied to real textile wastewater treatment.* Chemical Engineering Journal, 2015. **266**: p. 203-212.

46. Weller, C., S. Horn, and H. Herrmann, *Effects of Fe(III)-concentration, speciation, excitation-wavelength and light intensity on the quantum yield of iron(III)-oxalato complex photolysis.* Journal of Photochemistry and Photobiology A: Chemistry, 2013. **255**: p. 41-49.

47. Lucas, M.S. and J.A. Peres, *Degradation of Reactive Black 5 by Fenton/UV-C and ferrioxalate/H_2O_2/solar light processes.* Dyes and Pigments, 2007. **74**(3): p. 622-629.

48. Shu, H.-Y., M.-C. Chang, and H.-J. Fan, *Effects of gap size and UV dosage on decolorization of C.I. Acid Blue 113 wastewater in the UV/H_2O_2 process.* Journal of Hazardous Materials, 2005. **118**(1–3): p. 205-211.

49. Shah, N.S., X. He, H.M. Khan, J.A. Khan, K.E. O'Shea, D.L. Boccelli, and D.D. Dionysiou, *Efficient removal of endosulfan from aqueous solution by UV-C/peroxides: A comparative study.* Journal of Hazardous Materials, 2013. **263, Part 2**: p. 584-592.

50. Zhou, C., N. Gao, Y. Deng, W. Chu, W. Rong, and S. Zhou, *Factors affecting ultraviolet irradiation/hydrogen peroxide (UV/H_2O_2) degradation of mixed N-nitrosamines in water.* Journal of Hazardous Materials, 2012. **231–232**: p. 43-48.

51. Zalazar, C.S., M.D. Labas, R.J. Brandi, and A.E. Cassano, *Dichloroacetic acid degradation employing hydrogen peroxide and UV radiation.* Chemosphere, 2007. **66**(5): p. 808-815.

52. Basturk, E. and M. Karatas, *Decolorization of antraquinone dye Reactive Blue 181 solution by UV/H_2O_2 process.* Journal of Photochemistry and Photobiology A: Chemistry, 2015. **299**: p. 67-72.

53. Ghodbane, H. and O. Hamdaoui, *Decolorization of antraquinonic dye, C.I. Acid Blue 25, in aqueous solution by direct UV irradiation, UV/H_2O_2 and UV/Fe(II) processes.* Chemical Engineering Journal, 2010. **160**(1): p. 226-231.

54. Toor, A.P., A. Verma, C.K. Jotshi, P.K. Bajpai, and V. Singh, *Photocatalytic degradation of Direct Yellow 12 dye using UV/TiO_2 in a shallow pond slurry reactor.* Dyes and Pigments, 2006. **68**(1): p. 53-60.

55. Huang, M., C. Xu, Z. Wu, Y. Huang, J. Lin, and J. Wu, *Photocatalytic discolorization of methyl orange solution by Pt modified TiO_2 loaded on natural zeolite.* Dyes and Pigments, 2008. **77**(2): p. 327-334.

56. Shu, H.-Y., *Degradation of dyehouse effluent containing C.I. Direct Blue 199 by processes of ozonation, UV/H_2O_2 and in sequence of ozonation with UV/H_2O_2.* Journal of Hazardous Materials, 2006. **133**(1–3): p. 92-98.

57. Alaton, I.A., I.A. Balcioglu, and D.W. Bahnemann, *Advanced oxidation of a reactive dyebath effluent: comparison of O_3, H_2O_2/UV-C and TiO_2/UV-A processes.* Water Research, 2002. **36**(5): p. 1143-1154.

58. Pérez-Urquiza, M. and J.L. Beltrán, *Determination of the dissociation constants of sulfonated azo dyes by capillary zone electrophoresis and spectrophotometry methods.* Journal of Chromatography A, 2001. **917**(1–2): p. 331-336.

59. Gomes, A.C., L.R. Fernandes, and R.M.S. Simões, *Oxidation rates of two textile dyes by ozone: Effect of pH and competitive kinetics.* Chemical Engineering Journal, 2012. **189–190**: p. 175-181.

60. Yazdanbakhsh, M.R., A. Ghanadzadeh, and E. Moradi, *Synthesis of some new azo dyes derived from 4-hydroxy coumarin and spectrometric determination of their acidic dissociation constants.* Journal of Molecular Liquids, 2007. **136**(1–2): p. 165-168.

61. Ebead, Y.H., H.M.A. Salman, M. Khodari, and A.A. Ahmed, *Spectrophotometric investigations of the role of the organic solvent on the acid dissociation constants of some azo dyes derived from 2-aminobenzothiazole.* Journal of Molecular Liquids, 2010. **154**(1): p. 52-57.

62. Ebead, Y.H., *The role of the medium on the acid dissociation constants of some azo dyes in view of experimental and theoretical data.* Journal of Molecular Structure, 2010. **982**(1–3): p. 100-106.

63. Silva, T.F.C.V., R. Ferreira, P.A. Soares, D.R. Manenti, A. Fonseca, I. Saraiva, R.A.R. Boaventura, and V.J.P. Vilar, *Insights into solar photo-Fenton reaction parameters in the oxidation of a sanitary landfill leachate at lab-scale.* Journal of Environmental Management, 2015. **164**: p. 32-40.

64. Daneshvar, N., M.A. Behnajady, M.K.A. Mohammadi, and M.S.S. Dorraji, *UV/H_2O_2 treatment of Rhodamine B in aqueous solution: Influence of operational parameters and kinetic modeling.* Desalination, 2008. **230**(1–3): p. 16-26.

65. Jasper, J.T. and D.L. Sedlak, *Phototransformation of wastewater-derived trace organic contaminants in open-water unit process treatment wetlands.* Environmental science & technology, 2013. **47**(19): p. 10781-10790.

66. Zeng, T. and W.A. Arnold, *Pesticide photolysis in prairie potholes: probing photosensitized processes.* Environmental science & technology, 2012. **47**(13): p. 6735-6745.

67. De Laat, J. and T.G. Le, *Kinetics and modeling of the Fe (III)/H_2O_2 system in the presence of sulfate in acidic aqueous solutions.* Environmental science & technology, 2005. **39**(6): p. 1811-1818.

68. Neta, P., R.E. Huie, and A.B. Ross, *Rate constants for reactions of inorganic radicals in aqueous solution.* Journal of Physical and Chemical Reference Data, 1988. **17**(3): p. 1027-1284.

69. Chan, C.Y., S. Tao, R. Dawson, and P.K. Wong, *Treatment of atrazine by integrating photocatalytic and biological processes.* Environmental Pollution, 2004. **131**(1): p. 45-54.

70. Evans, M.G. and N. Uri, *The dissociation constant of hydrogen peroxide and the electron affinity of the HO_2 radical.* Transactions of the Faraday Society, 1949. **45**: p. 224-230.

71. Muruganandham, M. and M. Swaminathan, *Decolourisation of Reactive Orange 4 by Fenton and photo-Fenton oxidation technology.* Dyes and Pigments, 2004. **63**(3): p. 315-321.

72. Gierer, J. and K. Jansbo, *Formation of Hydroxyl Radicals from Hydrogen Peroxide and their Effect on Bleaching of Mechanical Pulps.* Journal of Wood Chemistry and Technology, 1993. **13**(4): p. 561-581.

73. Karci, A., I. Arslan-Alaton, T. Olmez-Hanci, and M. Bekbölet, *Transformation of 2,4-dichlorophenol by H_2O_2/UV-C, Fenton and photo-Fenton processes: Oxidation products and toxicity evolution.* Journal of Photochemistry and Photobiology A: Chemistry, 2012. **230**(1): p. 65-73.

74. Sanz, J., J.I. Lombraña, and A. de Luis, *Temperature-assisted UV/H_2O_2 oxidation of concentrated linear alkylbenzene sulphonate (LAS) solutions.* Chemical Engineering Journal, 2013. **215–216**: p. 533-541.

75. Santos, A., P. Yustos, S. Rodriguez, E. Simon, and F. Garcia-Ochoa, *Abatement of phenolic mixtures by catalytic wet oxidation enhanced by Fenton's pretreatment: Effect of H_2O_2 dosage and temperature.* Journal of Hazardous Materials, 2007. **146**(3): p. 595-601.

76. Skoumal, M., C. Arias, P.L. Cabot, F. Centellas, J.A. Garrido, R.M. Rodríguez, and E. Brillas, *Mineralization of the biocide chloroxylenol by electrochemical advanced oxidation processes.* Chemosphere, 2008. **71**(9): p. 1718-1729.

77. Souza, B.M., M.W.C. Dezotti, R.A.R. Boaventura, and V.J.P. Vilar, *Intensification of a solar photo-Fenton reaction at near neutral pH with ferrioxalate complexes: A case study on*

diclofenac removal from aqueous solutions. Chemical Engineering Journal, 2014. **256**: p. 448-457.

78. Garcia-Segura, S., A. El-Ghenymy, F. Centellas, R.M. Rodríguez, C. Arias, J.A. Garrido, P.L. Cabot, and E. Brillas, *Comparative degradation of the diazo dye Direct Yellow 4 by electro-Fenton, photoelectro-Fenton and photo-assisted electro-Fenton.* Journal of Electroanalytical Chemistry, 2012. **681**: p. 36-43.

79. Olmez-Hanci, T., D. Dursun, E. Aydin, I. Arslan-Alaton, B. Girit, L. Mita, N. Diano, D.G. Mita, and M. Guida, *$S_2O_8^{2-}$/UV-C and H_2O_2/UV-C treatment of Bisphenol A: Assessment of toxicity, estrogenic activity, degradation products and results in real water.* Chemosphere, 2015. **119, Supplement**: p. S115-S123.

80. Skoumal, M., R.M. Rodríguez, P.L. Cabot, F. Centellas, J.A. Garrido, C. Arias, and E. Brillas, *Electro-Fenton, UVA photoelectro-Fenton and solar photoelectro-Fenton degradation of the drug ibuprofen in acid aqueous medium using platinum and boron-doped diamond anodes.* Electrochimica Acta, 2009. **54**(7): p. 2077-2085.

6 Assessment of AOPs as a polishing step in the decolourisation of bio-treated textile wastewater: technical and economic considerations[4]

This chapter reports on the decolourisation of a bio-treated real textile wastewater using UVC/H_2O_2 and photo-Fenton oxidation processes, as a polishing step. The efficiency of hydrogen peroxide photolysis using UVC radiation on the wastewater decolourisation was evaluated at different reaction conditions. The effect of radiation source, iron concentration, pH value and H_2O_2 concentration on the photo-Fenton reaction was also assessed. The viability of the photo-Fenton reaction enhanced by ferric-organic ligands using artificial solar radiation was also under consideration. In addition, the costs associated with the processes studied were evaluated and compared.

[4]This Chapter is based on the research article: "Soares, P.A., Silva, Tânia F. C. V., Arcy, A. R., Selene M. A. Guelli U., Boaventura, Rui A. R., Vilar, Vítor J. P., *Assessment of AOPs as a polishing step in the decolourisation of bio-treated textile wastewater: technical an economic considerations.* Journal of Photochemistry and Photobiology A: Chemistry. 2016 317: p. 26-38.

6.1 Introduction

Wastewaters discharged from textile plants have a considerable recalcitrant organic fraction, normally associated with dyes, surfactants and other additives [1]. In addition, wastewaters from the textile dyeing processes have a strong coloration which is difficult to remove, causing serious environmental impacts [2]. In response to increasingly stringent legislation, environmental engineers are looking for eco-efficient and environmentally sound technologies for the decolourisation and mineralisation of textile wastewaters [2-5]. The combination of biological and physical/chemical processes, such as coagulation/flocculation, is currently the most common approach applied to textile wastewater treatment [6]. Biological oxidation systems have provided good results for the mineralisation of the non-recalcitrant organic fraction of textile wastewater, especially when it is mixed with biodegradable wastewaters, e.g., domestic sewage [7]. On the other hand, it is known that biological processes are not always efficient as regards wastewater decolourisation, mainly due to the recalcitrant characteristic of most synthetic organic dyes. In the case of coagulation/flocculation systems, the contaminants are merely transferred from the wastewater to the sludge, which then needs careful disposal [8].

Recently, other technologies for the decolourisation of textile wastewater have been emerging, such as advanced oxidation processes (AOPs). In this regard, the photo-Fenton (PF) process using solar light has shown to be a promising low cost technique, since solar radiation as a UV–Vis photon source represents an extra mechanism for $^{\bullet}OH$ generation through the photolysis of iron complexes [9]. However, several drawbacks associated with the application of this process in the treatment of textile wastewaters have been reported in the literature [10], for instance: i) textile wastewaters are usually alkaline and thus high amounts of acid are required in the acidification step of the photo-Fenton reaction, with the subsequent need for neutralisation; and ii) ferric-dissolved organic matter complexes can be formed, limiting the photoreduction of Fe^{3+}, hindering the decomposition of H_2O_2 in the Fenton reaction and decreasing the overall efficiency of the photo-Fenton process [11, 12]. The enhancement of the photo-Fenton reaction can be achieved through the use of ferricarboxylate complexes [13], minimizing the formation of undesirable poorly photoactive and/or insoluble ferric-organic matter complexes and making it possible to work under near neutral pH conditions.

On the other hand, UVC/H_2O_2 is one of the most commonly applied AOPs [14-16], where hydroxyl radicals are generated through the photolysis of hydrogen peroxide under UVC radiation. UVC/H_2O_2 has been extensively investigated for the degradation of different organic pollutants, such as phenol derivatives [17, 18], pesticides [19], EDTA [20] and antibiotics [21]. In recent years, UVC light emitting diodes (UV-LEDs), which are a mercury-free source of monochromatic UVC radiation, have been

shown to be a promising UV light source for the photolysis of H_2O_2 [22, 23]. Although UVC/H_2O_2 has also been efficiently used for the decolourisation of several dye solutions on the lab scale [8, 24-26], the lack of information related to the treatment of real textile wastewaters is one of the main reasons for the absence of real applications in this field.

The aim of this study was to assess the decolourisation of a bio-treated real textile wastewater using UVC/H_2O_2 and the photo-Fenton oxidation process as polishing step. The efficiency of hydrogen peroxide photolysis under UVC radiation in relation to the decolourisation of the wastewater was evaluated at different pH values, H_2O_2 concentrations and temperatures. The effect of the radiation source (UVC, UVA or UVA-Visible), iron concentration, pH value and H_2O_2 concentration on the photo-Fenton reaction was also studied. The viability of the photo-Fenton reaction enhanced by ferric-organic ligands using artificial solar radiation was also evaluated at different iron concentrations, pH values and iron/organic ligand molar ratios. In addition, the costs associated with the studied processes were calculated and compared.

6.2 Material and Methods

All the chemicals and reagents used in this work, the detailed description of the lab-scale and pilot-plant scale experimental units, along with the corresponding experimental procedures, and, finally, the employed methods can be consulted in Chapter 2. The detailed operational conditions of the assays reported in this chapter are shown in Table 6.1 (lab-scale lamp photoreactor) and Table 6.2 (lab-scale sunlight simulator photoreactor).

Table 6.1. Operational conditions reactions under UVC radiation.

System	TDI[a]	T[b]	pH	Dosage of H_2O_2[c]
UVC/H_2O_2	-	30	2.8	2.1
UVC/Fe^{2+}/H_2O_2	0.5 1 2			
UVC/H_2O_2	-	15 30 45	Natural	2.1
		15 30 45	2.8	2.1
UVC/Fe^{2+}/H_2O_2	2	15 30 45	2.8	2.1
UVC/H_2O_2	-	30	Natural	0.7 1.3 2.1 4.2 6.9 10.0
UVC/Fe^{2+}/H_2O_2	2	30	2.8	0.7 1.3 2.1 4.2 6.9 10.0

[a]Dissolved iron concentration (mg L^{-1}); [b]Liquid phase temperature (ºC); [c](mM H_2O_2).

Table 6.2. Operational conditions for reactions under UVA-Visible radiation.

System	TDI[a]	Molar Ratio (Fe:LIG)	T[b]	pH	Dosage of H_2O_2[c]
UVA-Vis/Fe^{2+}/H_2O_2	10	-	30	2. 8	2.1
UVA-Vis/Fe^{3+}/H_2O_2/Oxalic acid		1:3			3.1
UVA-Vis/Fe^{3+}/H_2O_2/EDDS		1:1			2.1
UVA-Vis/Fe^{3+}/H_2O_2/Citric acid		1:1			3.1
UVA-Vis/Fe^{3+}/H_2O_2/Oxalic acid	10	1:3	30	2.8	3.1
		1:6			5.1
		1:9			5.1
UVA-Vis/Fe^{3+}/H_2O_2/Oxalic acid	2	1:3	30	2.8	2.1
	6				3.1
	10				3.1
	20				5.1
	40				9.8
UVA-Vis/Fe^{3+}/H_2O_2/Oxalic acid	6	1:3	30	2.9[d]	3.1
				3.7[d]	3.1
				4.1[d]	3.1
				4.9[d]	3.1
				5.5[d]	3.1
				5.9[d]	3.1
		1:6		6.1[d]	3.1

[a]Dissolved iron concentration (mg L^{-1}); [b]Liquid phase temperature (°C); [c](mM H_2O_2); [d]average pH.

6.3 Results and discussion

6.3.1 Characteristics of the textile wastewater

Table 2.7 (Materials and methods – Chapter 2) shows a brief characterisation of the bio-treated real textile wastewater used in this study. The wastewater presents a near neutral pH value (~7.8) and a low organic load (COD = 107 mg O_2 L^{-1} and DOC = 32 mg C L^{-1}). High concentrations were found for chloride and sodium ions (613 mg Cl^- L^{-1} and 659 mg Na^+ L^{-1}, respectively). The wastewater shows a reddish colour, equivalent to 160 mg Pt-Co L^{-1}. Furthermore, a greater absorbance was observed at DFZ_{436nm} compared with DFZ_{525nm} and DFZ_{620nm}, which indicates a predominance of violet with respect to green and orange in the wastewater absorption spectrum.

The bio-treated real textile wastewater was found to be in accordance with the Portuguese regulations for discharge into water bodies [27] with one exception, that is, the limits for colour. According to the cited standard, the wastewater has to be uncoloured at a 1:20 dilution. However, this quality criterion does not allow the colour removal efficiencies to be calculated and the results from different experiments to be compared.

In order to overcome this limitation, the German textile wastewater discharge standard [28] was used for the technical and economic assessment carried out in this study. This legislation was selected for two main reasons: i) a simple and efficient technique for colour measurement based on DIN EN ISO:7887 [29] is adopted; and ii) for the textile wastewater used in this study, the German legislation establishes 7 m^{-1} (DFZ_{436nm}), 5 m^{-1} (DFZ_{525nm}) and 3 m^{-1} (DFZ_{620nm}), which is in accordance with Portuguese legislation (uncoloured wastewater at 1:20 dilution).

6.3.2 Photo-Fenton decolourisation using different radiation sources

The decolourisation of the textile wastewater through the conventional photo-Fenton reaction was evaluated using different radiation sources (pH = 2.8; [Fe^{2+}] = 2 mg L^{-1}; T = 30ºC) (Figure 6.1). Although a similar colour reduction after acidification was obtained for all test conditions, i.e., ~38% (Pt-Co method), ~27% (DFZ_{436nm}), ~29% (DFZ_{525nm}) and ~44% (DFZ_{620nm}), negligible mineralisation was observed (Figure 6.2).

This may be caused by: i) the dissociation of some dyes, which leads to different absorption properties as a function of pH [30-34]; or/and ii) the precipitation of some dyes, e.g., sulphur and vat dyes [35],

which means that the dye molecules, before ionisation and water solubilisation in moderately alkali solution, become insoluble in water at acid pH [36-38]. Since the reduction in the colour was partial and textile dyes normally contribute to a low DOC in textile wastewaters, it is possible that the precipitation of a small part of these compounds would not be detected through DOC monitoring.

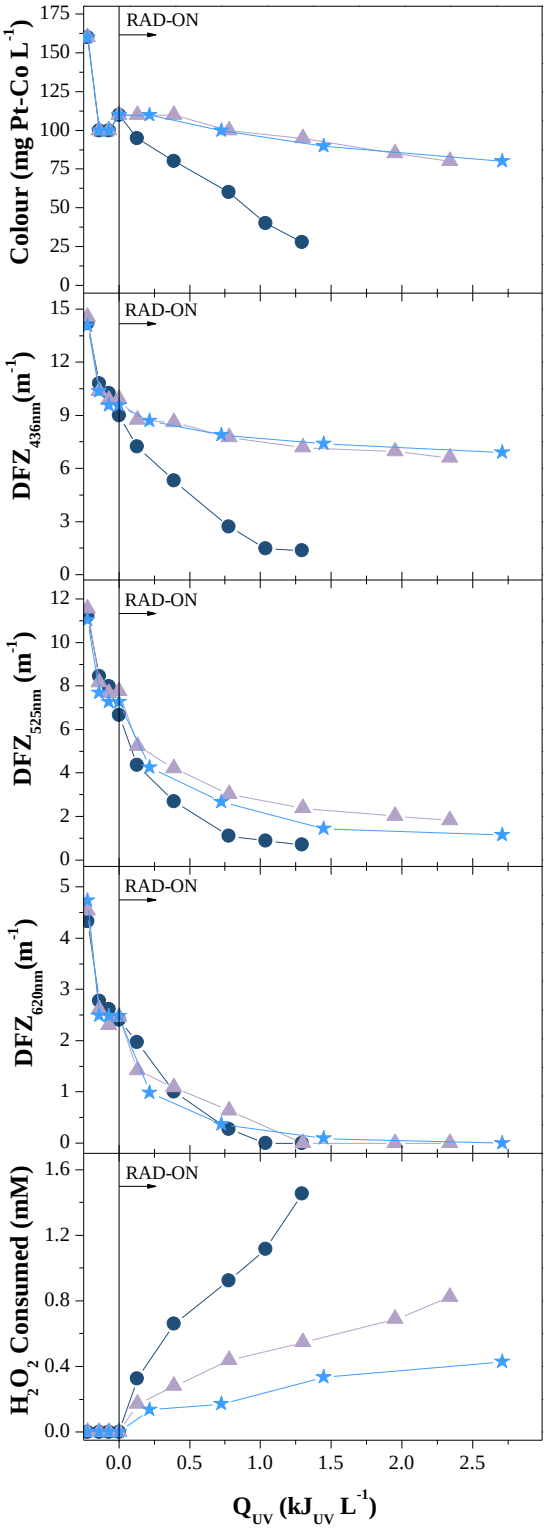

Figure 6.1. Decolourisation of the textile wastewater using different sources of radiation. ● - UVC/Fe^{2+}/H_2O_2; ▲ - UVA/Fe^{2+}/H_2O_2; ★ – UVA-Vis/Fe^{2+}/H_2O_2.

After the radiation was turned on, the photo-Fenton reaction under UVC radiation led to better results than when UVA and UVA-Visible light were used, as regards the colour removal associated with dye species absorbing in the lower range of visible light ($DFZ_{436\,nm}$ and Pt-Co). Similar results were obtained in the decolourisation of dye species which absorb at longer wavelengths, such as 525 nm and 620 nm. The evaluation of the decolourisation by the platinum-cobalt and DFZ_{436nm} methods showed good agreement with the visual observations.

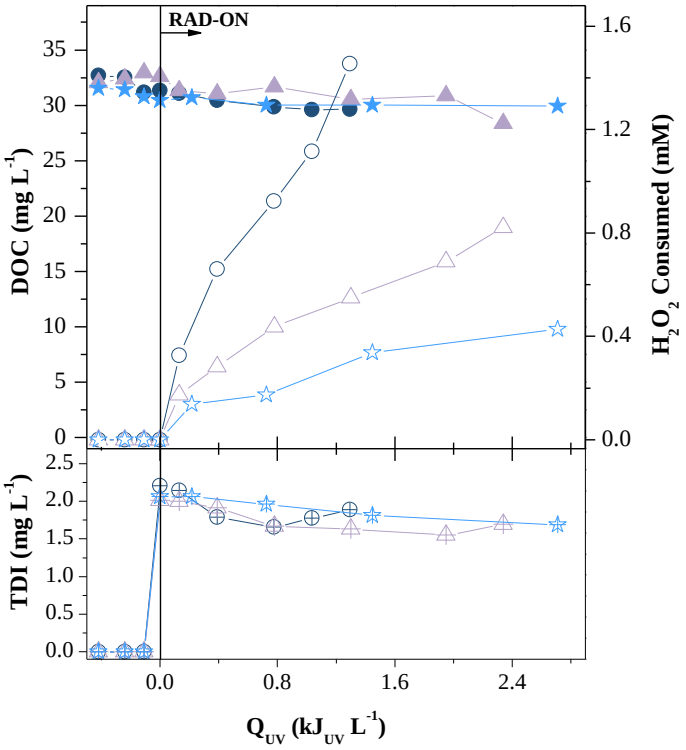

Figure 6.2. Mineralisation of the textile wastewater using different sources of radiation. Solid symbols – DOC; open symbols – H_2O_2 consumed; cross symbols – total dissolved iron (TDI). ● ○ ⊕ - UVC/Fe^{2+}/H_2O_2; ▲ △ ⊞ - UVA/Fe^{2+}/H_2O_2; ★ ☆ ✯ – UVA-Vis/Fe^{2+}/H_2O_2.

The low efficiency of the photo-Fenton reaction under UVA and UVA-Visible light may be associated with the formation of stable complexes between Fe^{3+} and organic pollutants present in the textile wastewater, which present low photoactivity under UVA and visible light, limiting the photoreduction of Fe^{3+}.

Under UVC radiation, the photo-Fenton reaction showed a high decolourisation efficiency related to the photolysis of hydrogen peroxide, leading to the formation of extra $^{\bullet}OH$ radicals. The photolysis of H_2O_2 has a low quantum yield under UVA and visible light. In addition, the beneficial effect of the use of UVC radiation can be related to the higher quantum yield of $FeOH^{2+}$ and other iron species for $^{\bullet}OH$ generation at lower wavelengths [39]. Further reactions under UVC radiation were performed in order

to evaluate the effect of different reaction variables, such as iron concentration, temperature, pH and hydrogen peroxide concentration.

6.3.3 Decolourisation under UVC reaction

6.3.3.1 Effect of iron concentration

Figure 6.3 shows the decolourisation results obtained for the photo-Fenton reaction under UVC radiation at different initial ferrous iron concentrations (0.5, 1.0 and 2.0 mg Fe^{2+} L^{-1}; T = 30ºC; pH = 2.8; $[H_2O_2]$ = 2.1 mM) and for the UVC/H_2O_2 system (T = 30ºC; pH = 2.8; $[H_2O_2]$ = 2.1 mM).

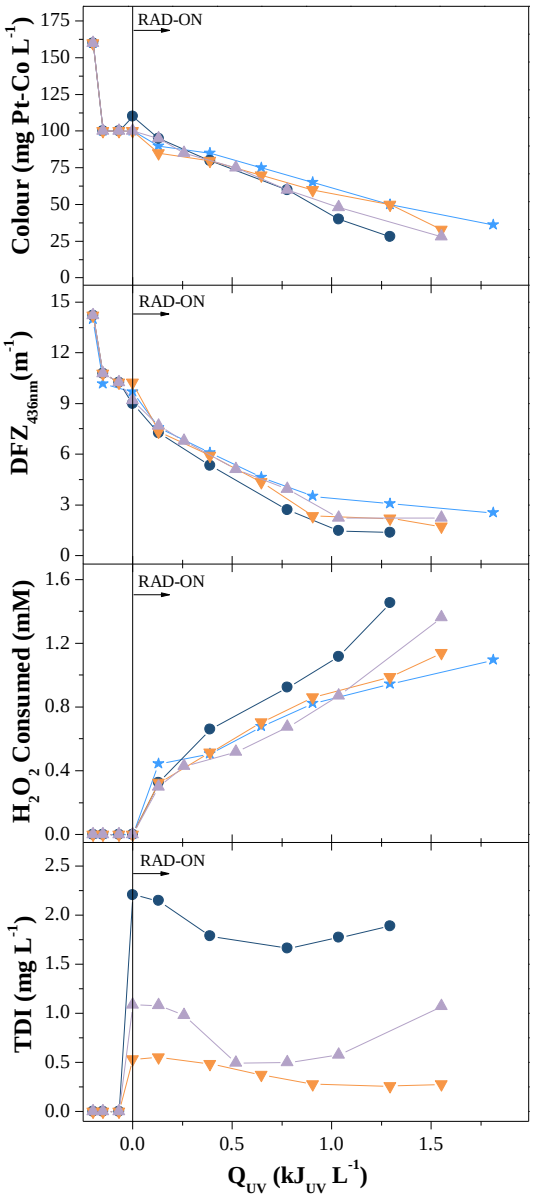

Figure 6.3. Decolourisation of the textile wastewater under UVC radiation using different iron concentrations. ● - $[Fe^{2+}]$ = 2 mg L^{-1}; ▲ - $[Fe^{2+}]$ = 1 mg L^{-1}; ▼ - $[Fe^{2+}]$ = 0.5 mg L^{-1}; ★ – without iron.

The decolourisation kinetics profiles show a very similar behaviour up to $Q_{UV} \approx 0.75$ kJ_{UV} L^{-1}, indicating that the photolysis of H_2O_2 is the predominant mechanism. For higher Q_{UV} values, a slight improvement in the decolourisation rate with an increase in the iron concentration is observed. This may be related to the breakdown of poorly photoactive iron-organic complexes due to •OH radicals generated from the photolysis of H_2O_2, and consequently more •OH radicals are generated from the H_2O_2 decomposition in the presence of ferrous iron as well as from the photoreduction of Fe(III)-hydroxy complexes.

6.3.3.2 Effect of solution temperature

Figure 6.4 shows the textile wastewater decolourisation profiles for different temperatures (15°C, 30°C, and 45ºC) resulting from: (a) the UVC/H_2O_2 system with the natural wastewater pH and acidic pH of 2.8, with a H_2O_2 dosage of 2.1 mM; and (b) the UVC/Fe^{2+}/H_2O_2 system with a pH value of 2.8, iron concentration of 2 mg Fe^{2+} L^{-1} and H_2O_2 dosage of 2.1 mM.

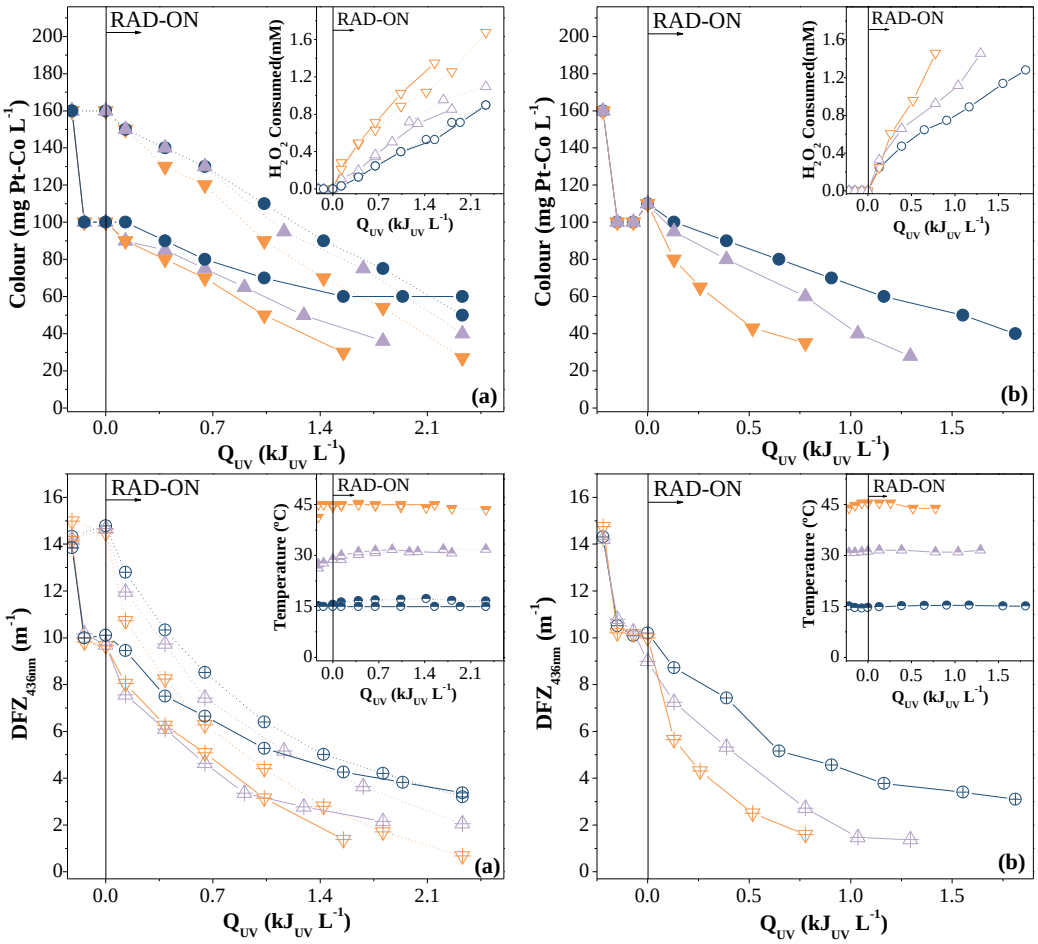

Figure 6.4. Textile wastewater decolourisation under UVC radiation at different temperatures. (a) UVC/H_2O_2 reactions; (b) UVC/Fe^{2+}/H_2O_2 reactions. Solid symbols – Colour on Pt-Co scale; open symbols – H_2O_2 consumed; cross symbols – Colour on DFZ_{436nm} scale; half painted symbols - Temperature. Continuous line – pH 2.8; dotted line – natural pH. ● ○ ⊕ ◓ – T=15ºC; ▲ △ ⟑ ◭ – T=30ºC; ▼ ▽ ⧩ ⧨ – T=45ºC.

An increase in temperature favours the decolourisation rates (Figure 6.4a and Table 6.3) of the textile wastewater using the UVC/H_2O_2 system, suggesting that the generation of •OH radicals through H_2O_2 photolysis is enhanced, i.e., the UV/H_2O_2 system is positively influenced by a temperature increase [40]. For the reactions at natural pH, although the decolourisation rate at 45ºC is 1.6 times higher than at 15ºC, the H_2O_2 consumption rate is almost 2.0 times higher at 45ºC; the same behaviour was observed at pH 2.8. This phenomenon can be explained by hydrogen peroxide decomposition into H_2O and O_2 (inactive species) and the formation of radicals with lower oxidation potential at high temperatures, and consequently the rate of decomposition of hydrogen peroxide can duplicate every time the temperature rises by 10ºC [41, 42].

Table 6.3. Operational conditions and pseudo-first-order kinetic constants for reaction under UVC radiation.

System	TDI[a]	T[b]	pH	Dosage of H_2O_2[c]	Kinetic parameters			
					Decolourisation[d]		H_2O_2 consumption	
					k[e]	R^2	k_H[f]	R^2
UVC/H_2O_2	-	30	2.8	2.1	0.57±0.08	0.991	0.56±0.09	0.919
UVC/Fe^{2+}/H_2O_2	0.5				0.7±0.2	0.974	0.7±0.3	0.916
	1				0.71±0.08	0.996	0.88±0.04	0.999
	2				1.0±0.1	0.993	1.0±0.2	0.979
UVC/H_2O_2	-	15	Natural	2.1	0.41±0.05	0.990	0.39±0.01	0.999
		30			0.6±0.1	0.970	0.59±0.07	0.994
		45			0.66±0.07	0.992	0.71±0.06	0.992
		15	2.8		0.35±0.04	0.992	0.36±0.03	0.995
		30			0.57±0.08	0.991	0.56±0.09	0.919
		45			0.8±0.2	0.980	0.9±0.2	0.981
UVC/Fe^{2+}/H_2O_2	2	15	2.8	2.1	0.54±0.04	0.993	0.7±0.1	0.986
		30			1.0±0.1	0.993	1.0±0.2	0.979
		45			1.6±0.3	0.990	1.87±0.05	0.999
UVC/H_2O_2	-	30	Natural	0.7	0.21±0.04	0.992	0.3±0.1	0.922
				1.3	0.43±0.05	0.994	0.53±0.05	0.990
				2.1	0.6±0.1	0.970	0.59±0.07	0.994
				4.2	1.3±0.3	0.970	0.8±0.1	0.985
				6.9	2.1±0.6	0.976	1.7±0.1	0.998
				10.0	2.2±0.4	0.969	3.0±0.2	0.994
UVC/Fe^{2+}/H_2O_2	2	30	2.8	0.7	0.69±0.09	0.995	0.41±0.05	0.993
				1.3	0.9±0.1	0.992	0.57±0.09	0.982
				2.1	1.0±0.1	0.993	1.0±0.2	0.979
				4.2	1.4±0.3	0.995	2.6±0.8	0.990
				6.9	1.9±0.1	0.996	5.6±0.9	0.987
				10.0	2.0±0.3	0.992	5.4±0.9	0.912

[a]Dissolved iron concentration (mg L^{-1}); [b]Liquid temperature (ºC); [c](mM H_2O_2); [d]Platinum-Cobalt method; [e]Pseudo-first-order kinetic constant (L kJ^{-1}); [f]H_2O_2 consumption rate (mmol kJ^{-1}).

Although the decolourisation rate for the UVC/H_2O_2 system is similar at neutral and acid pH values, the amount of UVC energy required to achieve the same decolourisation efficiency is higher under neutral pH conditions. This is mainly related to the marked contribution of the acidification procedure to the colour removal. It should be noted that at the end of the UVC/H_2O_2 assay performed at acid pH, the solution was neutralized using sodium hydroxide but the colour indicators (Pt-Co, DFZ_{436nm}) remained the same.

An increase in the temperature improved significantly the photo-Fenton decolourisation reaction rate (Figure 6.4b and Table 6.3), achieving a wastewater suitable for discharge to water bodies in accordance with the legislation [28], after 0.13 kJ_{UV} L^{-1} energy uptake and 0.3 mM H_2O_2 consumption. It has been previously reported that the molar fraction of the $FeOH^{2+}$ species increases with temperature [43] and therefore the beneficial effect of temperature on the reaction rates can be associated with two main factors: i) the presence of different amounts of photoactive species ($FeOH^{2+}$); and ii) higher levels of Fe^{3+} reduction through thermal Fenton reactions [10], which may also be associated with the fact that the H_2O_2 consumption rate in the photo-Fenton reactions was higher than in the UVC/H_2O_2 reactions.

6.3.3.3 Effect of H_2O_2 concentration

Figure 6.5a shows the decolourisation kinetics profiles for the textile wastewater using the UVC/H_2O_2 system at different initial hydrogen peroxide concentrations (0.7, 1.3, 2.1, 4.2, 6.9 and 10 mM) at the natural wastewater pH. The decolourisation rates increase significantly with the availability of hydrogen peroxide, being ten times higher for the initial H_2O_2 dose of 6.9 mM when compared with 0.7 mM. For H_2O_2 dosages higher than 6.9 mM the reaction rate remains almost unchanged.

As reported by other authors [8, 24, 44], the presence of excess hydrogen peroxide can lower the decolourisation efficiency, which occurs mainly because the $^{\bullet}OH$ radicals reach equilibrium with the concentration of hydrogen peroxide. Above the equilibrium concentration, an increase in the hydrogen peroxide does not enhance the free radical concentration [8]. In addition, the results of other studies also suggest that H_2O_2 itself can act as an effective $^{\bullet}OH$ radical scavenger at concentrations that are specific for each pollutant, and the presence of excess H_2O_2 can lower the treatment efficiency of AOPs [45].

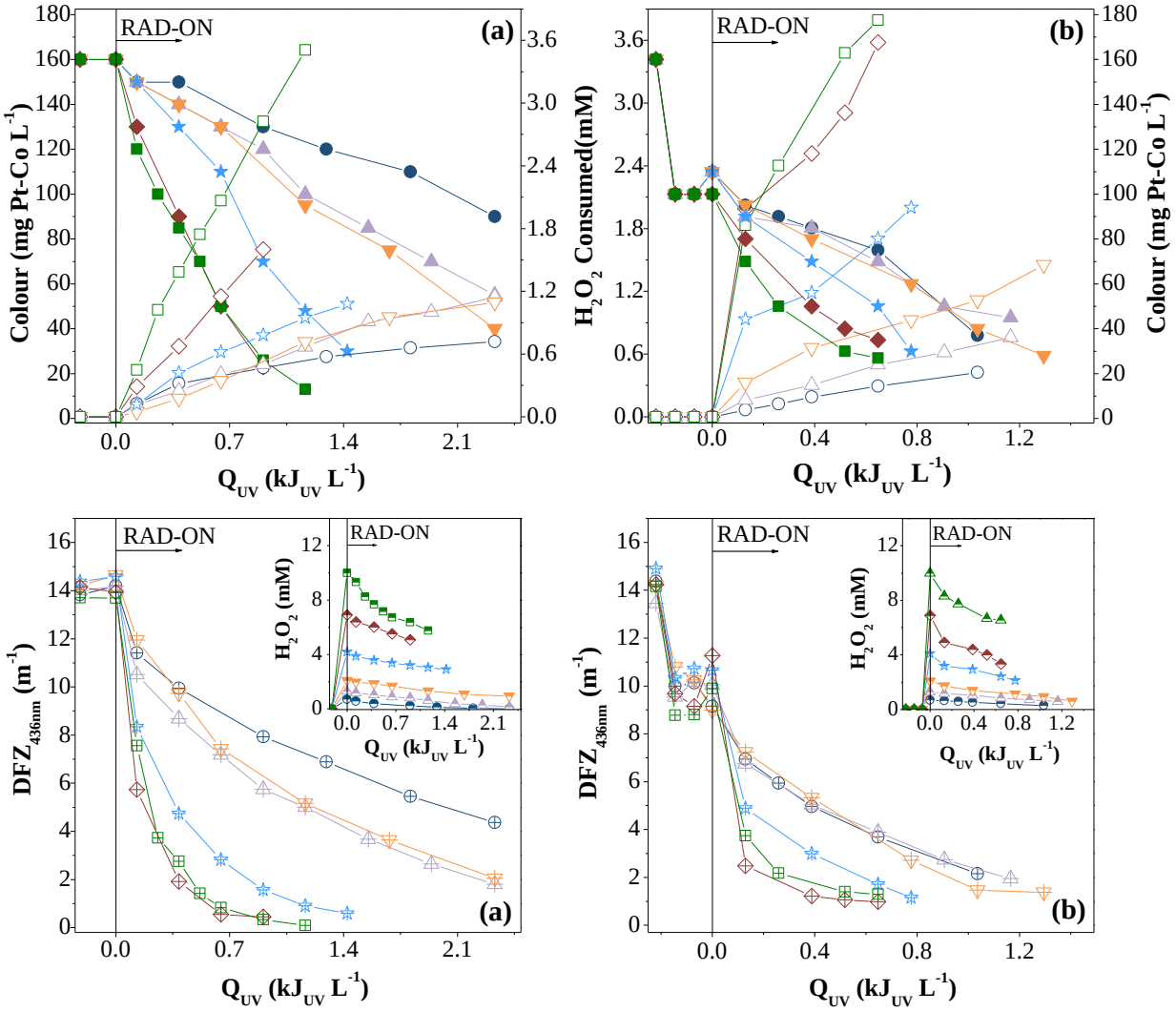

Figure 6.5. Textile wastewater decolourisation under UVC radiation at different H_2O_2 dosage. (a) UVC/H_2O_2 reactions; (b) UVC/ Fe^{2+}/H_2O_2 reactions. Solid symbols – Colour on Pt-Co scale; open symbols – H_2O_2 consumed; cross symbols – Colour on DFZ_{436nm} scale; half painted symbols – H_2O_2 concentration. ● ○ ⊕ ◓ – [H_2O_2] = 0.7 mM; ▲ △ ⧋ ▲ – [H_2O_2] = 1.3 mM; ▼ ▽ ⧩ ▽ – [H_2O_2] = 2.1 mM; ★ ☆ ☆ ★ – [H_2O_2] = 4.2 mM; ◆ ◇ ⊕ ◆ - [H_2O_2] = 6.9 mM; ■ □ ⊞ ◨ – [H_2O_2] = 10.0 mM.

In order to evaluate the role of photolysis and the effect of the applied peroxide dosage on the decolourisation, control experiments in the absence of UVC radiation or H_2O_2, at natural pH and pH 2.8, were carried out separately (Figure 6.6). Both systems showed a negligible decolourisation rate, which suggests that the wastewater studied is photolytically stable under UVC radiation and the oxidizing potential of H_2O_2 is not sufficient to decolorise the wastewater. As expected, acidification to pH 2.8 leads to a colour reduction. However, at the end of the assays the solutions were neutralized using sodium hydroxide and the colour indicators (Pt-Co, DFZ_{436nm}) provided values similar to those of the raw wastewater.

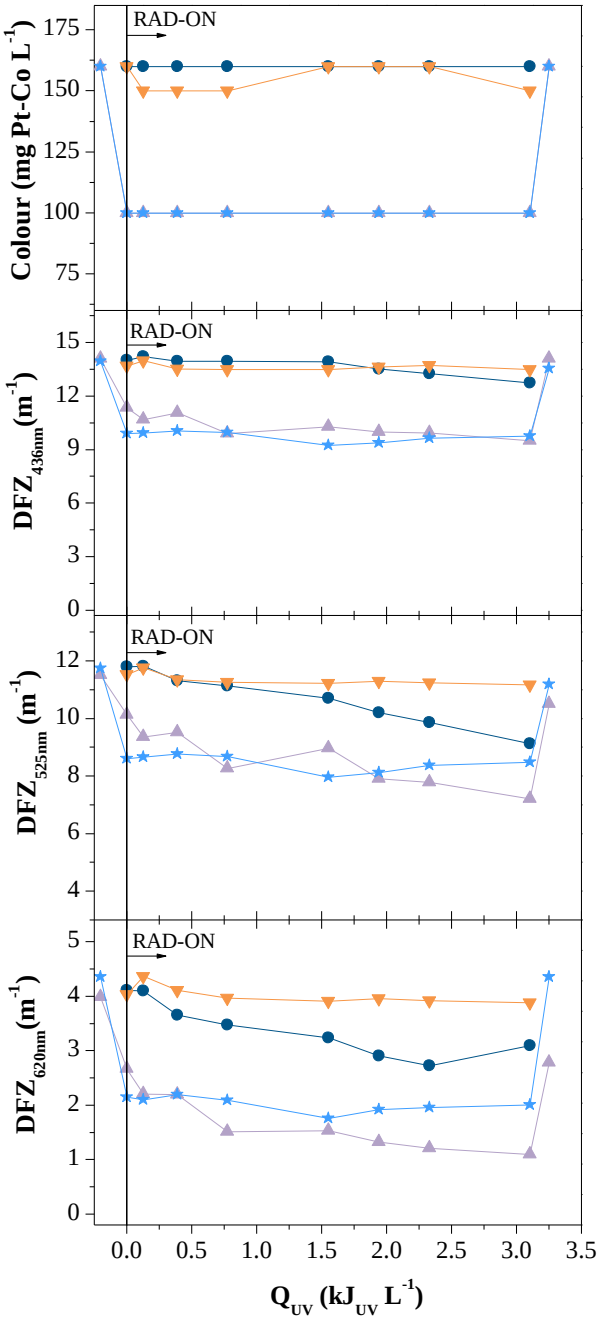

Figure 6.6. Decolourisation of the textile wastewater using UVC and H_2O_2 processes. ● – UVC radiation at natural pH; ▲ – UVC radiation at pH 2.8; ▼ – H_2O_2 process at natural pH and $[H_2O_2]$ = 6.9 mM; ★ – H_2O_2 process at pH 2.8 and $[H_2O_2]$ = 6.9 mM.

Figure 6.5b shows a significant increase in the decolourisation rate with the availability of H_2O_2 using the photo-Fenton reaction with UVC radiation under acidic conditions (pH = 2.8). The decolourisation rate using 6.9 mM of H_2O_2 is almost three times higher than that obtained with 0.7 mM. Although the decolourisation rate increases significantly with the H_2O_2 dosage, higher amounts of H_2O_2 are consumed. Also, higher residual H_2O_2 concentrations are obtained at the end of the experiments when using high

H_2O_2 dosages, a subsequent system being necessary to achieve the complete decomposition of the H_2O_2 present in the wastewater before its discharge to the aquatic system.

The results for pseudo-first-order kinetics constant versus H_2O_2 initial concentration, for both systems studied, are summarized in Figure 6.7. It can be observed that in the interval between 0.7 mM and 6.9 mM of H_2O_2 the initial H_2O_2 concentration had a greater effect in the UVC/H_2O_2 system than in the photo-Fenton process.

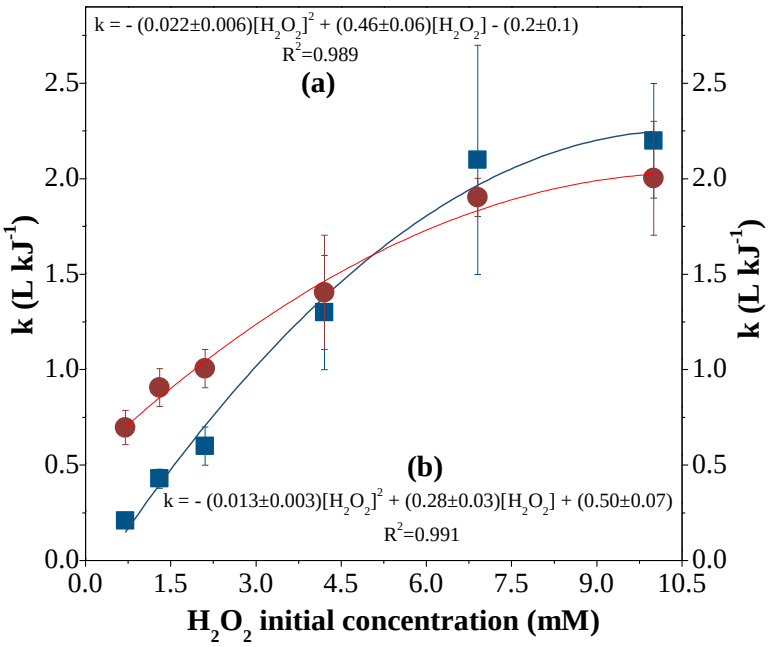

Figure 6.7. The pseudo-first-order kinetic constants vs. hydrogen peroxide initial concentration for (a) UVC/H_2O_2 reactions (natural wastewater pH and T = 30ºC) and for (b) UVC/Fe^{2+}/H_2O_2 reactions (pH = 2.8; T = 30ºC and [Fe^{2+}] = 2 mg L^{-1}). ■ – UVC/H_2O_2 reactions and ● - UVC/ Fe^{2+}/H_2O_2 reactions.

6.3.4 UVA-Visible decolourisation reactions

As demonstrated above (Figure 6.1), the photo-Fenton reaction exhibited a low performance under UVA-Visible radiation when compared with the reaction under UVC radiation. In order to improve the efficiency of the photo-Fenton reaction under UVA-Visible radiation, which enables the use of natural solar light, additional experiments were performed using ferrioxalate complexes (Table 6.4).

Table 6.4. Operational conditions and pseudo-first-order kinetic constants for reactions under UVA-Visible radiation.

System	TDI[a]	Molar Ratio (Fe:LIG)	T[b]	pH	Dosage of H_2O_2[c]	Kinetic parameters			
						Decolourisation[d]		H_2O_2 consumption	
						k[e]	R^2	k_H[f]	R^2
UVA-Vis/Fe^{2+}/H_2O_2	10	-	30	2. 8	2.1	0.21±0.09	0.966	0.32±0.04	0.994
UVA-Vis/Fe^{3+}/H_2O_2/Oxalic acid		1:3			3.1	1.4±0.3	0.994	1.0±0.7	0.990
UVA-Vis/Fe^{3+}/H_2O_2/EDDS		1:1			2.1	0.8±0.2	0.990	0.7±0.1	0.989
UVA-Vis/Fe^{3+}/H_2O_2/Citric acid		1:1			3.1	0.7±0.3	0.914	0.9±0.2	0.995
UVA-Vis/Fe^{3+}/H_2O_2/Oxalic acid	10	1:3	30	2.8	3.1	1.4±0.3	0.994	1.0±0.7	0.990
		1:6			5.1	0.7±0.2	0.966	1.6±0.5	0.990
		1:9			5.1	0.6±0.1	0.991	1.7±0.3	0.990
UVA-Vis/Fe^{3+}/H_2O_2/Oxalic acid	2	1:3	30	2.8	2.1	0.3±0.1	0.935	0.24±0.08	0.990
	6				3.1	1.3±0.1	0.998	0.7±0.3	0.926
	10				3.1	1.4±0.3	0.994	1.0±0.7	0.990
	20				5.1	1.2±0.2	0.995	2.4±0.9	0.990
	40				9.8	0.9±0.4	0.899	4.4±0.4	0.997
UVA-Vis/Fe^{3+}/H_2O_2/Oxalic acid	6	1:3	30	2.8	3.1	1.3±0.2	0.997	0.8±0.3	0.945
				3.5	3.1	1.3±0.5	0.980	1.1±0.4	0.940
				4.0	3.1	0.8±0.1	0.993	0.9±0.4	0.899
				4.5	3.1	0.4±0.1	0.900	1.0±0.4	0.900
				5.0	3.1	0.5±0.2	0.900	1.0±0.5	0.920
				5.5	3.1	0.16±0.07	0.950	0.7±0.2	0.958
		1:6		5.5	3.1	0.16±0.08	0.901	0.7±0.1	0.975

[a]Dissolved iron concentration (mg L^{-1}); [b]Liquid phase temperature (ºC); [c](mM H_2O_2); [d]Platinum-Cobalt method; [e]Pseudo-first-order kinetic constant (L kJ^{-1}); [f]H_2O_2 consumption rate (mmol kJ^{-1}); [g]average pH.

6.3.4.1 Effect of iron concentration

Figure 6.8 shows the effect of the iron concentration (2, 6, 10, 20 and 40 mg Fe^{3+} L^{-1}) on the decolourisation of the bio-treated textile wastewater using the UVA-Vis/Fe^{3+}/H_2O_2/Oxalic acid system. It can be observed that the addition of oxalic acid, as an organic ligand of ferric ions, enhanced significantly the photo-Fenton reaction under UVA-Visible radiation, for an iron concentration in the range of 6 to 10 mg Fe^{3+} L^{-1}. The reaction with 2 mg Fe^{3+} L^{-1} clearly did not achieved significant decolourisation, which can be explained by two possible facts: i) at this concentration the iron available was not able to absorb all available UV-visible photons, probably hampered by the presence of other light-absorbing species in solution, namely the dyes [13], or ii) the short lifetime of ferrioxalate complexes, which was not sufficient to destroy all of the dissolved organic pollutants responsible for the formation of unwanted iron complexes with low photoactivity.

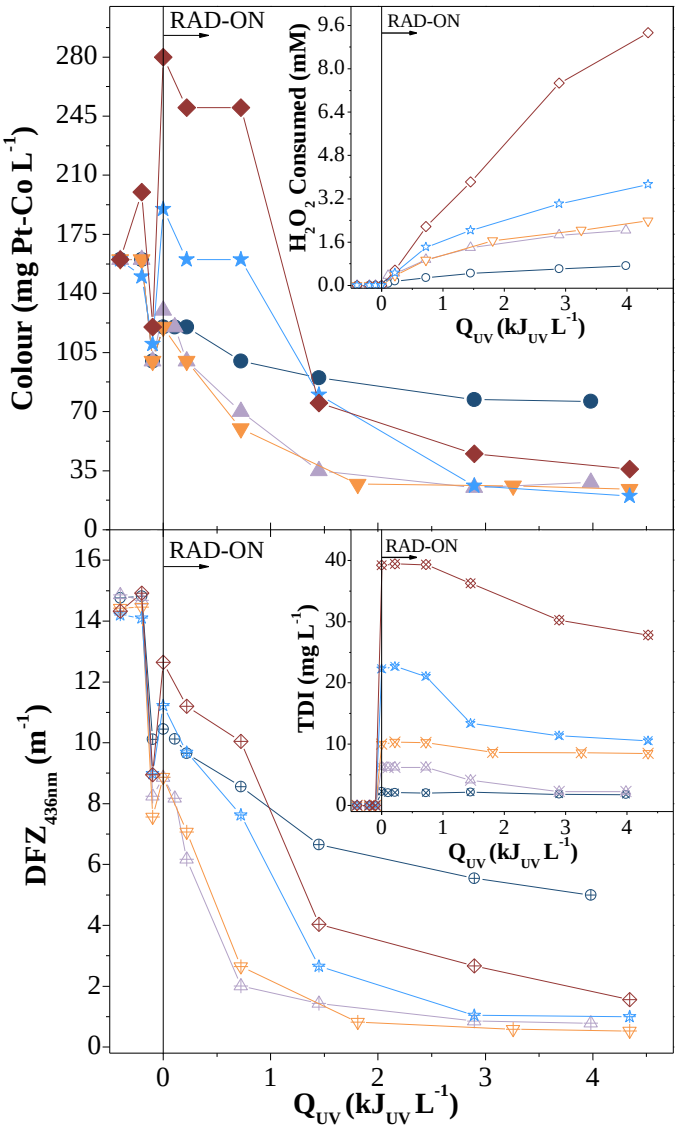

Figure 6.8. Decolourisation of the textile wastewater using UVA-Vis/Fe^{3+}/H_2O_2/Oxalic Acid reaction with different iron concentrations. Solid symbols – Colour on Pt-Co scale; open symbols – H_2O_2 consumed; cross symbols – Colour on DFZ_{436nm} scale; "x" within symbols - TDI concentration. ● ○ ⊕ ⊗ – [Fe^{2+}] = 2 mg L^{-1}; ▲ △ ⟁ ⟁ – [Fe^{2+}] = 6 mg L^{-1}; ▼ ▽ ▽ ▽- [Fe^{2+}] = 10 mg L^{-1}; ★ ☆ ☆ ☆- [Fe^{2+}] = 20 mg L^{-1}; ◆ ◇ ⟐ ⟐ - [Fe^{2+}] = 40 mg L^{-1}.

For the two highest iron concentrations tested, 20 and 40 mg Fe^{3+} L^{-1}, a large increase in the colour intensity was observed after the addition of oxalic acid and ferric ions, which indicates that ferrioxalate complexes affect significantly the colour results obtained by the Pt-Co method. After the total decarboxylation of ferrioxalate complexes, the decolourisation efficiency achieved for the two highest iron concentrations was similar to that obtained for 6 and 10 mg Fe^{3+} L^{-1} (Figure 6.9).

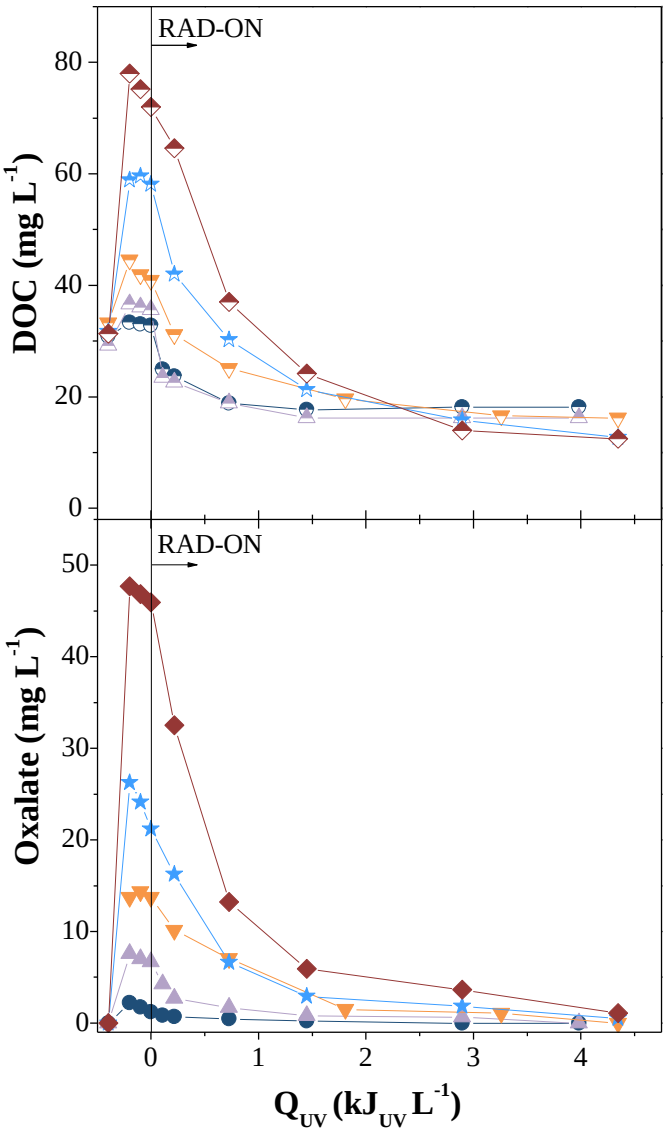

Figure 6.9. Mineralisation of the textile wastewater using UVA-Vis/Fe^{3+}/H_2O_2/Oxalic Acid reaction with different iron concentrations. Solid symbols – DOC; half-painted symbols - Oxalate. ● ◓ – [Fe^{2+}] = 2 mg L^{-1}; ▲ △ – [Fe^{2+}] = 6 mg L^{-1}; ▼ ▽ - [Fe^{2+}] = 10 mg L^{-1}; ★ ☆ - [Fe^{2+}] = 20 mg L^{-1}; ◆ ◇ - [Fe^{2+}] = 40 mg L^{-1}.

Higher iron concentrations require higher amounts of oxalic acid to be added in order to maintain the same iron/oxalate molar ratio. The added oxalate can act as an additional organic carbon source, competing with the target pollutant for hydroxyl radicals, and increasing the H_2O_2 consumption, which may be related to the increase in H_2O_2 consumption by a factor of 2.4 when the total dissolved iron was increased from 20 to 40 mg L^{-1}.

The enhancement of the photo-Fenton process was also assessed using citrate acid and EDDS, as ferric-organic ligands, with an iron/organic ligand molar ratio of 1:1, which corresponds to the most stable and strong complexes for these ligands [46-48]. The photo-Fenton reaction mediated by ferric-organic ligands performs much better than the conventional photo-Fenton reaction, and the Fe(III)-Oxalic system performs slightly better than Fe(III)-Citrate and Fe(III)-EDDS (Figure 6.10). Ferric ions form stable and

strong complexes with organic ligands, such as oxalic acid, EDDS and citric acid, avoiding the undesired interactions with other organic and inorganic species present in the wastewater while at the same time providing a quicker pathway for ferric iron regeneration in the presence of UV-Visible light [49-51].

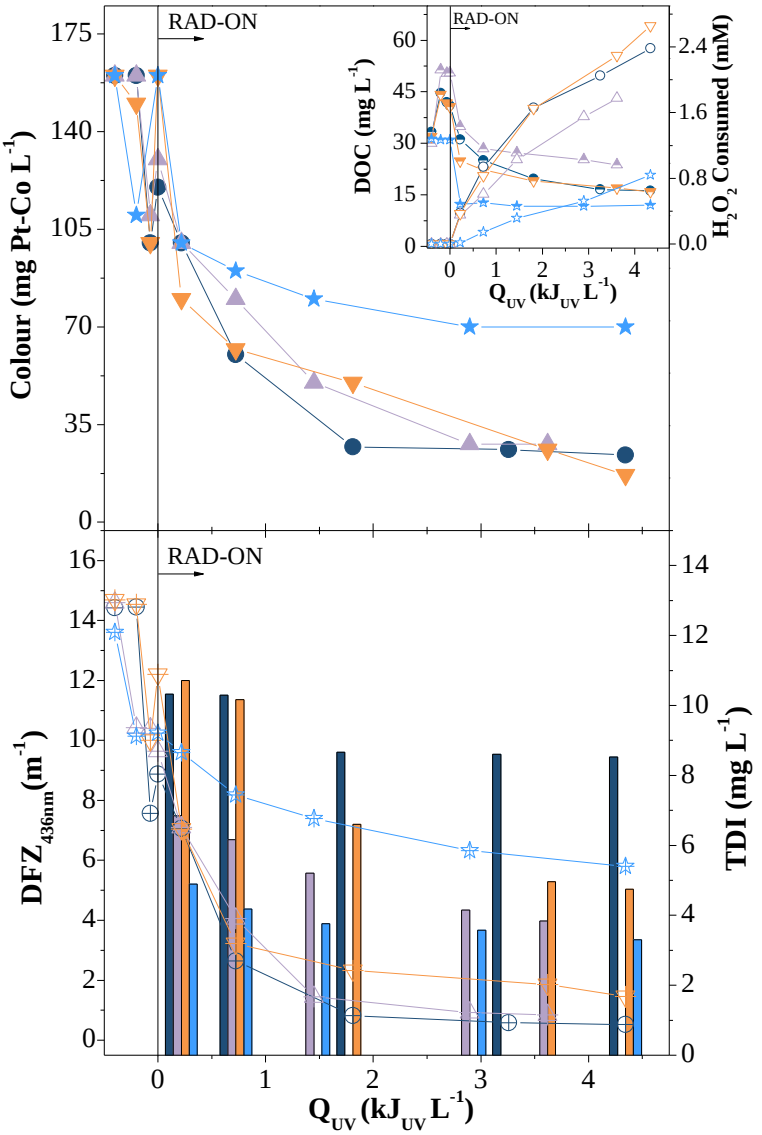

Figure 6.10. Decolourisation of the textile wastewater under UVA-Visible radiation with different iron ligands. Solid symbols – Colour on Pt-Co scale; open symbols – H_2O_2 consumed; cross symbols – Colour on DFZ_{436nm} scale; half-painted symbols – DOC; columns – TDI concentration. ★☆✲✲ – UVA-Vis/Fe^{2+}/H_2O_2; ●○⊕◓ – UVA-Vis/Fe^{3+}/H_2O_2/Oxalic Acid; ▲△△▲ – UVA-Vis/Fe^{3+}/H_2O_2/EDDS; ▼▽▽▼ – UVA-Vis/Fe^{3+}/H_2O_2/Citric Acid.

It is important to note that the discharge limit for total iron according to Portuguese legislation is 2 mg Fe L^{-1} [27]. Considering this regulation, in order to lower the iron concentration to within the legal limit, a subsequent step for iron precipitation has to be considered. However, when the German legislation [28] is considered, the additional precipitation step is not necessary.

6.3.4.2 Effect of iron/oxalate molar ratio

Reports in the literature state that the most stable ferric-oxalate complex results from the binding of three oxalate ions with one ferric ion [47]. However, due to the short lifetime of ferrioxalate complexes, as observed in the previous assays with different iron concentrations, higher amounts of oxalic acid may be required to avoid the formation of undesired ferric-organic complexes with low photoactivity [52]. Figure 6.11 shows that the increase in the stoichiometric molar ratio did not have a positive effect on the textile wastewater decolourisation. However, an increase in the oxalic acid concentration did affect significantly the colour reduction. For both decolourisation monitoring methods, the photo-Fenton reaction using an iron/oxalate ratio molar of 1:3 performs better compared with using ratios of 1:6 and 1:9.

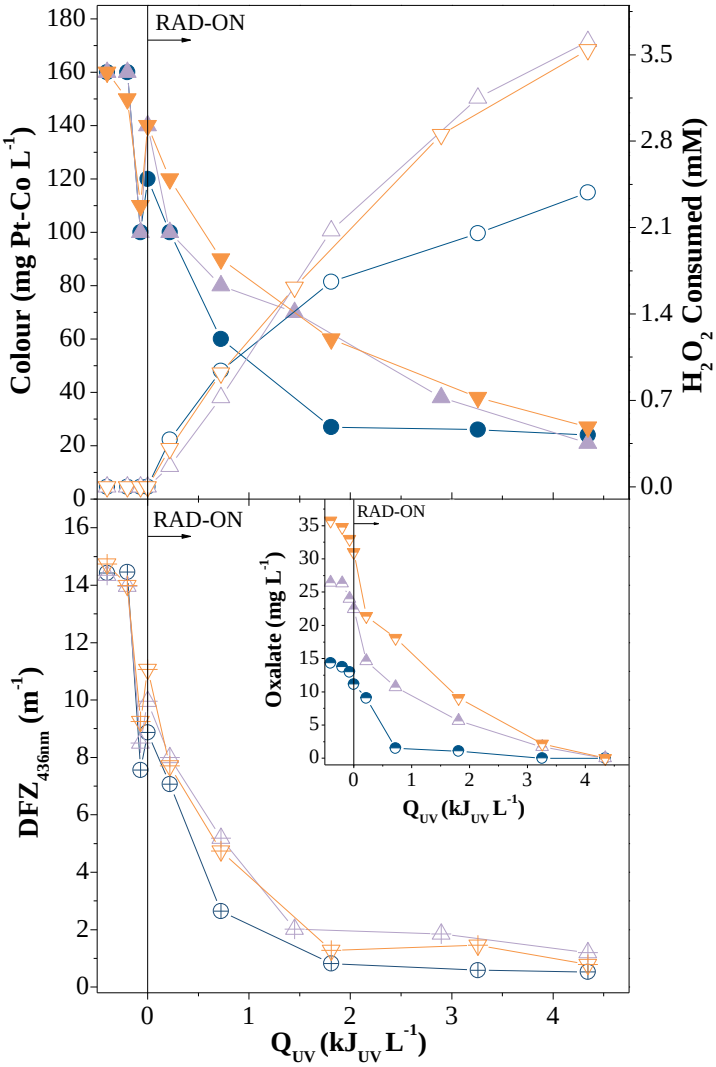

Figure 6.11. Decolourisation of the textile wastewater under UVA-Visible radiation with different iron/oxalate stoichiometry molar ratios. Solid symbols – Colour on Pt-Co scale; open symbols – H_2O_2 consumed; cross symbols – Colour on DFZ_{436nm} scale; half painted symbols – Oxalate. ● ○ ⊕ ◓ – iron/oxalate molar ratio of 1:3; ▲ △ ⊿ ◭ – iron/oxalate molar ratio of 1:6; ▼ ▽ ▽ ▼ - iron/oxalate molar ratio of 1:9.

6.3.4.3 *Effect of solution pH*

The high alkalinity of most textile wastewaters constitutes a limitation for the application of the photo-Fenton reaction, since pH is one of the critical operating parameters in this process. Not only does the consumption of reagents needed for acidification and subsequent neutralisation generate additional costs, but the salt load of the treated wastewater also increases [10]. In this regard, in order to assess the performance of the UVA-Vis/Fe^{3+}/H_2O_2/Oxalic acid reaction at higher pH values, experiments using 6 mg Fe^{3+} L^{-1}, a temperature of 30ºC, an iron/oxalate molar ratio of 1:3 and different initial pH values (2.8, 3.5, 4.0, 4.5, 5.0 and 5.5) were performed (Figure 6.12). Although the UVA-Vis/Fe^{3+}/H_2O_2/Oxalic acid reaction can be performed at higher pH values, a significant decrease in the decolourisation efficiency is observed. This phenomenon can be attributed to two main factors: i) the low photoactivity of the ferrioxalate complexes at near neutral pH values [53]; and ii) the short lifetime of ferrioxalate complexes leading to a fast iron precipitation.

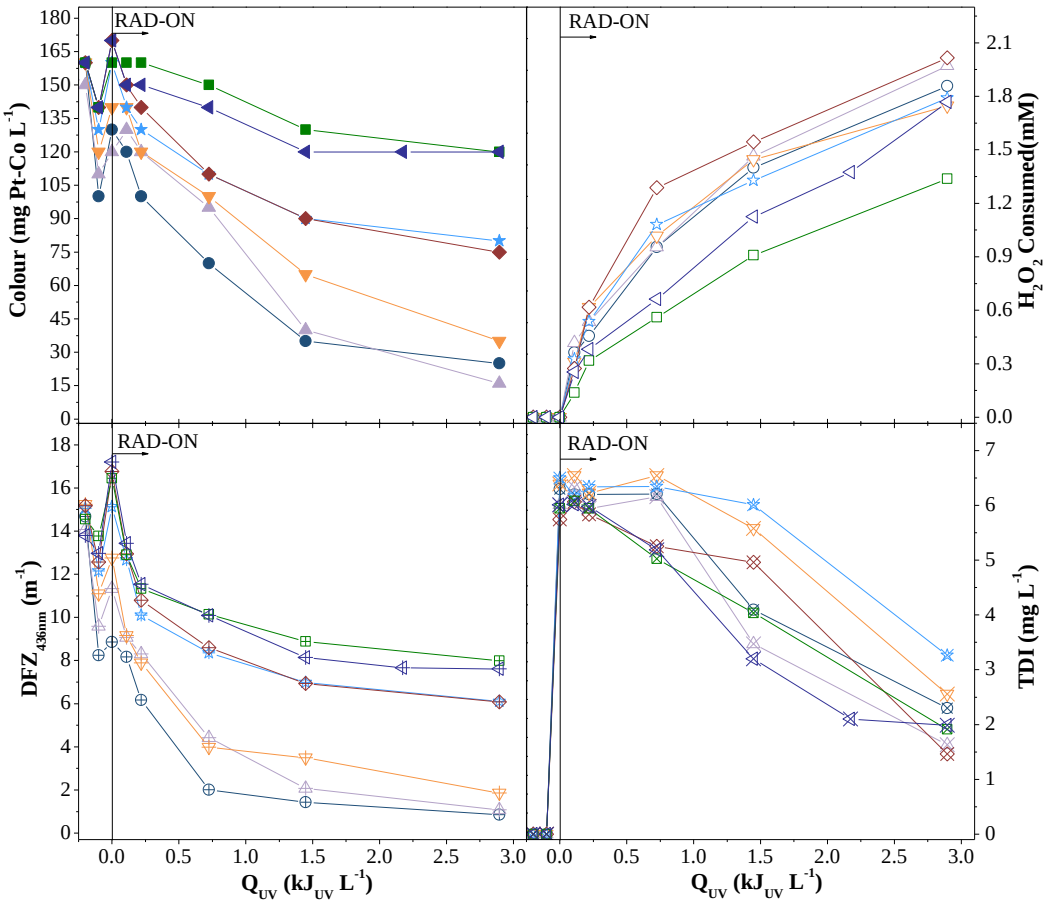

Figure 6.12. Decolourisation of the textile wastewater under UVA-Visible radiation with different initial pH values. Solid symbols – Colour on Pt-Co scale; open symbols – H_2O_2 consumed; cross symbols – Colour on DFZ_{436nm} scale; – "x" within symbols - TDI concentration. ● ○ ⊕ ⊗ – pH 2.8; ▲ △ ⟑ ⟑ – pH 3.5; ▼ ▽ ⩛ ⩛ – pH 4.0; ★ ☆ ☆ ☆ – pH 4.5; ◆ ◇ ⊕ ⊕ – pH 5.0; ■ □ ⊞ ⊠ – pH 5.5; ◀ ◁ ◀ ◀ – pH 5.5 and iron/oxalate molar ratio of 1:6.

The formation of stable iron complexes, with low photoactivity, between iron (III) and compounds present in the textile wastewater (e.g., dyes and textile auxiliaries), favoured by alkaline conditions, could be associated with the decrease in decolourisation efficiency at higher pH. However, additional assays without oxalate were carried out and the precipitation of iron at alkaline pH was observed (data not shown), demonstrating that stable iron complexes do not form under these conditions.

The iron speciation diagrams in Figure 6.13 demonstrate that the presence of oxalic acid extends the pH range available for the process application, since the precipitation of $Fe(OH)_3$ (s) begins at pH=4.8 for an initial iron/oxalate molar ratio of 1:3 and at pH 5.6 for an initial iron/oxalate molar ratio 1:6. However, on increasing the oxalic acid concentration, the decolourisation efficiency increased only slightly and higher amounts of oxalic acid could be required, making the process economically unfeasible.

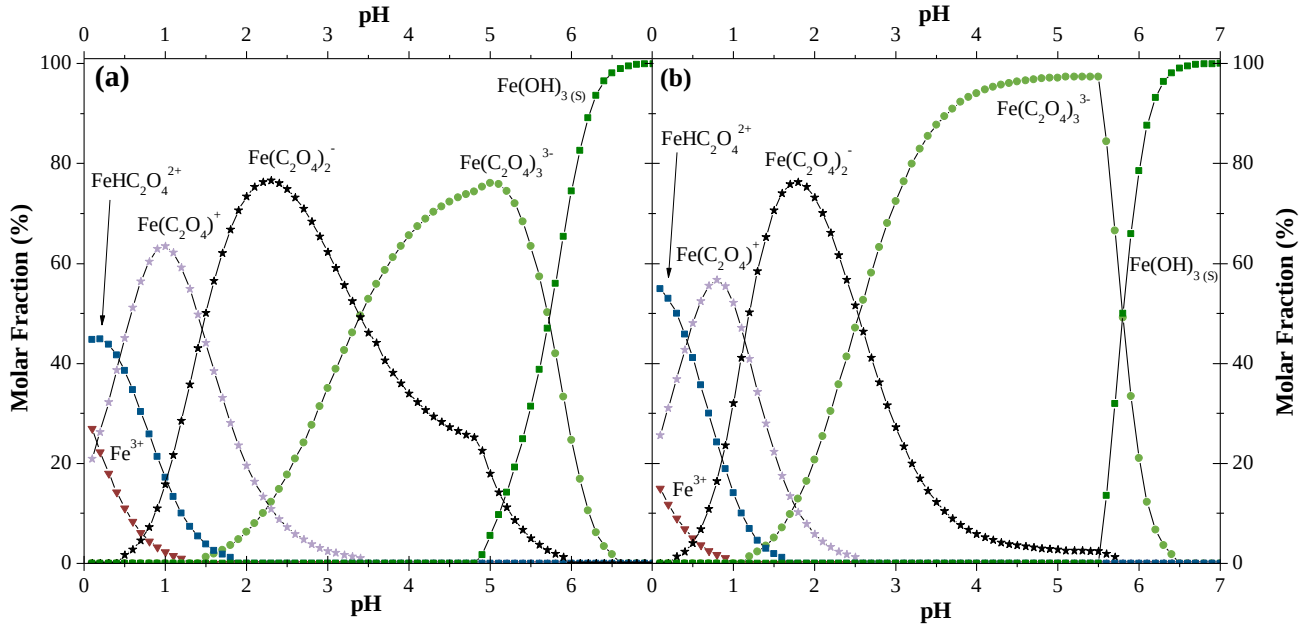

Figure 6.13. Speciation diagrams for ferric complexes as a function of pH for a solution containing $Fe^{3+}/SO_4^{2-}/Cl^-$ /Oxalic acid. Ionic strength = 0.03 M; T = 30ºC; $[Fe^{3+}]$ = 1.07×10^{-1} mM (6 mg L^{-1}); $[SO_4^{2-}]$ = 1.26 mM; $[Cl^-]$ = 17.3 mM; a) [Oxalic acid] = 3.22×10^{-1} mM and, b) [Oxalic acid] = 6.45×10^{-1} mM.

6.3.5 Assessment of treatment costs

An assessment of the costs associated with the required treatment to achieve a wastewater colour values of 7 m^{-1} (DFZ_{436nm}), 5 m^{-1} (DFZ_{525nm}) and 3 m^{-1} (DFZ_{620nm}), according to the German regulations for discharge into water bodies [28], which is also in agreement with Portuguese legislation (uncoloured at 1:20 dilution), was carried out.

In the economic assessment of the photocatalytic plant the treatment of a textile wastewater obtained from a biological pre-oxidation process was considered, applying the following operating conditions: (a) initial pH = 2.8, T = 30ºC, [H_2O_2] = 2.1 mM, UVC radiation; (b) natural pH, T = 30ºC, [H_2O_2] = 2.1 mM, UVC radiation; (c) initial pH = 2.8, T = 30ºC, [H_2O_2] = 2.1 mM, [Fe^{2+}] = 2 mg L^{-1}, UVC radiation; (d) initial pH = 2.8, T = 30ºC, [H_2O_2] = 2.1 mM, [Fe^{2+}] = 10 mg L^{-1}, UVA-Visible radiation; (e) initial pH = 2.8, T = 30ºC, [H_2O_2] = 2.1 mM, [Fe^{2+}] = 6 mg L^{-1}, iron/oxalate molar ratio of 1:3, UVA-Visible radiation; and (f) initial pH = 5.0, T = 30ºC, [H_2O_2] = 3.1 mM, [Fe^{2+}] = 6 mg L^{-1}, iron/oxalate molar ratio of 1:3, UVA-Visible radiation.

Table 6.5 shows the main process operation variables required for the economical assessment, considering the decolourisation of bio-treated textile wastewater. Values for yearly UV radiation and accumulated UV energy were obtained considering fixed solar energy collectors oriented southward (northern hemisphere) in order to capture the maximum amount of global UV energy, and tilted from the horizontal to a degree equal to the latitude (city of Porto: 41º) (Figure 6.14).

Table 6.5. Operation data for the treatment of 30,240 m^3 per day of textile wastewater.

Parameter	Values
Daily flow – Q_d (m^3 day^{-1})	30,240
Yearly volume - V_y (m^3)	11,037,600
Yearly average global UV irradiation – I_m[a] (W m^{-2})	21.2
Total yearly hours of insolation – t_{ins}[a] (h)	2547
Yearly accumulated UV energy – E_y[b] (kJ_{UV} m^{-2})	194,479
Lamp, Ballast and accessories[c] – unit cost (€)	1,838
Lamp reactor – unit cost (€)	500
Electric energy – cost (€ kWh^{-1})	0.10
H_2SO_4 98% - cost[d] (€ ton^{-1})	180
NaOH 30% - cost[d] (€ ton^{-1})	270
Ferrous sulphate ($FeSO_4$) – cost[d] (€ ton^{-1})	290
Ferric chloride ($FeCl_3$) – cost[d] (€ ton^{-1})	350
Hydrogen peroxide (H_2O_2) 50% – cost[d] (€ ton^{-1})	450
Oxalic acid ($H_2C_2O_4$) – cost[d] (€ ton^{-1})	2,000

[a]Values obtained from the integration of the yearly UV radiation data from April 2014 to February 2015, using 4 W m^{-2} as the integration limit; [b]Accumulated UV energy from April 2014 to February 2015 ($E_y = 3.6 \times I_m \times t_{ins}$); [c]UV-Lamps with 12 kW and 1.8 kW of UVC radiation flow and 20,000 hours of total operation; [d]Average prices in 2015.

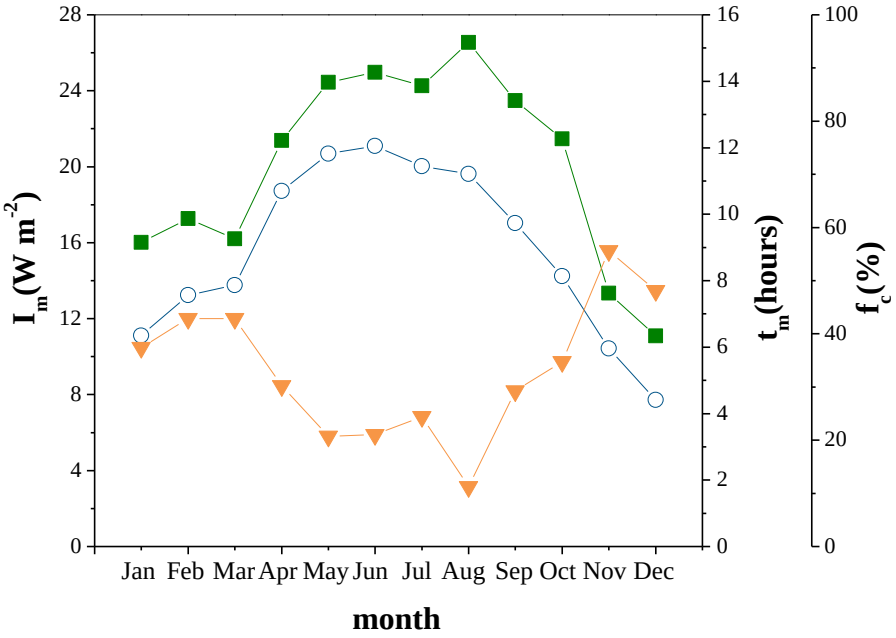

Figure 6.14. Average global UV irradiance. ■ - I_m, insolation, ○ - t_m and 'cloud factor', ▼ - f_c for global UV irradiance from March 2014 to February 2015, Porto, Portugal.

Total collectors area (A_{CPC}) needed for the treatment of 30,240 m^3 of bio-treated textile wastewater per day was calculated based on Eq. (6.1) [5]:

$$A_{CPC} = \frac{Q_{UV} \times V_y}{I_m \times t_{ins}} \tag{6.1}$$

were Q_{UV} is the accumulated UV energy required for the treatment, Vy is the yearly volume of textile wastewater, I_m is the yearly average global UV radiation power and t_{ins} is the total yearly hours of insolation.

Table 6.6 shows the annual costs for two radiation sources: UVA-Visible radiation (solar light) and UVC radiation (artificial light-lamps). Furthermore, the treatment costs for the systems using iron (UVC radiation) and oxalic acid (UVA-Visible radiation) at near neutral or acidic pH were also assessed. Table 6.6 shows that for the UVC/H_2O_2 system the treatment costs are lower at natural pH than at acidic pH (conditions (a) and (b)), which is mainly associated with a substantial reduction in the expenses related to consumables (acids and bases) (0.131 € m^{-3}), while the increase in capital expenditure is not so expressive (0.010 € m^{-3}) (Figure 6.15).

Table 6.6. Yearly cost associated to pre-treated real textile wastewater treatment under UVA-Visible radiation (using CPC technology) and under UVC radiation (using lamps) considering different operation conditions.

Description of costs	Under UVC radiation			Under UVA-Visible radiation		
	UVC/H_2O_2		$UVC/Fe^{2+}/H_2O_2$	$UVA\text{-}Vis/Fe^{2+}/H_2O_2$	$UVA\text{-}Vis/Fe^{3+}/H_2O_2$/Oxalic acid	
	Acid pH[a]	Basic pH[b]	Acid pH[c]	Acid pH[d]	Acid pH[e]	pH 5.0[f]
Direct Cost:						
CPCs area (m^2)	-	-	-	164,362	12,327	82,181
Total collector cost	-	-	-	21,154,148.73 €	1,586,561.15 €	10,577,074.37 €
Lamps number	222	398	133	-	-	-
Lamp, ballast and accessories	408,036.00 €	731,524.00 €	244,454.00 €	-	-	-
Reactor cost	111,000.00 €	199,000.00 €	66,500.00 €	-	-	-
Piping and tanks[g]	126,009.38 €	226,735.07 €	75,597.84 €	1,692,331.90 €	126,924.89 €	846,165.95 €
Auxiliary equipment and controls[h]	157,511.73 €	283,418.84 €	94,497.30 €	2,115,414.87 €	158,656.12 €	1,057,707.44 €
Others[i]	236,267.59 €	425,128.27 €	141,745.94 €	3,173,122.31 €	237,984.17 €	1,586,561.15 €
Total Direct Cost (TDC)	**1,038,824.70 €**	**1,865,806.18 €**	**622,795.08 €**	**28,135,017.81 €**	**2,110,126.34 €**	**14,067,508.91 €**
Indirect Cost:						
Contingencies[j]	124,658.96 €	223,896.74 €	74,735.41 €	3,376,202.14 €	253,215.16 €	1,688,101.07 €
Spare parts[k]	10,388.25 €	18,658.06 €	6,227.95 €	281,350.18 €	21,101.26 €	140,675.09 €
Total Capital Required (TCR)	**1,173,871.91 €**	**2,108,360.99 €**	**703,758.44 €**	**31,792,570.13 €**	**2,384,442.76 €**	**15,896,285.07 €**
Yearly Cost:						
Capital[l]	140,864.63 €	253,003.32 €	84,451.01 €	3,815,108.42 €	286,133.13 €	1,907,554.21 €
Consumables	2,090,177.36 €	637,077.78 €	2,243,264.02 €	2,835,817.97 €	8,356,553.73 €	7,268,828.75 €
Operation and maintenance	108,000.00 €	108,000.00 €	108,000.00 €	36,000.00 €	36,000.00 €	36,000.00 €
Electricity	262,537.20 €	470,674.80 €	157,285.80 €	-	-	-
Lamp replacement	160,439.40 €	287,634.60 €	96,119.10 €	-	-	-
Labour cost of replacement	5,250.74 €	9,413.50 €	3,145.72 €	-	-	-
Total Yearly Cost (TYC)	**2,767,269.33 €**	**1,765,803.99 €**	**2,692.265.65 €**	**6,686,926.38 €**	**8,678,686.87 €**	**9,212,382.96 €**
Unit Cost (UC)	**0.25 € m^{-3}**	**0.16 € m^{-3}**	**0.24 € m^{-3}**	**0.61 € m^{-3}**	**0.79 € m^{-3}**	**0.83 € m^{-3}**

[a]Operational conditions: initial pH = 2.8; T = 30ºC; $[H_2O_2]$ = 2.1 mM; [b]Operational conditions: natural pH; T = 30ºC; $[H_2O_2]$ = 2.1 mM; [c]Operational conditions: initial pH = 2.8; T = 30ºC; $[H_2O_2]$ = 2.1 mM; $[Fe^{2+}]$ = 2 mg L^{-1}; [d]Operational conditions: initial pH = 2.8; T = 30ºC; $[H_2O_2]$ = 2.1 mM; $[Fe^{2+}]$ = 10 mg L^{-1}; [e]Operational conditions: initial pH = 2.8; T = 30ºC; $[H_2O_2]$ = 2.1 mM; $[Fe^{2+}]$ = 6 mg L^{-1}; iron/oxalate molar ratio of 1:3; [f]Operational conditions: initial pH = 5.0; T = 30ºC; $[H_2O_2]$ = 3.1 mM; $[Fe^{2+}]$ = 6 mg L^{-1}; iron/oxalate molar ratio of 1:3; [g]8% of total collector cost; [h]10% of total collector cost; [i]15% of total collector cost; [j]12% of total direct cost; [k]1% of total direct cost; [l]12% of total capital required, 20 years.

However, the addition of iron (condition (c): UVC/Fe^{2+}/H_2O_2) resulted in more efficient energy consumption in the photo-Fenton reaction and, as a consequence, lower expenses associated with electricity, lamps and labour costs related to lamp replacement and capital spending. The only increase in the cost of the consumables is due to the addition of iron.

On comparing the total unit cost for the systems using different radiation sources, it was verified that the use of solar radiation does not result in a cost reduction when compared to systems using UVC radiation. As can be seen in Figure 6.15, capital spending causes a significant increase in the total cost of solar treatment systems, representing up to 57% of the total cost of the treatment (condition (d): UVA-Vis/Fe^{2+}/H_2O_2). In addition, the expenses associated with consumables were even lower for the systems using UVC radiation as the energy source.

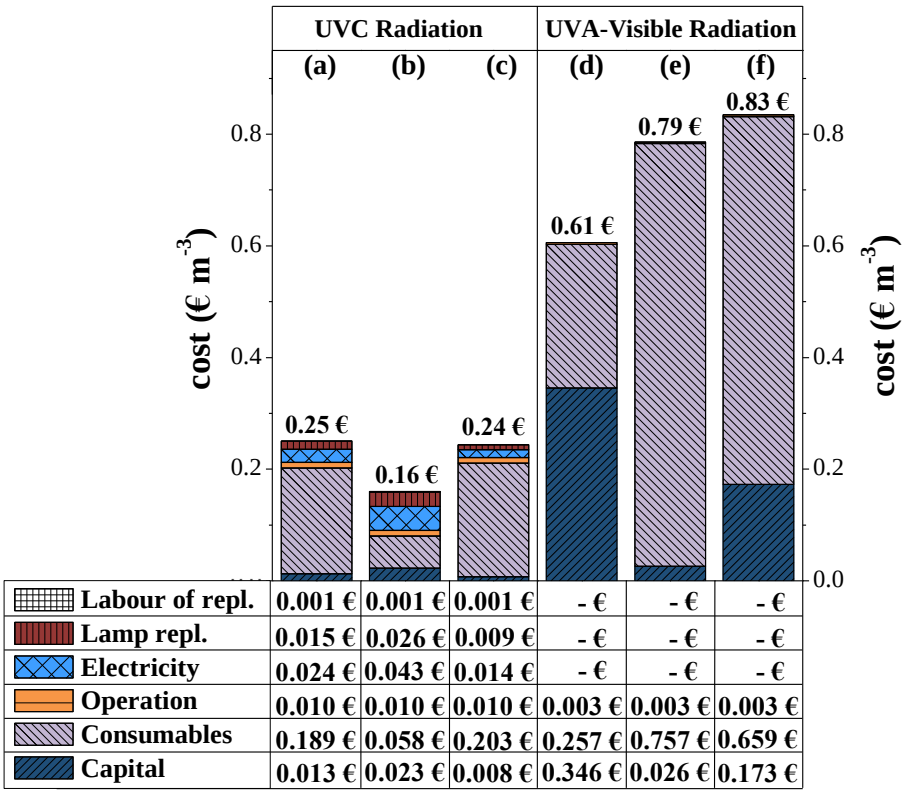

Figure 6.15. Comparative cost of treatment under UVA-Visible radiation with CPCs and UVC radiation with lamps. Assessed operational conditions: (a) initial pH = 2.8; T = 30ºC; [H_2O_2] = 2.1 mM; (b) natural pH; T = 30ºC; [H_2O_2] = 2.1 mM; (c) initial pH = 2.8; T = 30ºC; [H_2O_2] = 2.1 mM; [Fe^{2+}] = 2 mg L^{-1}; (d) initial pH = 2.8; T = 30ºC; [H_2O_2] = 2.1 mM; [Fe^{2+}] = 10 mg L^{-1};(e) initial pH = 2.8; T = 30ºC; [H_2O_2] = 2.1 mM; [Fe^{2+}] = 6 mg L^{-1}; iron/oxalate molar ratio of 1:3; (f) initial pH = 5.0; T = 30ºC; [H_2O_2] = 3.1 mM; [Fe^{2+}] = 6 mg L^{-1}; iron/oxalate molar ratio of 1:3.

In an effort to reduce the energy required for the treatment under UVA-Visible radiation, reducing the required CPC area and capital costs, the use of oxalic acid as the iron ligand was evaluated (condition

(e): UVA-Vis/Fe^{3+}/H_2O_2/Oxalic acid). As a result, the capital spending decreased 93% due to a reduction in the energy dosage required for the treatment. Furthermore, the spending related to consumables increased 195% (up to 0.757 € m^{-3}), representing 96% of the total treatment cost, mainly due to the high price of oxalic acid. The costs associated with UVA-Vis/Fe^{3+}/H_2O_2/Oxalic acid at near neutral pH conditions were also assessed (condition (f)). This condition resulted in a 10% reduction in the spending related to consumables, but the capital costs are five times higher than those for the system operating at acidic pH due to the increased energy demand and, as a consequence, the extra CPC area required.

The land requirement for the implementation of the treatment plant was not considered in the cost calculation for all conditions assessed. The significant volume of textile wastewater considered in the cost calculations (11,037,600 m^3 $year^{-1}$, current operating volume of the WWTP) resulted in the need for a huge land area for the implementation of CPCs, which is equivalent to 80 football fields. However, if land costs were considered in the calculations, the addition of oxalic acid would probably result in a global cost reduction, since the area required for the CPCs would be significantly reduced (from 164,362 to 12,327 m^2), which means a 92% reduction in land area.

Gumy *et al.*, [5] estimated a unitary treatment cost of 7.2 € m^{-3}, considering the treatment of 1000 m^3 per year of a biodegradable azo-dye found in textile wastewaters, through the solar-photo-Fenton reaction. Rodrigues *et al.*, [3] reported the integration of the SBR (sequential batch reactor) with the Fenton reaction for the treatment of three different types of synthetic textile wastewater. The researchers obtained estimated costs of 2.9, 7.5 and 14.8 € m^{-3} for polyester, cotton and acrylic wastewater, respectively. It should be noted that in this study the significant costs associated with the disposal and/or treatment of the sludge were not considered, which is an important factor in relation to the Fenton reaction.

6.4 Conclusions

UVC/H_2O_2, UVC/Fe^{2+}/H_2O_2 and UV-Vis/Fe^{2+}/H_2O_2/oxalic acid advanced oxidation processes showed promising results as polishing step for the decolourisation of a bio-treated textile wastewater. The use of UVC radiation enhanced significantly the textile wastewater decolourisation rates mainly when associated with hydrogen peroxide photolysis and a quantum yield of $FeOH_2^+$ for the formation of hydroxyl radicals. A higher hydrogen peroxide dosage and wastewater temperature showed a positive influence on the UVC/H_2O_2 and UVC/Fe^{2+}/H_2O_2 systems. Although natural solar radiation, such as a UV-visible light source, can be used to promote the photo-Fenton reaction, high amounts of energy are required to achieve wastewater decolourisation, mainly due to the formation of iron-organic pollutant complexes which present low photoactivity. The addition of organic ligands, especially oxalic acid, enhanced significantly the photo-Fenton reaction, minimizing the formation of ferric-organic pollutant complexes and ensuring lower energy consumption. An increase in the stoichiometric iron/oxalate molar ratio did not have a positive effect on the textile wastewater decolourisation. The optimum iron concentration under the tested conditions was 6 mg Fe^{3+} L^{-1} for an iron/oxalate stoichiometric molar ratio of 1:3. Although the photo-Fenton reaction mediated by ferrioxalate can be carried out at near neutral pH, the decolourisation rate decreases significantly when compared to acidic conditions.

The economic assessment using UVA-Visible radiation (solar light) or UVC radiation (lamps) based on the operation variables obtained, for the treatment of 30,240 m^3 per day of a textile wastewater after a biological pre-oxidation process, in order to achieve the values required by German regulations for discharge into water bodies, allowed the following conclusions: i) at acidic pH values the addition of iron to the UVC/H_2O_2 reaction enhanced the decolourisation rates, resulting in a lower treatment cost when compared to neutral pH conditions; ii) the UVC/H_2O_2 system at natural wastewater pH is cheaper than at acid pH, mainly due to the need for acids and bases; iii) the use of solar radiation (UVA-Visible) increases the treatment costs, mainly due to an increase in the capital spending associated with CPCs; iv) the addition of oxalic acid to the photo-Fenton reaction decreases the capital spending (high reaction rates), but the cost of consumables increases significantly, making the treatment more costly; and v) the photo-Fenton system mediated by ferrioxalate at near neutral pH using solar radiation is the most costly treatment process, due to the low decolourisation rates and high consumption of reactants, especially oxalic acid.

6.5 References

1. Karci, A., I. Arslan-Alaton, and M. Bekbolet, *Advanced oxidation of a commercially important nonionic surfactant: Investigation of degradation products and toxicity.* Journal of Hazardous Materials, 2013. **263, Part 2**: p. 275-282.
2. Chowdhury, S. and R. Balasubramanian, *Graphene/semiconductor nanocomposites (GSNs) for heterogeneous photocatalytic decolorization of wastewaters contaminated with synthetic dyes: A review.* Applied Catalysis B: Environmental, 2014. **160**: p. 307-324.
3. Rodrigues, C.S.D., L.M. Madeira, and R.A.R. Boaventura, *Synthetic textile dyeing wastewater treatment by integration of advanced oxidation and biological processes – Performance analysis with costs reduction.* Journal of Environmental Chemical Engineering, 2014. **2**(2): p. 1027-1039.
4. Manenti, D.R., P.A. Soares, A.N. Módenes, F.R. Espinoza-Quiñones, R.A.R. Boaventura, R. Bergamasco, and V.J.P. Vilar, *Insights into solar photo-Fenton process using iron(III)–organic ligand complexes applied to real textile wastewater treatment.* Chemical Engineering Journal, 2015. **266**: p. 203-212.
5. Gumy, D., P. Fernández-Ibáñez, S. Malato, C. Pulgarin, O. Enea, and J. Kiwi, *Supported Fe/C and Fe/Nafion/C catalysts for the photo-Fenton degradation of Orange II under solar irradiation.* Catalysis Today, 2005. **101**(3–4): p. 375-382.
6. Pearce, C., J. Lloyd, and J. Guthrie, *The removal of colour from textile wastewater using whole bacterial cells: a review.* Dyes and pigments, 2003. **58**(3): p. 179-196.
7. Fibbi, D., S. Doumett, L. Lepri, L. Checchini, C. Gonnelli, E. Coppini, and M. Del Bubba, *Distribution and mass balance of hexavalent and trivalent chromium in a subsurface, horizontal flow (SF-h) constructed wetland operating as post-treatment of textile wastewater for water reuse.* Journal of Hazardous Materials, 2012. **199–200**: p. 209-216.
8. Shu, H.-Y., M.-C. Chang, and H.-J. Fan, *Effects of gap size and UV dosage on decolorization of C.I. Acid Blue 113 wastewater in the UV/H_2O_2 process.* Journal of Hazardous Materials, 2005. **118**(1–3): p. 205-211.
9. Oller, I., S. Malato, and J.A. Sánchez-Pérez, *Combination of Advanced Oxidation Processes and biological treatments for wastewater decontamination—A review.* Science of The Total Environment, 2011. **409**(20): p. 4141-4166.
10. Soares, P.A., M. Batalha, S.M.A.G.U. Souza, R.A.R. Boaventura, and V.J.P. Vilar, *Enhancement of a solar photo-Fenton reaction with ferric-organic ligands for the treatment of acrylic-textile dyeing wastewater.* Journal of Environmental Management, 2015. **152**: p. 120-131.
11. Spuhler, D., J. Andrés Rengifo-Herrera, and C. Pulgarin, *The effect of Fe^{2+}, Fe^{3+}, H_2O_2 and the photo-Fenton reagent at near neutral pH on the solar disinfection (SODIS) at low temperatures of water containing Escherichia coli K12.* Applied Catalysis B: Environmental, 2010. **96**(1–2): p. 126-141.
12. De la Cruz, N., J. Giménez, S. Esplugas, D. Grandjean, L.F. de Alencastro, and C. Pulgarín, *Degradation of 32 emergent contaminants by UV and neutral photo-fenton in domestic wastewater effluent previously treated by activated sludge.* Water Research, 2012. **46**(6): p. 1947-1957.
13. Malato, S., P. Fernández-Ibáñez, M.I. Maldonado, J. Blanco, and W. Gernjak, *Decontamination and disinfection of water by solar photocatalysis: Recent overview and trends.* Catalysis Today, 2009. **147**(1): p. 1-59.

14. Liu, K., F.A. Roddick, and L. Fan, *Impact of salinity and pH on the UVC/H_2O_2 treatment of reverse osmosis concentrate produced from municipal wastewater reclamation.* Water Research, 2012. **46**(10): p. 3229-3239.

15. Lopez-Lopez, C., J. Purswani, J. Martín-Pascual, M.V. Martínez-Toledo, M.M. Muñío, and J.M. Poyatos, *Toxic effect of H_2O_2 in H_2O_2/UV, photo-Fenton and heterogeneous photocatalysis (TiO_2/H_2O_2/UV) systems to treat textile wastewater.* Desalination and Water Treatment, 2014: p. 1-10.

16. Litter, M.I., R.J. Candal, and J.M. Meichtry, *Advanced oxidation technologies: Sustainable solutions for environmental treatments*. 2014: CRC Press.

17. Karci, A., I. Arslan-Alaton, T. Olmez-Hanci, and M. Bekbolet, *Degradation and detoxification of industrially important phenol derivatives in water by direct UV-C photolysis and H_2O_2/UV-C process: A comparative study.* Chemical Engineering Journal, 2013. **224**(0): p. 4-9.

18. Karci, A., I. Arslan-Alaton, M. Bekbolet, G. Ozhan, and B. Alpertunga, *H_2O_2/UV-C and Photo-Fenton treatment of a nonylphenol polyethoxylate in synthetic freshwater: Follow-up of degradation products, acute toxicity and genotoxicity.* Chemical Engineering Journal, 2014. **241**: p. 43-51.

19. Antoniou, M.G. and H.R. Andersen, *Comparison of UVC/$S_2O_8^{2-}$ with UVC/H_2O_2 in terms of efficiency and cost for the removal of micropollutants from groundwater.* Chemosphere, 2015. **119**: p. S81-S88.

20. Rekab, K., C. Lepeytre, M. Dunand, F. Dappozze, J.-M. Herrmann, and C. Guillard, *H_2O_2 and/or photocatalysis under UV-C irradiation for the removal of EDTA, a chelating agent present in nuclear waste waters.* Applied Catalysis A: General, 2014. **488**: p. 103-110.

21. Jung, Y.J., W.G. Kim, Y. Yoon, J.-W. Kang, Y.M. Hong, and H.W. Kim, *Removal of amoxicillin by UV and UV/H_2O_2 processes.* Science of The Total Environment, 2012. **420**: p. 160-167.

22. Carra, I., J.A. Sánchez Pérez, S. Malato, O. Autin, B. Jefferson, and P. Jarvis, *Application of high intensity UVC-LED for the removal of acetamiprid with the photo-Fenton process.* Chemical Engineering Journal, 2015. **264**: p. 690-696.

23. Umar, M., F.A. Roddick, L. Fan, O. Autin, and B. Jefferson, *Treatment of municipal wastewater reverse osmosis concentrate using UVC-LED/H_2O_2 with and without coagulation pre-treatment.* Chemical Engineering Journal, 2015. **260**: p. 649-656.

24. Alaton, I.A., I.A. Balcioglu, and D.W. Bahnemann, *Advanced oxidation of a reactive dyebath effluent: comparison of O_3, H_2O_2/UV-C and TiO_2/UV-A processes.* Water Research, 2002. **36**(5): p. 1143-1154.

25. Basturk, E. and M. Karatas, *Decolorization of antraquinone dye Reactive Blue 181 solution by UV/H_2O_2 process.* Journal of Photochemistry and Photobiology A: Chemistry, 2015. **299**: p. 67-72.

26. Zuorro, A., M. Fidaleo, and R. Lavecchia, *Response surface methodology (RSM) analysis of photodegradation of sulfonated diazo dye Reactive Green 19 by UV/H_2O_2 process.* Journal of Environmental Management, 2013. **127**: p. 28-35.

27. Portugal, *Decreto-Lei nº.236/98*. 1998, Ministério do Ambiente: Diário da República. p. 47.

28. Abwasserverordnung, *Verordnung über Anforderungen an das Einleiten von Abwasser in Gewässer (Abwasserverordnung - AbwV)*, B. I, Editor. 2004, Bundesministerium der Justiz: Bundesrepublik Deutschland.

29. *DIN EN ISO 7887:2012-04, Wasserbeschaffenheit - Untersuchung und Bestimmung der Färbung*. 2012, Deutsches Institut für Normung - DIN.

30. Pérez-Urquiza, M. and J.L. Beltrán, *Determination of the dissociation constants of sulfonated azo dyes by capillary zone electrophoresis and spectrophotometry methods.* Journal of Chromatography A, 2001. **917**(1–2): p. 331-336.

31. Gomes, A.C., L.R. Fernandes, and R.M.S. Simões, *Oxidation rates of two textile dyes by ozone: Effect of pH and competitive kinetics.* Chemical Engineering Journal, 2012. **189–190**(0): p. 175-181.

32. Yazdanbakhsh, M.R., A. Ghanadzadeh, and E. Moradi, *Synthesis of some new azo dyes derived from 4-hydroxy coumarin and spectrometric determination of their acidic dissociation constants.* Journal of Molecular Liquids, 2007. **136**(1–2): p. 165-168.

33. Ebead, Y.H., H.M.A. Salman, M. Khodari, and A.A. Ahmed, *Spectrophotometric investigations of the role of the organic solvent on the acid dissociation constants of some azo dyes derived from 2-aminobenzothiazole.* Journal of Molecular Liquids, 2010. **154**(1): p. 52-57.

34. Ebead, Y.H., *The role of the medium on the acid dissociation constants of some azo dyes in view of experimental and theoretical data.* Journal of Molecular Structure, 2010. **982**(1–3): p. 100-106.

35. Goswami, P. and M. Basak, *Sulfur Dyes*, in *Kirk-Othmer Encyclopedia of Chemical Technology*. 2000, John Wiley & Sons, Inc.

36. Aksu, Z., *Application of biosorption for the removal of organic pollutants: a review.* Process Biochemistry, 2005. **40**(3–4): p. 997-1026.

37. Leube, H., W. Rüttiger, G. Kühnel, J. Wolff, G. Ruppert, M. Schmitt, C. Heid, M. Hückel, H.-J. Flath, W. Beckmann, R. Brossmann, M. Söll, and U. Sewekow, *Textile Dyeing*, in *Ullmann's Encyclopedia of Industrial Chemistry*. 2000, Wiley-VCH Verlag GmbH & Co. KGaA.

38. Tehrani-Bagha, A.R. and K. Holmberg, *Solubilization of hydrophobic dyes in surfactant solutions.* Materials, 2013. **6**(2): p. 580-608.

39. Benkelberg, H.-J. and P. Warneck, *Photodecomposition of Iron(III) Hydroxo and Sulfato Complexes in Aqueous Solution: Wavelength Dependence of OH and SO_4^- Quantum Yields.* The Journal of Physical Chemistry, 1995. **99**(14): p. 5214-5221.

40. Sanz, J., J.I. Lombraña, and A. de Luis, *Temperature-assisted UV/H2O2 oxidation of concentrated linear alkylbenzene sulphonate (LAS) solutions.* Chemical Engineering Journal, 2013. **215–216**: p. 533-541.

41. Monteagudo, J.M., A. Durán, J.M. Corral, A. Carnicer, J.M. Frades, and M.A. Alonso, *Ferrioxalate-induced solar photo-Fenton system for the treatment of winery wastewaters.* Chemical Engineering Journal, 2012. **181–182**: p. 281-288.

42. Santos, A., P. Yustos, S. Rodriguez, E. Simon, and F. Garcia-Ochoa, *Abatement of phenolic mixtures by catalytic wet oxidation enhanced by Fenton's pretreatment: Effect of H_2O_2 dosage and temperature.* Journal of Hazardous Materials, 2007. **146**(3): p. 595-601.

43. Moreira, F.C., R.A.R. Boaventura, E. Brillas, and V.J.P. Vilar, *Degradation of trimethoprim antibiotic by UVA photoelectro-Fenton process mediated by Fe(III)–carboxylate complexes.* Applied Catalysis B: Environmental, 2015. **162**: p. 34-44.

44. Shu, H.-Y., C.-R. Huang, and M.-C. Chang, *Decolorization of mono-azo dyes in wastewater by advanced oxidation process: A case study of acid red 1 and acid yellow 23.* Chemosphere, 1994. **29**(12): p. 2597-2607.

45. Shah, N.S., X. He, H.M. Khan, J.A. Khan, K.E. O'Shea, D.L. Boccelli, and D.D. Dionysiou, *Efficient removal of endosulfan from aqueous solution by UV-C/peroxides: A comparative study.* Journal of Hazardous Materials, 2013. **263, Part 2**: p. 584-592.

46. Seraghni, N., S. Belattar, Y. Mameri, N. Debbache, and T. Sehil, *Fe(III)-Citrate-Complex-Induced Photooxidation of 3-Methylphenol in Aqueous Solution.* International Journal of Photoenergy, 2012. **2012**.

47. Monteagudo, J.M., A. Durán, M. Aguirre, and I.S. Martín, *Photodegradation of Reactive Blue 4 solutions under ferrioxalate-assisted UV/solar photo-Fenton system with continuous addition of H_2O_2 and air injection.* Chemical Engineering Journal, 2010. **162**(2): p. 702-709.

48. Zhang, C., *Photodegradation of Organic Pollutants Induced by Iron-carboxylate Complexes in Aqueous Solutions*, in *Department of Chemistry*. 2009, University Blaise Pascal.

49. Ito, H., M. Fujii, Y. Masago, C. Yoshimura, T.D. Waite, and T. Omura, *Mechanism and kinetics of ligand exchange between ferric citrate and desferrioxamine B.* J Phys Chem A, 2011. **115**(21): p. 5371-9.

50. Weller, C., S. Horn, and H. Herrmann, *Effects of Fe(III)-concentration, speciation, excitation-wavelength and light intensity on the quantum yield of iron(III)-oxalato complex photolysis.* Journal of Photochemistry and Photobiology A: Chemistry, 2013. **255**: p. 41-49.

51. Klamerth, N., S. Malato, A. Agüera, and A. Fernández-Alba, *Photo-Fenton and modified photo-Fenton at neutral pH for the treatment of emerging contaminants in wastewater treatment plant effluents: A comparison.* Water Research, 2013. **47**(2): p. 833-840.

52. Safarzadeh-Amiri, A., J.R. Bolton, and S.R. Cater, *Ferrioxalate-mediated photodegradation of organic pollutants in contaminated water.* Water Research, 1997. **31**(4): p. 787-798.

7 Main conclusions and future work

This final chapter presents the most pertinent results and conclusions stated in the previous Chapters, complemented with some recommendations for future work.

7.1 Main conclusions

The main goal of this thesis was to study alternative strategies combining biological and advanced oxidation processes (AOPs), such as Fenton, photo-Fenton, UV/TiO_2, UV/H_2O_2, UV/TiO_2/H_2O_2 and UVC/H_2O_2, for the treatment of textile wastewaters with different characteristics, targeting an effective decolourisation and mineralisation at low operating cost. Considering that textile wastewaters are known to show different compositions, an integrated treatment strategy was applied to four different textile wastewaters, two real textile wastewaters and two synthetic ones, taking into account their main characteristics.

In this way, for two wastewaters (from a real cotton dyeing process and from a synthetic acrylic dyeing process), both with high percentage of recalcitrant organic matter, an AOP followed by a biological oxidation treatment was proposed. For the other two wastewaters (a real bio-treated textile wastewater and other one from a synthetic polyester-cotton dyeing), both with high percentage of biodegradable organic matter, a biological oxidation treatment followed by an AOP was proposed.

7.1.1 Advanced Oxidation processes followed by biological oxidation

In Chapter 3 the efficiency of different AOPs, namely UVA-Vis; UVA-Vis/TiO_2; UVA-Vis/H_2O_2; UVA-Vis/TiO_2/H_2O_2 and UVA-Vis/Fe^{2+}/H_2O_2, in the treatment of a real cotton-textile dyeing wastewater at pilot scale under natural sunlight, was compared. The solar-photo-Fenton treatment was the most efficient of all solar AOPs studied, enhancing the biodegradability of the wastewater and making possible its combination with a biological oxidation process, in order to achieve a wastewater quality in agreement with the discharge limits imposed by legislation. A subsequent study was performed in order to evaluate the influence of the main photo-Fenton reaction variables, such as iron concentration, pH, temperature and irradiance, in a lab-scale prototype under controlled conditions using artificial solar radiation. The results obtained in this study lead to the following conclusions:

- Although the kinetic constants increase with iron concentration, the increment is very small for concentrations higher than 60 mg L^{-1}, being necessary higher amounts of H_2O_2;
- Although the photo-Fenton reaction was more efficient at pH 2.8, the reaction rates remained very similar up to pH 3.6, which can reduce the costs associated with acid and base consumption;

- The increase of solution temperature favoured the photo-Fenton efficiency, principally from 10 to 30ºC, which was associated with the increment of the molar fraction of the most photoactive species ($FeOH_2^+$), as well as to the thermal reactions involved in the reduction of ferric ions, which use radiation of wavelengths higher than 500 nm. This condition favours the textile wastewater treatment since textile dyeing wastewaters normally present temperatures higher than 30ºC;

- The reaction rate remained approximately constant within the range of UVA irradiance studied, therefore, during spring and summer, considering the path length of the photoreactors, energy losses are negligible, and, over autumn and winter, the kinetic reaction rate remains constant in terms of accumulated UV energy, but the photo-Fenton reaction can take a longer time;

- Finally, considering the combination of an AOP with a biological oxidation system, the energy dose required for the photo-Fenton reaction was 0.5 kJ_{UV} L^{-1} (T = 30ºC; pH = 2.8) consuming 7.5 mM of hydrogen peroxide and leading to 58.4% mineralisation (DOC_f = 62.9 mg C L^{-1}).

In Chapter 4 it was reported that the traditional solar-photo-Fenton process showed limited efficiency in the mineralisation of the synthetic acrylic-textile dyeing wastewater, which was attributed to the iron complexation with the dyeing auxiliaries products. The photo-Fenton process was enhanced by ferric-organic ligands (oxalic acid, citrate acid and EDDS-Ethylenediamine-N,N'-disuccinic acid), on a lab-scale prototype under controlled conditions, using artificial solar radiation. The addition of organic ligands enhanced the photo-Fenton reaction significantly, minimising the formation of ferric complexes with the dyeing auxiliary products. The catalytic activity of the organic ligands toward the ferrous catalysed system followed the order: Fe(III)-Oxalate>Fe(III)-Citrate>Fe(III)-EDDS. The influence of the main ferrioxalate-solar-photo-Fenton reaction variables, such as iron concentration, pH, temperature, UV irradiance and H_2O_2 concentration and dosage strategy was also investigated, and the following considerations emerged from the obtained results:

- The optimum iron concentration must be evaluated taking into account the variability on the UV irradiance (amount of photons available for the reaction);

- The addition of small amounts of H_2O_2 during the photo-Fenton reaction improves the mineralisation rates, as also minimizes the consumption rate of H_2O_2;

- Acetic acid formation was observed during the reaction. This carboxylic acid can form a stable complex with ferric ions, which has a low photoactivity under UVA-visible light and is very

resistant to the attack of hydroxyl and other reactive oxygen species, almost stopping the photo-Fenton reaction.

The effect of the hydrodynamic conditions, on a lab-scale prototype using artificial solar radiation and on a pilot scale under natural sunlight, was also assessed both in the dark and light parts of the system. The results obtained demonstrated that the design of a CPC plant must take into account not only the need of a turbulent regime inside the tubular photoreactors, but also promoting the mixing of the wastewater in the dark system (recirculation tank).

Finally, the ferrioxalate induced photo-Fenton process achieved 87% mineralisation after 9.3 kJ_{UV} L^{-1}, and allowing working until pH 5.0. As expected, the biodegradability of the textile wastewater was significantly enhanced by the photo-Fenton treatment, achieving a value of 73%, consuming 32.4 mM of H_2O_2 and 5.7 kJ_{UV} L^{-1}.

7.1.2 Biological oxidation followed by Advanced Oxidation processes

Chapter 5 regards an integrated treatment strategy for synthetic polyester-cotton dyeing wastewater, combining biological and photochemical oxidation processes. The biodegradability of all constituents, dyes and dyeing auxiliary products, present in the synthetic polyester dyeing textile wastewater, was firstly assessed through a Zahn-Wellens test. More than 80% of the constituents are easily biodegradable, being possible to achieve their complete removal by biological oxidation. Consequently, the synthetic wastewater was firstly subjected to a biological oxidation, achieving a DOC removal of 76%, resulting in a bio-treated wastewater with 84 mg L^{-1} of DOC. However, colour reduction was less than 5% (Pt-Co scale), 9% (DFZ_{436nm}), 3% (DFZ_{525nm}) and 0% (DFZ_{620nm}).

Different chemical oxidation systems, such as UVC/H_2O_2, UVC/Fe^{2+}/H_2O_2 and UVC/Fe^{3+}/H_2O_2/Oxalic acid, were used as a polishing treatment step, regarding the wastewater decolourisation. The photo-Fenton reaction did not promote wastewater decolourisation. The low iron concentration used was not able to suppress the inner filter effects related to other light-absorbing species present in the solution. Beyond that, complexes of ferric ions with organic and inorganic species (e.g., auxiliary products) present in the textile wastewater show low photoactivity and recalcitrant characteristic to further mineralisation by hydroxyl radical attack. The addition of oxalic acid, as a ferric ions ligand, did not lead to an increase of the wastewater decolourisation.

On the other hand, the photolysis of hydrogen peroxide using UVC radiation showed decolourisation efficiencies of 71% (Pt-Co scale), 86% ($DFZ_{436\ nm}$) and 97% ($DFZ_{525\ nm}$) and more than 40% of

mineralisation, consuming 14.1 mM H_2O_2 and 2.5 kJ_{UV} L^{-1} of energy (time = 95 min; 6W UVC lamp; natural pH = 8.4; T = 30ºC). The effect of hydrogen peroxide dosage, lamp power, solution pH and temperature, on the UVC/H_2O_2 system was evaluated, leading to the following conclusions:

- The decolourisation rates increased significantly with the availability of hydrogen peroxide, being almost six times higher for the initial H_2O_2 dose of 42 mM when compared with 10 mM. A higher H_2O_2 dose was necessary to break the dyes molecules and other auxiliary products into smaller molecules and further conversion into carbon dioxide, water and inorganic acids;

- It was demonstrated that a detailed study considering the optical length of the reactor and linking the lamp power to peroxide dosage should always be done in order to avoid unnecessary expenses with reagents and energetic costs;

- Alkaline and acidic wastewaters inhibited the decolourisation of the bio-treated wastewater using the UVC/H_2O_2 system;

- Decolourisation and mineralisation rates are favoured at higher temperatures, especially when the temperature raised from 15 to 30ºC. This behaviour was associated with the increase of the generation of $^{\bullet}OH$ radicals through H_2O_2 photolysis as temperature increases.

During the photochemical reaction some low-molecular-weight carboxylic acids were detected, as oxalic acid, maleic acid and tartaric acid, which is an indirect indicator of the biodegradability enhancement. Finally, the integrated treatment strategy was able to achieve a wastewater quality in agreement with the discharge limits imposed by legislation.

In Chapter 6 it was assessed the decolourisation of a bio-treated real textile wastewater using UVC/H_2O_2 and photo-Fenton oxidation processes, as a polishing step. The photolysis of hydrogen peroxide using UVC radiation showed decolourisation efficiencies of 86% (Pt-Co scale) and 96% (DFZ_{436nm}), consuming 1.6 mM H_2O_2 after 0.9 kJ_{UV} L^{-1} (time = 35 min; 6 W UVC lamp; natural pH = 7.8; T = 30ºC). The efficiency of hydrogen peroxide photolysis under UVC radiation on the wastewater decolourisation was evaluated at different pH values, H_2O_2 concentration and temperature. Although the decolourisation rate is similar for the UVC/H_2O_2 system at neutral and acid pH values, the amount of UVC energy required to achieve the same decolourisation efficiency is higher at neutral pH conditions. This is mainly related to the high fraction of decolourisation obtained in the acidification procedure. The initial concentration of hydrogen peroxide, for the dosage range studied, showed a higher effect on the UVC/H_2O_2 system than on the photo-Fenton system. The photo-Fenton reaction was promoted by

different radiation sources (UVC, UVA or UVA-Visible), showing better results under UVC light. Decolourisation efficiencies of 78% (Pt-Co scale) and 93% (DFZ_{436nm}), were achieved by the UVC/Fe^{2+}/H_2O_2 system at pH = 2.8 and T = 30ºC, consuming 3.6 mM H_2O_2 after 0.6 kJ_{UV} L^{-1} (time = 25 min; 6 W UVC lamp). The efficiency of the UVC/Fe^{2+}/H_2O_2 system was also studied for different iron concentrations, H_2O_2 availability and pH values, resulting in the following conclusions:

- The decolourisation kinetic profiles show a very similar behaviour in the initial part of curves of the different tested concentrations of iron, indicating that the photolysis of H_2O_2 is the predominant mechanism. In the second part of the curves, a slight improvement on the decolourisation rate with the increase of iron concentration was observed;

- The increase of the textile wastewater temperature improved significantly the decolourisation reaction rate using the photo-Fenton reaction, which was associated with two main factors: i) presence of different amounts of photoactive species ($FeOH^{2+}$); ii) higher Fe^{3+} reduction through Fenton's thermal reactions.

Aiming at using solar energy, additional photo-Fenton assays mediated by ferric-organic ligands under UVA-Visible radiation were also performed, considering the effect of the type of ferric-organic ligand, iron/ferric-organic ligand molar ratio, iron concentration and pH. Maximum values of decolourisation achieved by the UVA-Vis/Fe^{3+}/H_2O_2/Oxalic acid system were 84% (Pt-Co scale) and 94% (DFZ_{436nm}), consuming 1.9 mM H_2O_2 after 2.9 kJ_{UV} L^{-1} (pH = 2.8):

- The addition of organic ligands, especially oxalic acid, enhanced significantly the photo-Fenton reaction, minimising the formation of ferric-organics complexes and ensuring lower energy consumption;

- The optimum iron concentration in the tested conditions was 6 mg Fe^{3+} L^{-1} for an iron/oxalate stoichiometric molar ratio of 1:3. The increase of stoichiometric iron/oxalate molar ratio did not produce positive effect on the textile wastewater decolourisation. Considering the Portuguese regulation, a subsequent step for iron precipitation has to be considered in order to meet the legal limit for the iron concentration;

- Although the photo-Fenton reaction mediated by ferrioxalate can be carried out at near neutral pH, the decolourisation rates decrease significantly when compared to acidic conditions;

Finally, the total unit costs for the optimal conditions were estimated, aiming at achieving the legal wastewater discharge requirements, leading to the following conclusions: i) at acidic pH values the

addition of iron to the UVC/H_2O_2 reaction enhanced the decolourisation rates, resulting in a lower treatment cost when compared to neutral pH conditions; ii) the UVC/H_2O_2 system at natural wastewater pH is cheaper than at acid pH; iii) the use of solar radiation increases the treatment costs, due to an increase in the capital spending associated with CPCs; iv) the addition of oxalic acid to the photo-Fenton reaction decreases the capital spending (high reaction rates), but the cost of consumables increases, making the treatment more costly; and v) the photo-Fenton system mediated by ferrioxalate at near neutral pH using solar radiation is the most expensive treatment process, due to the low decolourisation rates and high consumption of reactants, especially oxalic acid.

7.2 Recommendations for future work

According to the obtained results, some suggestions for further investigations can be proposed.

In order to overcome the restrictions of working at neutral pH levels, a possible strategy can be the use of immobilized photocatalysts, as well as, tests with other iron-carboxylate complexes. Moreover, Electrochemical Advanced Oxidation Processes, considering their capacity for in situ generation of H_2O_2, could be also tested for textile wastewater treatment. Another strategy could be the development of photocatalytic membranes (separation function/photocatalytic activity), which would enhance their antifouling properties and at the same time would lead to membrane concentrates with lower organic loads.

Efforts must be also spent on the possible combination of natural and artificial radiation, development of new designs for photocatalytic reactors using artificial radiation through computational fluid dynamics (CFD) tool, optimization of the optical system for sunlight capture, based in CPCs systems, in terms of photon and thermal flux (high temperatures favour the reaction rate) and, volumetric capacity per unit of collector area using nonimaging optics (NIO) techniques.